POWER SYSTEMS DEVELOPMENT FACILITY

TECHNICAL PROGRESS REPORT FOR KELLOGG BROWN & ROOT TRANSPORT REACTOR TRAIN WITH SIEMENS-WESTINGHOUSE PARTICULATE CONTROL DEVICE

TC02: APRIL — MAY 1998

DOE Cooperative Agreement Number
DE-FC21-90MC25140

Prepared by:
Southern Company Services, Inc.
Power Systems Development Facility
P.O. Box 1069
Wilsonville, AL 35186

June 1999

DISCLAIMER

This report was prepared as an account of work sponsored by an agency of the United States Government. Neither the United States Government nor any agency thereof, nor any of their employees, nor Southern Company Services, Inc., nor any of its employees, nor any of its subcontractors, makes any warranty, expressed or implied, or assumes any legal liability or responsibility for the accuracy, completeness, or usefulness of any information, apparatus, product, or process disclosed, or represents that its use would not infringe privately owned rights. Reference herein to any specific commercial product, process, or service by trade name, trademark, manufacturer or otherwise, does not necessarily constitute or imply its endorsement, recommendation, or favoring by the United States Government or any agency thereof. The views and opinions of authors expressed herein do not necessarily state or reflect those of the United States Government or any agency thereof.

Available to the public from the National Technical Information Service, U.S. Department of Commerce, 5285 Port Royal Road, Springfield, VA 22161. Phone orders accepted at (703) 487-4650.

Contents

CONTENTS

Section Page

Inside Cover
Disclaimer

Listing of Tables and Figures v

1.0 EXECUTIVE SUMMARY 1.1-1

1.1 Operation Status 1.1-1
1.1.1 Transport Reactor 1.1-3
1.1.2 Siemens-Westinghouse PCD 1.1-4

1.2 PSDF Accomplishments 1.2-1
1.2.1 Transport Reactor Train 1.2-1
1.2.2 PCD-Related Systems 1.2-2

1.3 Future Plans 1.3-1

2.0 INTRODUCTION 2.1-1

2.1 The Power Systems Development Facility 2.1-2
2.2 Transport Reactor System Description 2.2-1
2.3 Westinghouse Particulate Control Device 2.3-1

3.0 PARTICLE FILTER SYSTEM 3.1-1

3.1 TC02 PCD Overview 3.1-1
3.1.1 Run Summary 3.1-1
3.1.2 TC02 Accomplishments 3.1-1
3.1.3 Developmental Areas 3.1-2
3.1.4 Future Plans 3.1-3

3.2 PCD Operations During Test Run TC02 ..... 3.2-1
3.2.1 Run Summary 3.2-1
3.2.2 Test Objectives 3.2-1
3.2.3 Observations/Events 3.2-2
3.2.4 Run Outcome 3.2-5

3.3 TC02 Inspection Report 1 ..... 3.3-1
3.3.1 Run Summary 3.3-1
3.3.2 Thermal Event 3.3-1

3.3.3 PCD Inspection and Dustcake Observations 3.3-1
3.3.4 Inspection Results....3.3-2

3.4 TC02 Inspection Report 2....3.4-1
3.4.1 Run Summary....3.4-1
3.4.2 PCD Inspection and Dustcake Observations 3.4-1
3.4.3 Inspection Results....3.4-1

3.5 TC02 Ash Characteristics and PCD Performance....3.5-1
3.5.1 Measurements of Particulate Mass Loadings....3.5-1
3.5.2 Measurements of Particle-Size Distributions....3.5-4
3.5.3 Cut-Size Tests....3.5-4
3.5.4 Chemical Analyses 3.5-5
3.5.5 Measurements of Physical Properties 3.5-8

3.6 Coax Valve Testing After Modification 3.6-1
3.6.1 Test Objectives....3.6-1
3.6.2 Introduction....3.6-1
3.6.3 Test Procedure 3.6-1
3.6.4 Results and Observations 3.6-2
3.6.5 Conclusions 3.6-4
3.6.6 References for Section 3.6....3.6-4

3.7 Plenum Pressure Measurements....3.7-1
3.7.1 Test Objectives....3.7-1
3.7.2 Introduction....3.7-1
3.7.3 Test Procedure 3.7-1
3.7.4 Conclusions 3.7-2

3.8 Coors P-100A-1 Filter Element Operational Experience and Analysis 3.8-1
3.8.1 Introduction....3.8-1
3.8.2 Coors P-100-A-1 Test History at the PSDF....3.8-2
3.8.3 Analysis of Data....3.8-6
3.8.4 Filter Element Thermocouples....3.8-10
3.8.5 Thermal/Mechanical Analysis of Coors Vs Other Ceramic Filter Elements 3.8-12
3.8.6 Conclusions and Future Plans 3.8-15
3.8.7 Acknowledgments for Section 3.8 ....3.8-17
3.8.8 References for Section 3.8....3.8-18

4.0 TRANSPORT REACTOR....4.1-1

4.1 Transport Reactor TC02 Run Summary 4.1-1
4.2 TC02 Heat and Material Balance....4.2-1

4.3 SO_2, SO_3, and Solids Analyses 4.3-1
4.4 NO_x Emissions 4.4-1
4.5 Flow Regimes in the Transport Reactor 4.5-1
4.5.1 Literature Review on Flow Regimes in a CFB 4.5-1
4.5.2 Test Results and Discussion 4.5-3
4.5.3 Conceptual Model and Discussion 4.5-5
4.5.4 Summary 4.5-7
4.5.5 References for Section 4.5 ..... 4.5-7

4.6 Feed Systems 4.6-1
4.6.1 Feedstock Preparation 4.6-1
4.6.2 Reactor Feedstock Injection and Ash Removal Systems 4.6-1

TERMS ..... PSDF Terms-1

Listing of Tables and Figures

Listing of Tables

Table		Page
2.2-1	Major Equipment in the Transport Reactor Train	2.2-3
2.2-2	Major Equipment in the Balance-of-Plant	2.2-4
3.2-1	TC02 Run Statistics	3.2-6
3.2-2	TC02 Major Events	3.2-7
3.5-1	PCD Inlet Particulate Mass Loading Data for Test Program TC02	3.5-11
3.5-2	PCD Outlet Particulate Mass Loading Data for Test Program TC02	3.5-11
3.5-3	PCD Particulate Collection Efficiencies for Test Program TC02	3.5-12
3.5-4	Elemental Analysis of Selected TC02 Hopper Samples	3.5-13
3.5-5	Elemental Analysis of TC02 In Situ Samples	3.5-14
3.5-6	Elemental Analysis and Characteristics of Layered TC02 Dustcake Samples	3.5-15
3.5-7	Elemental Analysis and Characteristics of Layers Compared to Entire Cake	3.5-16
3.5-8	Characteristics of Dustcake Samples Taken From Various Types of Filter Elements	3.5-17
3.5-9	Physical Properties of TC02 In Situ Samples	3.5-18
3.5-10	Physical Properties of Selected TC02 Hopper Samples	3.5-19
3.6-1	Test Arrangements	3.6-5
3.8-1	Coors P-100A-1 Filters Installed in April 1997	3.8-19
3.8-2	Coors Filters Installed in July 1997	3.8-19
3.8-3	Coors Filters Installed in September 1997	3.8-19
3.8-4	Coors Filter Element Ultimate Tensile Strength	3.8-20
3.8-5	Filter Elements Installed in April 1998	3.8-20
3.8-6	Coefficient of Thermal Expansion, Strain-to-Failure, and Estimated Thermal Gradient Required to Initiate Microcracking in a Filter Element	3.8-21
3.8-7	Thermal Diffusitivity of Ceramic Filter Materials	3.8-21
4.1-1	TC02 Operating Conditions	4.1-4
4.2-1	Average Reactor Conditions on May 2	4.2-2
4.2-2	Overall Material Balance	4.2-2
4.2-3	Component Material Balances	4.2-2
4.3-1	TC02 SO_2 and SO_3 Data From May 7 and May 11	4.3-8
4.3-2	TC02 SO_2 and SO_3 Data From May 7 and May 11	4.3-8
4.4-1	Reactor Operating Conditions	4.4-3

Listing of Figures

Figure Page

2.2-1 Flow Diagram of the Transport Reactor Train in Combustion Mode of Operation....2.2-7

2.3-1 Sketch of Westinghouse PCD....2.3-2

3.2-1 First Filter Element Layout for TC02 April 5 to April 13 (Layout No. 7)....3.2-9
3.2-2 Second Filter Element Layout for TC02 April 18 to May 13 (Layout No. 8)....3.2-10
3.2-3 TC02 Summary Information....3.2-11
3.2-4 TC02 Summary Information....3.2-12
3.2-5 TC02 Summary Information....3.2-13
3.2-6 TC02 Summary Information....3.2-14
3.2-7 TC02 Summary Information....3.2-15
3.2-8 TC02 Summary Information....3.2-16
3.2-9 TC02 Summary Information....3.2-17
3.2-10 TC02 Summary Information....3.2-18
3.2-11 TC02 Summary Information....3.2-19
3.2-12 TC02 Summary Information....3.2-20
3.2-13 TC02 Summary Information....3.2-21
3.2-14 TC02 Summary Information....3.2-22
3.2-15 TC02 Summary Information....3.2-23
3.2-16 TC02 Summary Information....3.2-24
3.2-17 TC02 Summary Information....3.2-25

3.3-1 Bottom Plenum on April 16, 1998....3.3-3
3.3-2 Broken Blasch Filter Elements....3.3-3
3.3-3 Broken Specific Surface Filter Element....3.3-4
3.3-4 Broken Coors Element Close-Up....3.3-4
3.3-5 Two Broken Coors Elements....3.3-5
3.3-6 Layout 7....3.3-6
3.3-7 Layout 7 Failures....3.3-7
3.3-8 Broken Blasch Elements Removed....3.3-8
3.3-9 Final Arrangement TC02 Run....3.3-9

3.4-1 Removal of PCD Plenum May 19, 1998....3.4-2
3.4-2 Leaking Gaskets on 3M Candles....3.4-3
3.4-3 Dustcake on the Elements....3.4-3
3.4-4 Ash Accumulation on the Filter Flanges....3.4-4
3.4-5 Dust Ridges on the Elements....3.4-4
3.4-6 Element Layout for TC03....3.4-5

3.5-1 Differential Mass Distributions of Selected Inlet Particulate Samples 3.5-20
3.5-2 Cumulative Percentage Mass Distribution Measured at PCD Outlet (Average of Three Cascade Impactor Runs)..... 3.5-21
3.5-3 Differential Mass Distribution Measured at PCD Outlet (Average of Three Cascade Impactor Runs)..... 3.5-22
3.5-4 Drag-Equivalent Diameter Versus Calcium Content of TC02 Dustcake Samples 3.5-23
3.5-5 Drag-Equivalent Diameter Versus Calcium Content of TC02 Hopper Samples..... 3.5-24
3.5-6 Drag-Equivalent Diameter Versus Calcium Content for All TC02 Dustcake and Hopper Samples..... 3.5-25

3.6-1 Mass Discharge Vs Valve Differential Pressure at t = 0.4 sec 3.6-6
3.6-2 Fully Open Time Vs Valve Differential Pressure at t = 0.4 sec 3.6-6
3.6-3 Response Time Vs Valve Differential Pressure at t = 0.4 sec.....3.6-7
3.6-4 Mass Discharge Vs Valve Differential Pressure for SV3112B at t = 0.9 sec.....3.6-7
3.6-5 Fully Open Time Vs Valve Differential Pressure for SV3112B at t = 0.9 sec.....3.6-8
3.6-6 Response Time Vs Valve Differential Pressure for SV3112B at t = 0.9 sec.....3.6-8
3.6-7 Mass Discharge Vs Valve Differential Pressure for SV3112B at t = 1.2 sec.....3.6-9
3.6-8 Fully Open Time Vs Valve Differential Pressure for SV3112B at t = 1.2 sec.....3.6-9
3.6-9 Response Time Vs Valve Differential Pressure for SV3112B at t = 1.2 sec..... 3.6-10
3.6-10 Mass Discharge Vs Valve Differential Pressure for SV3112A at t = 0.2 sec..... 3.6-10
3.6-11 Fully Open Time Vs Valve Differential Pressure for SV2112A at t = 0.2 sec..... 3.6-11
3.6-12 Response Time Vs Valve Differential Pressure for SV3112A at t = 0.2 sec..... 3.6-11
3.6-13 Mass Discharge Vs Electrical Pulse Duration for SV3112A at ΔP = 225 psi..... 3.6-12
3.6-14 Fully Open Time Vs Electrical Pulse Duration for SV3112A at ΔP = 225 psi..... 3.6-12

3.7-1 Schematic of Plenum Pressure Rise Measurements..... 3.7-3

3.8-1 Tubesheet Map for April 1997..... 3.8-22
3.8-2 Time/Temperature Operating History of PCD From April 1997 to July 1997 ..... 3.8-23
3.8-3 Tubesheet Map for July 1997 ..... 3.8-24
3.8-4 PCD Temperatures During Start-Up on August 31/September 1, 1997..... 3.8-25
3.8-5 Tubesheet Map Showing Location of Broken Coors Filters..... 3.8-26
3.8-6 Tubesheet Map for September 1997..... 3.8-27

3.8-7 PCD Temperatures During Start-Up on September 7, 1997 ....3.8-28
3.8-8 PCD Outlet Loadings During the September to December 1997 Test Campaign 3.8-28
3.8-9 PCD Temperatures During Element Failure of September 19, 1997 ....3.8-29
3.8-10 PCD Temperatures During Coal Feeder Upset on November 2, 1997 ....3.8-29
3.8-11 Broken Coors Filters After Transient of November 2, 1997 ....3.8-30
3.8-12 Location of Broken Filters After Transient of November 2, 1997 ....3.8-31
3.8-13 Location of Instrumented Filter Elements of April 1998 ....3.8-32
3.8-14 PCD Temperatures During Candle Failures of April 9, 1998 ....3.8-33
3.8-15 Broken Coors Filter Element Hanging From Thermocouple 3.8-34
3.8-16 Probable Axial Tensile Stress-Strain Responses for Coors P-100A-1 Filter Element 3.8-35
3.8-17 Thermal Expansion of Coors P-100A-1 Filter Element 3.8-35
3.8-18 Cutting Plan for O-Ring Testing of Coors Filter 3.8-36
3.8-19 Hoop Tensile Strength of Coors P-100A-1 ....3.8-37
3.8-20 Crack Propogating Through Hoop Tensile Specimens of Coors Filter Element KC007 ....3.8-38
3.8-21 Diagram of Cracks in Broken Coors P-100-A1 Element KC013 ....3.8-39
3.8-22 Approximate Locations of ID and OD Thermocouples 3.8-40
3.8-23 Thermocouples on Pall and Coors Filter Elements 3.8-41
3.8-24 Broken Filters After Start-Up on April 9, 1998 ....3.8-42
3.8-25 Pall Filter Element Thermocouple Response on April 9, 1998 ....3.8-43
3.8-26 Thermal Expansion of Various Ceramic Filter Materials 3.8-43
3.8-27 Axial Tensile Stress-Strain Response of Various Ceramic Filter Material 3.8-44
3.8-28 Thermal Conductivity of Coors, Pall, and Schumacher Filter Elements 3.8-44
3.8-29 SRI Flat Plate Thermal Model 3.8-45
3.8-30 Calculated Thermal Gradient From SRI Flat Plate Model 3.8-46
3.8-31 ANSYS Finite Element Model of Filter Element 3.8-46
3.8-32 Thermal Gradient Applied to "Hot Spot" 3.8-47
3.8-33 Results of ANSYS Model for Coors Filter 3.8-48
3.8-34 Results of ANSYS Model for Schumacher TF20 Filter 3.8-49
3.8-35 Gradient Calculated by ANSYS for Coors, Pall, and Schumacher Filter Elements 3.8-50

4.1-1 C00201 System Profile 4.1-5
4.1-2 Start-Up Bruner Flow/Temperature 4.1-5
4.1-3 System Pressures Downstream of PCD 4.1-5
4.1-4 Total Gas In/Out Flow Rates 4.1-6
4.1-5 Reactor Mixing Zone and Riser Temperature 4.1-6
4.1-6 Standpipe Temperatures 4.1-6
4.1-7 Cyclone Dipleg Temperatures 4.1-7
4.1-8 Temperature Profiles Downstream of Reactor 4.1-7
4.1-9 Reactor Pressure/Riser Differential Pressure Profiles 4.1-7
4.1-10 Standpipe Differential Pressure Profiles 4.1-8

4.1-11 Dipleg Differential Pressure Profiles 4.1-8
4.1-12 Coal Feed Rate Based on Gas Analysis 4.1-8

4.3-1 TC02 Daily Average Temperatures and Pressures....4.3-9
4.3-2 TC02 Daily Average SO_2 Emissions and Coal Feed Rate....4.3-9
4.3-3 TC02 Coal Sulfur and Ash Weight Percents.... 4.3-10
4.3-4 TC02 Coal Particle-Size and Bulk Density.... 4.3-10
4.3-5 TC02 Coal Particle-Size Distribution May 1, 1998 (20:00).... 4.3-11
4.3-6 TC02 Dolomite Particle-Size and Bulk Density.... 4.3-11
4.3-7 TC02 Dolomite Particle-Size Distribution May 1, 1998 (4:00).... 4.3-12
4.3-8 TC02 Calcium/Sulfur Ratio and SO_2 Emissions.... 4.3-12
4.3-9 TC02 Reactor Solids Particle-Size and Bulk Density 4.3-13
4.3-10 TC02 Reactor Solids Particle-Size Distribution May 8, 1998 (0:00).... 4.3-13
4.3-11 TC02 PCD Solids Particle-Size and Bulk Density 4.3-14
4.3-12 TC02 PCD Solids Particle-Size Distribution May 10, 1998 (0:00) 4.3-14
4.3-13 TC02 PCD Solids $CaCO_3$ and $CaSO_4$ Concentrations 4.3-15
4.3-14 TC02 PCD Solids CaO•MgO & MgO Concentrations.... 4.3-15
4.3-15 TC02 PCD Solids Unburned Carbon and Inerts Concentrations.... 4.3-16
4.3-16 TC02 May 10 to May 12 SO_2 and Ca/S Ratio Data.... 4.3-16
4.3-17 TC02 May 10 to May 11 SO_2 and SO_3 Data.... 4.3-17
4.3-18 SO_2 - SO_3 Equilibrium and TC02 Data for May 11, 1998.... 4.3-17
4.3-19 Equilibrium Line for SO_2 - SO_3 and TC02 Data.... 4.3-18

4.4-1 Transport Reactor Train Loop Schematic....4.4-3
4.4-2 Effect of Staging Air and Excess Air on NO_x Emissions 4.4-4
4.4-3 Effect of Primary Air Distribution on NO_x Emissions 4.4-4
4.4-4 Effect of Temperature on NO_x Emissions....4.4-5
4.4-5 Effect of Coal Feed Rate on NO_x Emissions....4.4-5
4.4-6 Effect of Dolomite Addition on NO_x Emissions....4.4-6

4.5-1 Bulk Density, Gas Velocity, and Void Fraction Varying With the Height of the Transport Reactor on May 7, 1998....4.5-9
4.5-2 Bulk Density, Gas Velocity, and Void Fraction Varying With the Height of the Transport Reactor on April 29, 1998 ....4.5-9
4.5-3 Bulk Density, Gas Velocity, and Void Fraction Varying With the Height of the Transport Reactor on April 22, 1998 .... 4.5-10
4.5-4 Illustration of an Equation of Flooding Line in the Transport Reactor.... 4.5-10
4.5-5 Illustration of an Equation of Flooding Line in the Transport Reactor.... 4.5-11

Section 1.0

Executive Summary

1.0 EXECUTIVE SUMMARY

1.1 OPERATION STATUS

This report discusses test campaign TC02 of the Kellogg Brown & Root (KBR)[1] transport reactor train with a Siemens-Westinghouse particle filter system at the Power Systems Development Facility (PSDF) located in Wilsonville, Alabama. The transport reactor is an advanced circulating fluidized-bed reactor designed to operate as either a combustor or a gasifier using one of two possible hot-gas clean-up filter technologies (particulate control device technology or PCDs). The transport reactor was operated as a pressurized combustor during TC02.

The objectives of the PSDF are to:

1. Develop advanced coal-fired power generation technologies through testing and evaluation of hot-gas clean-up systems and other major components at the pilot scale.

2. Assess and demonstrate the performance of the components in an integrated mode of operation.

The primary focus of the PSDF project is to demonstrate and evaluate high-temperature PCDs, which are the single most important component required for successful development of advanced power generation systems. High-temperature PCDs are a common component of advanced gasification and Advanced Pressurized Fluidized-Bed Combustion (APFBC) technologies, both of which will be evaluated at the facility. The facility is sized to test the components at capacities that are readily scaleable to commercial systems.

Commissioning activities began in September 1995 and proceeded in parallel with construction activities. Construction of the transport reactor and associated equipment was completed in early summer of 1996. By midsummer all separate components and subsystems were fully operational, and commissioning work was focused on integration issues for the entire transport reactor train. The first coal fire was achieved on August 18, 1996. A series of characterization tests was initiated to develop an understanding of reactor system operations.

Test runs CCT1, CCT2, and CCT3 were completed by December 1996. During these test runs solids carryover from the reactor to the PCD was found to be excessive. A number of start-up and design problems associated with various equipment were successfully addressed.

Three additional sets of characterization test runs, CCT4, CCT5, and CCT6, and one major test campaign, TC01, were undertaken during 1997. The major accomplishments in 1997 included the following:

[1] During the preparation of this report, the M. W. Kellogg Company was merged with Brown & Root to become Kellogg Brown & Root.

- Operating the Siemens-Westinghouse PCD for over 1,200 hours on coal in combustion mode without ash bridging at PCD inlet temperatures between 1,350 and 1,400°F.

- Demonstrating stable reactor operations by successfully addressing the excessive solids carryover problem.

- Achieving over 1,980 hours on coal and approximately 2,600 hours of solids circulation in 1997.

- Achieving nearly 100-percent on-line availability during the last 12 days of test run TC01.

Excluding the outages caused by the inherent testing nature of the transport reactor and PCD, the on-line availability (based on coal) for the entire TC01 test run was about 71 percent. The major bottleneck for sustained high on-line availability was the unreliability of the coal feed and fine ash removal systems. Test run modifications were made in the second half of test run TC01 to the fine ash removal system that significantly increased its availability. Also, modifications made to the coal feed system improved its availability to nearly 100 percent in the last 2 weeks of the test run.

With these achievements, TC02 was planned for reactor parametric testing to better quantify the effect of different variables on reactor operation. Test run TC02 was started on April 5, 1998, and was completed on May 11, 1998. The major accomplishments and observations during TC02 include the following:

1. Higher temperatures were achieved with the start-up burner before feeding coal. The start-up burner firing, originally designed for 3.6 MBtu/hr was increased to 7.5 MBtu/hr, which resulted in a PCD inlet starting temperature of 920°F and a reactor starting temperature of 1,200°F.

2. The TC02 test run included the longest continuous trouble-free operations (298 hours) to date. A total of 559 hours on coal feed was accumulated during this run. To date, PSDF has achieved over 2,760 hours of operation on coal feed and about 3,950 hours of solids circulation.

3. Coal feed system modifications were effective and the system operated reliably over a longer period of time.

4. The Siemens-Westinghouse PCD operated without ash bridging with one coal/sorbent at PCD inlet temperatures over 1,350°F.

5. Monitoring and controlling ash level in the PCD continued to be successful.

6. The pulse valves supplied with the PCD were modified and the modifications were proven successful.

7. The 3M Company resolved an issue of dust leaking around the 3M elements, an issue resulting from the filter-vessel-supplied gasketing scheme, by designing a ceramic insert to allow use of the "standard" gasketing scheme.

1.1.1 Transport Reactor

TC02 was planned as a 500-hour test run for reactor parametric testing to better quantify the effect of different variables on reactor operation. The objectives of test run TC02 for the transport reactor were:

- *Perform reactor capacity test.* Determine the maximum coal feed rate, solids circulation rate, and reactor pressure.
- *Evaluate effects of reactor conditions on NO_x emissions.* Vary excess air, primary/secondary air ratio, and operation temperature.
- *Evaluate effects of reactor conditions on SO_x emissions.* Vary Ca/S molar ratio, solids inventory, and operation temperature.
- *Investigate the effect of increasing the mixing zone density.* Decrease various aeration flows and increase solids inventory.

Overall, this test run was quite successful. There were 692 hours of solid circulation and 559 hours of coal feed attained. The process availability for the transport reactor train, excluding an induced outage on the PCD, was much higher (at 95 percent) than previous test runs due to the higher reliability of all dense-phase systems. Another important factor was that the dolomite feed rate could be controlled at desired low-feed rates and excess dolomite feed was not needed to maintain the reactor solids inventory.

Most of the tests planned were successfully completed. However, one staging air test could not be completed because of operating difficulties with the cyclone dipleg and reactor pressure limitations of 200 psig. These reactor pressure limitations were capacity limitations of the main air compressor and the nitrogen system and problems with the recycle gas system. High heat-release rates and solids circulation rates were achieved.

In addition to improved reactor operations there were several other notable findings. Greater than 99-percent sulfur capture was achieved with dolomite at Ca/S molar feed ratios of less than 1:5. Concerning sulfur removal, a higher than expected sulfur oxidization within the reactor was found. Without addition of dolomite, the SO_3 level detected was approximately 2 times the SO_2 level. The NO_X emissions were low at 0.08 lb NO_X/MBtu and varied up to 0.35 lb NO_X/MBtu as process parameters were varied to study their effect. The NO_X emissions increased with increased excess air and with increased air through the lower level of primary combustion air. The NO_X emissions decreased as the amount of staging air was increased. NO_X formation was observed to be significantly higher when dolomite was fed to the reactor.

1.1.2 Siemens-Westinghouse PCD

The Siemens-Westinghouse PCD operated for slightly over 550 hours on coal during TC02. Thermocouples were attached to a Pall 326 and a Coors P100-A-1 element to gain a better understanding of what occurs in the failure of monolithic oxide elements. These thermocouples proved invaluable during a failure event on April 9, 1998, when during transition to coal, large temperature spikes were recorded by the thermocouples. This lead to speculation that burning coal was blown over into the PCD from the transport reactor. Nine elements failed, including six Blasch, two Coors, and one Specific Surface element. The thermocouple data from the April 9, 1998, failure event became a key component of understanding the root cause of the Coors P100-A-1 filter failures (see section 3.8).

Southern Research Institute's (SRI) particulate collection system continued its flawless operation. Additionally, SRI requested a dirty shutdown of the PCD vessel to study the ash cake just prior to back-pulsing. It was discovered during this outage that ash was leaking around the 3M filters due to the Siemens-Westinghouse-supplied gasketing scheme; 3M has since redesigned the flange of their elements so that the "standard" gasketing scheme can be used.

Operation of the PCD and auxiliary systems greatly improved during TC02. No downtime was attributed to the ash removal systems as in previous runs. A design change with the spheri valve seal material was the major reason for the improvements. Problems with the fine ash screw cooler, however, required attention during the run, and leaking shaft rider seals required additional monitoring by plant personnel. Operation staff continued to monitor ash level in the PCD with great success; rising ash levels became an issue of concern several times during the run but at no time did the ash level approach the filter elements. The modifications made to the pulse valves were characterized and confirmed to have been successful (see section 3.6).

1.2 PSDF ACCOMPLISHMENTS DURING TC02

Major accomplishments of test run TC02 are summarized in sections 1.2.1 and 1.2.2. These accomplishments include either improved equipment and process design, higher availability, improved process performance, or better understanding of the transport reactor and PCD operations.

1.2.1 Transport Reactor Train

1. Higher temperatures were achieved with the start-up burner before transitioning to coal. The start-up burner firing was increased to 7.5 MBtu/hr that provided a PCD inlet starting temperature of 920°F and a reactor starting temperature of 1,200°F. Also, the burner was successfully operated up to a reactor pressure of 135 psig. The start-up burner was originally designed for 3.6 MBtu/hr of operation at 60 psig.

2. Test run TC02 included the longest continuous trouble-free operations (298 hours) to date. Totals including 559 hours on coal feed and 692 hours of solids circulation were accumulated during this run. Over 2,760 hours of operation on coal and 3,950 hours of solids circulation were achieved in this test run.

3. Unlike previous test runs, no make-up solids were necessary for reactor solids inventory.

4. Coal feed system modifications were effective and the system operated reliably over a longer period of time.

5. The test was completed within the scheduled time period due to stable reactor operations.

6. Over-aeration of the standpipe could cause cyclone dipleg instability.

7. Over 99-percent sulfur capture was achieved with dolomite at a Ca/S molar feed ratio of less than 1.5.

8. Low-NO_X emissions of 0.08 lb NO_X/MBtu of fuel fired were achieved.

9. Without addition of dolomite, the SO_3 level detected was approximately 2 times the SO_2 level.

10. An increase in dolomite feed increased the NO_X formation significantly.

1.2.2 PCD-Related Systems

1. The Siemens-Westinghouse PCD was operated for over 550 hours on coal in combustion without ash bridging with one coal/sorbent at PCD inlet temperatures over 1,350°F.

2. The process of monitoring and controlling ash level in the PCD continued to be successfully proven.

3. The pulse valves supplied with the PCD were modified, and these modifications were proven to be successful.

4. Concerns were identified with the current filter-element-gasketing arrangement and installation. Dust leakage around the 3M elements was due to the Siemens-Westinghouse-supplied gasketing scheme. The issue was resolved by 3M designing a ceramic insert to allow use of the "standard" gasketing scheme.

5. Isokinetic ash samples on both the PCD inlet and outlet continued to be reliably, safely, and routinely taken. Outlet loadings were relatively high (1 to 12 ppmw) due to the dust leakage around the 3M filters.

6. Ash characteristics were studied further. Samples of both the transient and residual dust cake were taken by shutting down the system without back-pulsing.

7. The acoustic detectors were redesigned and installed prior to TC02. However, electrical cross talk between the inlet and outlet probe prevented the obtaining of meaningful data.

8. There are currently 2,420 hours of coal combustion experienced on a significant number of Pall 442T (21) and Pall 326 (4) filter elements. Six types of filter elements (Coors P100A, Pall 326, Pall 442T, Schumacher TF20, Schumacher T10-20, and 3M type 203) have been tested to date and these elements are at various levels of exposure.

9. PSDF is continuing work with Roger Chen to develop acoustic methods for nondestructive evaluation of monolithic ceramic filter material.

10. New seal materials with lower temperature ratings in the spent fines transporter system allowed for runs with no seal failures. A new seal material was developed and delivered to the site.

11. Changes based on operational experience began to be incorporated in a new design for the spent-fines-transport-system screw cooler.

12. Cut-size tests were performed to help determine the amount of ash removed from the PCD by cyclonic action.

13. New filter elements were introduced into the filter system. These include elements from DuPont, Blasch, McDermott, IF&P, Specific Surface, 3M (oxide), and Fe-Al elements from Pall.

14. The first filter element supplier review meeting was held at the PSDF facility in January 1998. Previous tests were discussed with the suppliers in these meetings as well as all operational problems (filter element failures, etc.), so that suppliers could get a better understanding of what the filter elements are subjected to during operation. Suppliers were allowed to see the filter elements installed in the Siemens-Westinghouse plenum with the residual dust cake essentially intact. Similar periodic meetings are planned for the future.

15. There was a hot-gas clean-up symposium in Birmingham in April 1998 jointly sponsored by the U. S. Department of Energy (DOE) and Electric Power Research Institution (EPRI). Technical papers were presented on PSDF activities and a tour of the PSDF was provided as part of this event.

1.3 FUTURE PLANS

The plans for the remainder of 1998 and 1999 are shown below.

1. The next test run, TC03, was scheduled for the second and third quarters of 1998.

2. The plans are to stay in combustion on the KBR transport reactor throughout 1998. This would allow operational hours for the continued development of both the transport reactor and PCD. Gasification is scheduled for August 1999.

3. The biggest "hurdle" of the year continues to be the start-up of the FW combustion system with its PCD that contains 273 filters. Installation of the plenums and filter elements was scheduled to begin in the second quarter of 1998.

4. A system is planned to be built that will be essentially identical to FL0301 as the PCD for the FW carbonizer. This Request for Proposal (RFP) is out to suppliers.

5. Material testing, both destructive and nondestructive, should continue to gain momentum for the remainder of 1998 as materials gain hours of exposure.

6. New filter elements will be introduced into the filter system for the first time at the PSDF. These include elements from Ensto; 2-meter-long 3M oxide elements; 2-meter-long Pall 326 elements; Pall 181 elements; and a new Pall Fe-Al element.

Section 2.0

Introduction

2.0 INTRODUCTION

This report provides an account of test campaign TC02 with the Kellogg Brown & Root (KBR)[1] transport reactor and the Westinghouse filter vessel at the Power Systems Development Facility (PSDF) located in Wilsonville, Alabama, 40 miles southeast of Birmingham. The PSDF is sponsored by the U. S. Department of Energy (DOE) and is an engineering-scale demonstration of two advanced coal-fired power systems. In addition to DOE, Southern Company Services, Inc., (SCS), Electric Power Research Institute (EPRI), and Peabody Holding Company are cofunders. Other cofunding participants supplying services or equipment include KBR, Foster Wheeler (FW), Westinghouse, and Combustion Power Company. SCS is responsible for constructing, commissioning, and operating the PSDF.

The transport reactor is an advanced circulating fluidized-bed reactor acting as either a combustor or as a gasifier using one of two possible hot gas clean-up filter technologies (particulate control devices or PCDs) at a component size readily scaleable to commercial systems. Design and construction of the transport reactor and required associated equipment were completed in early summer of 1996. All separate components and subsystems were fully operational by midsummer and commissioning work was focused on integration issues for the entire reactor system. At the same time, the first set of ceramic candles was loaded into the Westinghouse PCD. Initial operation of the transport reactor as a combustor was completed in late August, with further combustion commissioning tests completed in the last quarter of 1996. Combustion characterization tests were then performed and the first major test campaign, TC01, was completed by the end of 1997.

Test campaign TC02 was then planned for reactor parametric testing to better quantify the effect of different variables on reactor and candle filter operation. This test run began on April 2, 1998, in the combustion mode of operation after the reactor inspections, preventive maintenance activities, and process modifications were completed. The test run ended on May 11, 1998. The previous test run, TC01, focused on exposing the PCD candles to process gas for 1,000 hours at temperatures from 1,350 to 1,400°F and on achieving more stable reactor operations. The objectives of test run TC02 for the transport reactor were:

- *Perform reactor capacity test.* Determine the maximum coal feed rate, solids circulation rate, and reactor pressure.

- *Evaluate effects of reactor conditions on NO_x emissions.* Vary excess air, primary/secondary air ratio, and operation temperature.

- *Evaluate effects of reactor conditions on SO_x emissions.* Vary Ca/S molar ratio, solids inventory, and operation temperature.

- *Investigate the effect of increasing the mixing zone density.* Decrease various aeration flows and increase solids inventory.

[1] During the preparation of this report, the M. W. Kellogg Company was merged with Brown & Root to become Kellogg Brown & Root.

The supplemental objectives for the PCD included the following:

- Support the primary (see bulleted list above) objective and accumulate exposure time for the filter elements at a PCD operating temperature of approximately 1,350°F (730°C).
- Obtain data from the elements equipped with thermocouples.
- Characterize the newly redesigned pulse valves.
- Measure the plenum pressure rise with each back-pulse.
- Perform cut-size testing for the ash collected from the PCD.

2.1 THE POWER SYSTEMS DEVELOPMENT FACILITY

SCS entered into an agreement with DOE/Federal Energy Technology Center (FETC) for the design, construction, and operation of a hot gas clean-up test facility for gasification and pressurized combustion. The purpose of the PSDF is to provide a flexible test facility suitable for the development of advanced power system components, evaluation of advanced turbine system configurations, and assessment of the integration and control issues of these advanced power systems. The facility would provide a resource for rigorous, long-term testing and performance assessment of hot-stream clean-up devices and other components in an integrated environment.

The PSDF will consist of five modules for systems and component testing. These modules include:

- An advanced pressurized fluidized-bed combustion module (APFBC).
- A transport reactor module.
- A hot-gas clean-up module.
- A compressor/turbine module.
- A fuel cell module.

The APFBC module consists of FW technology for second-generation PFBC. This module relies on partial conversion of coal to fuel gas in a carbonizer, with the remaining char converted in a PFBC. Both the fuel gas and PFBC exhaust gas streams are filtered to remove particulates and are then combined to fire a combustion turbine. The advanced gasifier module includes MWK transport technology for pressurized combustion and gasification to provide either oxidizing or reducing gas for parametric testing of hot-particulate control devices.

The filter systems that will be tested at PSDF include PCDs supplied by Combustion Power Company from Menlo Park, California, and Westinghouse from Pittsburgh, Pennsylvania. A Request for Proposal (RFP) has been issued for the PCD that treats the carbonizer.

2.2 TRANSPORT REACTOR SYSTEM DESCRIPTION

The transport reactor train operating in the combustion mode is shown schematically in figure 2.2-1. A taglist of all major equipment in the process train and associated balance-of-plant is provided in tables 2.2-1 and -2. Two PCDs are shown in this flow diagram; however, during operations only one PCD is tested with the transport reactor at any given time. The intent is to have the capability to install, change out, or provide maintenance on a second PCD while one is tested, which provides increased flexibility for the test facility and reduces downtime. The facility is sized to process nominally 2 tons/hour of coal. This size generates sufficient gas to test the PCDs at a nominal 1,000 ACFM of gas at the PCD inlet. Indirect cooling of the gas from the transport reactor allows testing of the PCDs with inlet temperatures between 600 and 1,400°F and at pressures ranging from 150 to 305 psia. The PCD in this train receives particulate-laden gas from the transport reactor, which can operate in either gasification or combustion mode. In the gasification mode, the gas exiting the PCDs is oxidized, cooled, and filtered in a baghouse before being discharged from a stack. The ash and char produced in the gasification mode are oxidized in a sulfator prior to disposal.

Coal is ground to a nominal average particle diameter of 100 and 200 microns, respectively, when the transport reactor is operated in gasification mode and combustion mode. Sorbent is ground to a nomimal average particle diameter of 100 microns. Both coal and sorbent are pneumatically fed continuously into the transport gasifier/combustor by feeders at a controlled rate.

Air is compressed to about 350 psia in the main air compressor and fed directly to the transport reactor. For start-up purposes, a burner (BR0201) is provided at the reactor mixing zone. Liquefied propane gas (LPG) is used as start-up fuel. Fuel, sorbent, and gas feeds enter the reactor in a mixing zone at the bottom where they mix with recycled solids from the disengager cyclone. Coal conversion begins in this zone and the reaction mixture flows upward at high velocity into the more narrow riser section and then flows to the disengager.

The reactor typically operates at temperatures of 1,600 to 1,625°F in combustion mode. Provision is made to inject air at several different points along the riser to control the formation of NO_X. Limestone/dolomitic sorbents fed with the coal are used for sulfur capture, which eliminates the need for downstream facilities otherwise needed to reduce plant sulfur emissions.

Solids and gases leaving the reactor flow to the disengager for bulk separation of the two phases. Most of the solids collected in the disengager are recycled to the reactor. Coal ash and spent sorbent are discharged from the transport reactor to maintain the solids inventory in the system. In the combustion mode, heat removal from the reactor system is necessary to control the reactor temperature. This is accomplished by removing solids from the disengager, cooling the solids in the combustor heat exchanger (HX0203), and returning the solids to the reactor system.

The gas leaving the disengager still contains a high loading of particulates. This gas is then sent to a cyclone system for additional solids recovery prior to being fed to the PCDs. The cyclone is provided with spoiling gas to vary the solids loading into the effluent gas. The conditioned gas enters the PCD where essentially all of the remaining particulates in the gas are removed. The cleaned gas leaving the PCD is sent to a secondary gas cooler (HX0402) and ultimately cooled to

about 600°F. All gas stream cooling is accomplished by generating steam. A portion of the cooled gas is further cooled in the compressor feed cooler (HX0405) and sent to the recycle gas booster compressor (CO0401), which increases the pressure to about 400 psia. This gas is for aeration-fluidization gas in the combustor heat exchanger.

The main gas stream from the secondary gas cooler is cooled further by dilution air and cleaned in a baghouse of any remaining particulates before being discharged to the atmosphere through a stack.

Table 2.2-1

Major Equipment in the Transport Reactor Train

TAG NAME	DESCRIPTION
BR0201	Reactor Start-Up Burner
BR0401	Thermal Oxidizer
BR0602	Sulfator Start-Up/PCD Preheat Burner
CO0201	Main Air Compressor
CO0401	Recycle Gas Booster Compressor
CO0601	Sulfator Air Compressor
CY0201	Primary Cyclone in the Reactor Loop
CY0207	Disengager in the Reactor Loop
CY0601	Sulfator Cyclone
DR0402	Steam Drum
DY0201	Feeder System Air Dryer
FD0206	Spent Solids Screw Cooler
FD0210	Coal Feeder System
FD0220	Sorbent Feeder System
FD0502	Fines Screw Cooler
FD0510	Spent Solids Transporter System
FD0520	Fines Transporter System
FD0530	Spent Solids Feeder System
FD0602	Sulfator Solids Screw Cooler
FD0610	Sulfator Sorbent Feeder System
FL0301	PCD — Westinghouse
FL0302	PCD — Combustion Power
FL0401	Compressor Intake Filter
HX0202	Primary Gas Cooler
HX0203	Combustor Heat Exchanger
HX0204	Transport Air Cooler
HX0402	Secondary Gas Cooler
HX0405	Compressor Feed Cooler
HX0601	Sulfator Heat Recovery Exchanger
ME0540	Heat Transfer Fluid System
RX0201	Transport Reactor
SI0602	Spent Solids Silo
SU0601	Sulfator

Table 2.2-2 (Page 1 of 3)

Major Equipment in the Balance-of-Plant

TAG NAME	DESCRIPTION
BO2920	Auxiliary Boiler
BO2921	Auxiliary Boiler - Superheater
CL2100	Cooling Tower
CO2201A-D	Service Air Compressor A-D
CO2202	Air-Cooled Service Air Compressor
CO2203	High-Pressure Air Compressor
CO2601A-C	Reciprocating N_2 Compressor A-C
CR0104	Coal and Sorbent Crusher
CV0100	Crushed Feed Conveyor
CV0101	Crushed Material Conveyor
DP2301	Baghouse Bypass Damper
DP2303	Inlet Damper on Dilution Air Blower
DP2304	Outlet Damper on Dilution Air Blower
DY-2201A-D	Service Air Dryer A-D
DY2202	Air-Cooled Service Air Compressor Air Dryer
DY2203	High-Pressure Air Compressor Air Dryer
FD0104	MWK Coal Transport System
FD0111	MWK Coal Mill Feeder
FD0113	Sorbent Mill Feeder
FD0140	Coke Breeze and Bed Material Transport System
FD0154	MWK Limestone Transport System
FD0810	Ash Unloading System
FD0820	Baghouse Ash Transport System
FL0700	Baghouse
FN0700	Dilution Air Blower
HO0100	Reclaim Hopper
HO0105	Crushed Material Surge Hopper
HO0252	Coal Surge Hopper
HO0253	Sorbent Surge Hopper
HT2101	MWK Equipment Cooling Water Head Tank
HT2103	SCS Equipment Cooling Water Head Tank
HT0399	60-Ton Bridge Crane
HX2002	MWK Steam Condenser
HX2003	MWK Feed Water Heater

Table 2.2-2 (Page 2 of 3)

Major Equipment in the Balance-of-Plant

TAG NAME	DESCRIPTION
HX2004	MWK Subcooler
HX2103A	SCS Cooling Water Heat Exchanger
HX2103C	MWK Cooling Water Heat Exchanger
LF0300	Propane Vaporizer
MC3001-3017	MCCs for Various Equipment
ME0700	MWK Stack
ME0701	Flare
ME0814	Dry Ash Unloader for MWK Train
ML0111	Coal Mill for MWK Train
ML0113	Sorbent Mill for Both Trains
PG2600	Nitrogen Plant
PU2000A-B	MWK Feed Water Pump A-B
PU2100A-B	Raw Water Pump A-B
PU2101A-B	Service Water Pump A-B
PU2102A-B	Cooling Tower Make-Up Pump A-B
PU2103A-D	Circulating Water Pump A-D
PU2107	SCS Cooling Water Make-Up Pump
PU2109A-B	SCS Cooling Water Pump A-B
PU2111A-B	MWK Cooling Water Pump A-B
PU2300	Propane Pump
PU2301	Diesel Rolling Stock Pump
PU2302	Diesel Generator Transfer Pump
PU2303	Diesel Tank Sump Pump
PU2400	Fire Protection Jockey Pump
PU2401	Diesel Fire Water Pump #1
PU2402	Diesel Fire Water Pump #2
PU2504A-B	Waste Water Sump Pump A-B
PU2507	Coal and Limestone Storage Sump Pump
PU2700A-B	Demineralizer Forwarding Pump A-B
PU2701	SCS Closed-Loop System Make-Up Pump
PU2711	Corrosion Inhibitor Pump
PU2713	Waste Water Alum Pump
PU2714	Waste Water Caustic Pump
PU2720	Acid Pump
PU2721	Waste Water Acid Pump

Table 2.2-2 (Page 3 of 3)

Major Equipment in the Balance-of-Plant

TAG NAME	DESCRIPTION
PU2730	MWK Steam System Phosphate Pump
PU2740	Cooling Tower Sodium Bisulfate Pump
PU2741	Cooling Tower Sodium Bisulfate Pump
PU2750	MWK Steam System O_2 Scavenger and pH Pump
PU2900A-C	Chemical Injection Pump A-C
PU2920A-B	Auxiliary Boiler Feed Water Pump A-B
SB3001	125V DC Station Battery
SB3002	UPS
SC0700	Baghouse Screw Conveyor
SG3000-3005	4160V, 480V Switchgear Buses
SI0101	MWK Crushed Coal Storage Silo
SI0103	Crushed Sorbent Storage Silo
SI0111	MWK Pulverized Coal Storage Silo
SI0113	MWK Limestone Silo
SI0114	FW Limestone Silo
SI0810	Ash Silo
ST2601	N_2 Storage Tube Bank
TK2000	MWK Condensate Storage Tank
TK2001	FW Condensate Tank
TK2100	Raw Water Storage Tank
TK2300A-D	Propane Storage Tank A-D
TK2301	Diesel Storage Tank
TK2401	Fire Water Tank
XF3000A	230/4.16 kV Main Power Transformer
XF3001B-5B	4160/480V SS Transformer No. 1-5
XF3001G	480/120V Miscellaneous Transformer
XF3010G	120/208 Distribution Transformer
XF3012G	UPS Isolation Transformer
VS2203	High-Pressure Air Receiver

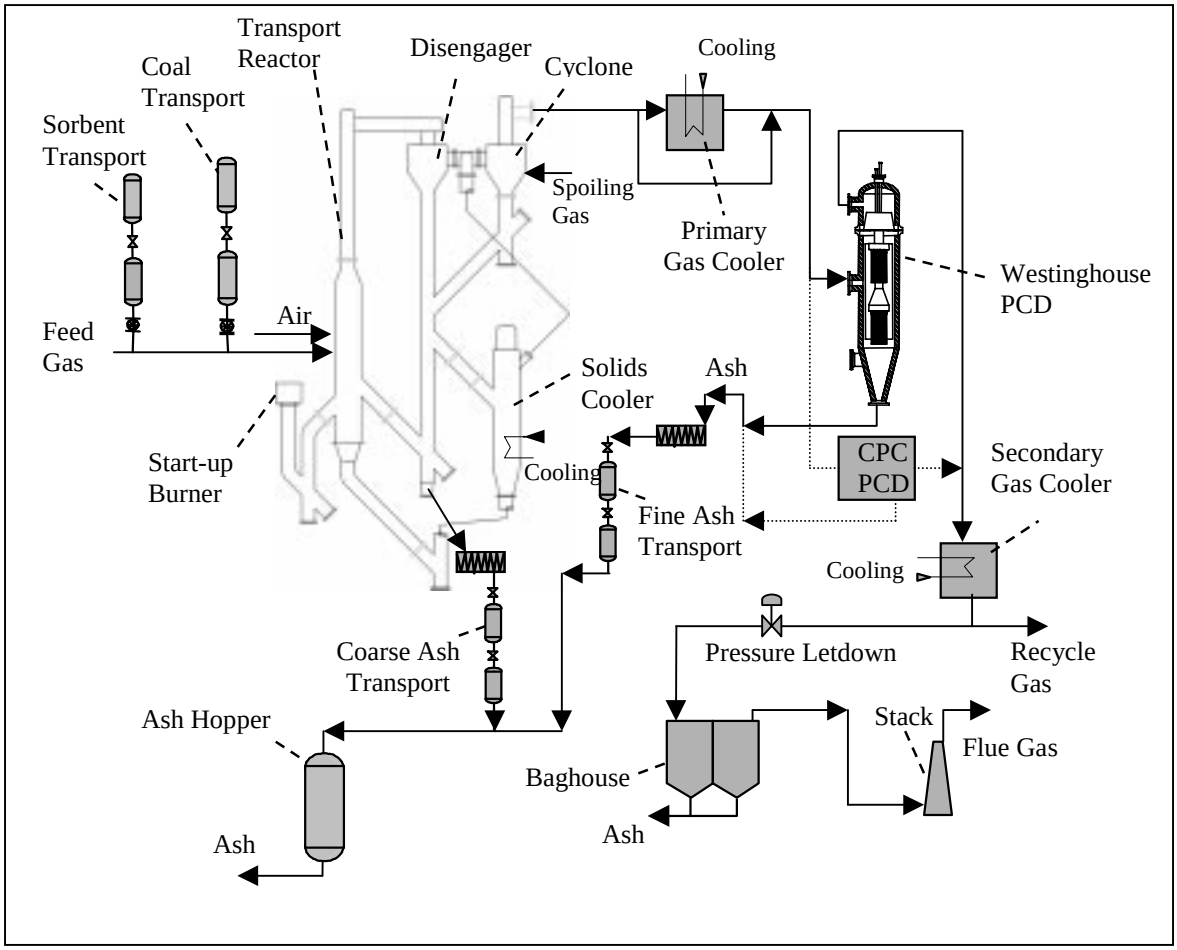

Figure 2.2-1 Flow Diagram of the Transport Reactor Train in Combustion Mode of Operation

2.3 WESTINGHOUSE PARTICULATE CONTROL DEVICE

Plans for the PSDF call for a variety of PCDs to be evaluated on the transport reactor train. The first PCD, commissioned in 1996 and used in the all 1997 and 1998 testing, was the filter system designed by Westinghouse. Dirty gas enters the PCD below the tubesheet and flows through the filter elements; the ash collects on the outside of the filter. The clean gas passes from the plenum/filter element assembly through the plenum pipe to the outlet pipe. As ash collects on the outside surface of the filter elements the pressure drop across the filter system gradually increases. The filter cake resulting from ash collection is periodically dislodged by injecting a high-pressure gas pulse to the clean side of the candles. The cake then falls to the discharge hopper.

The transport reactor had been operated only in the combustion mode at the time this report is being written. Initially, high-pressure air was used as the pulse gas for the PCD. However, the pulse gas was changed to nitrogen early in 1997. The pulse gas was routed individually to the two-plenum/filter element assemblies via injection tubes mounted on the top head of the PCD vessel. The pulse duration was typically 0.1 to 0.5 seconds.

A sketch of the Westinghouse PCD is shown in figure 2.3-1.

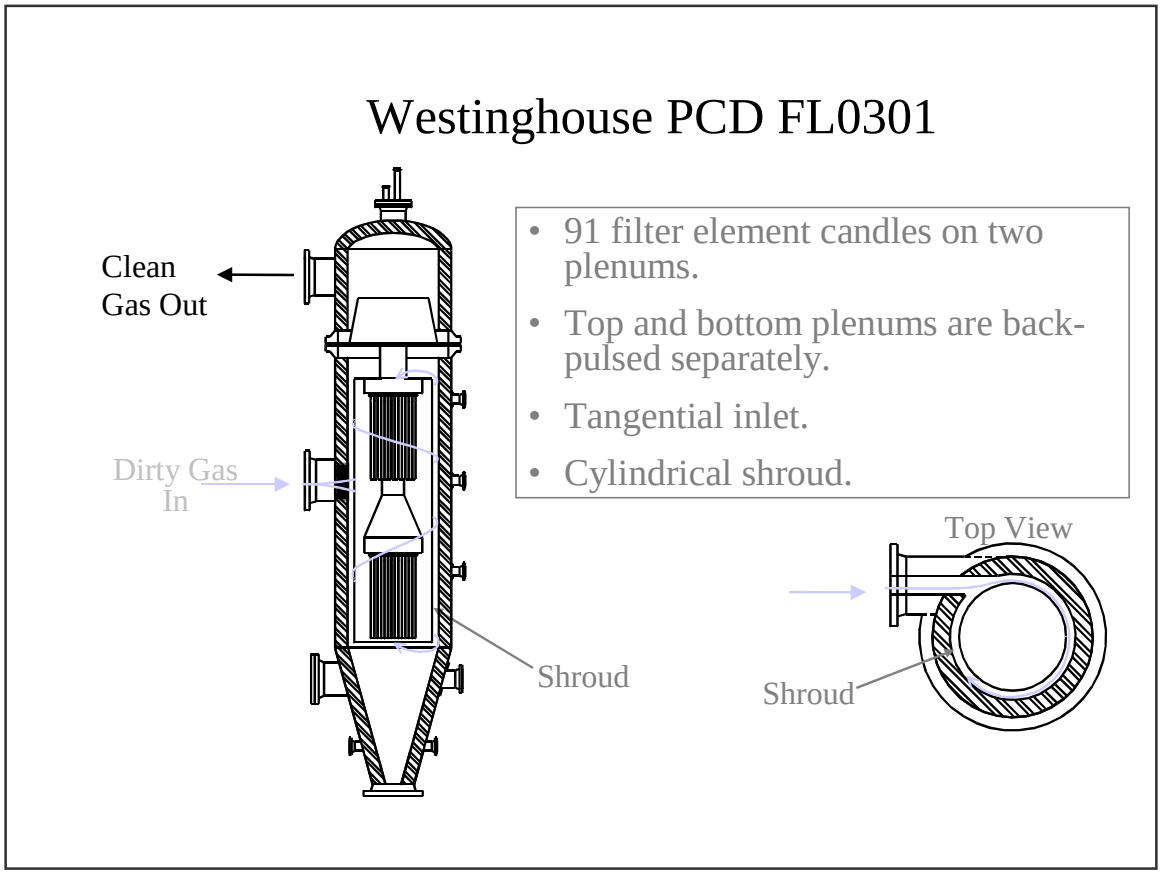

Figure 2.3-1 Sketch of the Westinghouse PCD

Section 3.0

Particle Filter System

3.0 PARTICLE FILTER SYSTEM

3.1 TC02 PCD OVERVIEW

3.1.1 Run Summary

The Westinghouse PCD operated for slightly over 550 hours on coal in TC02. Thermocouples were attached to a Pall 326 and a Coors P100-A-1 element to obtain a better understanding of the mechanism for the failure of the monolithic oxide elements. These thermocouples proved invaluable during a failure event on April 9, 1998. During transition to coal, large temperature spikes were recorded by the thermocouples, leading to the speculation that burning coal was blown over into the PCD from the transport reactor. Nine elements failed including six Blasch, two Coors, and one Specific Surface element. The thermocouple data from the April 9, 1998, failure event became a key component to understanding the root cause of the Coors P100-A-1 filter failures (see section 3.8).

The Southern Research Institute (SRI) particulate collection system continued its flawless operation. Additionally, SRI requested a dirty shutdown of the PCD vessel to study the ash cake just prior to back-pulsing. It was discovered during the outage that ash was leaking around the 3M filters due to the Westinghouse-supplied-gasketing scheme. The flange of 3M elements has since been redesigned so that the "standard" gasketing scheme can be used.

Operation of the PCD and auxiliary systems greatly improved during TC02. No downtime was attributed to the ash removal systems as in previous runs. A design change with the spheri valve seal material was the major reason for the improvements. Problems with the fine ash screw cooler, however, required attention during the run. Leaking shaft-rider seals required additional monitoring by plant personnel. Operation staff continued monitoring ash level in the PCD with great success. Rising ash levels became an issue for concern several times during the run, but at no time did the ash level approach the filter elements. The modifications made to the pulse valves were characterized and confirmed to have been successful and are discussed in section 3.6.

3.1.2 TC02 Accomplishments

The accomplishments for TC02 include:

- The Westinghouse PCD was operated for over 550 hours on coal in combustion without ash bridging and with only one coal/sorbent at PCD inlet temperatures over 1,350°F.

- A process of monitoring and controlling ash level in the PCD continued to be successfully proven.

- The pulse valves supplied with the PCD were modified and the modifications were proven to be successful.

- Concerns were identified with the current filter element gasketing arrangement and installation. Dust leakage around the 3M elements was due to the Westinghouse-supplied-gasketing scheme; 3M resolved the issue by designing a ceramic insert which allowed use of the "standard" gasketing scheme.

- Isokinetic ash samples, on both the PCD inlet and outlet, continued to be reliably, safely, and routinely taken. Outlet loadings were relatively high (1 to 12 ppmw) due to the leaking around the 3M filters.

- Ash characteristics were studied further. Samples of both the transient and residual dust cakes were taken by shutting down the system without back-pulsing.

- The acoustic detectors were redesigned and installed prior to TC02. However, electrical cross talk between the inlet and outlet probe prevented the obtaining of meaningful data.

- At the time of this report, there are 2,420 hours of coal combustion experienced on a significant number of Pall 442T filter elements (21) and on Pall 326 (4). Six types of filter elements have been tested to date and are at various levels of exposure (Coors P100A, Pall 326, Pall 442T, Schumacher TF20, Schumacher T10-20, and 3M Type 203).

- The PSDF is continuing work with Roger Chen to develop acoustic methods for nondestructive evaluation of monolithic ceramic filter material.

- New seal materials with lower temperature ratings in the spent fines transporter system allowed for runs without seal failures. A new seal material was developed and delivered to the site.

- Based on operational experience, changes began to be incorporated in a new design for the spent fines transport system screw cooler.

- Cut-size tests were performed to help determine the amount of ash removed from the PCD by cyclonic action.

- New filter elements were introduced into the filter system. These include elements from DuPont, Blasch, McDermott, IF&P, Specific Surface, 3M (oxide), and Fe-Al elements from Pall.

3.1.3 Developmental Areas

The system was performing well by the end of TC02. The previous problems with the spent fines removal system were less apparent during this run than ever before. However, there are still areas of concern that require further evaluation in the future. These include the following:

- Performance of fail-safes and filter gaskets continue to need attention. Different gasketing materials for the fail-safe were experimented with during the run. Work continues with Westinghouse to improve both the design and the installation of the filter gaskets.

- The failure of the Coors P100A filter elements is still under investigation. The data from the thermocouples are being evaluated. Hopefully, this information will shed additional light on why these filter elements failed.

- Modifications to the screw cooler are being manufactured for delivery to the plant by the end of the year.

3.1.4 Future Plans

The plans for the remainder of 1998 and 1999 are shown below.

- The next test run, TC03, was scheduled for the second and third quarters of 1998.

- The biggest "hurdle" of the year continues to be the start-up of the Foster Wheeler combustion system with its PCD that contains 273 filters. Installation of the plenums and filter elements is scheduled to begin in the second quarter of 1998.

- The plans are to stay in combustion on the KBR transport reactor throughout 1998. This would allow operational hours to continue development on the issues raised in section 3.1.3. Gasification is scheduled for August 1999.

- A system essentially identical to FL0301 is planned to be built as the PCD for the Foster Wheeler Carbonizer. This request for proposal (RFP) is out to suppliers.

- Material testing, both destructive and nondestructive, should continue to gain momentum for the remainder of 1998 as materials gain hours of exposure.

- New filter elements will be introduced into the filter system for the first time at the PSDF. These include elements from Ensto, 2-meter-long 3M oxide elements, 2-meter-long Pall 326 elements, Pall 181 elements, and a new Pall Fe-Al element.

3.2 PCD OPERATION DURING TEST RUN TC02

3.2.1 Run Summary

Test campaign TC02 began early in the morning of April 5, 1998, for the purpose of evaluating the transport reactor performance. Based on the multiple failures of monolithic oxide filters in 1997, thermocouples were attached to two filter elements in an attempt to measure thermal gradients that might be causing the failures. Neoprene seals were reinstalled in the spent fines transport system (FD0520) for this run because of their success in test run TC01.

Due to the length of the previous outage the refractory had to be recured. This provided time for characterization of the newly modified back-pulse valves. A detailed report is included in section 3.6. The thermocouple temperatures were monitored with a fast data acquisition device during the transition to coal which, upon evaluation, revealed the possibility of carryover of burning coal from the transport reactor to the particulate control device (PCD). A detailed report of this carryover event is included in section 3.8. The PCD attained 1,350°F (730°C) temperature early in the afternoon of April 9, 1998. Complications with the ash removal system began early in the morning of April 10, 1998, when continued slow depressurization of the lock vessel tripped the unit. Small pieces of candles were removed that afternoon. Early in the morning of April 11, 1998, additional pieces were removed from the FD0520 system. Coincidentally, at approximately 3 a.m. that same day, the top plenum back-pulse valve stopped operating. It was repaired and returned on-line at 7 a.m. By 2 p.m. on April 11, 1998, the FD0520 system was plugged with a large volume of filter element pieces. A large volume of ash backed up in the PCD cone while these pieces were being removed. The coal feeder tripped, and the subsequent upset of the transport reactor dipleg forced the unit to come off-line due to concern about additional ash buildup in the PCD cone. Coal feed was resumed early in the morning of Monday, April 13, 1998, but quickly stopped just after noon when outlet ash concentrations were measured at 700 ppm. Speculation was that one of the instrumented elements had broken with the resulting flow through the modified fail-safe above the element contributing to the high-outlet loading. The run was resumed in the early afternoon of April 18, 1998, following a brief outage to repair the broken candles. The operation of the PCD was uneventful from this date until May 13, 1998. The run ended when the upper neoprene spheri valve seal on FD0520 failed on May 13, 1998.

3.2.2 Test Objectives

The primary objective of TC02 was to characterize reactor performance. Supplemental objectives for the PCD included:

1. Accumulating exposure time for the filter elements at a PCD operating temperature of approximately 1,350°F (730°C).
2. Obtaining data from the elements equipped with thermocouples.
3. Characterizing the newly redesigned pulse valves.
4. Measuring the plenum pressure rise with each back-pulse.
5. Performing cut-size testing for the ash collected from the PCD.

3.2.3 Observations/Events

Letter designations beside the information listed below are shown on the figures at the end of this section as events occurring during run TC02. Refer to the Terms section at the end of this report for explanation and/or definition of abbreviations found in this information. Descriptions of equipment tag names (e.g., description for FD0520) are found in tables 2.2-1 and -2.

A. Test Started–April 5 at 08:30. The main air compressor (MAC) was started April 5, 1998, to begin TC02A.

B. Start-Up Burner Lit–April 6 at 11:10.

C. Back-Pulse Valve Testing Began–April 7 at 11:55. The new back-pulse valves were tested at various differential pressures, open times, and pilot pressures in order to determine the flow characteristics.

D. Sand Addition Began–April 7 at 14:37.

E. Back-Pulse Valve Testing Ended–April 7 at 18:30.

F. Back-Pulse Timer Set to 40 Minutes–April 8 at 08:05.

G. Plant Power Failure–April 8 at 23:00. Severe thunderstorms caused a plantwide power failure.

H. Candle Data Acquisition Began–April 9 at 13:10. The fast data acquisition system began recording data from the elements and fail-safes outfitted with thermocouples.

I. Coal Feed Began–April 9 at 13:43.

J. Began Propane to Coal Transition–April 9 at 17:15.

K. Stopped Propane Feed–April 9 at 20:05.

L. Dipleg Upset; Solids Sent to PCD–April 9 at 20:35.

M. FD0520 Problems–April 10 at 05:25. Slow depressurization of the FD0520 system caused multiple trips of the unit during the early morning hours.

N. Dipleg Upset; Solids Sent to PCD–April 10 at 07:02. The back-pulse upset the dipleg.

O. FD0520 Set on Timer–April 10 at 16:06. The level probe repeatedly failed to operate correctly. The lockhopper logic was changed so that it would cycle on a timer instead of the level probe.

P. FD0520 Problems–April 10 at 18:30. Slow depressurization of the FD0520 system caused multiple trips of the unit. The drilled gate valve was opened one round but the problem still persisted.

Q. Back-Pulse Valve Failure–April 11 at 03:00. The back-pulse valve on the top plenum stopped operating. It was repaired after 4 hours. It was not discovered as a problem until 05:30.

R. FD0520 Problems–April 11 at 06:00. Small candle pieces were removed from FD0520.

S. FD0520 Plugged; Operation Stopped–April 11 at 02:00. A large volume of candle pieces was removed from FD0520. The system was down for 6 hours for removal of the broken elements.

T. Coal Feeder Tripped–April 11 at 16:10. The coal feed rates were dropped to minimal levels while waiting for repair of FD0520. The coal feeder system tripped during this time and upset the dipleg. The system was taken off coal feed due to the preexisting problems with the FD0520 system.

U. Started Start-Up Burner–April 11 at 19:15. The decision was made to not resume coal feed that evening. The burner was started to maintain reactor temperature.

V. FD0520 Resumed Operation–April 11 at 20:00. The candle pieces had been removed from FD0520; the system was put back in service to begin emptying accumulated ash from the cone for FL0301.

W. Resumed Coal Feed–April 13 at 03:52. Coal feed was restarted early in the morning so a steady state outlet particulate concentration could be obtained.

X. Dipleg Upset; Solids Sent to PCD–April 13 at 09:02.

Y. High-Outlet Loading From PCD Detected–April 13 at 11:00. The decision was made to shut down and repair broken elements when 700 ppm outlet concentration from the PCD was detected.

Z. Run Resumed–April 18 at 13:46.

AA. Main Compressor Off–April 19 at 20:00. A leak in the start-up burner igniter cooling purge line forced a shutdown.

BB. Main Compressor Started–April 20 at 09:00.

CC. Burner Firing Increased to Maximum–April 21 at 10:00.

DD. Coal Feed Started–April 21 at 10:35.

EE. Dipleg Upset–April 22 at 05:04.

FF. Dipleg Upset–April 22 at 13:25.

GG. Dipleg Upset–April 24 at 12:30.

HH. Recycle Gas Compressor Run Stopped–April 26 at 9:00. A leaking intake filter was found while testing the recycle gas compressor.

II. Coal Feeder Tripped–April 29 at 12:12.

JJ. Coal Feed Increased–May 2 at 05:00. Slumping temperatures forced an increase in coal feed.

KK. Coal Feeder Tripped–May 3 at 06:15.

LL. Coal Feed Problems–May 3 at 09:40. Continued problems with the coal feeder level probe caused intermittent coal feed for approximately 5 hours.

MM. Coal Feeder Stopped–May 3 at 21:30. The feeder was stopped to fix the continued problems.

NN. Coal Feed Started–May 4 at 15:40.

OO. Dipleg Upset–May 4 at 19:20.

PP. Dipleg Upset–May 7 at 05:45.

QQ. Dipleg Upset–May 7 at 11:06.

RR. Dipleg Upset–May 7 at 15:08.

SS. Coal Feed Stopped–May 9 at 13:58.

TT. Propane Burner Started–May 9 at 15:38.

UU. Coal Feed Started–May 9 at 23:50.

VV. Foxboro System Down–May 10 at 00:05. The Foxboro system was impaired for approximately 5 hours.

WW. Solids Sent to PCD–May 10 at 06:20.

XX. Dipleg Upset–May 12 at 05:20.

YY. Coal Feed Stopped (Leak on FD0520 Top Seal)–May 13 at 12:16.

ZZ. Run Ended–May 13 at 13:13.

3.2.4 Run Outcome

Thermocouples on Elements

A Pall 326 element and a Coors P-100A element were outfitted with thermocouples during the first half of the run to attempt measurement of any thermal gradients that could be causing monolithic oxide filters to fail. Additionally, an instrumented fail-safe was placed above a Pall 326 and Coors P-100A element. These elements, or their remnants, were removed on April 16, 1998. Measurements taken are reported in section 3.8 that describe the operation experience for Coors elements.

FL0301

The plenum assembly was pulled on April 16, 1998, after the first failure event. Nine filter elements had failed during the run: six Blasch; two Coors P-100A; and one Specific Surface. Two of these Blasch elements were previously exposed elements from Karhula. Additionally, during inspection of the plenum, a Dupont PRD66 was accidentally broken. For evaluation purposes, a 3M Oxide element, the remaining Specific Surface element, the two remaining intact Blasch elements, and a Schumacher TF20 belonging to Roger Chen were removed and replaced. A detailed report of this failure event is in section 3.8 and an inspection report is included in section 3.3.

The plenum was pulled and inspected once again at the conclusion of TC02. The run was terminated just prior to a normally scheduled back-pulse in order for Southern Research Institute (SRI) to inspect the dust cake prior to back-pulsing. A gradually increasing leak was detected near the end of TC02, which lead to speculation that the gaskets for the 3M elements may be providing a leak path. A detailed report of this inspection is in section 3.4.

FD0502/FD0520

Leaking around the shaft-rider seal packing glands on FD0502 during the run required constant attention. The follower for the packing glands was tightened as a means to remedy the leaking. Consequently, all four bolts on the follower broke. The follower was braced with angle iron and the leakage was remedied for the remainder of the run. No significant seal problems were noticed in spite of the broken follower. The neoprene seals experienced 5,966 cycles for the upper seal and 6,301 cycles for the lower seal during test run TC02. A failure of the upper seal forced an end to the run.

Table 3.2-1

TCO2 Run Statistics

Start Time:	4/5/98 08:30
End Time:	5/13/98 13:13
Coal Type:	Calumet Alabama Bituminous
Hours on Coal:	559:00
Sorbent Type:	Plum Run Dolomite
Number of Filter Elements:	88 (First Half)
Filter Element Layout No.:	7 and 8 (figure 3.2-4)
Filtration Area:	240.7 ft^2 (22.4 m^2)
Pulse Valve Open Time:	0.2 sec.
Pulse Time Trigger:	20 to 40 min.
Pulse Pressure:	400 to 470 psig (26 to 33 bar,g)
Pulse DP Trigger:	140 inWG (348 mbar,g)

Table 3.2-2 (Page 1 of 2)

TC02 Major Events

Event	Description	Date at Time
A	Test Started	April 5 at 08:30
B	Start-Up Burner Lit	April 6 at 11:10
C	Back-Pulse Valve Testing Began	April 7 at 11:55
D	Sand Addition Began	April 7 at 14:37
E	Back-Pulse Valve Testing Ended	April 7 at 18:30
F	Back-Pulse Timer set to 40 Minutes	April 8 at 08:05
G	Plant Power Failure	April 8 at 23:00
H	Candle Data Acquisition Began	April 9 at 13:10
I	Coal Feed Began	April 9 at 13:43
J	Began Propane to Coal Transition	April 9 at 17:15
K	Stopped Propane Feed	April 9 at 20:05
L	Dipleg Upset; Solids Sent to PCD	April 9 at 20:35
M	FD0520 Problems	April 10 at 05:25
N	Dipleg Upset: Solids Sent to PCD	April 10 at 07:02
O	FD0520 Set on Timer	April 10 at 16:06
P	FD0520 Problems	April 10 at 18:30
Q	Back-Pulse Valve Failure	April 11 at 03:00
R	FD0520 Problems	April 11 at 06:00
S	FD0520 Plugged; Operation Stopped	April 11 at 14:00
T	Coal Feeder Tripped	April 11 at 16:10
U	Started Start-Up Burner	April 11 at 19:15
V	FD0520 Resumed Operation	April 11 at 20:00
W	Resumed Coal Feed	April 13 at 03:52
X	Dipleg Upset; Solids Sent to PCD	April 13 at 09:02
Y	High-PCD-Outlet Loading Detected/Operation Stopped	April 13 at 11:00
Z	Run Resumed	April 18 at 13:46
AA	Main Compressor Off	April 19 at 20:00
BB	Main Compressor Started	April 20 at 09:00

Table 3.2-2 (Page 2 of 2)

TCO2 Major Events

Event	Description	Date at Time
CC	Burner Firing Increased to Maximum	April 21 at 10:00
DD	Coal Feed Started	April 21 at 10:35
EE	Dipleg Upset	April 22 at 05:04
FF	Dipleg Upset	April 22 at 13:25
GG	Dipleg Upset	April 24 at 12:30
HH	Recycle Gas Compressor Run Stopped	April 26 at 09:00
II	Coal Feeder Tripped	April 29 at 12:12
JJ	Coal Feed Increased	May 2 at 05:00
KK	Coal Feeder Tripped	May 3 at 06:15
LL	Coal Feed Problems	May 3 at 09:40
MM	Coal Feeder Stopped	May 3 at 21:30
NN	Coal Feed Started	May 4 at 15:40
OO	Dipleg Upset	May 4 at 19:20
PP	Dipleg Upset	May 7 at 05:45
QQ	Dipleg Upset	May 7 at 11:06
RR	Dipleg Upset	May 7 at 15:08
SS	Coal Feed Stopped	May 9 at 13:58
TT	Propane Burner Started	May 9 at 15:38
UU	Coal Feed Started	May 9 at 23:50
VV	Foxboro System Down	May 10 at 00:05
WW	Solids Sent to PCD	May 10 at 06:20
XX	Dipleg Upset	May 12 at 05:20
YY	Coal Feed Stopped, Leak on FD0520 Top Seal	May 13 at 12:16
ZZ	Run Ended	May 13 at 13:13

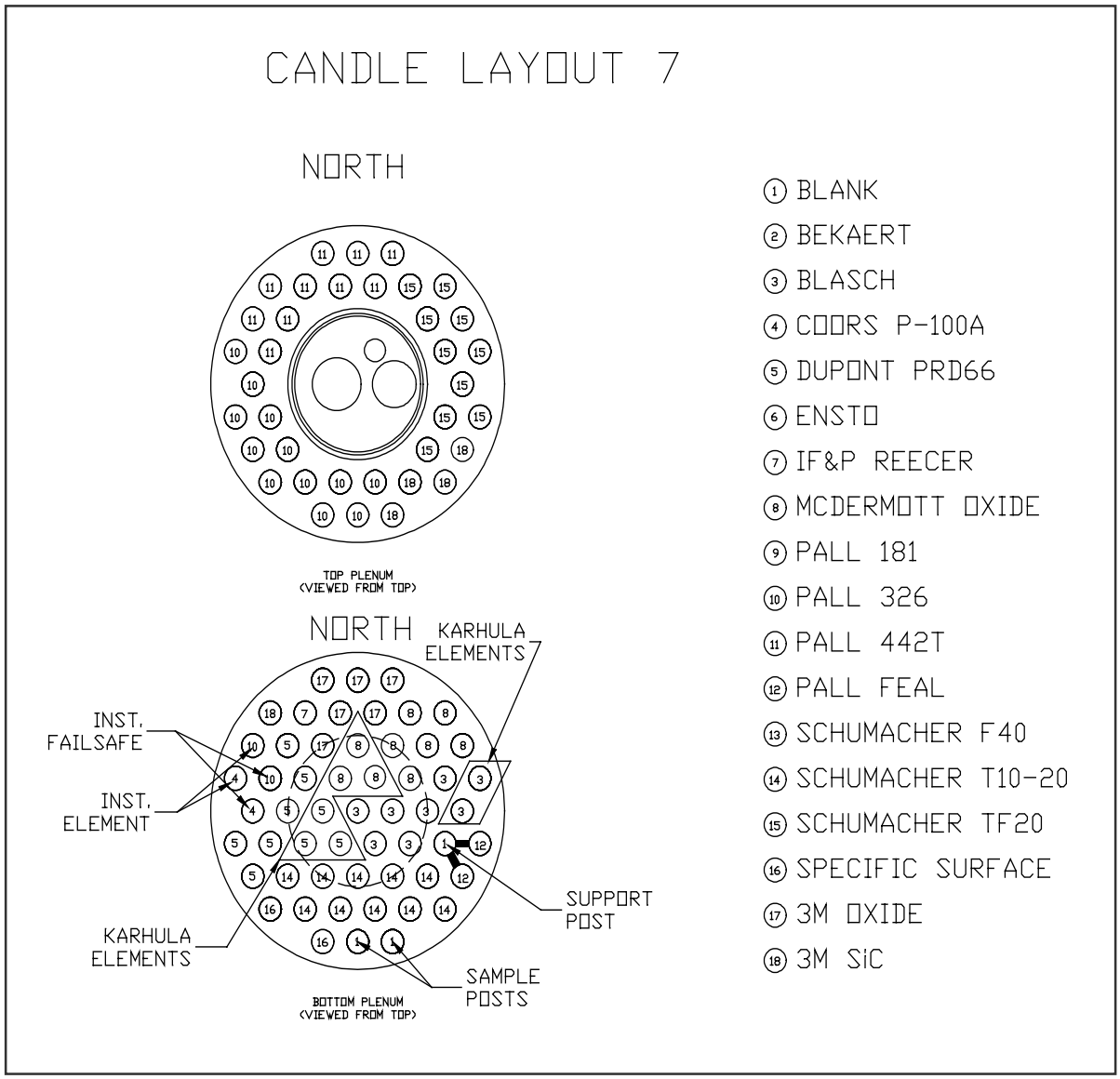

Figure 3.2-1 First Filter Element Layout for TCO2 April 5 to April 13 (Layout No. 7)

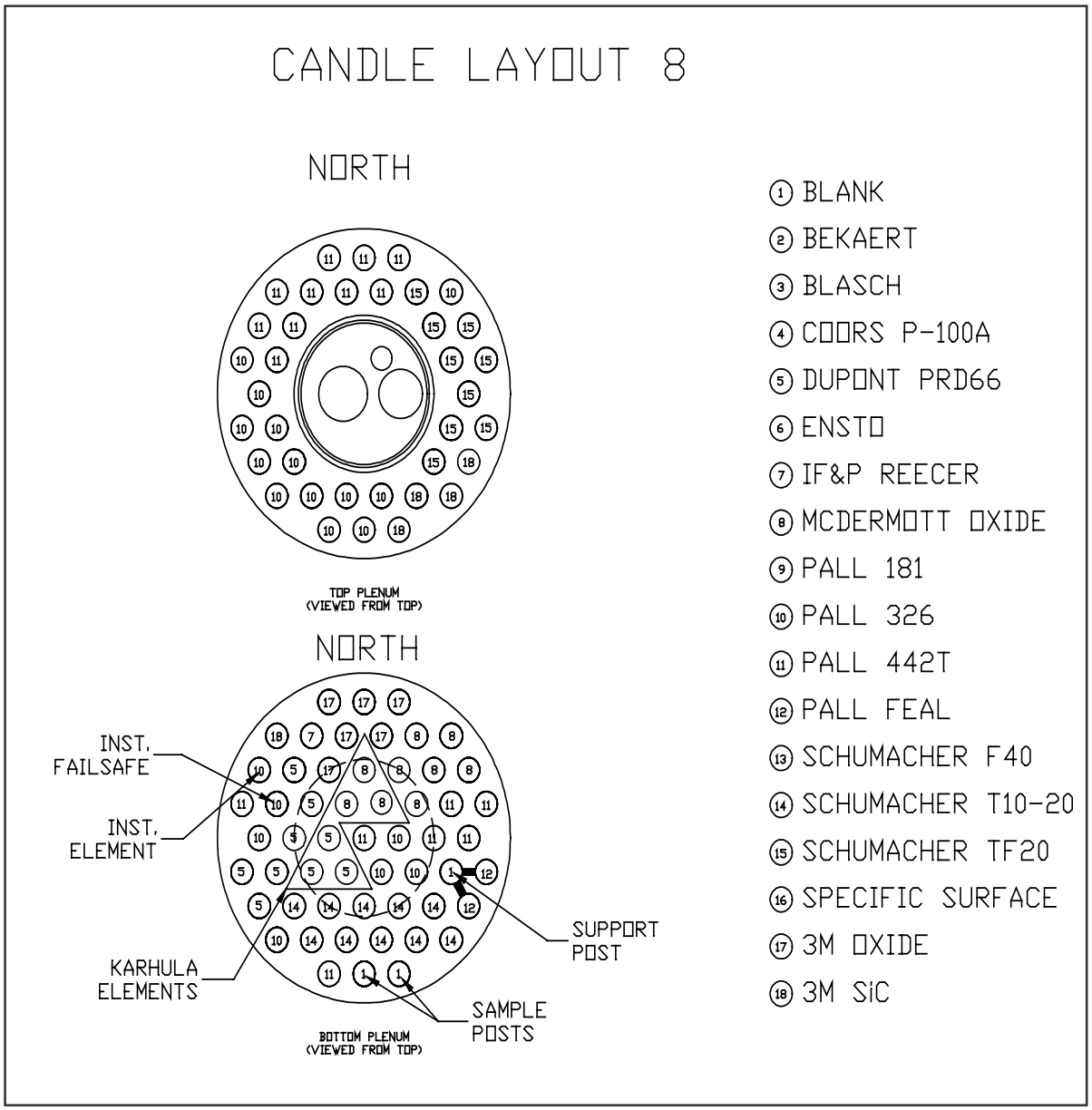

Figure 3.2-2 Second Filter Element Layout for TC02 April 18 to May 13 (Layout No. 8)

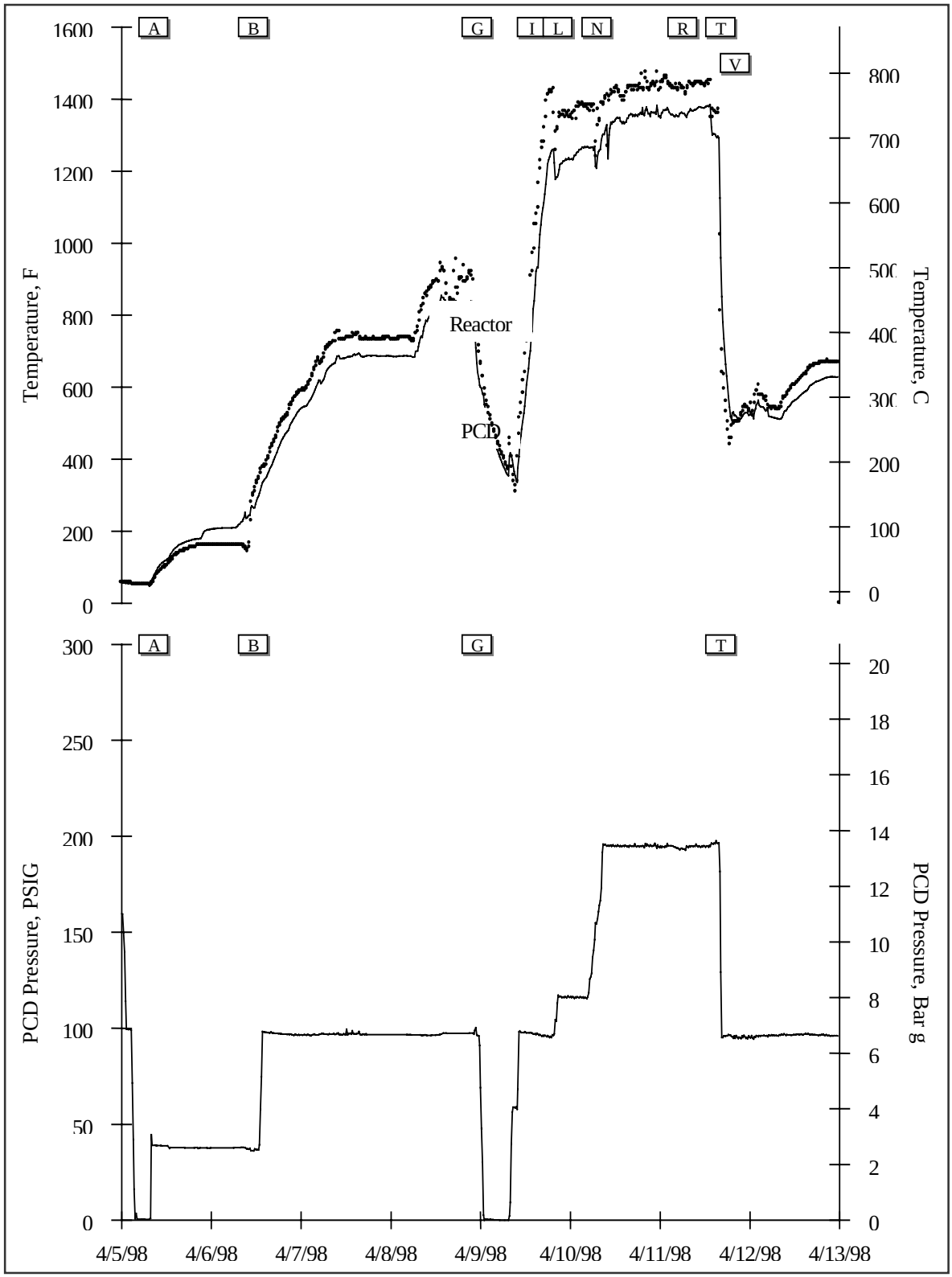

Figure 3.2-3 TCO2 Summary Information

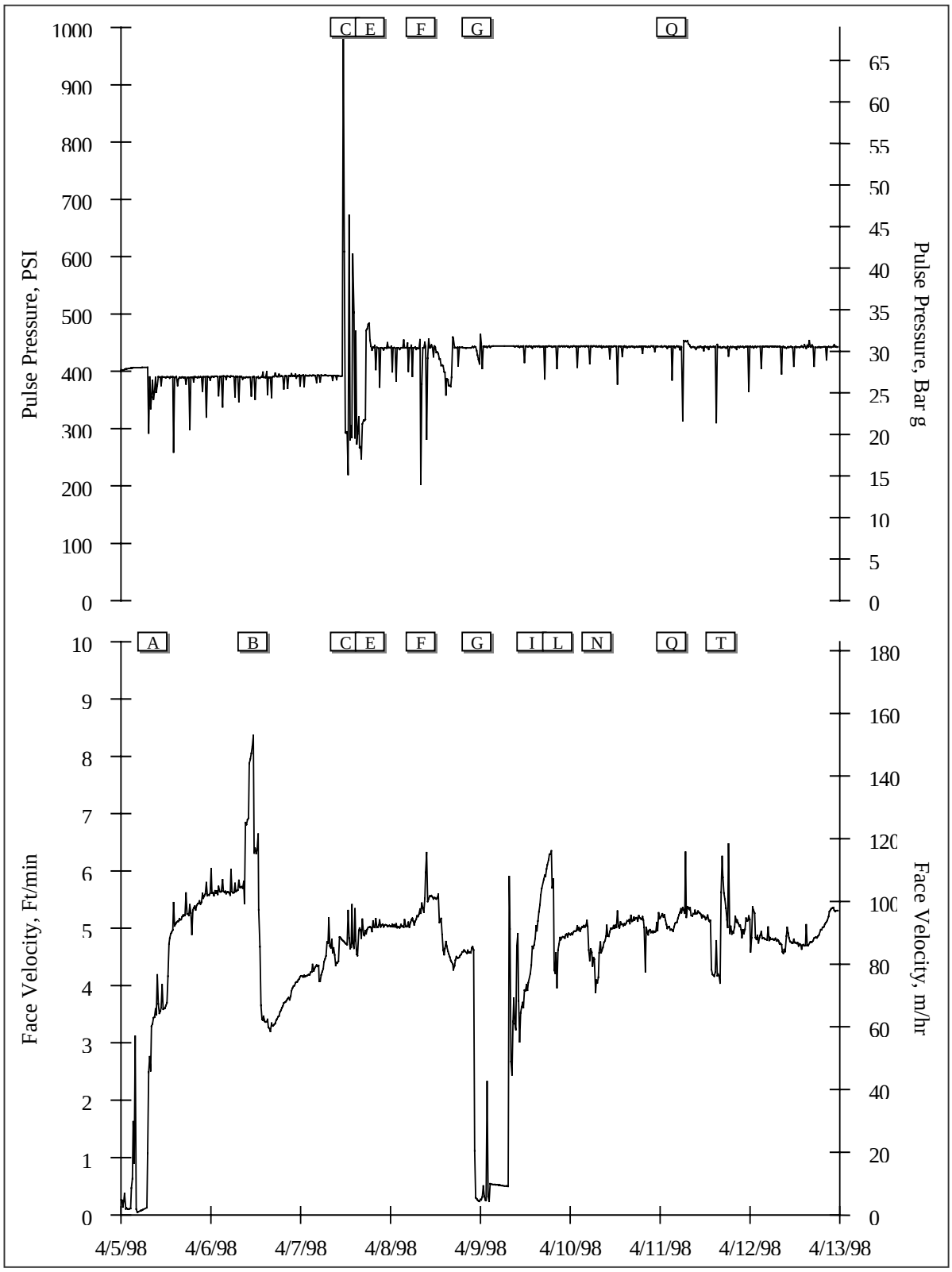

Figure 3.2-4 TC02 Summary Information

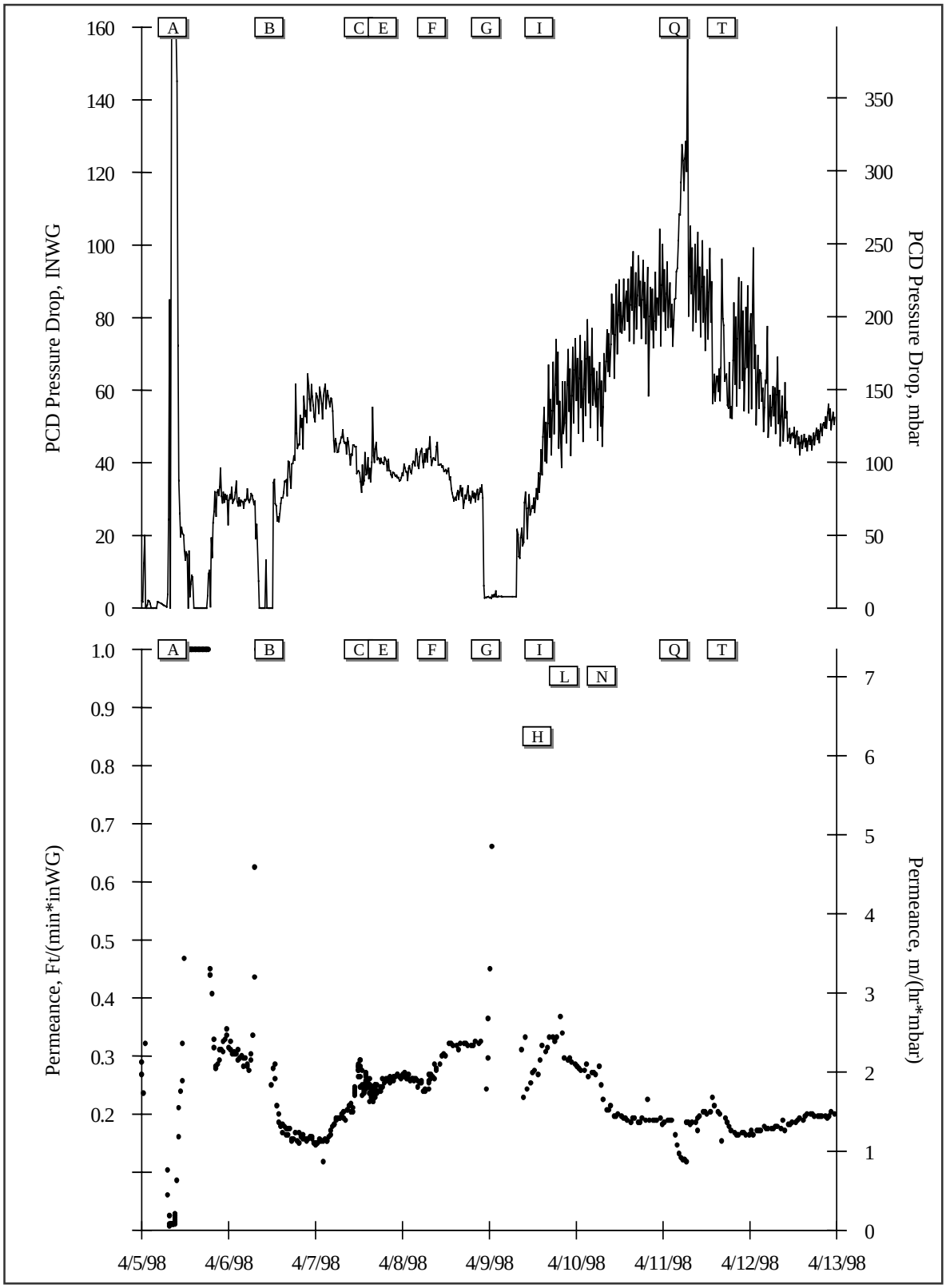

Figure 3.2-5 TCO2 Summary Information

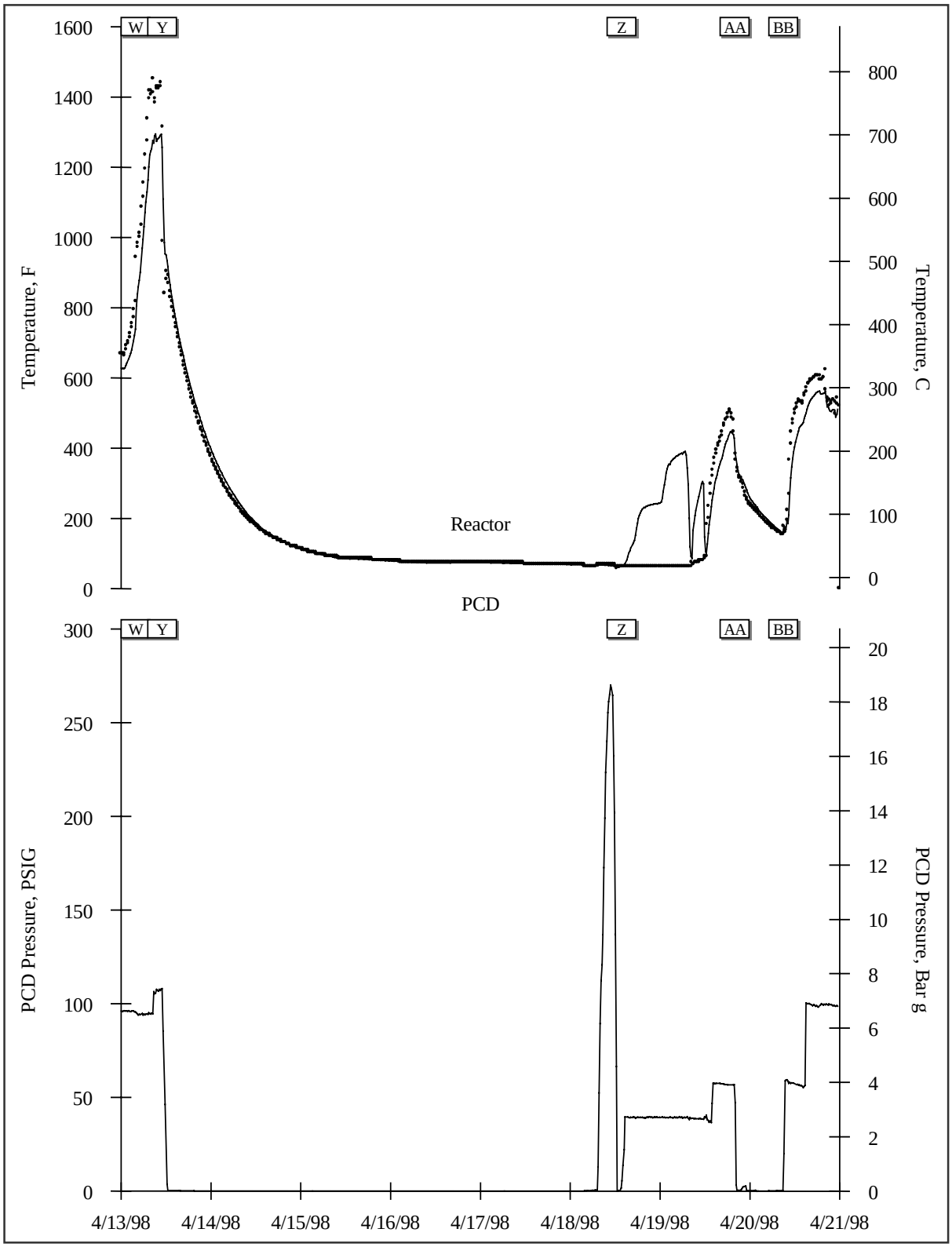

Figure 3.2-6 TC02 Summary Information

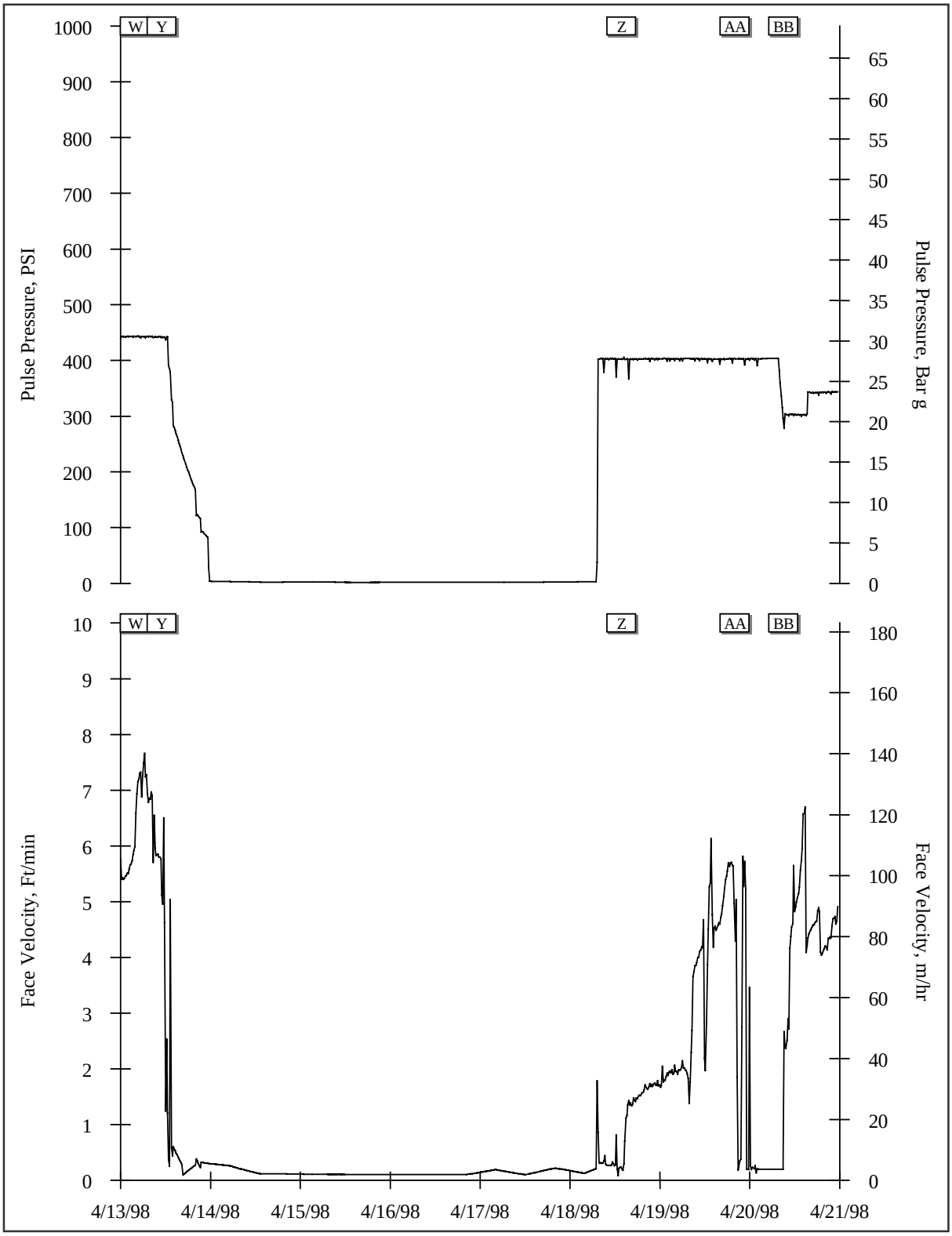

Figure 3.2-7 TCO2 Summary Information

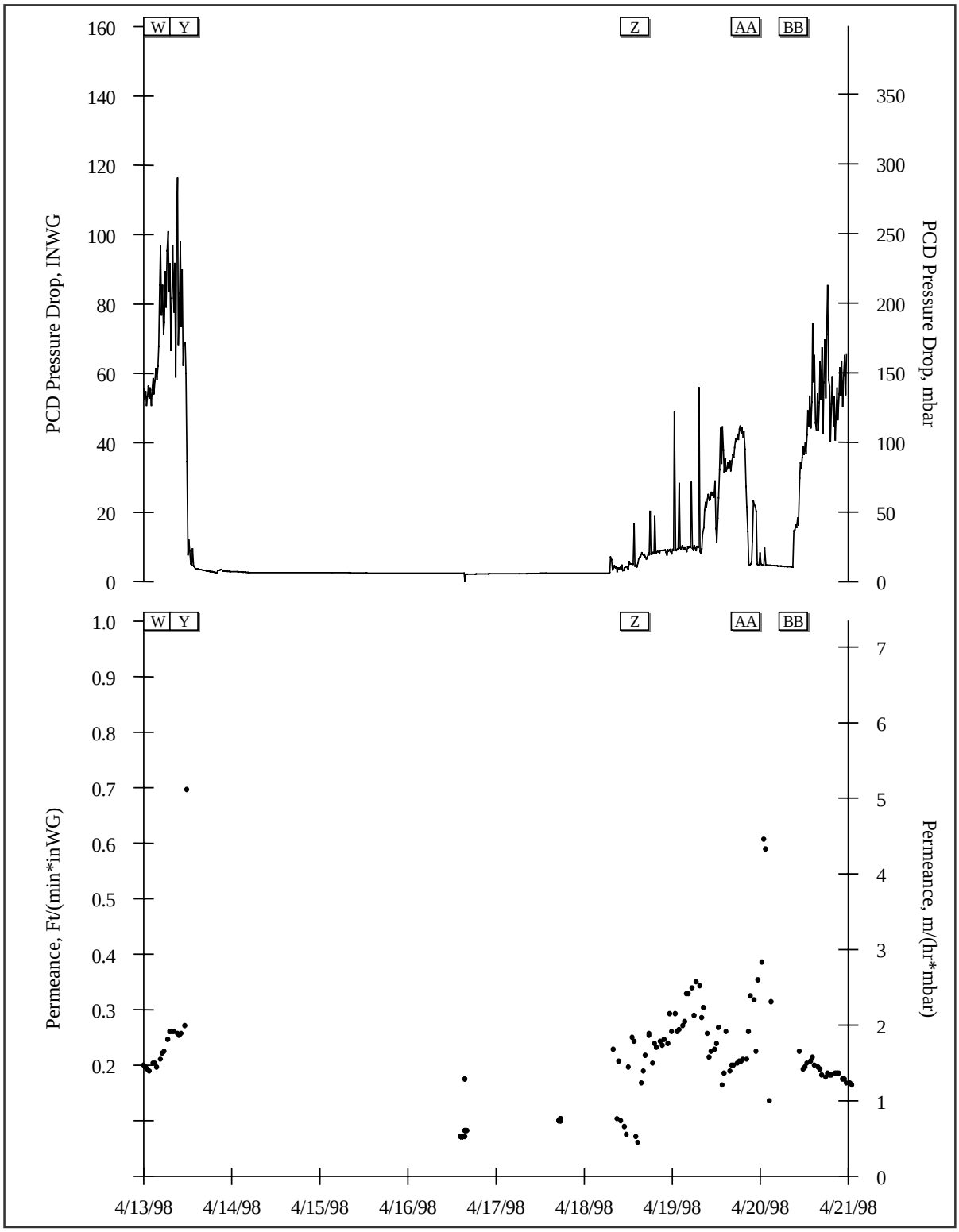

Figure 3.2-8 TC02 Summary Information

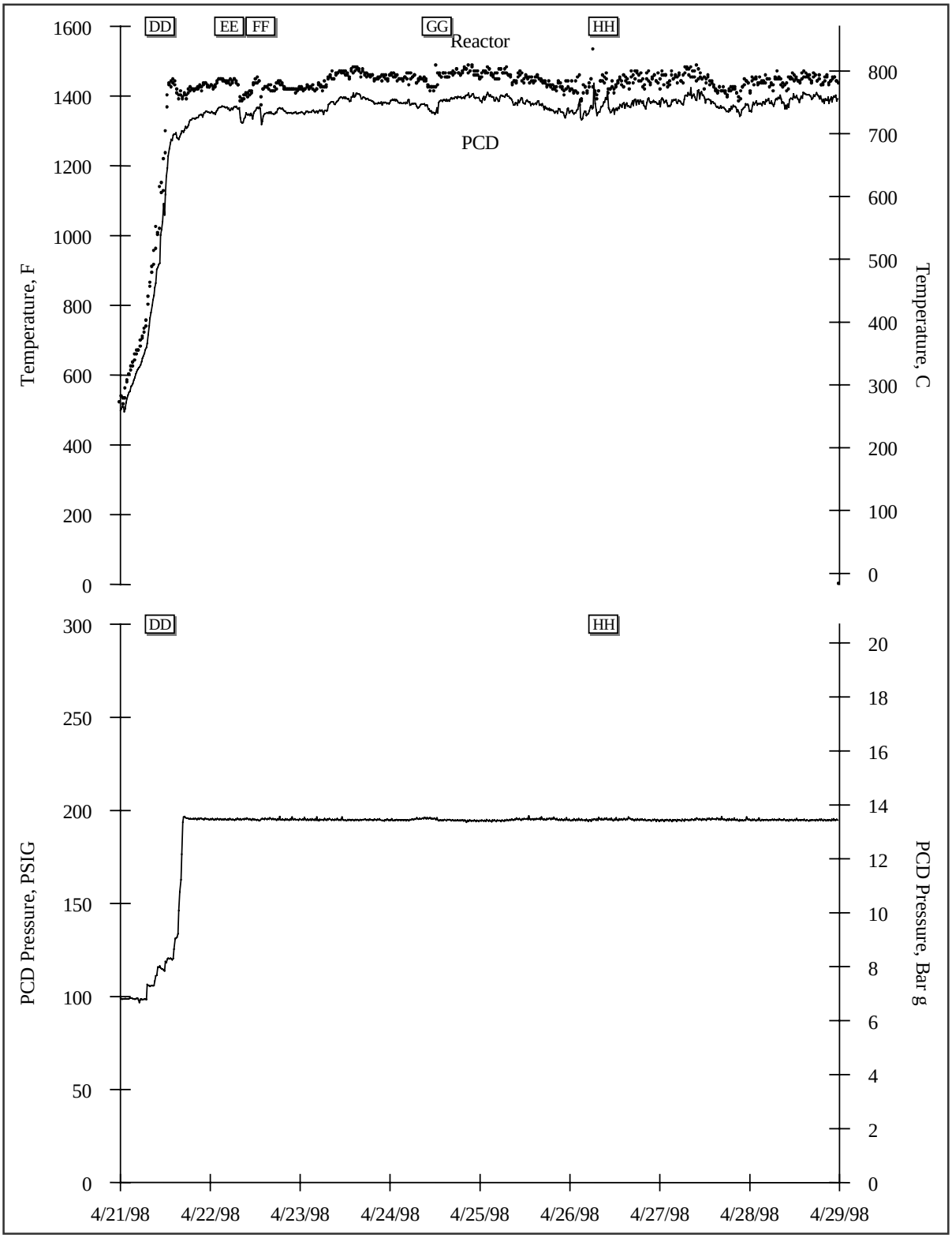

Figure 3.2-9 TCO2 Summary Information

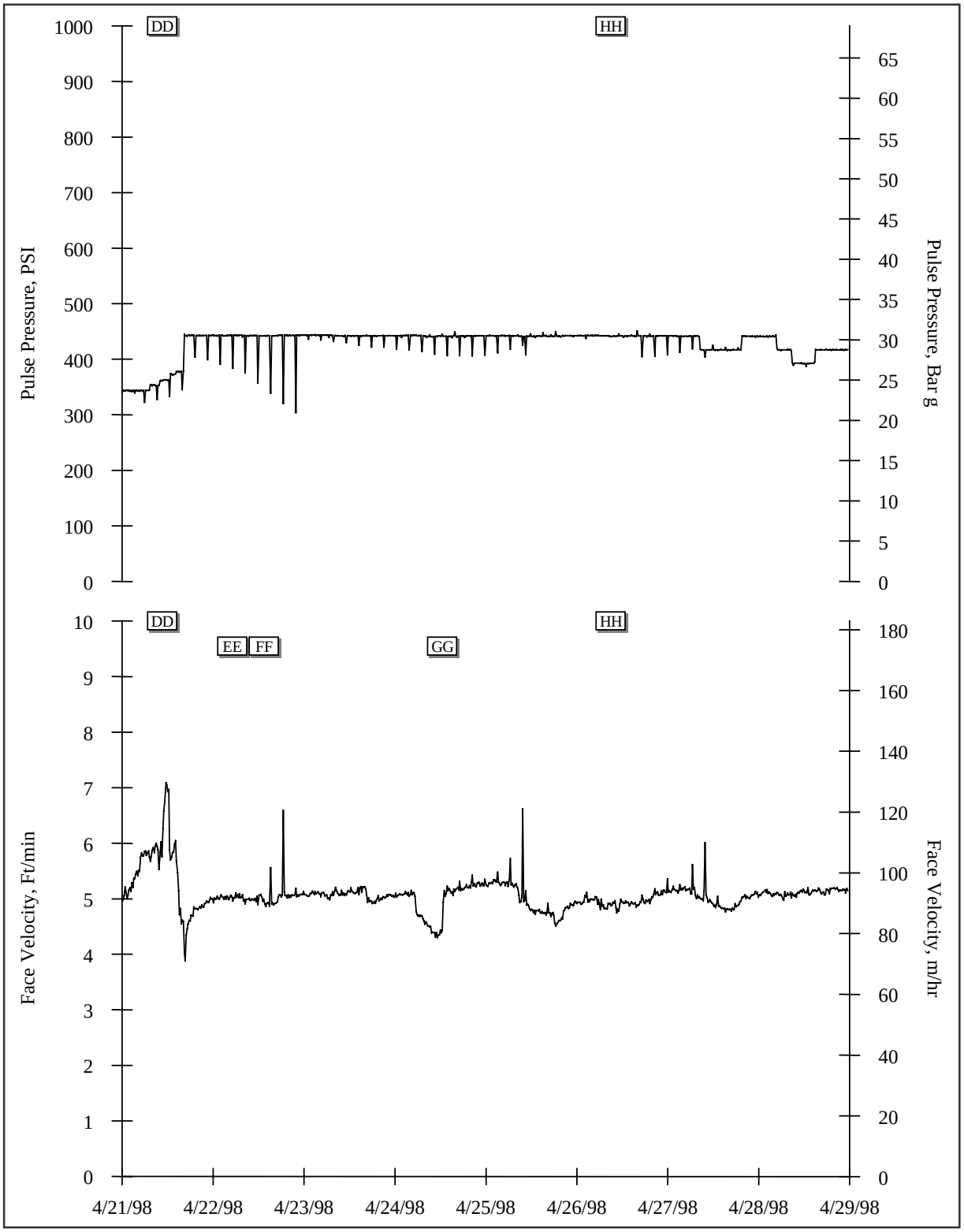

Figure 3.2-10 TCO2 Summary Information

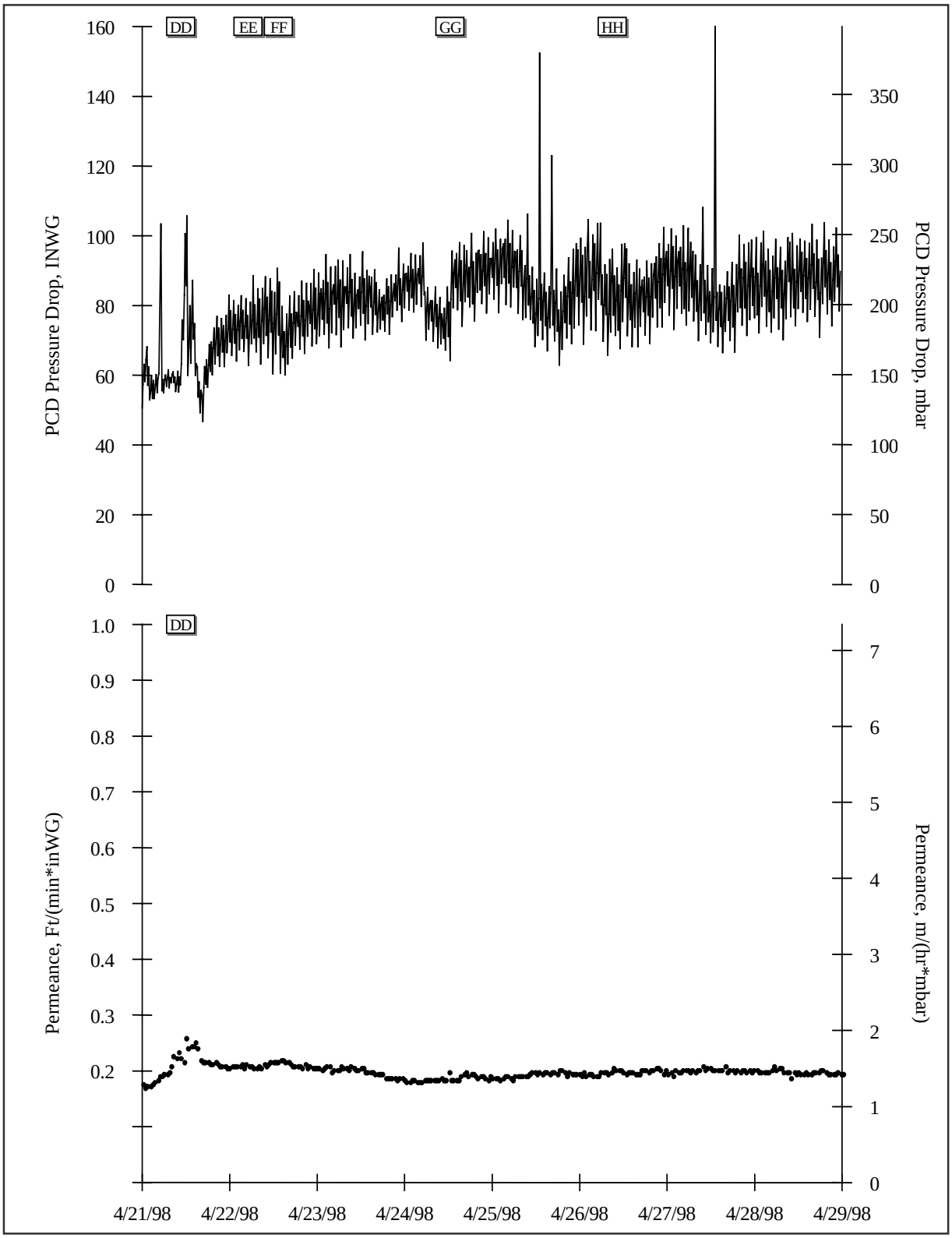

Figure 3.2-11 TCO2 Summary Information

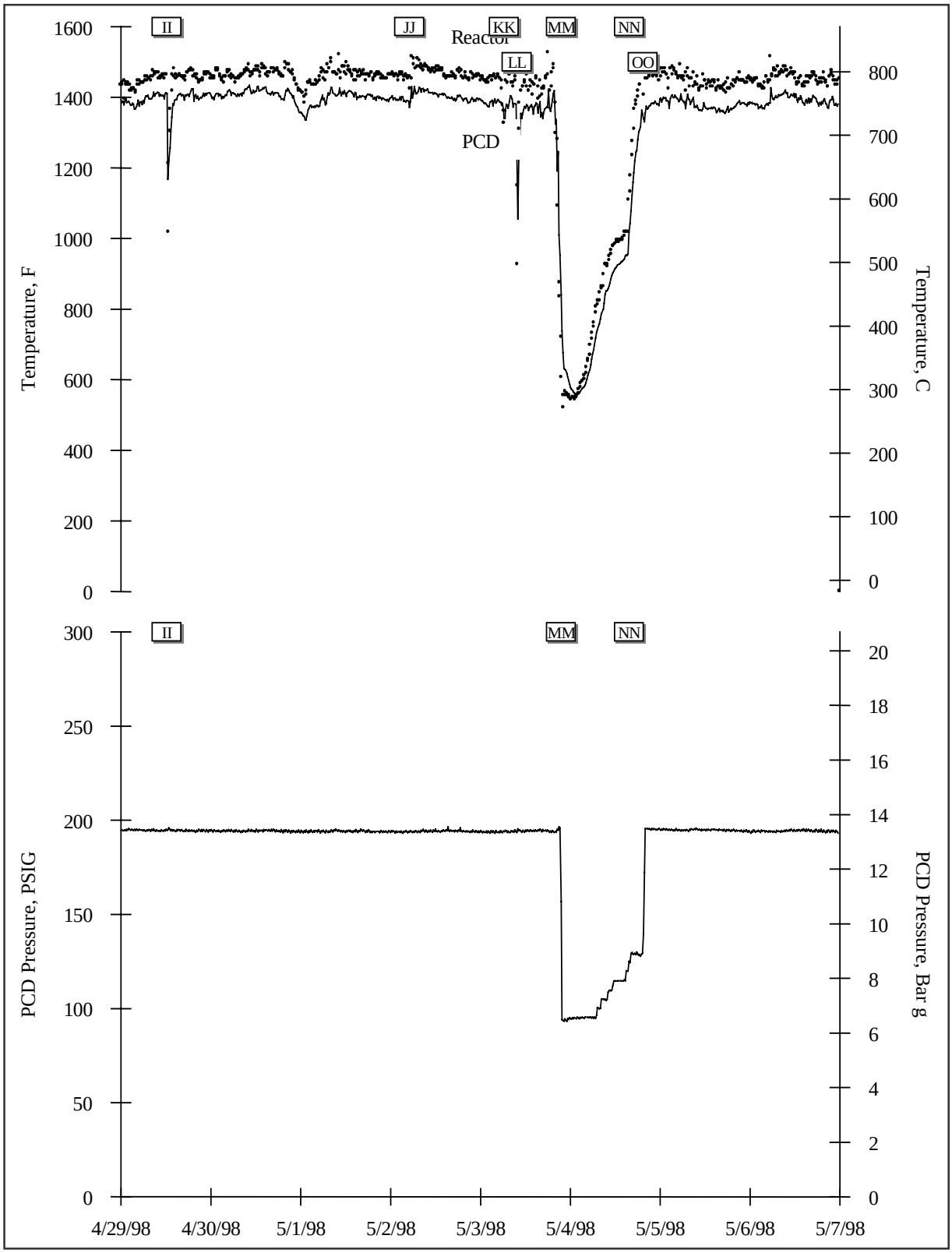

Figure 3.2-12 TC02 Summary Information

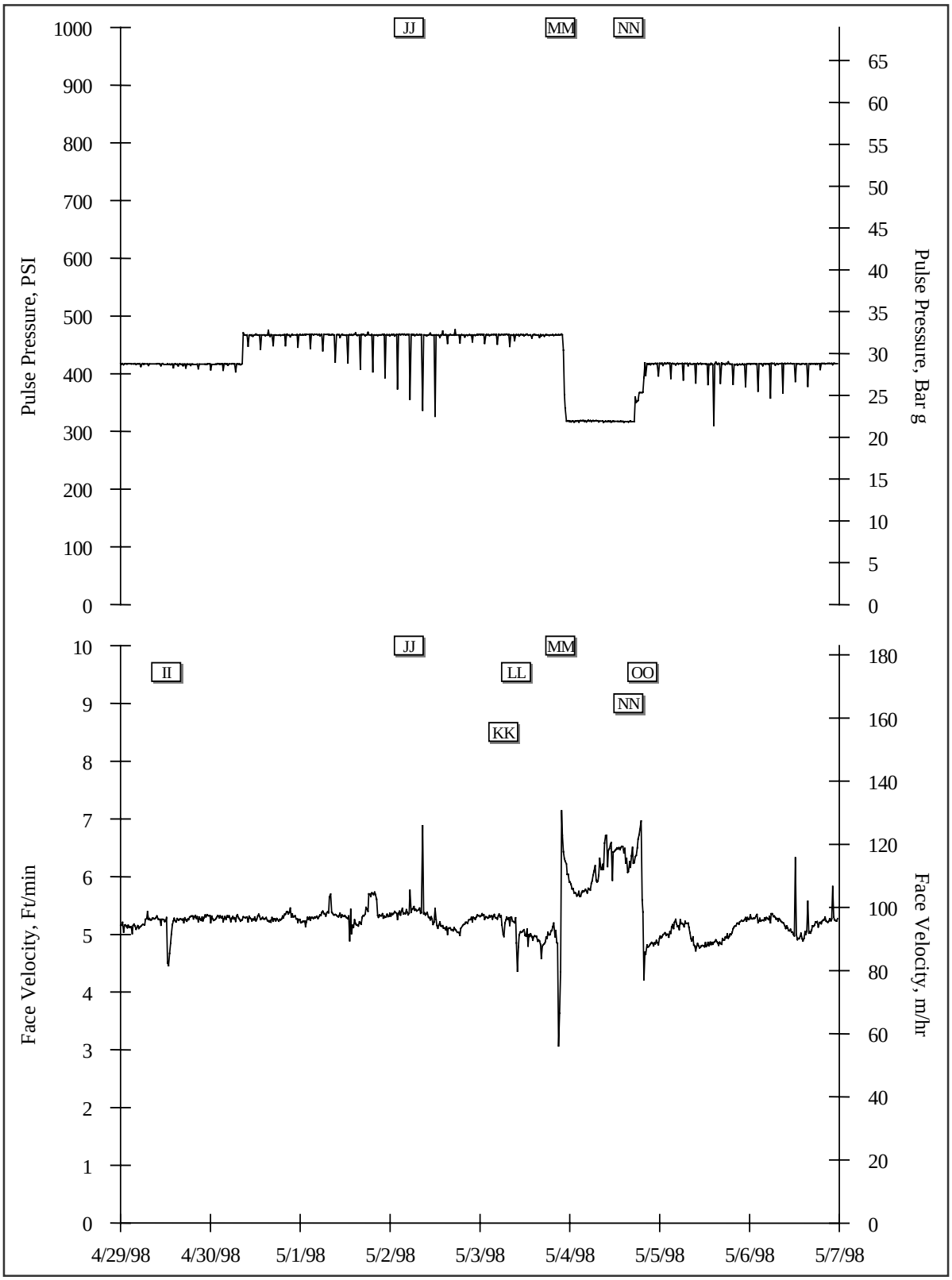

Figure 3.2-13 TCO2 Summary Information

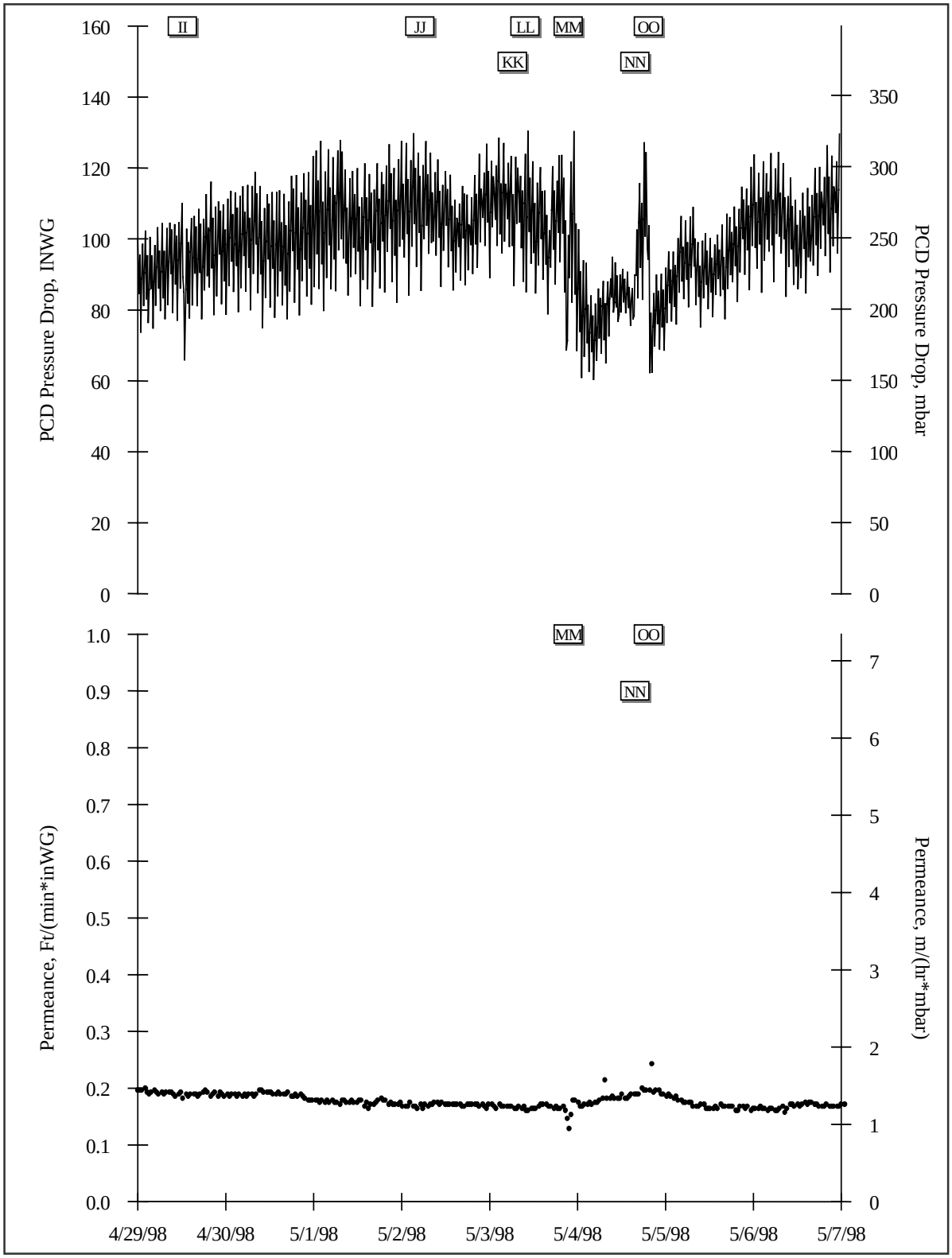

Figure 3.2-14 TC02 Summary Information

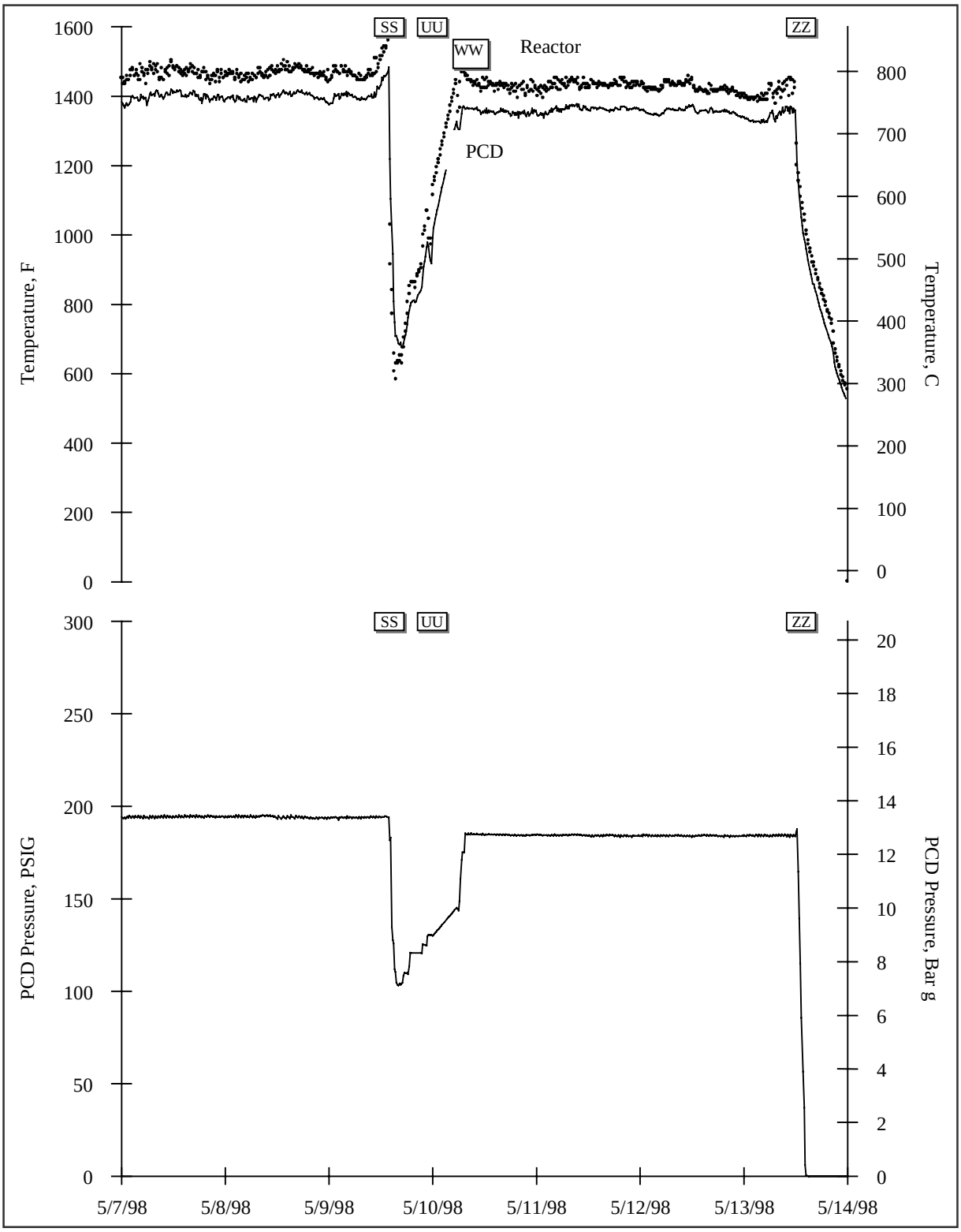

Figure 3.2-15 TCO2 Summary Information

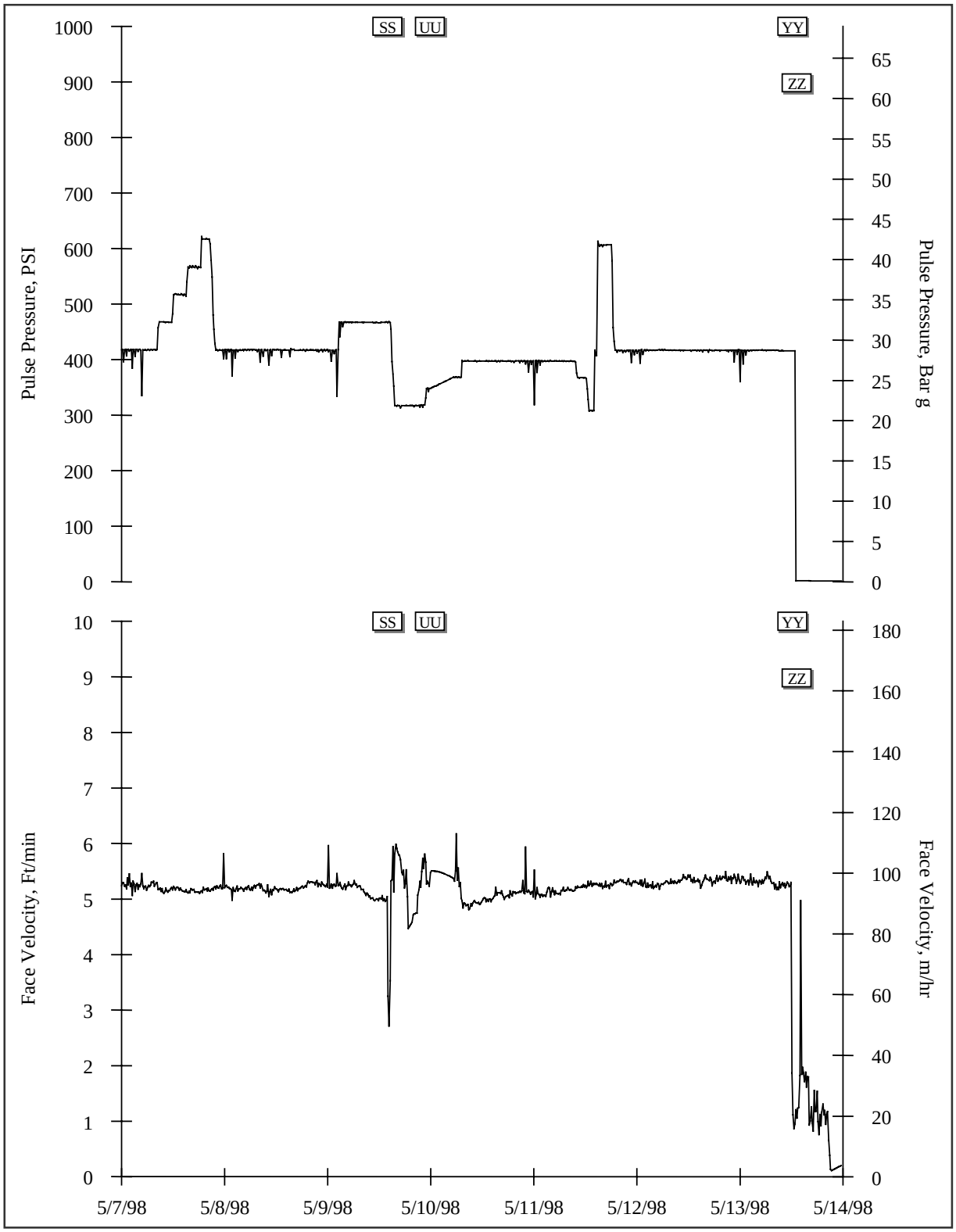

Figure 3.2-16 TC02 Summary Information

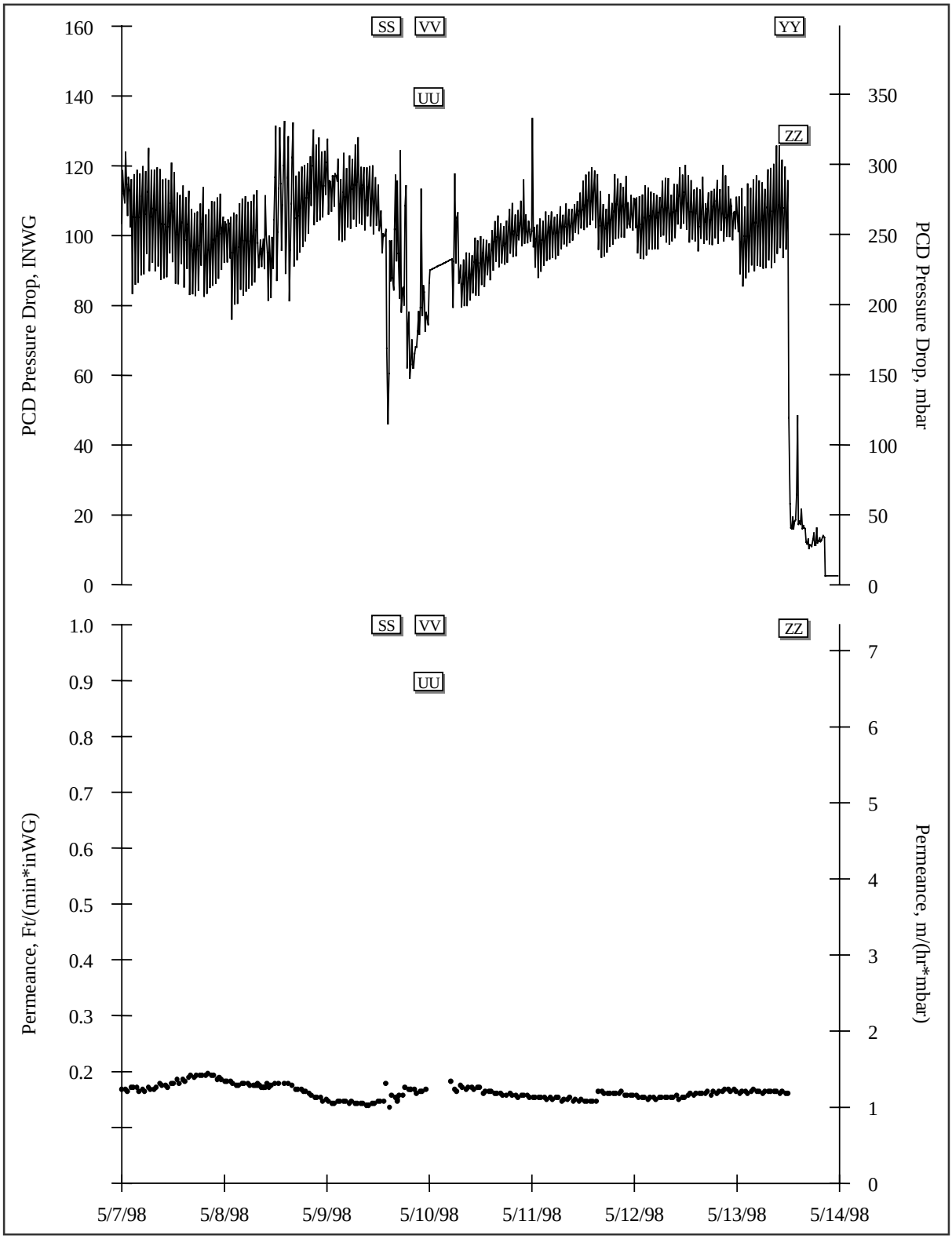

Figure 3.2-17 TCO2 Summary Information

3.3 TC02 INSPECTION REPORT 1

3.3.1 Run Summary

Test campaign TC02 was interrupted on April 13, 1998, after a large quantity of ceramic filter fragments were found in the PCD fines removal system; outlet loading suggested multiple candle failures. The transport reactor was shut down and the PCD allowed to cool to permit removal of the internals since several elements appeared to be involved. The PCD tubesheet and elements were lifted from the vessel on April 16 and placed in the maintenance bay for inspection. The inspection revealed that nine filter elements had failed during the run. Of these elements, six were Blasch, two were Coors P-100A, and one was a Specific Surface element. Two of these Blasch elements were previously exposed elements from Karhula. Additionally, during inspection of the plenum, a Dupont PRD66 was accidentally broken. A 3M oxide element, the remaining Specific Surface element, the two remaining intact Blasch elements, and a Schumacher TF20 belonging to Roger Chen were removed and replaced for evaluation purposes.

3.3.2 Thermal Event

There is suspicion that during initial start-up, while transitioning to coal, burning coal was being carried over from the transport reactor to the PCD. A detailed report of this event is included in the section 3.8. There is indication that elements outfitted with thermocouples experienced a rapid rise in temperature that was not recorded by plant instrumentation. Approximately 1 day after the thermal event, the fines transport system (FD0520) began plugging with element pieces indicating that elements had failed.

3.3.3 PCD Inspection and Dustcake Observations

Upon opening the PCD head it was immediately apparent that all failures occurred on the bottom plenum. Figure 3.3-1 shows the plenum as it was removed from the vessel. Six of the eight Blasch filter elements, two Coors P100A elements, and one Specific Surface element failed during operation. Figures 3.3-2 and -3 show views of the broken elements. One of the failed Coors elements was hanging loosely by only the thermocouple wires is shown in figures 3.3-4 through -5.

A fail-safe had been modified to allow for the thermocouple wires to be fed through a 1/4-in. tube and into the plenum above one of the Coors P100A elements that had been outfitted with thermocouples. This modified fail-safe showed signs of leakage and is suspected as a major cause of the 700 ppmw outlet loading. The Coors P100A element with an instrumented fail-safe also failed.

The remaining damaged elements were removed and inspected. Fail-safes were also examined. Several surrounding elements were temporarily removed during the outage so as to obtain access to the broken elements.

An element layout showing the damaged elements and a location map are shown in figures 3.3 6 and -7 for reference to the locations of the failed and damaged elements in the plenum assembly. Figure 3.3-6 shows the elements installed and figure 3.3-7 shows the elements that were damaged. It was also noticed that ash had accumulated on the top of the tube sheet. This ash was vacuumed off prior to reinstallation of the plenum in the vessel.

A close-up of the broken Blasch elements is shown in figure 3.3-2. Some of the elements showed additional cracking in a spider web fashion, as seen before with Coors element failures. Most of the breaks were of a V-shape typical of thermal failures. Figure 3.3-8 shows a close-up of the broken Blasch filters. SRI took samples of the elements for further testing. A Dupont PRD66 element was inadvertently broken during the removal process. Additionally, the failed Specific Surface element was removed as well as the intact one. The intact element was sent to SRI for study and the remaining pieces of the broken element were taken by the manufacturer.

3.3.4 Inspection Results

The failure of the six Blasch elements prompted the removal of all elements. The thermocouples were helpful in gaining understanding of what could be causing the failure events even though problems were known to be present with Coors P100A elements prior to their installation for test run TC02. The data obtained from the Pall 326 and Coors P100A elements equipped with thermocouples helped to determine the probability of carryover of burning coal. Additionally, one Schumacher TF20 element from Roger Chen and one 3M oxide element were removed for analysis. Fifteen elements were removed from the plenum. Those elements consisted of eight Blasch (six of which were broken), two Specific Surface (one of which was broken), one 3M oxide, two Coors, one Dupont PRD66 (broken during inspection), and one Schumacher TF20 (for Roger Chen). Figure 3.3-9 shows the final element arrangement as installed for the remainder of TC02.

Figure 3.3-1 Bottom Plenum on April 16, 1998

Figure 3.3-2 Broken Blasch Filter Elements

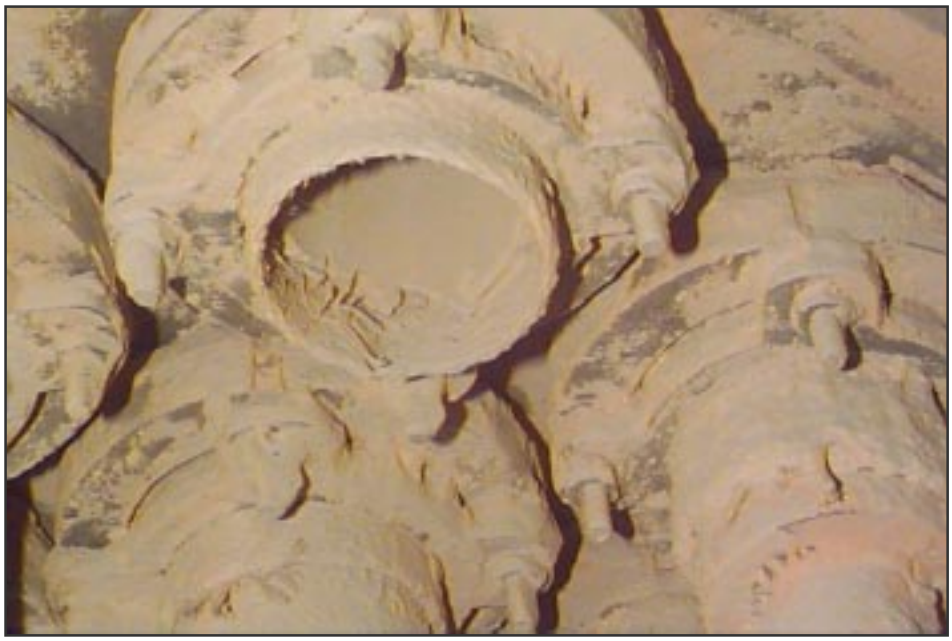

Figure 3.3-3 Broken Specific Surface Filter Element

Figure 3.3-4 Broken Coors Element Close-Up

Figure 3.3-5 Two Broken Coors Elements

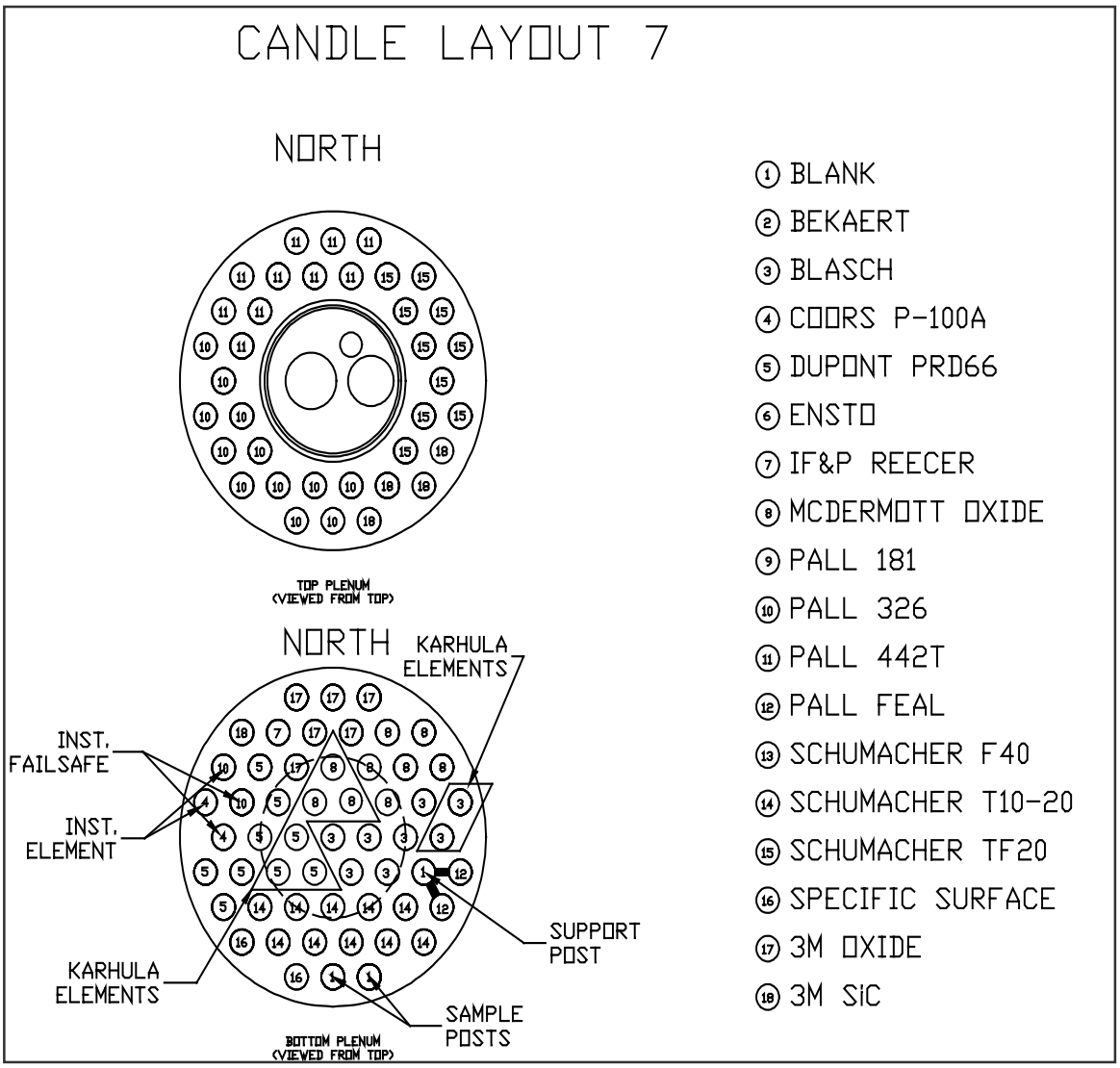

Figure 3.3-6 Layout 7

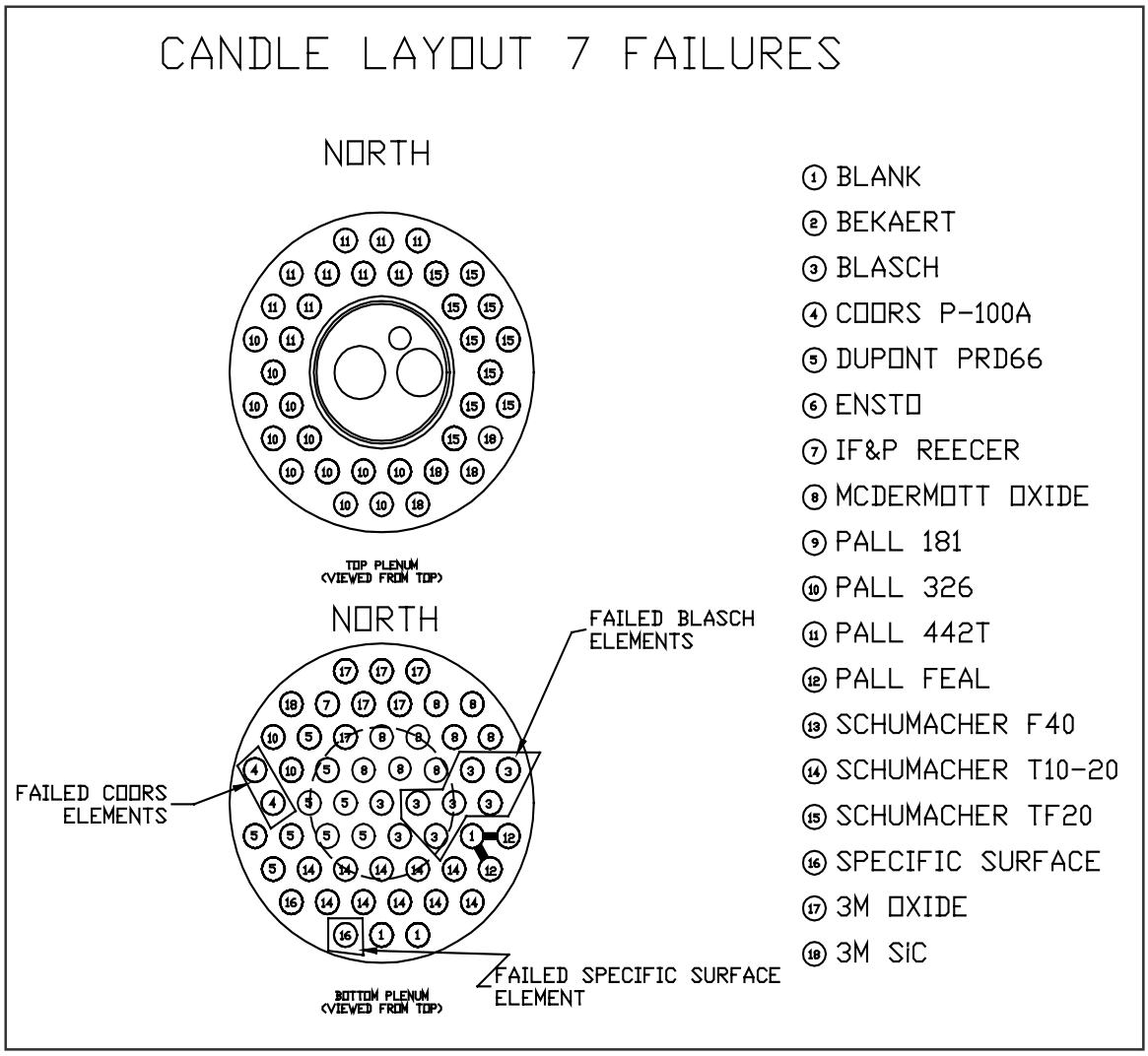

Figure 3.3-7 Layout 7 Failures

Figure 3.3-8 Broken Blasch Elements Removed

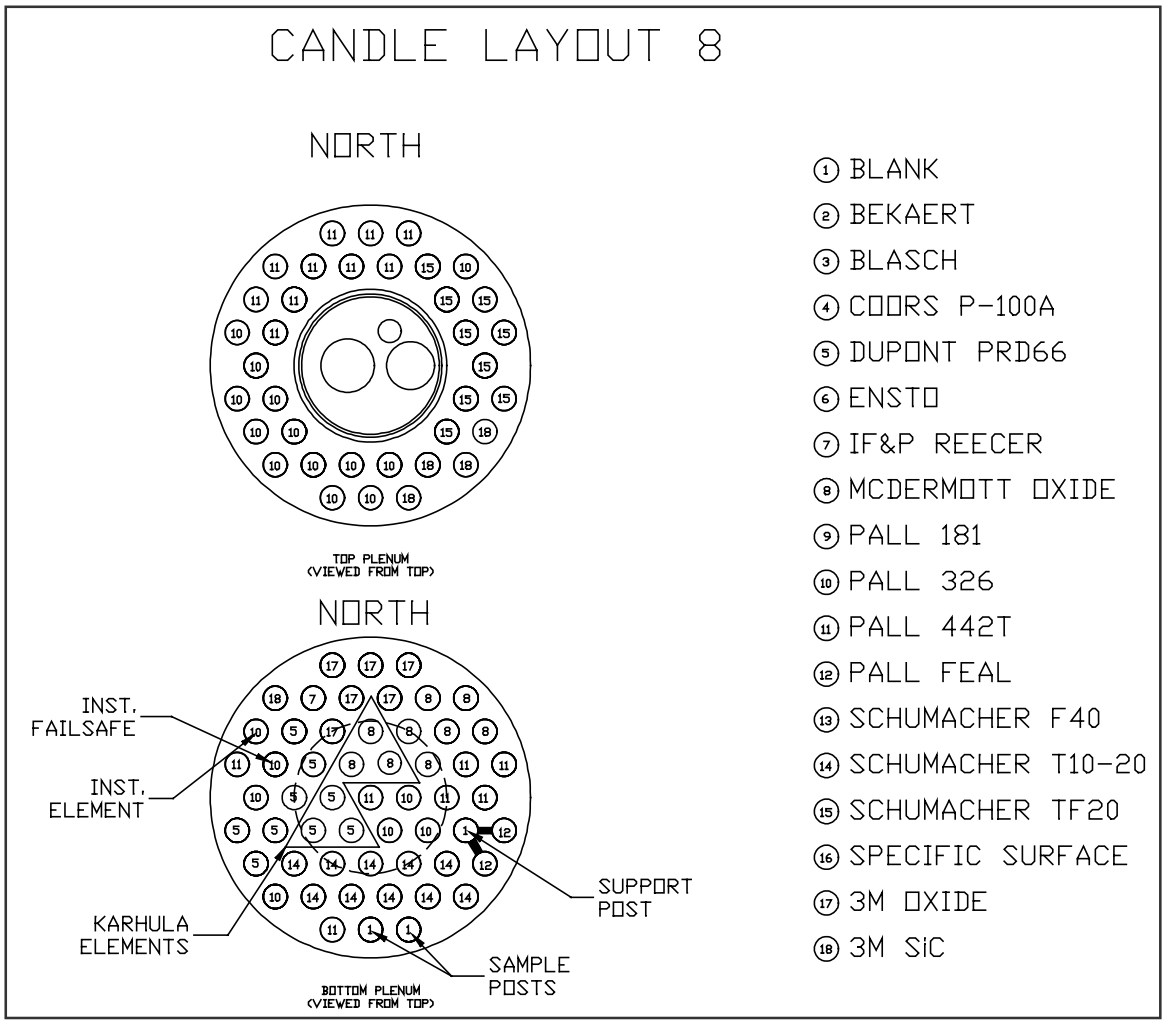

Figure 3.3-9 Final Arrangement TCO2 Run

3.4 TC02 INSPECTION REPORT 2

3.4.1 Run Summary

Test campaign TC02 was concluded with a normally scheduled shutdown on May 13, 1998. The plenum was pulled and inspected once again. The run was terminated just prior to a normally scheduled back-pulse in order for Southern Research Institute (SRI) to inspect the dustcake prior to back-pulsing. A gradually increasing leakage was detected towards the end of TC02, which lead to speculation that the gaskets for the 3M elements could be providing a leak path. This was found to be true, prompting the removal of all installed 3M elements. A total of 20 elements were removed, including 11 3M, 5 Pall, and 4 Schumacher elements.

3.4.2 PCD Inspection and Dustcake Observations

The PCD was removed on May 18, 1998. Figure 3.4-1 shows the bottom plenum after removal. Upon closer inspection, several gaskets for the 3M elements showed signs of leaking at the interface between the filter and the tubesheet. The element itself was not leaking; however, because of the gasket arrangement dust was leaking around the fail-safe. Figure 3.4-2 shows the leakage around the gaskets. Because of this, all of the installed 3M filters (oxide and SiC) were removed. Since SRI wanted to observe a dirty shutdown the candles had a noticeably thicker dustcake. Figures 3.4-3 through -5 show the appearance of the candles. Additionally, the Pall 326 element equipped with thermocouples and the fail-safe with thermocouples were removed. Ash was visible on many of the fail-safes due to the previous failure event during TC02. A total of 11 3M elements, 5 of which were 3M type 203 and 6 of which were 3M Oxides, were removed. In addition, 4 Pall 326 elements, 4 Schumacher TF20 elements, and 1 Pall 442T element were removed, for a total of 20. The elements removed were replaced by 2 McDermott Oxides, 2 Dupont PRD66 elements, 2 3M oxides with modified flange assemblies, and 14 Schumacher TF20 (5 of which were test elements owned by Roger Chen).

3.4.3 Inspection Results

Speculation about the leakage around the gaskets on the 3M filters prompted the manufacturer to modify the flange to conform to the standard element design. No other significant issues came from this inspection. The plenum was reinstalled in the vessel in preparation for TC03. Figure 3.4-6 shows the element layout as installed for TC03.

Figure 3.4-1 Removal of PCD Plenum on May 19, 1998

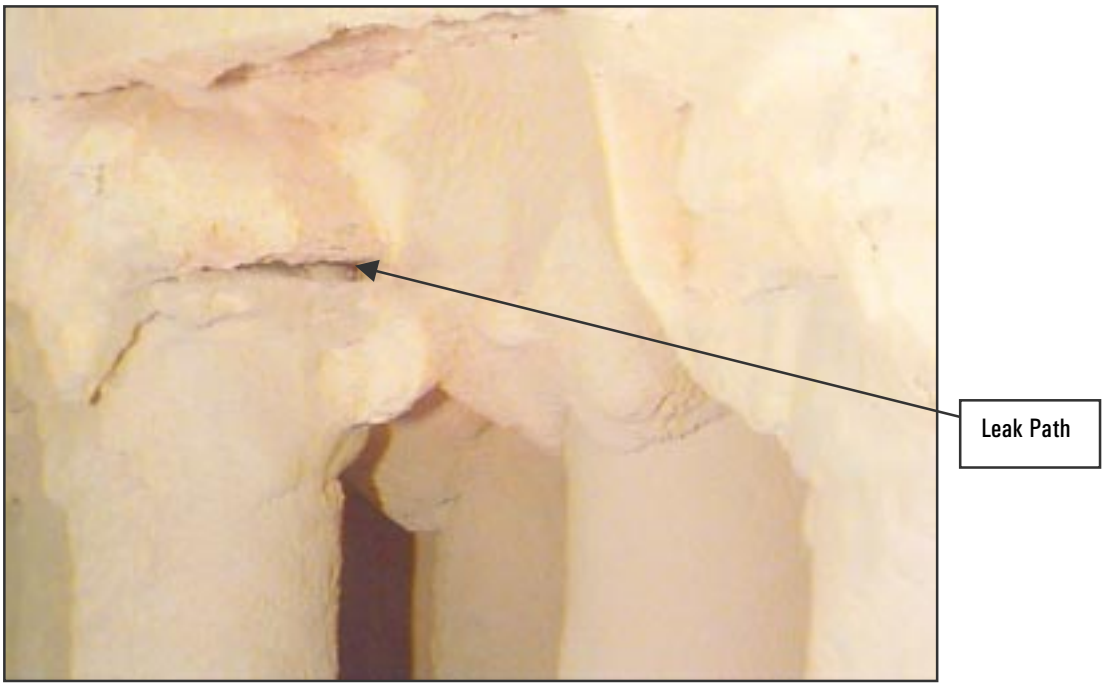

Figure 3.4-2 Leaking Gaskets on 3M Candles

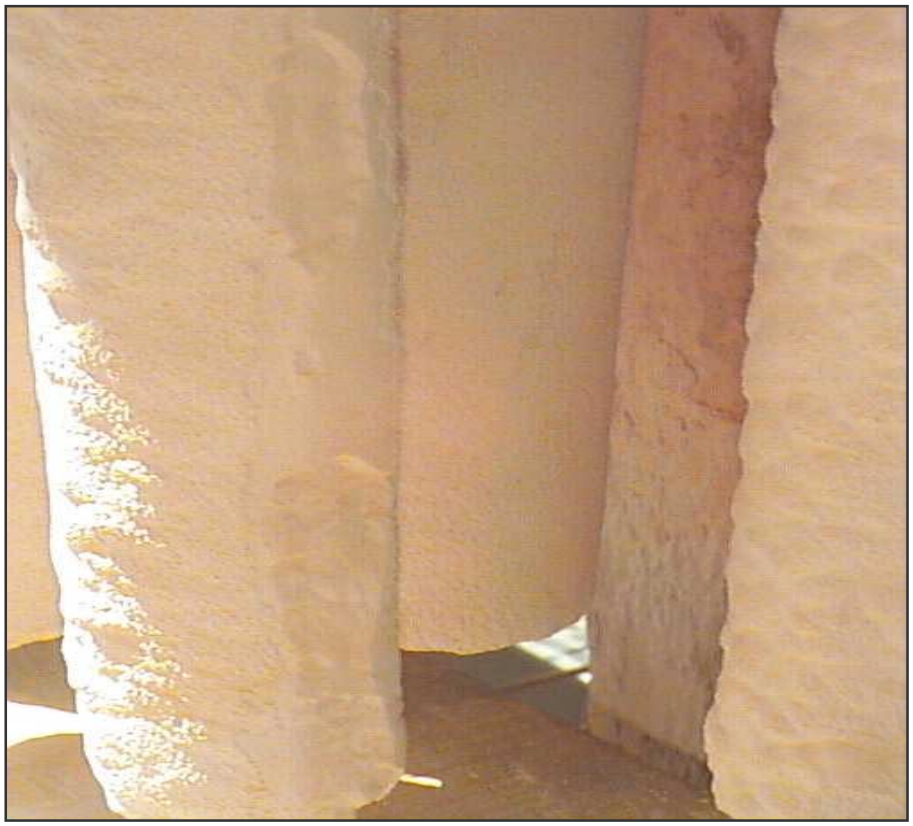

Figure 3.4-3 Dustcake on the Elements

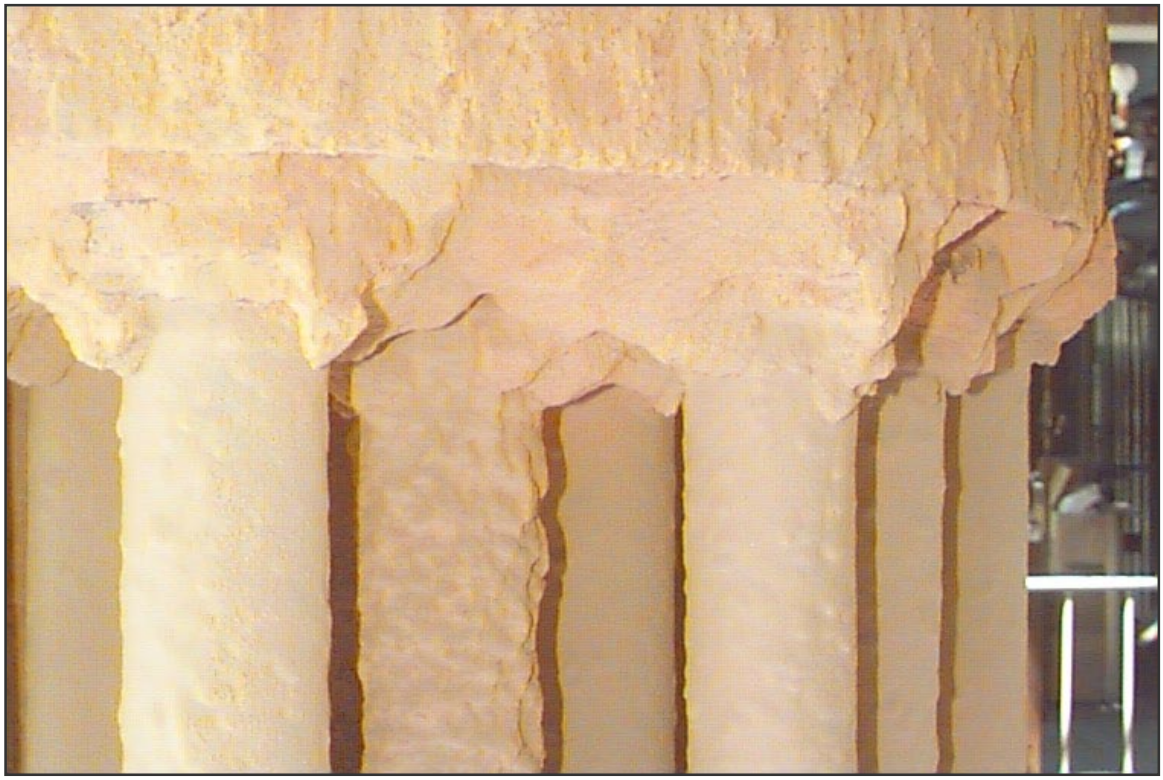

Figure 3.4-4 Ash Accumulation on the Filter Flanges

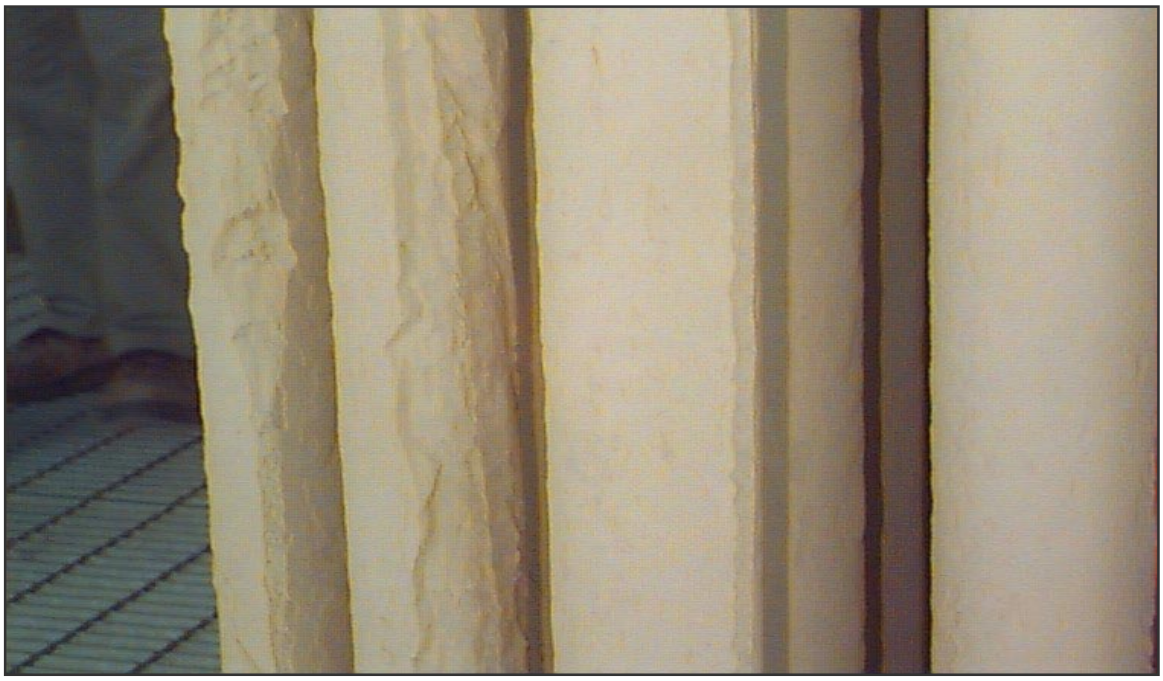

Figure 3.4-5 Dust Ridges on the Elements

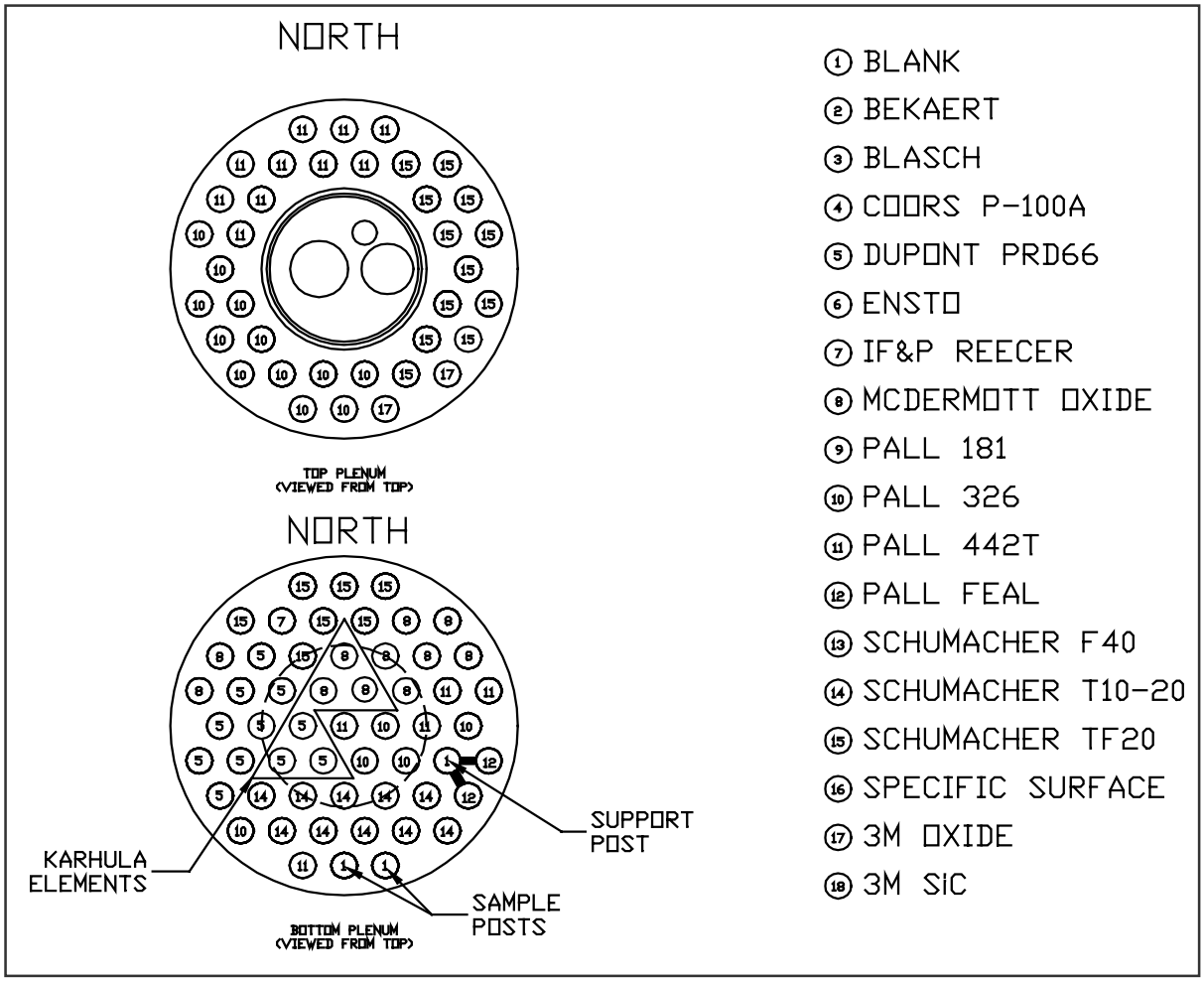

Figure 3.4-6 Element Layout for TC03

3.5 TC02 ASH CHARACTERISTICS AND PCD PERFORMANCE

In test campaign TC02 in situ particulate sampling runs were performed on a regular basis at the PCD inlet and outlet. Initial sampling runs performed at the PCD inlet were directed at monitoring changes in solids carryover from the transport reactor system during start-up solids circulation and during transition to coal. One inlet sampling run was performed in the absence of sorbent addition to better define the contribution of the sorbent to the total particulate loading. Three cut-size tests were also performed to quantify the fraction of solids that drops out ahead of the filter elements. Sampling runs were also performed at the PCD outlet to quantify particle penetration through the PCD during TC02. The in situ particulate samples collected during TC02 included eight samples of the particulate mass entering the PCD and nine samples of the particulate mass exiting the PCD. All of the samples collected at the PCD inlet and six of the samples collected at the PCD outlet were total particulate mass samples collected on a single filter (mass samples). Three of the samples collected at the PCD outlet were size-segregated samples collected in a cascade impactor.

This report summarizes the particulate mass loadings determined from the TC02 sampling runs, along with PCD collection efficiencies calculated from the inlet and outlet loadings. Particle-size distributions determined by cascade impactor and by particle-size analysis in the laboratory are discussed and compared to particle-size measurements from previous test series. Significant physical and chemical characteristics of the in situ samples are presented and compared to the characteristics of ash samples taken from the PCD hopper and of dustcake samples taken from the filter elements after the dirty shutdown in May.

3.5.1 Measurements of Particulate Mass Loadings

Inlet Measurements. Table 3.5-1 gives a summary of the results of all PCD inlet particle mass concentration measurements performed during all segments of TC02. To evaluate the effects of start-up on the characteristics of the initial dustcake buildup on the PCD candles, the first two measurements were made under unstable start-up conditions. The first measurement (TC02IMT-01) was made during start-up on propane with circulation of hot-bed material. The second measurement (TC02IMT-02) was made during the transition to coal combustion with relatively low-feed rates of coal and dolomite. Table 3.5-1 shows that the loading measured during the start-up condition (11,400 ppmw) was significantly higher than the loading measured on the next day during the transition to coal (2,800 ppmw). The relatively high loading obtained during hot-solids circulation was the result of inefficient operation of the primary cyclone under the low-flow start-up conditions. The lower loading obtained during the transition to coal is consistent with the relatively low-solids feed rates and low-circulation rates during the transition period.

Four tests were conducted during conditions that would be described as normal operation for TC02. Tests TC02IMT-03, -04, -05, and -06 were measured under stable operating conditions with dolomite addition. The measured particle loadings ranged from 9,100 to 11,100 ppmw and was generally within the range of loadings measured during TC01 (11,400 ± 2,300 ppmw). Except for run TC02IMT-05, the tests were conducted so that the sample was collected between PCD back-pulses, therefore avoiding any material carryover caused by a cyclone dipleg upset.

However, TC02IMT-05 results did not indicate any effect on mass concentration (TC02IMT-05 was conducted during a back-pulse).

One test was conducted with dolomite addition turned off in order to evaluate the effects of sorbent addition on SO_X removal (discussed elsewhere). The addition of dolomite had been terminated about 20 hours prior to the sampling run so that SO_X concentrations could stabilize in the absence of sorbent. Table 3.5-1 shows that the loading measured without dolomite addition (5,100 ppmw) was roughly half that measured during dolomite addition (9,100 to 11,100 ppmw). The magnitude of this effect is greater than expected, since the dolomite reaction products ($CaCO_3$, $CaSO_4$, CaO•MgO, and MgO) typically account for only 25 percent of the total particulate mass. The gas-flow rate was about the same during the tests done with and without dolomite addition, so there was presumably no difference in the collection efficiencies of the primary cyclone during these tests. This result may suggest that the presence of dolomite in the transport reactor loop has a secondary effect on the particulate carryover from the loop (i.e., the addition of dolomite may increase the carryover of coal ash particles through a secondary effect on the gas-particle flow dynamics).

After the dolomite feed was resumed operations personnel were unable to maintain the seal on the cyclone dipleg, resulting in large fluctuations in particulate carryover. The last sampling run (TC02IMT-08) was performed under these unstable conditions and yielded a particulate loading of 18,500 ppmw, almost double the loading measured during stable operation. After this run an adherent coating of fine ash was found on the sampler surfaces that faced into the gas flow. Particle impaction seems to be the most likely formation mechanism since the coating was present on only the surfaces that faced into the flow. The coating could not be removed by brushing or scraping and remained on the metal surfaces even after cleaning the parts in an ultrasonic bath. Prior to this sampling run no such coating had ever been observed on any of the samplers used at the PSDF. No unusual thermal excursions or other process upsets were detected during the sampling run. Process engineers and operating personnel were unable to offer any explanation for the formation of this tightly bonded film of ash on the sampler. The cause and significance of this incident remains unknown but it suggests that the transport reactor system can produce ultrafine, sticky ash particles under certain conditions.

Outlet Measurements. The outlet particulate measurements made during TC02 are summarized in table 3.5-2. Prior to the first outlet measurement filter element fragments were recovered from the ash discharge system on Saturday, April 11. Since this incident occurred on a Saturday operations personnel decided to discontinue the coal feed while keeping the transport reactor system hot until SRI personnel could make a measurement of the outlet particulate loading on Monday, April 13. Coal feed was restarted at about 6:00 a.m. Monday and an outlet sampling run was begun when suitable operating conditions were established at 8:20 a.m. As shown in the table, the results of the first run (TC02OMT-01) suggested that there was significant leakage (720 ppmw) from the dirty side to the clean side of the filter system after the incident mentioned above. The transport reactor system was immediately shut down and the filter internals were removed, revealing nine broken elements. Normally, nine broken elements with properly installed fail-safes would not produce a leak as large as 720 ppmw. In this instance, however, the leak was much larger than normal, because one of the broken elements was equipped with a modified fail-safe that contained a feedthrough for instrumentation wiring. The instrumentation feedthrough was apparently providing a significant leakage path through the fail-safe on that

broken element. Future design of the instrumentation wiring will be modified to avoid any potential leakage paths in the event of a filter failure.

The outlet runs performed after the broken elements were replaced (TC02OMT-02 and -03) confirmed that the leakage had been dramatically reduced (4.6 to 4.8 ppmw), although there was apparently still some penetration of ash through the filter system. (Experience has shown that the outlet loadings are normally below 1 ppmw when all the filter elements are intact and properly installed.)

Inadequate gasketing between 3M fiber-reinforced elements and their fail-safes was suspected as the source of the relatively minor leak since 3M elements differ from the other elements in the design of the flanged end that mates to the fail-safe. (Subsequent inspection of the element flange and fail-safe gasketing revealed that the leakage was actually occurring around the outside of the fail-safe. With thermal cycling, the difference in thermal expansion between the metal fail-safe and the ceramic filter element was apparently causing compression of the fail-safe gasketing. This gasket compression allowed the fail-safe to slip downward, opening up a gap at the fail-safe flange.)

The results of subsequent outlet measurements (TC02OMT-04, -05, and -06) showed that the leakage, which was at a level of 4.6 to 4.8 ppmw in late April, was increasing. As noted in the table, the leakage reached a level of 11.8 ppmw on May 13, when inability to maintain the cyclone dipleg seal forced a shutdown of the transport reactor system. Subsequent inspection of the filter internals during the shutdown confirmed that there was a sealing problem between the 3M elements and the fail-safes as discussed above. The 3M Corporation has since developed a ceramic insert that provides better sealing at the fail-safe flange and this modification has solved this leakage problem.

Collection Efficiency. The particle collection performance of the PCD was calculated from the inlet and outlet mass concentrations and the results are shown in table 3.5-3. The table contains both values of PCD collection efficiency (the percentage of particle mass collected) and the particle penetration of the PCD (percentage of particle mass that escapes collection). The outlet sampling runs were much longer in duration than the inlet runs (typically 6 hours versus 30 minutes) because of the great difference in mass concentration at the inlet and outlet. Since the inlet and outlet samples were not simultaneous, and because of considerable variability in the inlet concentration, the PCD performance values were calculated based on an inlet loading of 10,150 ppmw, which is the average of the four runs performed during stable operation with coal and dolomite. The very low collection efficiency recorded on April 13 is a consequence of particle penetration through the instrumented fail-safe discussed earlier. The other collection efficiencies are generally lower than those recorded during TC01, because of the leakage around the 3M element fail-safes discussed previously. Nevertheless, these efficiencies are still quite good compared to the performance of most particulate control systems that are currently operating on coal-fired power plants.

3.5.2 Measurements of Particle-Size Distributions

Inlet Measurements. Figure 3.5-1 shows particle-size distributions measured on two of the in situ mass samples discussed previously (TC02IMT-03 and -04). A representative particle-size distribution from one of the TC01 mass samples (TC01IMT-07) is also shown for comparison. All of these distributions were obtained by analyzing the mass samples on a Leeds & Northrup Microtrac X-100 particle-size analyzer. The results suggest that sample TC02IMT-04, which was collected on April 30, contained more fine particles ($D_p < 20$ µm) than did sample TC02IMT-03 collected on April 27. The higher concentration of fine particles may at least partially explain the higher mass loading measured on April 30 (10,900 ppmw versus 9,100 ppmw measured on April 27). The two mass loading measurements were made with nominally equivalent feed rates of coal and dolomite. The only intentionally introduced difference in process operating conditions was associated with changes in the staging of the combustion air implemented to examine the effect on NO_X emissions. Previous research has shown that the staging of combustion air can create localized reducing conditions that affect the volatilization of certain ash components, thereby altering fine-particle generation (Sarofim, et. al, *Combustion Science and Technology*, pgs. 187-201, 1977; Damle, et. al, *Aerosol Science and Technology*, pgs. 119-133, 1982).

Outlet Measurements. Figures 3.5-2 and -3 show particle-size distributions measured at the outlet of the PCD during TC02. These size distributions, which represent the average of three cascade impactor runs, confirm that the ash penetrating through the PCD is quite fine (mmd ≅ 3 µm). The cumulative percentage distribution is nearly linear when plotted in log-probability space (figure 3.5-2), indicating that the outlet-size distribution is almost perfectly log-normal and unimodal. A unimodal, log-normal size distribution usually indicates that the particles have been generated by a single mechanism or that one or more size modes have been eliminated by some sort of size-classifying mechanism. In this particular case the size-classifying mechanism could be associated with the leakage path between the tubesheet and the 3M filter elements discussed earlier. Preferential entrapment of large particles could produce an outlet-size distribution that is much finer than the inlet-size distribution, but some of the particles that penetrate through the PCD may still be large enough to be of concern from the standpoint of turbine blade erosion. In this particular case particles larger than 5 µm account for approximately 25 percent of the total particulate mass, or about 1.5 ppmw. While emissions of this magnitude may have an adverse impact on turbine operation, previous tests have documented that this particle penetration is substantially eliminated when all of the filter elements are intact and there is adequate sealing between the tubesheet, filter elements, and fail-safes.

3.5.3 Cut-Size Tests

Previous comparison of the particle-size distribution of dust collected on the PCD filters with the size distribution of dust suspended in the inlet gas stream has indicated the possibility that some particles may fall into the PCD hopper without reaching the filters. Since knowing the mass and size distribution of the dust actually collected on the PCD filters is critical to understanding PCD performance, three cut-size tests were performed to attempt to quantify this effect. These tests utilized the PCD ash removal system to attempt to collect only the particulate mass that settled into the hopper between back-pulses and to exclude the mass that entered the hopper after being pulsed off the filters. The drop-out mass was compared to the measured in

situ total mass concentration entering the PCD. The results of the measurements indicated that from 28 to 135 percent of the mass entering the PCD fell into the hopper before reaching the filters. Obviously these results are so scattered that they are not meaningful. Subsequent analysis of temperatures at the inlet and outlet of the screw cooler below the PCD hopper suggests that all of the ash from the most recent back-pulse may not have cleared the ash removal system when the "nonpulsed" dust was collected. Additional efforts will be made during TC03 to properly isolate the pulse versus drop-out mass.

3.5.4 Chemical Analyses

Table 3.5-4 summarizes the chemical composition of selected PCD hopper samples collected during TC02. Table 3.5-5 gives the same information for the isokinetically collected ash samples, while tables 3.5-6, -7, and -8 contain the data for the dustcake samples taken from the PCD candles during the post-TC02 PCD inspection. With the exception of the last table all of the analytical results are reported as the element on an ignited basis. The elemental concentrations are not reported in their oxide forms since calcium is predominantly present in the form of the sulfate and carbonate. Other ash constituents are also present as sulfates and carbonates as well as other forms such as silicates, aluminosilicates, halides, and sulfides.

Hopper Samples. Based on the hopper ash analyses shown in table 3.5-4 the calcium utilization (i.e., the percentage of the calcium that is converted to calcium sulfate on a molar basis) varied from about 41 to 88 percent depending on the test conditions and the amount of dolomite being added. These values of calcium utilization are generally in the range expected based on the observed SO_2 removals and the amount of dolomite injected. (At a dolomite-addition rate equivalent to a nominal Ca/S molar ratio of 2 to 1, the observed SO_2 removal was nearly 100 percent, which would correspond to a calcium utilization of 50 percent.) Since the raw dolomite contains equimolar amounts of calcium and magnesium and the inherent calcium in the coal is quite low (typically <1 percent of the coal ash) the calcium-to-magnesium molar ratio in the ash would be expected to be close to 1 to 1. The average value calculated from the hopper ash analysis is 0.99 to 1.0.

The hopper ash analyses were used to calculate the average chemical composition of the solids collected in the PCD assuming that all of the sulfur was present as $CaSO_4$ and all of the carbon was present as $CaCO_3$. Any remaining calcium that was not accounted for as $CaSO_4$ or $CaCO_3$ was assumed to be present as CaO•MgO. Any remaining magnesium that was not accounted for as CaO•MgO was assumed to be present as MgO. The balance of each sample was assumed to be ash and sand (bed material). The choice of these particular calcium and magnesium compounds was based on free-energy minimization calculations performed by Dr. L. Shadle at DOE/FETC as reported in the TC01 run report. The average TC02 chemical composition calculated in this manner is compared to the average composition for TC01 below.

	TC01 Hoppers (%)	TC02 Hoppers (%)
$CaSO_4$	9.3 to 13.3	10.6 to 17.0
CaO●MgO	6.5 to 11.5	0 to 9.2
$CaCO_3$	0.7 to 1.6	1.2 to 4.3
MgO	3.1 to 4.7	3.9 to 5.3
Ash/Sand	71.5 to 77.5	66.7 to 74.5

The lower limit of zero on the CaO●MgO was calculated for two hopper samples taken when the dolomite was turned off. While there is considerable overlap between the chemical compositions for TC01 and TC02 there appears to be a trend toward a higher degree of sulfation or higher calcium utilization during TC02.

In Situ Samples. Elemental analyses and calculated chemical compositions for the TC02 in situ samples are summarized in table 3.5-5. Calcium utilizations calculated for these samples tended to be slightly higher than the utilizations calculated for the hopper samples and are in closer agreement with observed SO_2 removals and nominal dolomite addition rates. The chemistry of the TC02 in situ samples cannot be compared to that of the TC01 in situ samples because the latter samples were not analyzed for sulfur. The information below compares the calculated chemical composition of the TC02 in situ samples to that of the hopper samples discussed above.

	TC02 In Situ (%)	TC02 Hoppers (%)
$CaSO_4$	6.4 to 15.5	10.6 to 17.0
CaO●MgO	0 to 9.4	0 to 9.2
$CaCO_3$	0.9 to 3.8	1.2 to 4.3
MgO	2.1 to 5.3	3.9 to 5.3
Ash/Sand	68.9 to 90.6	66.7 to 74.5

The lower limit of zero on the CaO●MgO for the in situ samples was calculated for one sample taken when the dolomite was turned off. As expected, in the absence of dolomite this same sample was 90.6-percent ash/sand. This effect was not evident in the hopper samples presumably because of the time-averaging effect of the ash collection and ash discharge systems. Overall, the calculated chemical compositions for in situ samples are generally in the same range as those of the hopper samples.

Dustcake Samples. Tables 3.5-6, -7, and -8 summarize the chemical and physical properties of several different types of dustcake samples removed during the PCD inspection at the end of TC02. Prior to the TC02 shutdown all system shutdowns had included extensive pulsing of the PCD during and after the shutdown, leaving only residual dustcake on the filter elements. The

shutdown executed at the end of TC02 followed a different procedure to also allow sampling of the transient dustcake. The coal feed was turned off at a point near the end of a filtration cycle, about 2 minutes before the next scheduled back-pulse. The back-pulse system was then disabled so as to preserve the entire (transient-plus-residual) dustcake on the filter elements. This procedure was intended to allow the collection of separate samples from the outer (so-called transient) layer and from the inner (so-called residual) layer, as well as samples of the entire dustcake. Characterization of these samples could then provide valuable information on the physical and chemical differences between these inner and outer layers of the dustcake and perhaps provide insight into the difference between the so-called transient and residual cakes. The following discussion will address the chemical differences. The differences in physical properties will be addressed in section 3.6 of this report.

Separate samples of the outer (transient) and inner (residual) layers were obtained by two different techniques. The transient layer in the first procedure was removed by gently tapping on the dustcake surface with a soft-bristle artist brush. The residual layer was then removed by scraping off all of the underlying material in the same area. In the second procedure the transient layer was removed using a scraper designed to leave behind a layer with a thickness of about 3/16 in. The residual, or 3/16-in. layer, was then removed by scraping off all the underlying material in the same area. These two methods of separating the dustcake into layers may or may not yield comparable results, depending on the actual thickness of the residual dustcake. Despite the possible differences in exactly where the dustcake is separated, either procedure should be sufficient for use in determining whether dustcake properties vary with thickness.

Table 3.5-6 illustrates the differences in chemical composition between the inner and outer layers of the dustcake. The most striking difference is in sulfur content. The transient layers contain 3.0- to 3.3-percent sulfur, expressed as the element, compared to 6.0- to 7.5-percent sulfur in the residual layers. It is very interesting that the molar ratio of calcium to sulfur in the residual layers is only 0.42 to 1 to 0.82 to 1, suggesting that the samples can contain over twice as much sulfur as expected if all of the sulfur were present as $CaSO_4$. The extra sulfur is presumably present as other sulfates (e.g., Na_2SO_4, K_2SO_4, and $Fe_2(SO_4)_3$) that are formed during the continuous, long-term exposure of the residual layer to SO_2. The following table compares the calculated compositions of the transient and residual dustcake layers to those of the hopper samples and in situ samples.

	Transient Cake (%)	Residual Cake (%)	TC02 In Situ (%)	TC02 Hoppers (%)
$CaSO_4$	13.0 to 14.2	24.0 to 31.8	6.4 to 15.5	10.6 to 17.0
CaO•MgO	0 to 2.1	0	0 to 9.4	0 to 9.2
$CaCO_3$	3.9 to 7.6	0.2 to 1.1	0.9 to 3.8	1.2 to 4.3
MgO	5.1 to 5.4	4.0 to 14.6	2.1 to 5.3	3.9 to 5.3
Ash/Sand	74.2 to 77.3	60.3 to 69.5	68.9 to 90.6	66.7 to 74.5

This comparison reveals that the composition of the transient dustcake is not substantially different from that of the hopper samples and the in situ samples. In contrast, the composition

of the residual dustcake is strikingly different from the composition of all other samples. The differences probably reflect the continued sulfation of any unreacted calcium in the residual dustcake. The absence of any CaO●MgO in the residual dustcake suggests that the sorbent has been completely converted to $CaSO_4$ and MgO.

Table 3.5-7 summarizes the chemical composition of the samples of the entire (transient plus residual) dustcake and compares them to the average properties of the transient and residual layers discussed above. The entire-cake samples were not removed from the same areas of the filter elements from which the separate transient and residual samples were obtained. Therefore, the dustcake properties given in table 3.5-7 are not directly comparable to those given previously in table 3.5-6. In terms of chemical composition the entire-cake samples contain more calcium and magnesium than either the transient or the residual layers. This difference in chemical composition cannot be explained by analytical variability and appears to indicate that there are significant variations in the make-up of the dustcake from one location to the next. (If this were not the case the composition of the entire-cake samples would lie somewhere between those of the transient cakes and those of the residual cakes.) Additional analyses to investigate these variations further were performed on dustcake samples obtained from each type of filter element. Results of these analyses are summarized in table 3.5-8 along with corresponding measurements of dustcake thickness and qualitative statements concerning dustcake tenacity. These results do not show any discernible trends with respect to variations in the chemical composition of the dustcake.

3.5.5 Measurements of Physical Properties

Tables 3.5-9 and -10 give a summary of physical measurements made on the TC02 in situ samples and hopper samples. The measured parameters included: true (skeletal particle) density, bulk density, uncompacted bulk porosity (UBP), BET surface area, mass median diameter (MMD), and drag-equivalent diameter (DED). The DED is not a physical size, but rather is a fitted parameter that can be used to rank the characteristic gas-flow resistance of ashes at equal porosities. Measurements of physical size generally correlate with DED, but the DED best expresses the fineness of an ash as it relates to its effect on gas-flow resistance (drag). Increasing values of DED indicate lower resistance to gas flow (less drag) at a given porosity. Using the DED as an indicator of flow resistance eliminates much of the ambiguity associated with drag measurements, which are a strong function of porosity. DED was measured on all of the hopper samples discussed previously and on all of the dustcake samples listed in tables 3.5-6 and -7. DED was not measured on the in situ samples because an inadequate amount of sample was left after other tests.

True density measurements were made by helium pycnometry using a Quantachrome Model 1000 Ultrapycnometer. Bulk density was determined by measuring the volume of a known weight of ash and uncompacted bulk porosity was calculated from the true density and bulk density. Specific surface area was determined by the BET method using a Micromeritics FloSorb-II analyzer and the MMD was based on particle-size analysis on a Leeds & Northrup Microtrac X-100 analyzer.

In situ Samples. Table 3.5-9 contains the physical properties measured for in situ samples collected during TC02. With the exception of the last in situ sample, which was obtained during a dipleg upset just prior to shutdown, all of the in situ samples have generally similar mean particle sizes in the range of 19 to 27 μm. In terms of other physical properties, however, differences can be seen when comparing the steady-state samples to samples obtained during start-up and during the dipleg upset just prior to shutdown.

Hopper Samples. Physical properties of selected TC02 hopper samples are summarized in table 3.5-10. These results suggest that the particles carried out of the transport reactor system during start-up (MMD ≅ 217 μm) are much larger than the particles generated during steady-state operation (MMD ≅ 27 to 51 μm). As noted in previous tests, the hopper samples are also generally coarser than the in situ samples.

Dustcake Samples. Dustcake properties given in tables 3.5-6, -7, and -8 are in conjunction with the elemental analyses of the samples. Before discussing the variation in physical properties shown in these tables it is important to understand some other observations concerning the dustcake thickness and tenacity. Considerable variation was noted in the thickness and tenacity of the dustcake during the post-TC02 inspection of the PCD internals. Measured thicknesses of the entire cake (transient plus residual) varied from 0.145 to 0.266 inchs. This variation in dustcake thickness is not too surprising given that the filter elements have different permeabilities. Since the total pressure drop across the filter element and dustcake must be the same for all elements the dustcake thickness must vary with the type of element. Even on a given filter element the thickness varied by as much as a factor of 2. This result is somewhat more surprising and may reflect variations in dustcake permeability related to particle-size effects or other differences. Since particle-size-fractionation mechanisms (i.e., swirl effects and settling) are at work in the filter vessel it is reasonable to expect that the mean-particle size in one location of the filter vessel may be different from the mean-particle size in another location. These particle-size differences would be expected to produce differences in dustcake permeability and corresponding variations in dustcake thickness.

Dustcake tenacity, judged qualitatively while brushing away portions of the cake, also revealed considerable variability from one filter element to the next but appeared to be relatively consistent on a given element. There was some indication that the residual dustcake was most easily released from the 3M oxide elements and the DuPont PRD-66 elements, which might be expected in view of the relatively smooth surface finish on these elements.

Table 3.5-6 shows two sets of inner-outer samples obtained from the bottom plenum and one set from the top plenum. Comparison of the physical properties of the outer (transient) and inner (residual) layers from the bottom plenum reveals the outer layers appear to have larger mean-particle sizes, lower specific-surface areas, and larger drag-equivalent diameters (i.e., lower flow resistances) than do the residual layers.

Table 3.5-7 shows the physical properties of the two dustcake layers as compared to the properties of the entire dustcake (transient and residual layers) taken from different locations within the PCD. In this comparison it is clear that the particle-size distribution was relatively coarse on the elements where the entire-dustcake samples were removed. This difference in

particle size is reflected in the lower specific surface areas and lower gas-flow resistance in the entire-cake samples.

Table 3.5-8 provides a comparison of the physical properties of entire dustcake samples taken from various types of filter elements. This comparison does not reveal any systematic variation in the dustcake properties as a function of the type of element on which the cake is collected. However, it is noteworthy that the thickest dustcake formed on the Pall 442T elements, which have the highest permeability of any of the elements tested. Additional testing is needed to investigate the relationship between dustcake thickness and filter element permeability.

Physical properties of the TC02 in situ, hopper, and dustcake samples are summarized and compared in the following table.

	Steady-State In Situ	Steady-State Hopper	Transient Cake	Residual Cake
True Density (g/cm^3)	2.48 to 2.66	2.51 to 2.66	2.59 to 2.64	2.66 to 2.71
Bulk Density (g/cm^3)	0.47 to 0.54	0.54 to 0.77	0.46 to 0.52	0.47 to 0.60
UBP (%)	79.1 to 82.1	71.2 to 78.5	80.3 to 82.6	77.4 to 83.2
Surface Area (m^2/g)	1.66 to 2.35	ND	2.21 to 2.51	2.48 to 3.18
MMD (μm)	19.3 to 25.9	27.4 to 51.1	8.8 to 13.7	8.4 to 9.3
DED (μm)	ND	3.1 to 4.2	2.0 to 2.2	1.7 to 1.9
Calcium (Wt %)	1.74 to 9.13	5.22 to 9.71	4.50 to 6.68	3.49 to 5.82

ND = Not Determined.

In terms of the physical properties listed above, the in situ samples and dustcake samples appear to have lower bulk densities and, therefore, higher porosities than do the hopper samples. As expected, the dustcake samples have smaller mean particle sizes than do the in situ and hopper samples. As mentioned earlier, the residual dustcake has smaller mean particle size and lower DED (i.e., more drag) than the transient dustcake.

Work is continuing to develop a better understanding of how flow resistance, or DED, varies with various parameters. Previous tests with fabric filters have shown a correlation between DED and calcium content (Bush, Snyder, and Chang, "Determination of Baghouse Performance from Coal and Ash Properties: Part II," *J. Air Pollut Control Assoc*, 39 (3), pp. 361-372). Figure 3.5-4 illustrates the results of several attempts to correlate these parameters using the data on TC02 dustcake samples. Figure 3.5-5 shows a plot of similar data for the TC02 hopper samples and figure 3.5-6 shows a combined plot of all TC02 dustcake and hopper data. Inadequate sample size precluded the measurement of DED values for the TC02 in situ samples. Although the regressions illustrated on these plots have relatively low-correlation coefficients ($r^2 < 0.79$) there definitely appears to be a trend toward increasing DED (decreasing drag) with increasing calcium content.

Table 3.5-1

PCD Inlet Particulate Mass Loading Data for Test Program TC02

SRI Run No.	Date	Start	End	Loading (ppmw)	Condition
TC02IMT-01	4/09/98	15:05	15:35	11,400	Start-up solids circulation
TC02IMT-02	4/10/98	14:30	15:00	2,800	Transition to coal
TC02IMT-03	4/27/98	10:50	11:15	9,100	Stable, No PCD back-pulse
TC02IMT-04	4/30/98	13:13	13:23	10,900	Stable, No PCD back-pulse
TC02IMT-05	5/01/98	13:20	13:50	9,500	Stable, PCD back-pulsed
TC02IMT-06	5/06/98	12:57	13:04	11,100	Stable, No PCD back-pulse
TC02IMT-07	5/11/98	8:55	9:25	5,100	Stable, No dolomite addition
TC02IMT-08	5/13/98	9:35	10:05	18,500	Unstable, Dipleg upset

Table 3.5-2

PCD Outlet Particulate Mass Loading Data for Test Program TC02

SRI Run No.	Date	Start	End	Loading (ppmw)	Condition
TC02OMT-01	4/13/98	8:20	9:20	720	Broken elements
TC02OMT-02	4/23/98	8:50	13:20	4.56	Leaks around gaskets
TC02OMT-03	4/24/98	8:45	13:15	4.78	Leaks around gaskets
TC02OMT-04	5/5/98	8:35	13:05	6.13	Leaks around gaskets
TC02OMT-05	5/7/98	9:35	13:25	8.19	Leaks around gaskets
TC02OMT-06	5/13/98	8:50	12:00	11.8	Leaks around gaskets

Table 3.5-3

PCD Particulate Collection Efficiencies for Test Program TCO2

SRI Outlet Run No	Outlet Run Date	Outlet Run Time		Loadings (ppmw)		Efficiency (%)	Penetration (%)
		Start	End	Inlet[1]	Outlet		
TCO2OMT-01	4/13/98	8:20	9:20	10,150	720	92.91	7.09
TCO2OMT-02	4/23/98	8:50	13:20	10,150	4.56	99.96	0.04
TCO2OMT-03	4/24/98	8:45	13:15	10,150	4.78	99.95	0.05
TCO2OMT-04	5/5/98	8:35	13:05	10,150	6.13	99.94	0.06
TCO2OMT-05	5/7/98	9:35	13:25	10,150	8.19	99.92	0.08
TCO2OMT-06	5/13/98	8:50	12:00	10,150	11.8	99.88	0.12

Note: 1. Inlet loading used in these calculations is the average value for the four inlet sampling runs performed during stable reactor operation with dolomite addition.

Table 3.5-4

Elemental Analysis of Selected TCO2 Hopper Samples[1]

I.D. No. (ABO-)	2772	2870	2968	2969	3084	3103	3118
Date Collected	4/10/98	4/27/98	4/30/98	5/1/98	5/11/98	5/11/98	5/13/98
Time of Day	16:15	08:00	16:00	00:00	08:00	16:00	08:00
Measured Composition							
Silicon (%)	37.98	23.11	20.44	21.49	25.99	26.90	21.21
Aluminum (%)	2.97	11.19	8.77	10.59	9.39	9.37	9.77
Titanium (%)	0.70	0.59	0.48	0.54	0.54	0.54	0.53
Iron (%)	1.67	3.06	2.55	2.92	2.96	2.95	2.70
Calcium (%)	1.24	7.67	9.71	8.53	5.22	5.65	8.43
Magnesium (%)	0.80	4.49	5.83	5.12	3.38	3.57	5.24
Potassium (%)	1.02	1.01	0.83	0.88	1.02	1.00	0.45
Sodium (%)	0.14	0.39	0.58	0.62	1.02	1.09	0.34
Phosphorous (%)	0.04	0.17	0.14	0.19	0.27	0.26	0.22
Sulfur (%)	0.00	2.49	3.16	3.16	3.69	3.99	2.85
Carbon (%)	0.30	0.29	0.58	0.54	0.41	0.35	0.93
Oxygen (%) (diff)	53.14	45.54	46.93	45.42	46.11	44.33	47.33
Calculated Parameters							
Utilization (%)[2]	0.00	40.6	40.7	46.3	88.4	88.3	42.3
Ca/S Molar Ratio	N/A	2.46	2.46	2.16	1.13	1.13	2.37
Ca/Mg Molar Ratio	0.94	1.04	1.01	1.01	0.94	0.96	0.98
$CaCO_3$ (%)	2.50	2.42	4.83	4.50	3.42	2.92	7.75
$CaSO_4$ (%)	0.00	10.58	13.43	13.43	15.68	16.96	12.11
CaO•MgO (%)	0.58	8.64	9.21	6.69	0.00	0.00	4.26
MgO (%)	1.08	3.83	5.81	3.43	5.61	5.92	6.91
Ash/Sand (%) (diff)	95.84	74.53	66.72	71.95	71.44	74.20	68.97

Notes: (1) Wt% ignited basis expressed as element (not oxide).
(2) Calcium utilization (i.e., % of Ca converted to $CaSO_4$ on a molar basis).

Table 3.5-5

Elemental Analysis of TCO2 In situ Samples[1]

I.D. No. (TCO2I-)	MT-1	MT-2	MT-3	MT-4	MT-5	MT-6	MT-7	MT-8
Date Collected	4/09/98	4/10/98	4/27/98	4/30/98	5/01/98	5/06/98	5/11/98	5/13/98
Time of Day	15:05	14:30	10:50	13:13	13:20	12:57	08:55	09:35
Time	15:35	15:00	11:15	13:23	13:50	13:04	09:25	10:05
Measured Composition								
Silicon (%)	39.19	30.82	19.67	22.33	21.67	19.69	26.03	30.11
Aluminum (%)	4.09	13.71	12.90	15.06	11.20	12.96	12.50	7.88
Titanium (%)	0.22	0.75	0.56	0.71	0.57	0.58	0.71	0.34
Iron (%)	1.40	3.95	3.08	3.77	3.28	3.61	3.80	4.12
Calcium (%)	1.23	0.86	9.13	8.65	7.15	8.55	1.74	6.23
Magnesium (%)	0.61	0.83	5.47	5.27	4.29	5.01	1.28	0.46
Potassium (%)	0.55	0.48	0.40	0.25	0.42	0.25	0.99	0.62
Sodium (%)	0.64	0.58	0.66	2.38	0.87	0.72	1.12	0.42
Phosphorous (%)	0.14	0.24	0.08	0.18	0.23	0.19	0.35	0.09
Sulfur (%)	0.58	0.62	3.04	3.29	3.65	3.58	1.50	3.15
Carbon (%)	0.48	0.22	0.46	0.19	0.13	0.31	0.11	0.54
Oxygen (%) (diff)	50.87	46.94	44.55	37.92	46.54	44.55	49.87	46.04
Calculated Parameters								
Utilization (%)[2]	58.9	90.1	41.6	47.5	63.8	52.3	107.7	63.2
Ca/S Molar Ratio	1.70	1.11	2.40	2.10	1.57	1.91	0.93	1.58
Ca/Mg Molar Ratio	0.74	0.63	1.01	1.00	1.01	1.04	0.83	8.23
$CaCO_3$ (%)	4.00	1.83	3.83	1.58	1.08	2.58	0.92	4.50
$CaSO_4$ (%)	2.47	2.64	12.92	13.98	15.51	15.22	6.38	13.39
CaO•MgO (%)	0.00	0.00	9.14	9.40	5.19	7.32	0.00	1.19
MgO (%)	1.01	1.38	5.25	4.81	4.94	5.25	2.12	0.26
Ash/Sand (%) (diff)	92.52	94.15	68.86	70.23	73.28	69.63	90.58	80.66

Notes: (1) Wt% ignited basis expressed as element (not oxide).
(2) Calcium utilization (i.e., % of Ca converted to $CaSO_4$ on a molar basis).

Table 3.5-6

Elemental Analysis and Characteristics of Layered TCO2 Dustcake Samples[1]

I.D. No. (ABO-)	3158	3157	3161	3159	3162	3160
Type of Sample	Transient[1]	Residual[1]	Transient[1]	Residual[1]	Transient[1]	Residual[2]
Plenum	Bottom	Bottom	Bottom	Bottom	Top	Top
Date Sampled	5/18/98	5/18/98	5/18/98	5/18/98	5/18/98	5/18/98
True Density (g/cm^3)	2.64	2.71	2.59	2.66	2.64	2.69
Bulk Density (g/cm^3)	0.46	0.47	0.51	0.60	0.52	0.49
Uncompacted Bulk Porosity	82.6	83.2	80.3	77.4	80.3	81.8
Surface Area (m^2/g)	2.31	3.18	2.21	2.48	2.51	2.61
Mass Median Diameter (μm)	13.70	9.26	11.74	9.28	8.75	8.43
Drag-Equivalent Diameter	NM[3]	NM[3]	2.19	1.86	1.97	1.73
Silicon (Wt% as Element)	20.41	18.69	22.10	17.89	20.37	19.56
Aluminum (Wt% as Element)	10.01	9.53	11.58	9.09	10.64	14.52
Calcium (Wt% as Element)	4.50	3.97	6.68	3.49	5.66	5.82
Magnesium (Wt% as	3.14	2.76	3.80	2.44	3.16	8.80
Iron (Wt% as Element)	4.22	3.76	3.77	3.68	3.51	4.00
Titanium (Wt% as Element)	0.60	0.65	0.66	0.59	0.63	1.07
Potassium (Wt% as Element)	1.64	1.47	.099	1.48	0.82	1.01
Sodium (Wt% as Element)	0.24	0.29	0.49	0.15	0.49	0.61
Phosphorous (Wt% as	0.34	0.33	0.28	0.31	0.26	0.32
Sulfur (Wt% as Element)	3.05	7.48	3.35	6.01	3.16	5.65
Carbon (Wt% as Element)	0.91	0.02	0.49	0.12	0.47	0.13
Oxygen (Wt% by Difference)	50.94	51.05	45.81	54.75	50.83	38.51
Ca-to-Mg Molar Ratio	0.87	0.87	1.07	0.87	1.09	0.40
Ca-to-S Molar Ratio	1.18	0.42	1.60	0.46	1.43	0.82

Notes:
1. Transient layer removed by brush technique described in text.
2. Transient layer removed by scraping as described in text.
3. Not measured; insufficient sample.

Table 3.5-7

Elemental Analysis and Characteristics of Layers Compared to Entire Cake

I.D. No. (ABO-)	3163	3164	Average	Average	Average
Type of Sample	Entire Cake	Entire Cake	Entire Cake	Transient	Residual
Plenum	Bottom	Top	Both	Both	Both
Date Sampled	5/18/98	5/18/98	5/18/98	5/18/98	5/18/98
True Density (g/cm^3)	2.62	2.61	2.62	2.62	2.69
Bulk Density (g/cm^3)	0.58	0.51	0.55	0.50	0.52
Uncompacted Bulk	77.9	80.5	79.16	81.06	80.80
Surface Area (m^2/g)	1.96	2.18	2.07	2.34	2.76
Mass Median Diameter	20.88	18.87	19.88	11.40	8.99
Drag-Equivalent Diameter	3.04	2.06	2.55	2.08	1.80
Silicon (Wt% as Element)	20.08	21.90	20.99	20.96	18.71
Aluminum (Wt% as	10.47	11.22	10.85	10.74	11.05
Calcium (Wt% as Element)	7.98	7.33	7.66	5.61	4.43
Magnesium (Wt% as	4.62	4.21	4.42	3.37	4.67
Iron (Wt% as Element)	3.39	3.67	3.53	3.83	3.81
Titanium (Wt% as Element)	0.60	0.64	0.62	0.63	0.77
Potassium (Wt% as	0.81	0.78	0.80	1.15	1.32
Sodium (Wt% as Element)	0.51	0.55	0.53	0.41	0.35
Phosphorous (Wt% as	0.25	0.28	0.27	0.29	0.32
Sulfur (Wt% as Element)	5.04	4.26	4.65	3.19	6.38
Carbon (Wt% as Element)	0.34	0.36	0.35	0.62	0.09
Oxygen (Wt% by	45.91	44.80	45.36	49.19	48.10
Ca-to-Mg Molar Ratio	1.05	1.06	1.05	1.01	0.71
Ca-to-S Molar Ratio	1.27	1.38	1.32	1.40	0.57

Table 3.5-8

Characteristics of Dustcake Samples Taken From Various Types of Filter Elements

Type of Element	Element Location	Dustcake Thickness (in.)	Dustcake Tenacity	MMD (μm)	Wt% SiO_2	Wt % Al_2O_3	Wt % CaO	Wt % MgO	Wt % SO_3	Ca/Mg Ratio	Ca/S Ratio
IF&P REECER	B-35	0.150	Intermediate	11.69	46.45	21.37	9.51	6.53	9.85	1.04	1.38
Schumacher T10-20	B-8	0.175	Intermediate	8.78	46.45	21.82	9.44	6.47	11.60	1.04	1.16
3M Oxide	B-18	0.206	Easily Released	10.75	44.41	20.31	9.01	6.38	11.08	1.01	1.16
Pall 326	B-32	0.210	Tenacious	8.48	44.69	20.65	9.11	6.19	11.23	1.05	1.16
DuPont PRD-66	B-14	0.219	Easily Released	10.84	46.00	21.33	9.40	6.28	12.85	1.07	1.05
Pall Iron Aluminide	B-6	0.226	Intermediate	8.97	48.54	22.39	8.54	5.74	9.68	1.06	1.26
3M Type 203	B-17	0.235	Intermediate	8.72	43.64	21.50	7.78	5.51	10.40	1.01	1.07
McDermott Oxide	B-20	0.237	Tenacious	9.09	48.89	23.32	8.49	5.67	10.38	1.07	1.17
Pall 442T	B-15	0.266	Tenacious	9.23	46.70	22.20	9.02	6.04	11.20	1.07	1.15

Table 3.5-9

Physical Properties of TCO2 In Situ Samples

Run Number	Date Sampled	Nominal Ca/S Ratio Injected	True Density (g/cm^3)	Bulk Density (g/cm^3)	UBP[1] (%)	Surface Area (m^2/g)	MMD[2] (μm)
Start-Up and Transition to Coal							
TCO2IMT-01	4/09/98	0	2.69	0.68	74.7	4.94	27.2
TCO2IMT-02	4/10/98	0	2.46	0.41	83.3	2.02	20.8
Average for Start-up and Transition			2.58	0.55	79.0	3.48	24.0
Steady-State With Dolomite							
TCO2IMT-03	4/27/98	2:1	2.62	0.53	79.8	2.10	25.9
TCO2IMT-04	4/30/98	2:1	2.66	0.50	81.2	2.35	21.5
TCO2IMT-05	5/01/98	1.5:1	2.58	0.54	79.1	2.28	19.5
TCO2IMT-06	5/06/98	2:1	2.62	0.47	82.1	1.66	19.3
Average for Steady-State With Dolomite			2.62	0.51	80.6	2.10	21.6
Steady-State Without Dolomite							
TCO2IMT-07	5/11/98	0	2.48	0.48	80.6	1.66	21.0
Dipleg Upset Just Prior to Shutdown							
TCO2IMT-08	5/13/98	1.5:1	2.64	0.84	68.2	0.99	72.1

Notes: (1) Uncompacted bulk porosity.
(2) Mass median diameter.

Table 3.5-10

Physical Properties of Selected TC02 Hopper Samples

Date Collected	Nominal Ca/S Ratio Injected	Lab ID No.	True Density (g/cm^3)	Bulk Density (g/cm^3)	UBP[1] (%)	Surface Area (m^2/g)	MMD[2] (μm)	DED[3] (μm)
Start-Up and Transition to Coal								
4/10/98	0	AB02772	2.64	1.48	43.9	N.D.[4]	216.9	23.7
Steady-State With Dolomite								
4/27/98	2:1	AB02870	2.54	0.69	72.8	N.D.	31.3	3.80
4/30/98	2:1	AB02968	2.67	0.77	71.2	N.D.	51.1	4.23
5/01/98	1.5:1	AB02969	2.66	0.71	73.3	N.D.	27.4	3.74
Average for Steady-State With Dolomite			2.62	0.72	72.4	N.D.	36.6	3.92
Steady-State Without Dolomite								
5/11/98	0	AB03084	2.51	0.54	78.5	N.D.	38.7	3.07
5/11/98	0	AB03103	2.51	0.56	77.7	N.D.	28.5	3.59
Average for Steady-State W/O Dolomite			2.51	0.55	78.1	N.D.	33.6	3.33
Dipleg Upset Just Prior to Shutdown								
5/13/98	1.5:1	AB03118	2.59	0.47	81.9	N.D.	29.24	3.10

Notes: (1) Uncompacted bulk porosity.
(2) Mass median diameter.
(3) Drag equivalent diameter.
(4) Not determined.

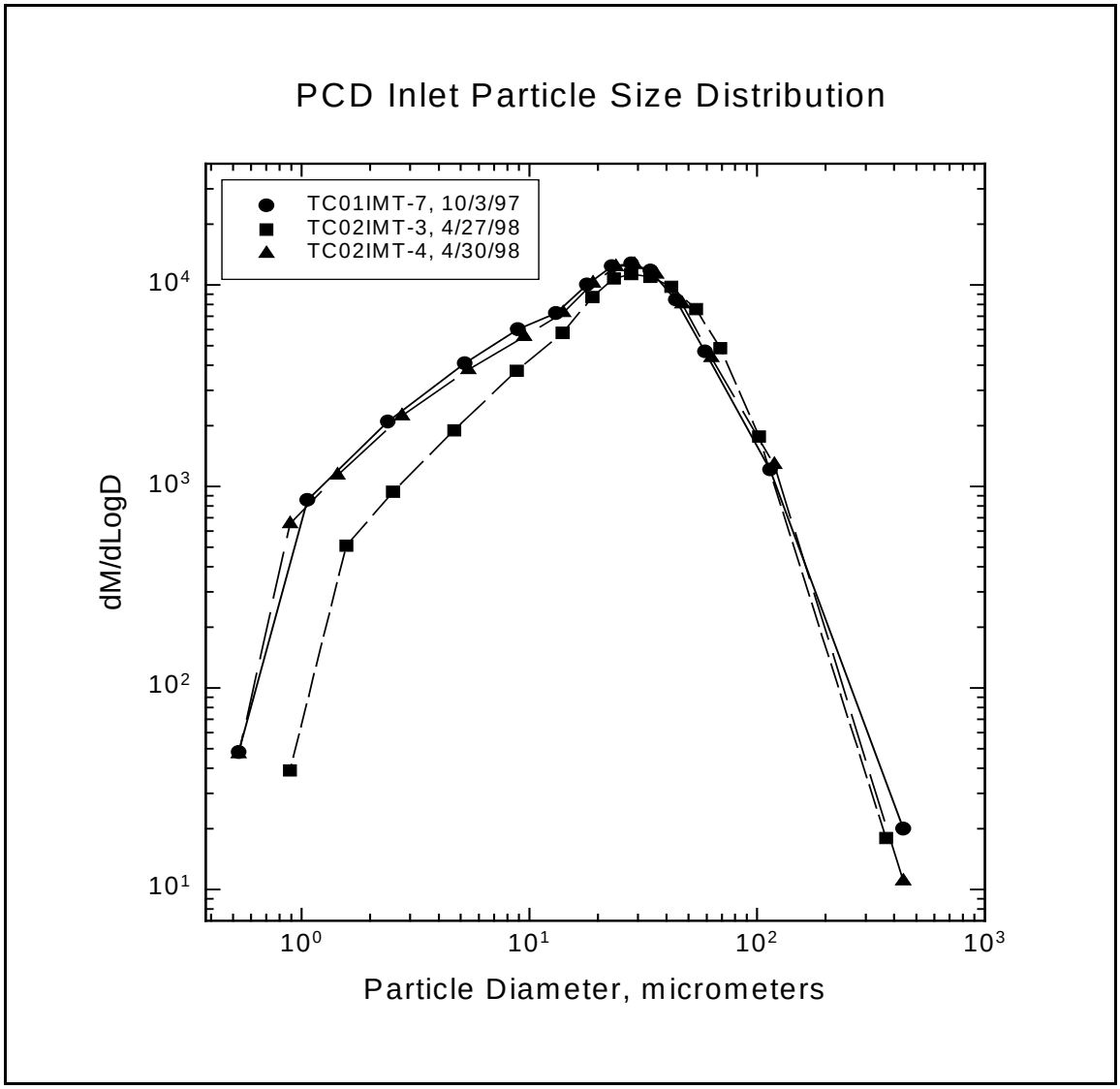

Figure 3.5-1 Differential Mass Distributions of Selected Inlet Particulate Samples

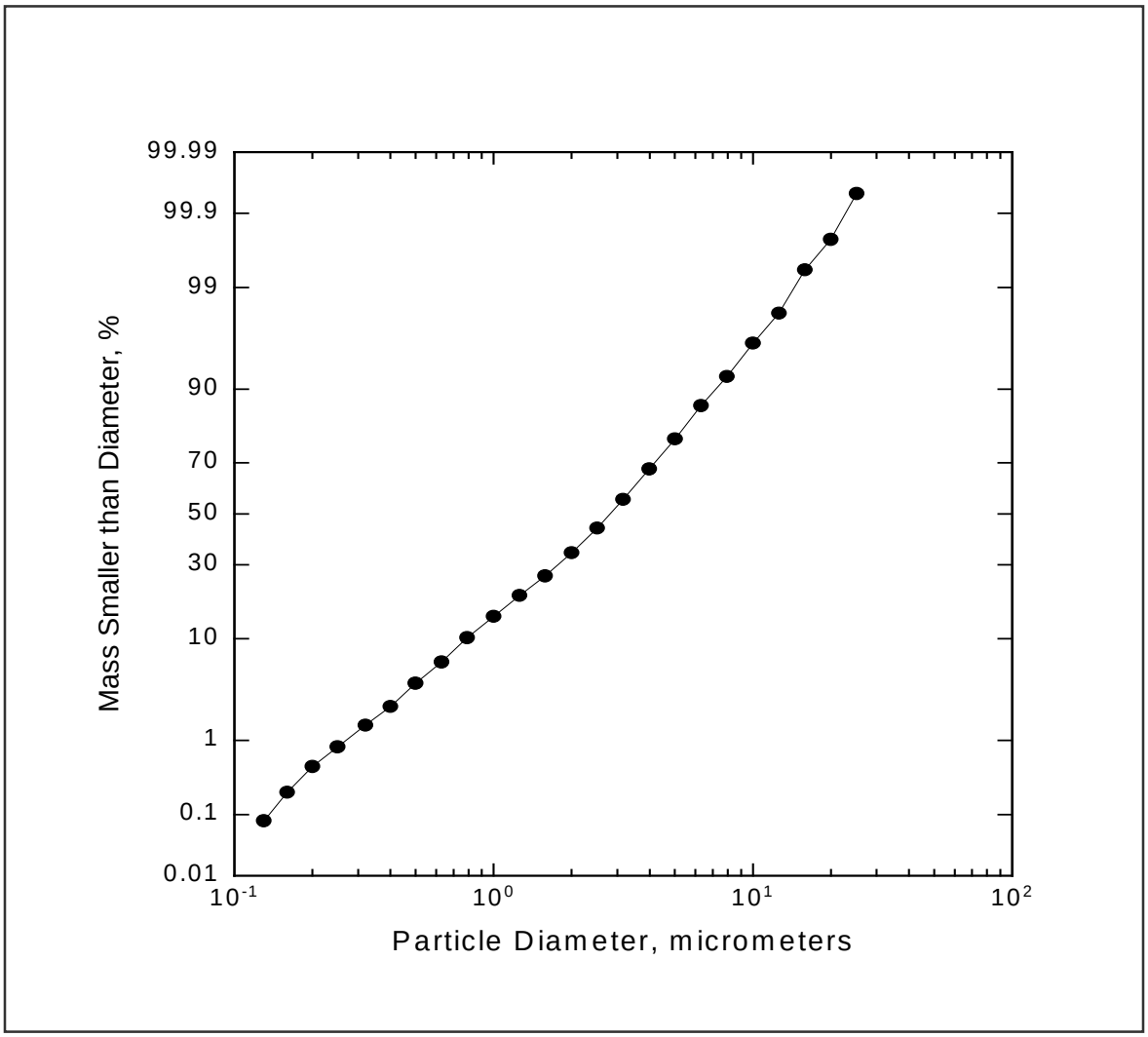

Figure 3.5-2 Cumulative Percentage Mass Distribution Measured at PCD Outlet (Average of Three Cascade Impactor Runs)

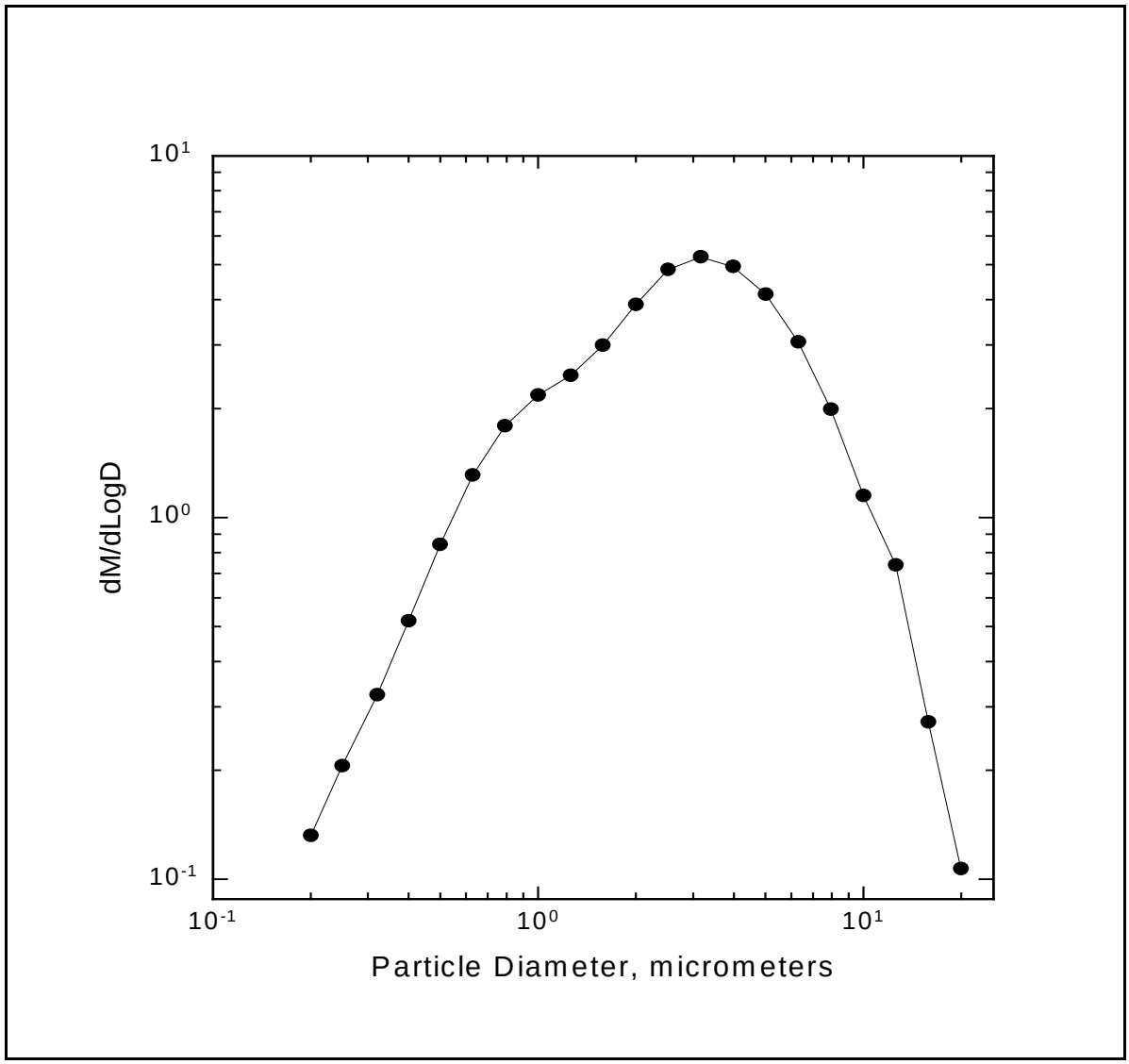

Figure 3.5-3 Differential Mass Distribution Measured at PCD Outlet
(Average of Three Cascade Impactor Runs)

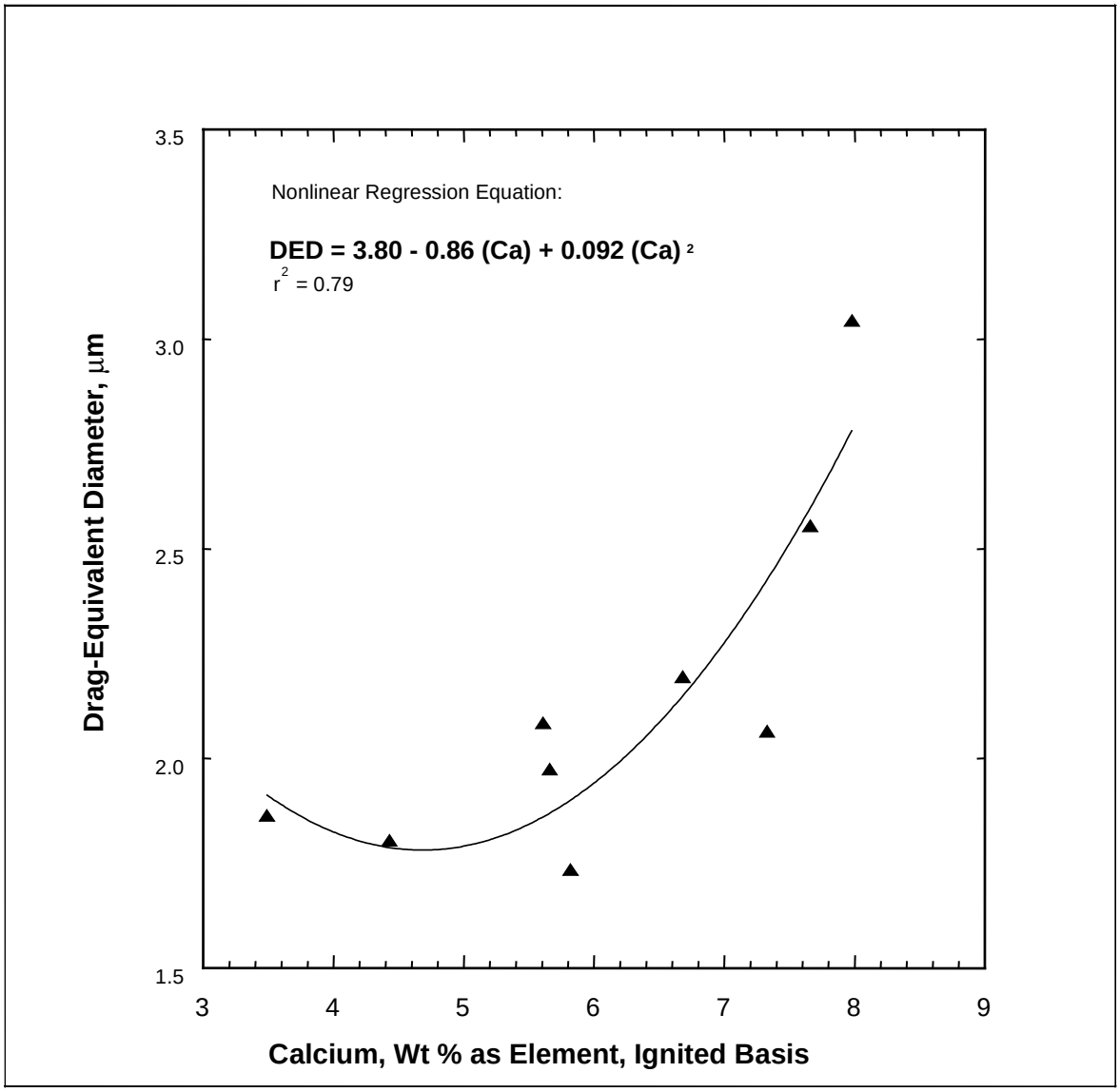

Figure 3.5-4 Drag-Equivalent Diameter Versus Calcium Content of TCO2 Dustcake Samples

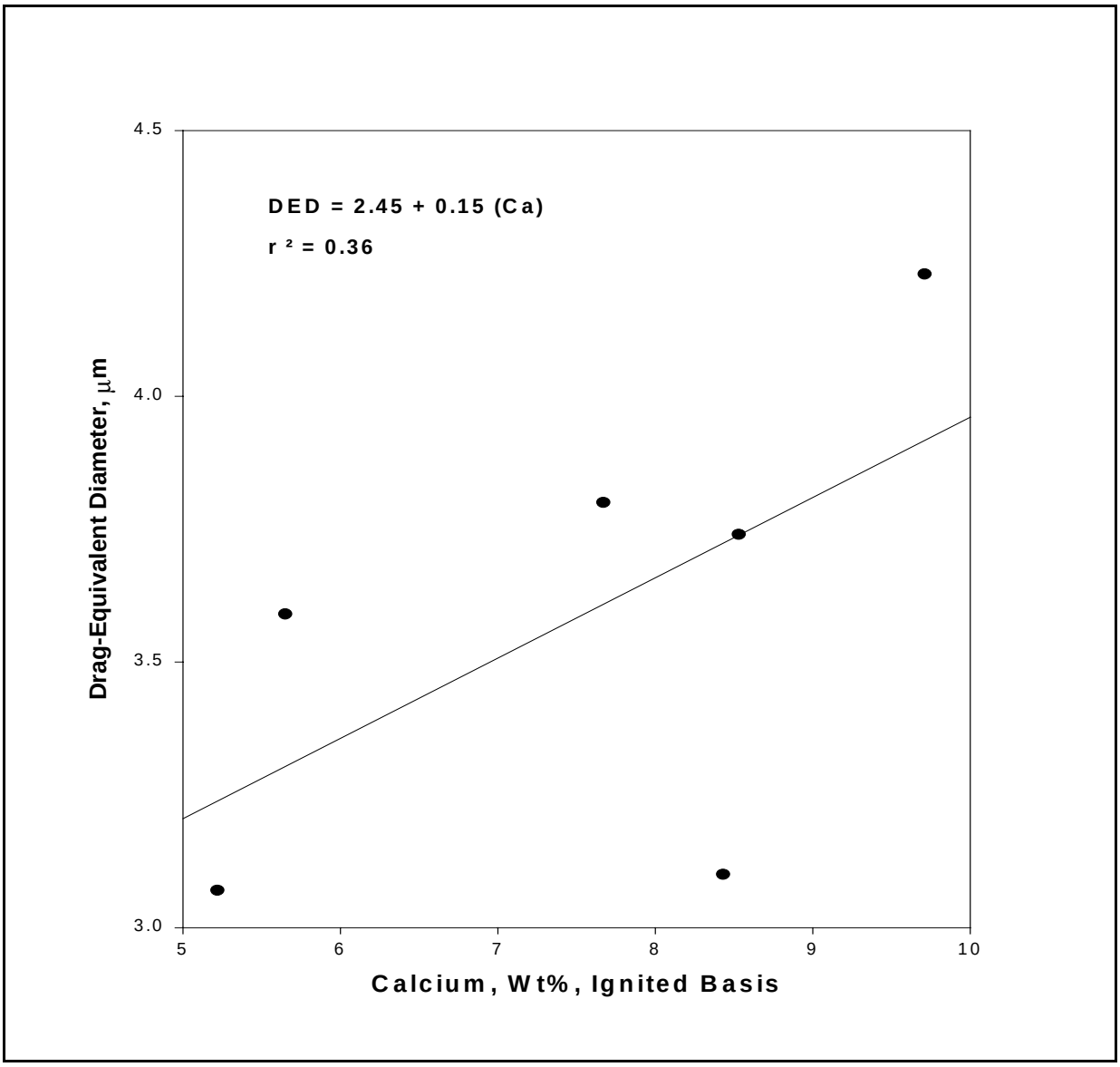

Figure 3.5-5 Drag-Equivalent Diameter Versus Calcium Content of TCO2 Hopper Samples

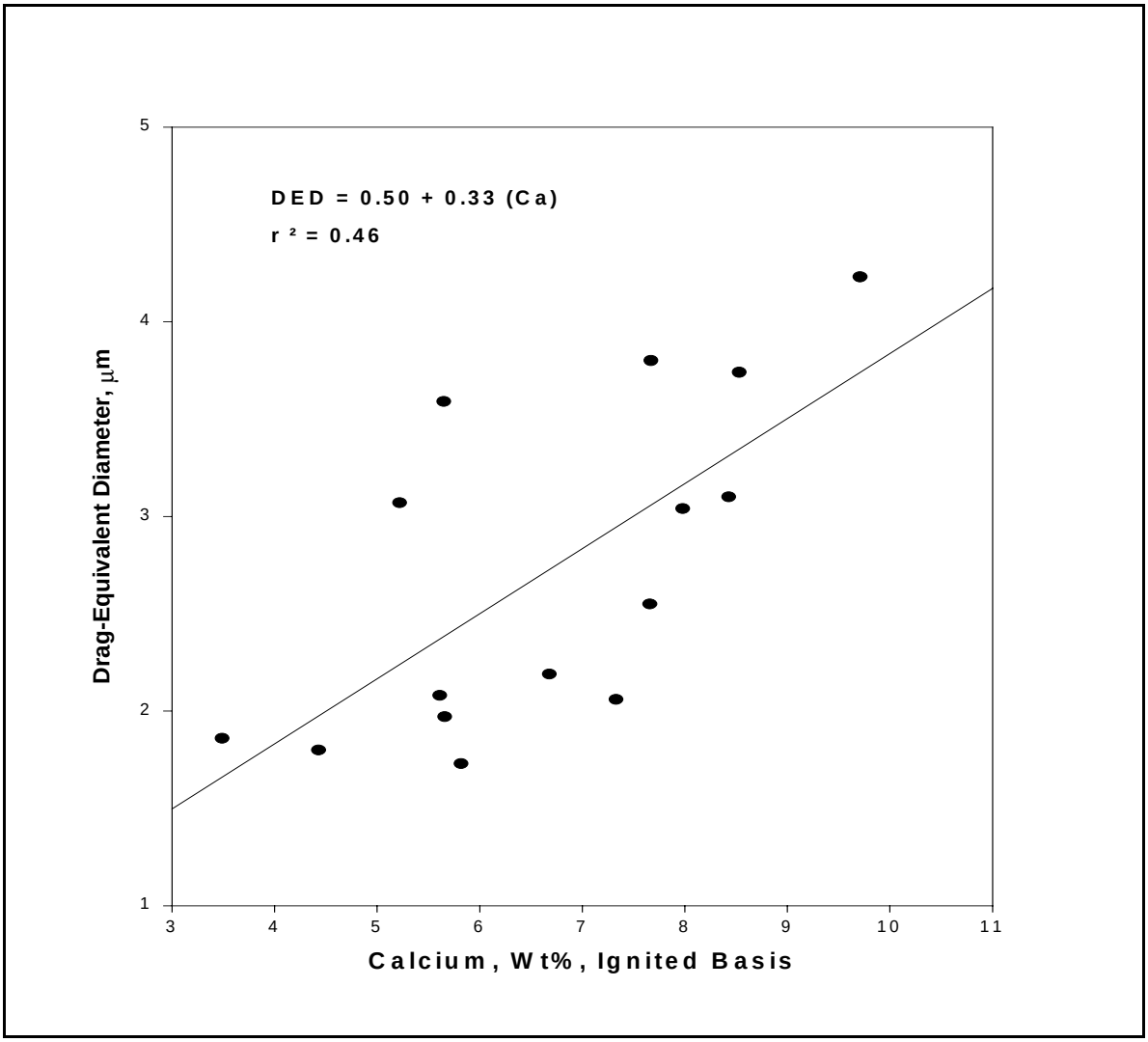

Figure 3.5-6 Drag-Equivalent Diameter Versus Calcium Content for All TCO2 Dustcake and Hopper Samples

3.6 COAX VALVE TESTING AFTER MODIFICATION

3.6.1 Test Objectives

The main objective of this testing was to evaluate the improvement of valve performance after the valve manufacturer modified the valves. More data was acquired to establish a database for controlling PCD operations.

3.6.2 Introduction

In previous operations the back-pulse valves (Müller SVS-F80) did not perform properly in the region of high-valve-differential pressure (ΔP, pressure difference between the accumulator tank and the PCD). Systematic valve testing in TC01 revealed that the mass discharge during a back-pulse decreased as the valve differential pressure exceeded a certain value[1]. Characteristic analysis concluded that the valves had design shortcomings that resulted in insufficient actuation force at high ΔP.

The valve manufacturer (Müller Coax) modified the valves after test run TC01 (four valves on the KBR side and four on the Foster Wheeler side). The major changes included a larger piston size, better seat profile, and seal modification. The valves were then reinstalled prior to test run TC02. The four valves on the KBR side were tested during the TC02 to verify the improvement of valve performance. The valve testing included consistency and characteristic tests.

Consistency testing was comprised of testing the four valves under the same operating conditions to confirm that the performance of the four valves was consistent. Three valves were extensively tested after the consistency was confirmed to characterize the opening behavior. The test data was analyzed and compared with data obtained before the valve modification. The results showed that the valve performance was significantly improved in the test region.

The detailed testing procedure and data analysis methods are not reported here (see reference (1) at the end of this chapter for the original testing prior to valve modifications).

3.6.3 Test Procedure

Table 3.6-1 shows the test parameters. Fourteen tests were conducted for different purposes. The electrical pulse duration "t" was varied from 0.1 to 1.2 seconds. The pilot pressure P_{pilot}, was either instrument air (IA, 105 psig) or nitrogen (N_2, 100-140 psig through a regulator). (It should be noted that the pressure gauge on the nitrogen pilot line had a +5 psi system error in the region of 100-140 psig.) The same gauge pressures (100, 120, and 140 psig) were used in this testing to keep the data comparable to the previous results.

[1] Technical Progress Report for M. W. Kellogg Transport Reactor Train With Westinghouse Particulate Control Device, January 1997 - December 1997, Section 3.27, prepared by Southern Company Services, Inc., DOE Cooperative Agreement Number DE-FC21-90MC25140, December 1998.

3.6.4 Results and Observations

Test results were analyzed in two categories: mass discharge and characteristic times. Mass discharge was calculated from the measured pressure and temperature changes in the accumulator tanks during a back-pulse. The characteristic times include fully open time, response time, time-to-open, and time-to-close (see reference (1) at the end of this chapter for detailed definitions).

3.6.4.1 Consistency Test

Consistency tests were conducted at P_{pilot} = 105 psig and t = 0.4 sec. Figures 3.6-1 to -3 show the mass discharge, fully open time, and response time as a function of valve differential pressure (ΔP), respectively. The trends are consistent for the four valves. The difference of the absolute values between different valves is due to the valve-to-valve variation. The results show that the four valves performed consistently.

3.6.4.2 Characteristic Test

Characteristic tests were conducted by varying the electrical pulse duration t and the pilot pressure P_{pilot}.

t = 0.9 seconds (SV3112B)

Figure 3.6-4 shows the mass discharge data. In the test region (ΔP = 200–650 psi) the mass discharge increased linearly with ΔP and was not affected by the pilot pressure. This indicates that the actuation force was sufficient and there was no mass reduction. The mass discharge reached about 31 lb at ΔP = 650 psi. Higher ΔP was not tested because the larger mass discharge would cause unfavorable effects on the reactor. The comparison of the data with the previous results clearly shows that the new curves linearly extend the initial linear portion of the old curves[1]. The old curves diverge at 350 to 400 psi as affected by the pilot pressure and the mass discharge started to decrease in the higher ΔP region.

Figure 3.6-5 shows the fully open time as a function of ΔP. The fully open time was about 100 ms less than the electrical pulse duration, which was consistent with the previous testing. The fully open time slightly decreased with ΔP in the test region. Again, the pilot pressure did not affect the fully open time. This trend explains the linear increase in the mass discharge. With the almost-constant valve-open time the mass flow was mainly controlled by ΔP (i.e., the higher the ΔP, the larger the mass discharge). By comparison, the fully open time before the modification was decreasing significantly with ΔP and was affected by the pilot pressure. The reduced open time caused the dramatic decrease in mass discharge.

Figure 3.6-6 shows the response time vs ΔP. The response time linearly increased with ΔP and was independent of the pilot pressure. The response time was longer than the previous value because the modified piston is a larger size and has inertial momentum. The response time had

[1] Ibid.

a slight increase in the high-ΔP region compared to the dramatic increase observed before the modification. With the properly modified valve structure the sufficient actuation force ensured a fast and stable opening process. An improved flow pattern around the modified seat also contributed to the fast response of the valve movement to actuation in the high-ΔP region.

The time-to-open and time-to-close were in the range of 80 to 90 ms and were very close to the previous data. This is expected because the movement of the valve internal part has a resistance contributed to by the friction of the seals, structures which were not significantly modified.

t = 1.2 seconds (SV3112B)

Figures 3.6-7 to -9 show the mass discharge, fully open time, and response time for t = 1.2 sec. Basically, the trends are the same as those for t = 0.9 sec. The linearity of the curves still exists. With the longer electrical pulse duration (t = 1.2 sec) the mass discharge was greater, the fully open time was longer, but the response time was almost the same compared to those for t = 0.9 sec. The time-to-open and time-to-close remained the same, in the range of 80 to 90 ms.

The comparison between the test data and previous results clearly shows that the valves were properly modified and the performance was significantly improved.

t = 0.1-0.4 seconds (SV3112A)

The valve performance was also tested at shorter electrical pulse duration. Figures 3.6-10 to -12 show the mass discharge, fully open time, and response time for t = 0.2 sec. As shown in figure 3.6-10, the mass discharge still corresponded linearly with ΔP at shorter t and relatively lower ΔP region. The valve was fully open and there was no dramatic increase in the response time.

When the electrical pulse duration varied the mass discharge deviated from the linear trend at t = 0.1 sec, as shown in figure 3.6-13. The reason is that the valve was not fully open at t = 0.1 sec (see figure 3.6-14). The measured data indicate that the valve was partially open at this point. The electrical pulse duration was so short that the moving piston did not have enough time to reach the open limit switch. This process, in turn, reduced the mass discharge. If the electrical pulse duration were further reduced the valve would not even have been partially open. The mass discharge would have decreased sharply. Increasing the pilot pressure could not help the opening process under such condition because it is controlled by the time span, not the actuation force. From a control point of view this operating condition should be avoided. In normal operation the valve should be operated at an electrical pulse duration equal to or longer than 0.2 sec to obtain a well-controlled back-pulse cleaning effect.

t = 0.1-0.4 seconds (SV3111A)

The test results are very close to those of SV3112A and, for brevity, are not included in this report.

3.6.5 Conclusions

- The valve manufacturer properly modified the back-pulse valves. The piston, seat, and seals were reconstructed to obtain a stronger actuation force and optimized flow pattern. The four valves tested behaved consistently. The valves have been working well since the modification.

- The valve performance has been significantly improved. In the test region with the electrical pulse duration longer than 0.1 sec the valves were fully open. The mass discharge increased linearly with the valve differential pressure. There was no dramatic increase in response time.

- In normal operation the valves should be operated at electrical pulse duration of 0.2 sec or longer.

3.6.6 References for Section 3.6

Technical Progress Report for M. W. Kellogg Transport Reactor Train With Westinghouse Particulate Control Device, January 1997 - December 1997, Section 3.27, prepared by Southern Company Services, Inc., DOE Cooperative Agreement Number DE-FC21-90MC25140, December 1998.

Table 3.6-1

Test Arrangements

Run	Date	Test	Valve	t (sec)	P_{pilot} (psig)	ΔP (psi, setting)
1	4/7/98	Consistency	SV3111A SV3112A	0.4	105 IA	200-650
2	4/7/98	Consistency	SV3111B SV3112B	0.4	105 IA	200-650
3	4/7/98	Characteristic	SV3112B	1.2	100 N_2	200-650
4	4/7/98	Characteristic	SV3112B	1.2	120 N_2	200-650
5	4/7/98	Characteristic	SV3112B	1.2	140 N_2	200-650
6	4/7/98	Characteristic	SV3112B	0.9	100 N_2	200-650
7	4/7/98	Characteristic	SV3112B	0.9	120 N_2	200-650
8	4/7/98	Characteristic	SV3112B	0.9	140 N_2	200-650
9	5/4/98 - 5/5/98	Characteristic	SV3111A SV3112A	0.4	105 IA	190-225
10	5/5/98 - 5/6/98	Characteristic	SV3111A SV3112A	0.3	105 IA	225
11	5/6/98	Characteristic	SV3111A SV3112A	0.2	105 IA	225
12	5/6/98	Characteristic	SV3111A SV3112A	0.1	105 IA	225
13	5/7/98 - 5/11/98	Characteristic	SV3111A SV3112A	0.2	105 IA	125-420
14	5/11/98	Characteristic	SV3111A SV3112A	0.4	105 IA	225

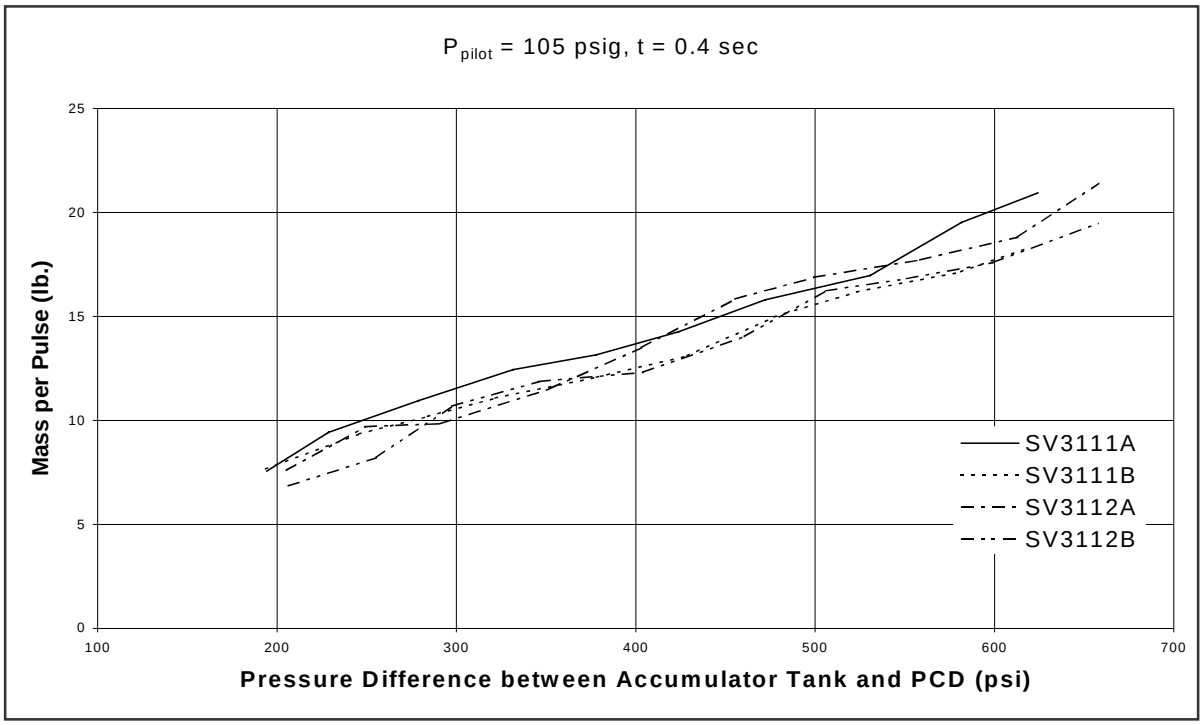

Figure 3.6-1 Mass Discharge Vs Valve Differential Pressure at t = 0.4 sec

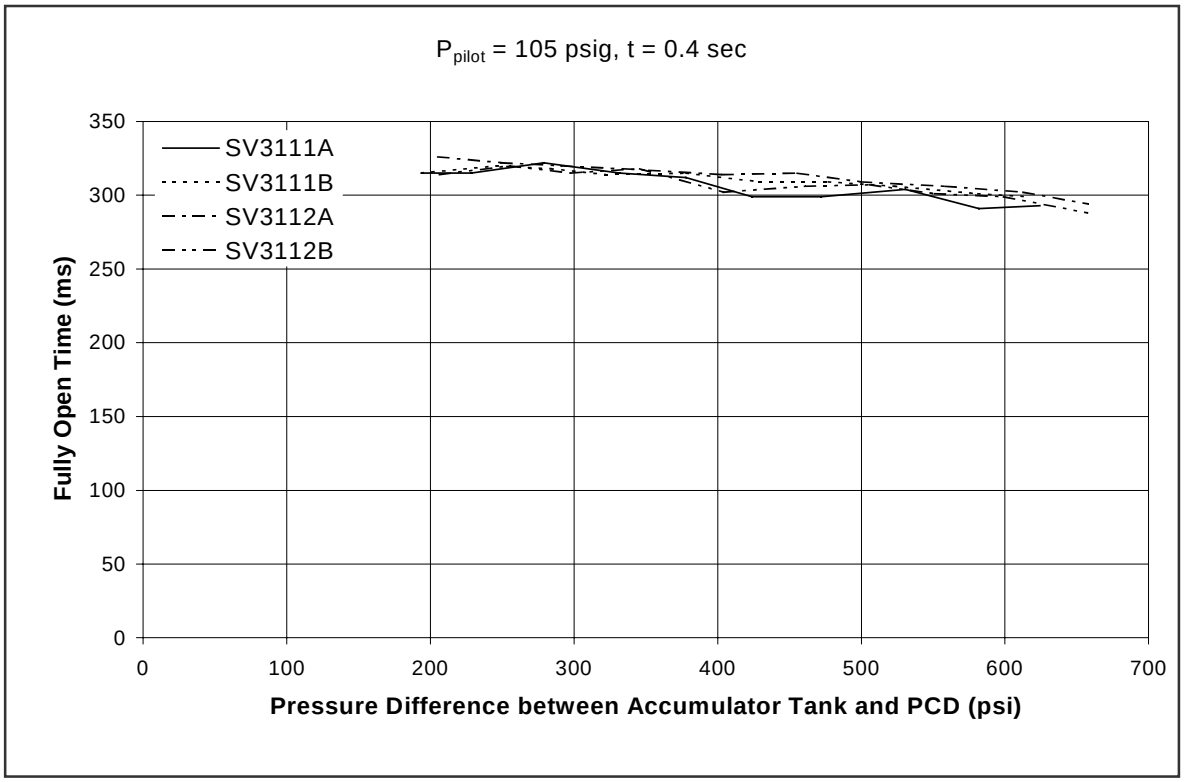

Figure 3.6-2 Fully Open Time Vs Valve Differential Pressure at t = 0.4 sec

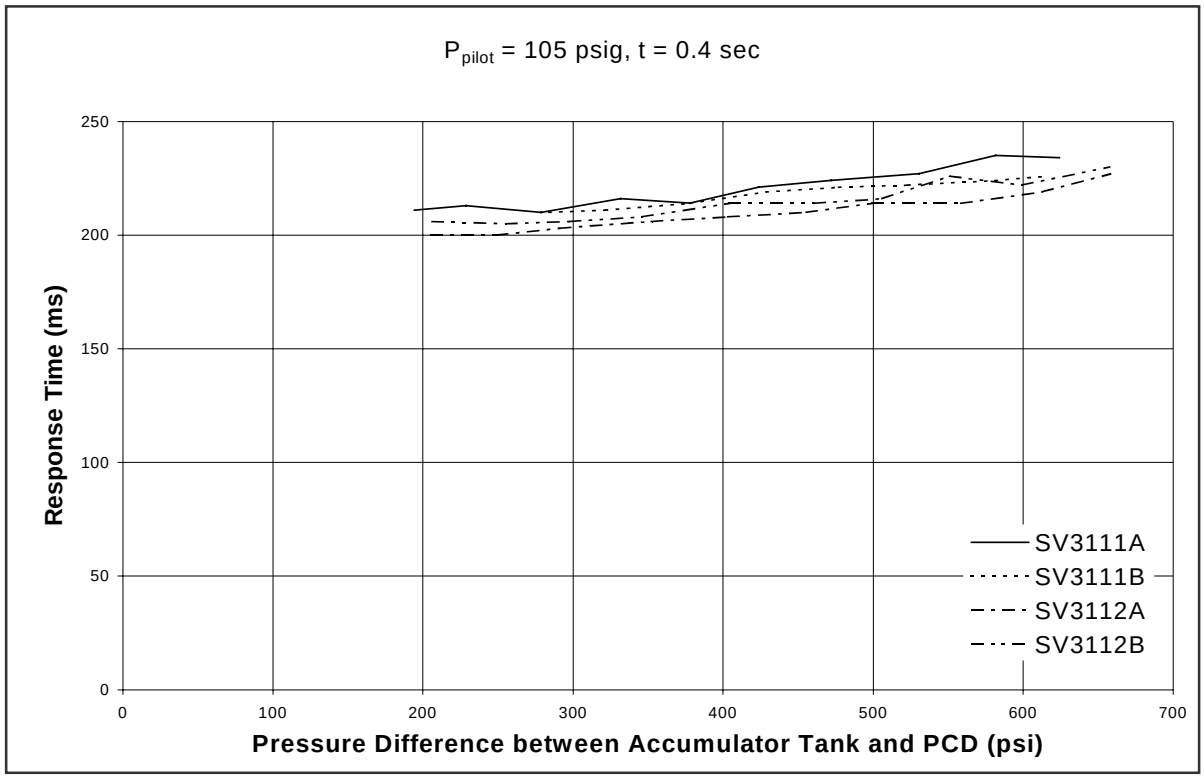

Figure 3.6-3 Response Time Vs Valve Differential Pressure at t = 0.4 sec

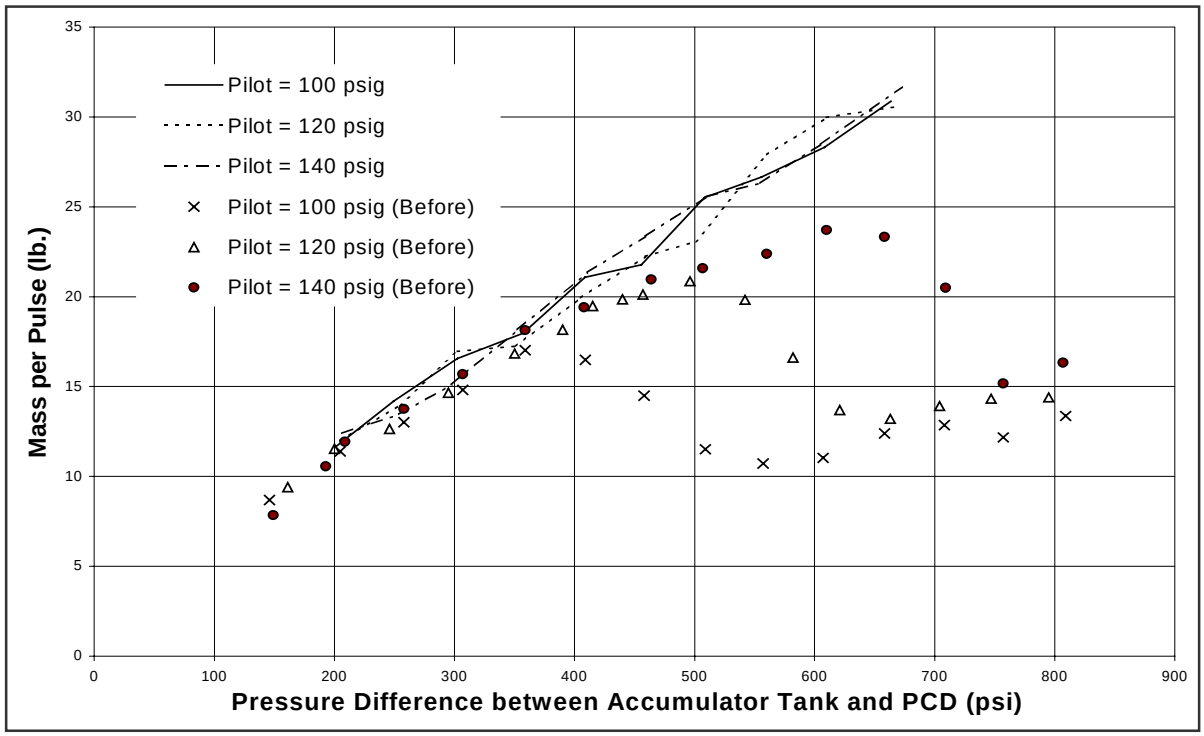

Figure 3.6-4 Mass Discharge Vs Valve Differential Pressure for SV3112B at t = 0.9 sec

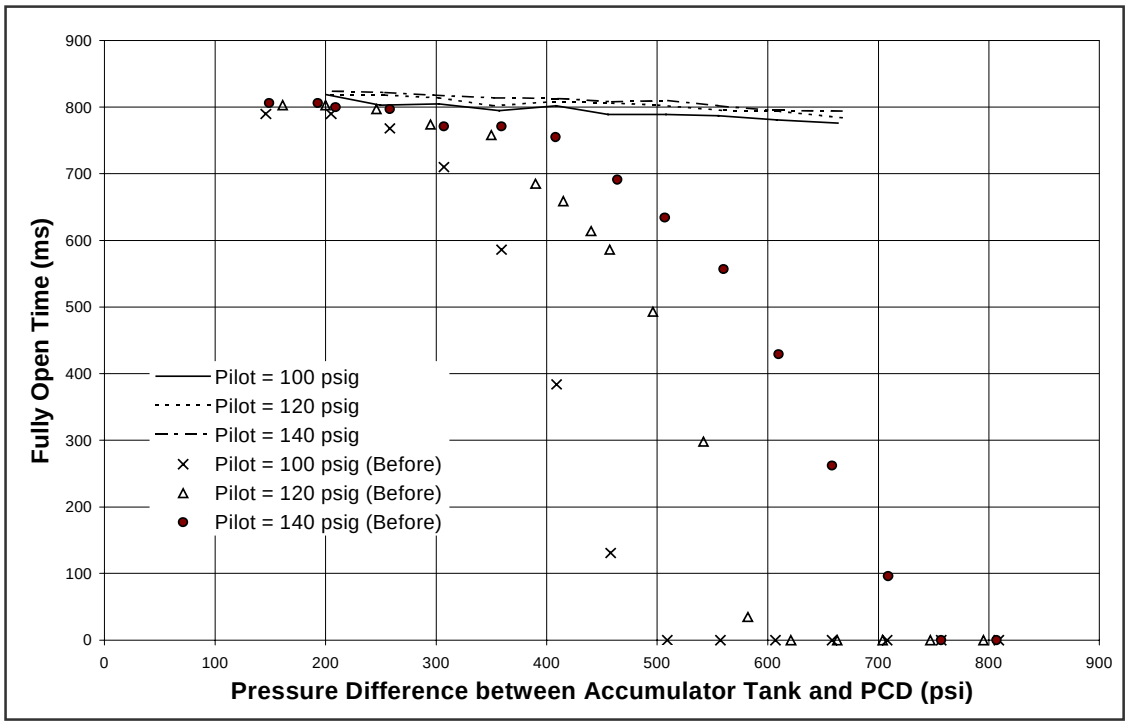

Figure 3.6-5 Fully Open Time Vs Valve Differential Pressure for SV3112B at t = 0.9 sec

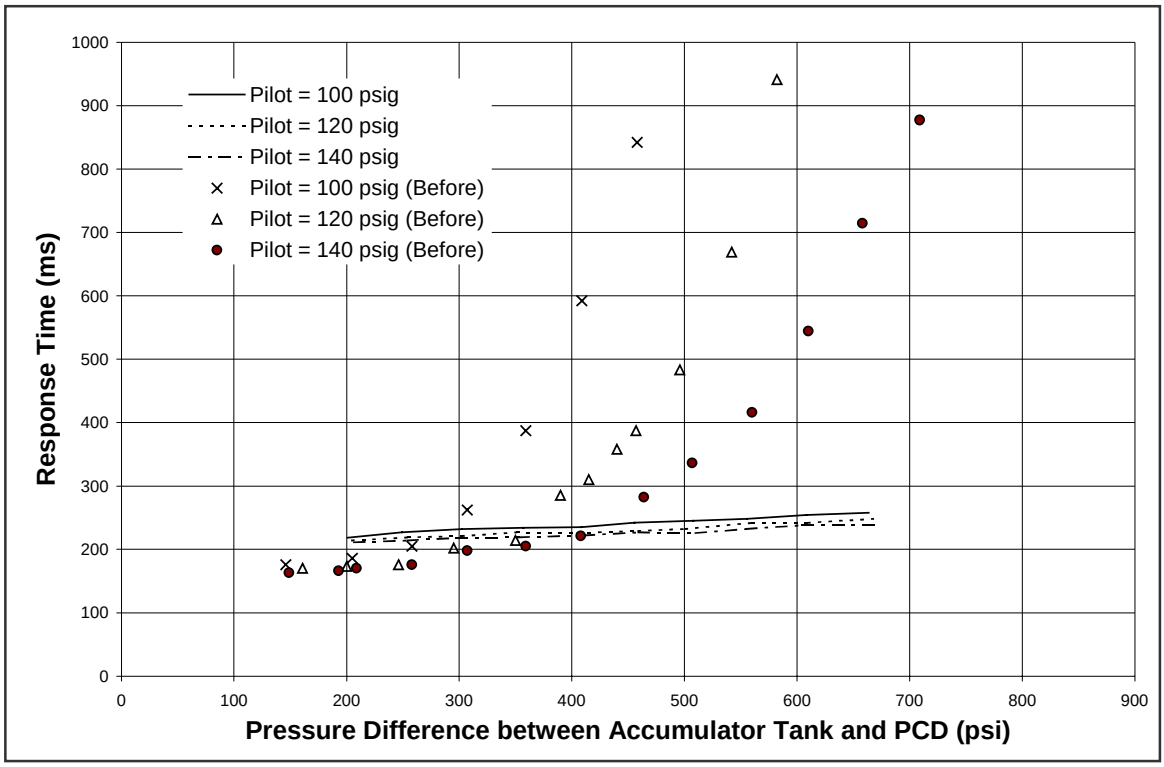

Figure 3.6-6 Response Time Vs Valve Differential Pressure for SV3112B at t = 0.9 sec

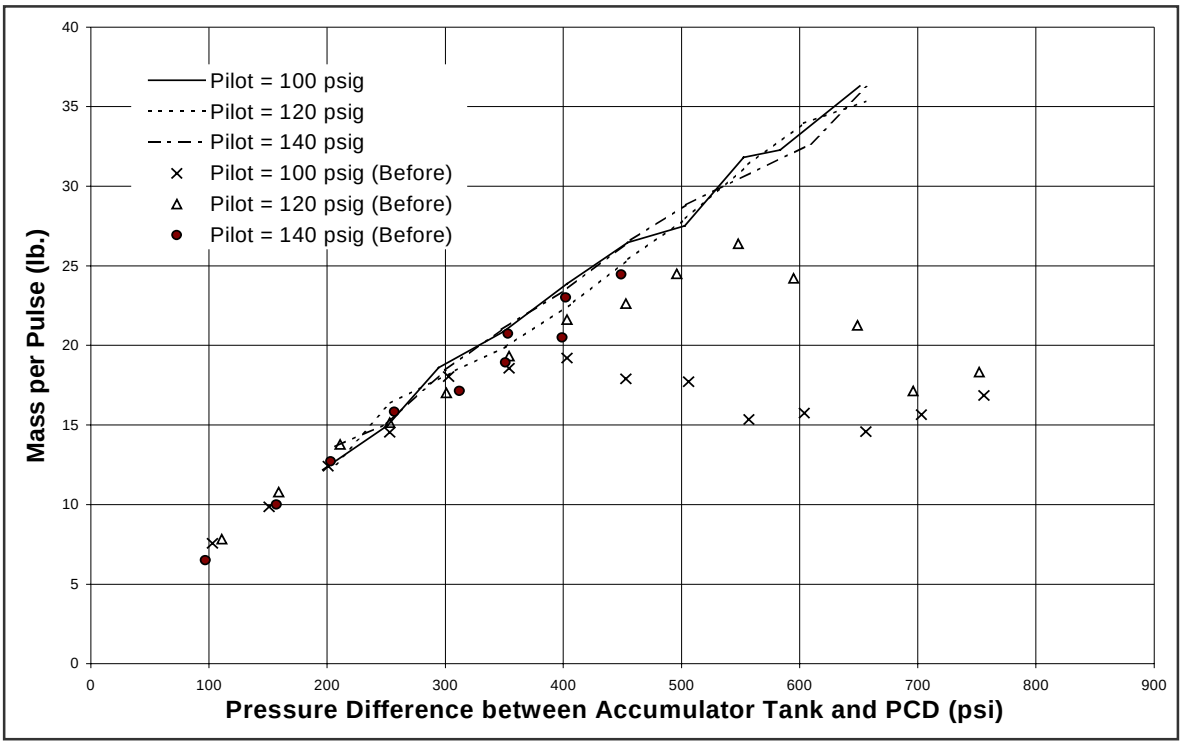

Figure 3.6-7 Mass Discharge Vs Valve Differential Pressure for SV3112B at t = 1.2 sec

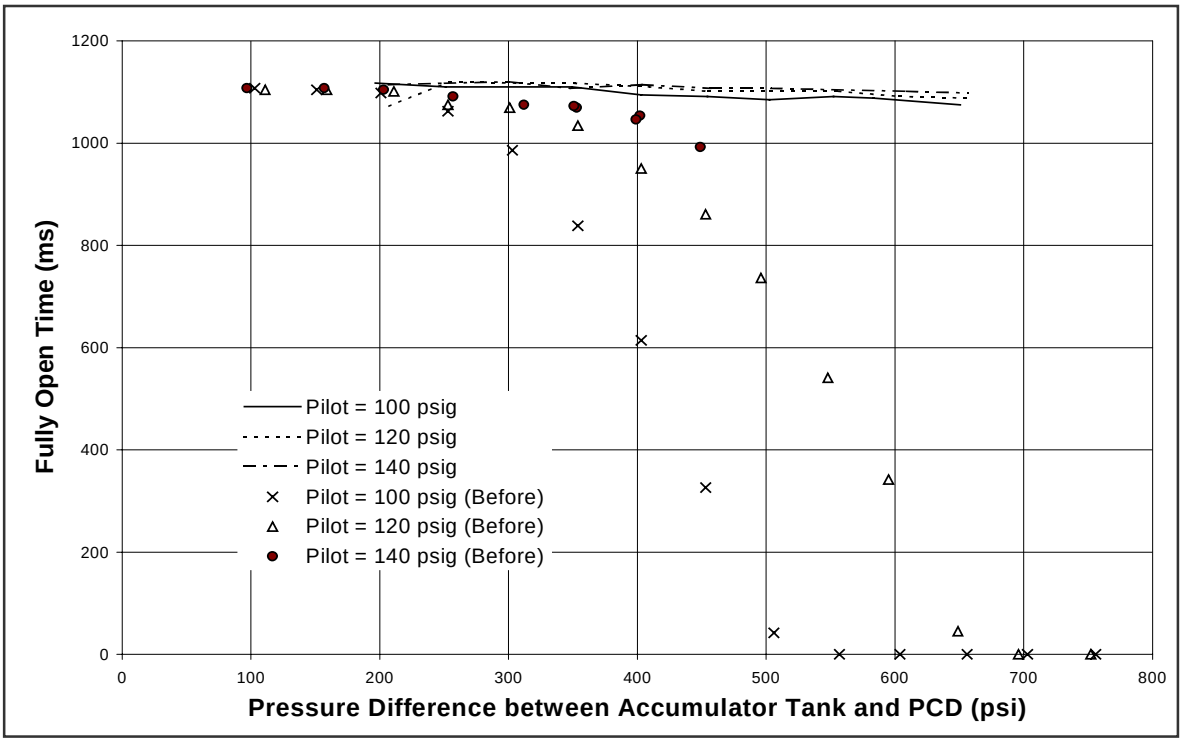

Figure 3.6-8 Fully Open Time Vs Valve Differential Pressure for SV3112B at t = 1.2 sec

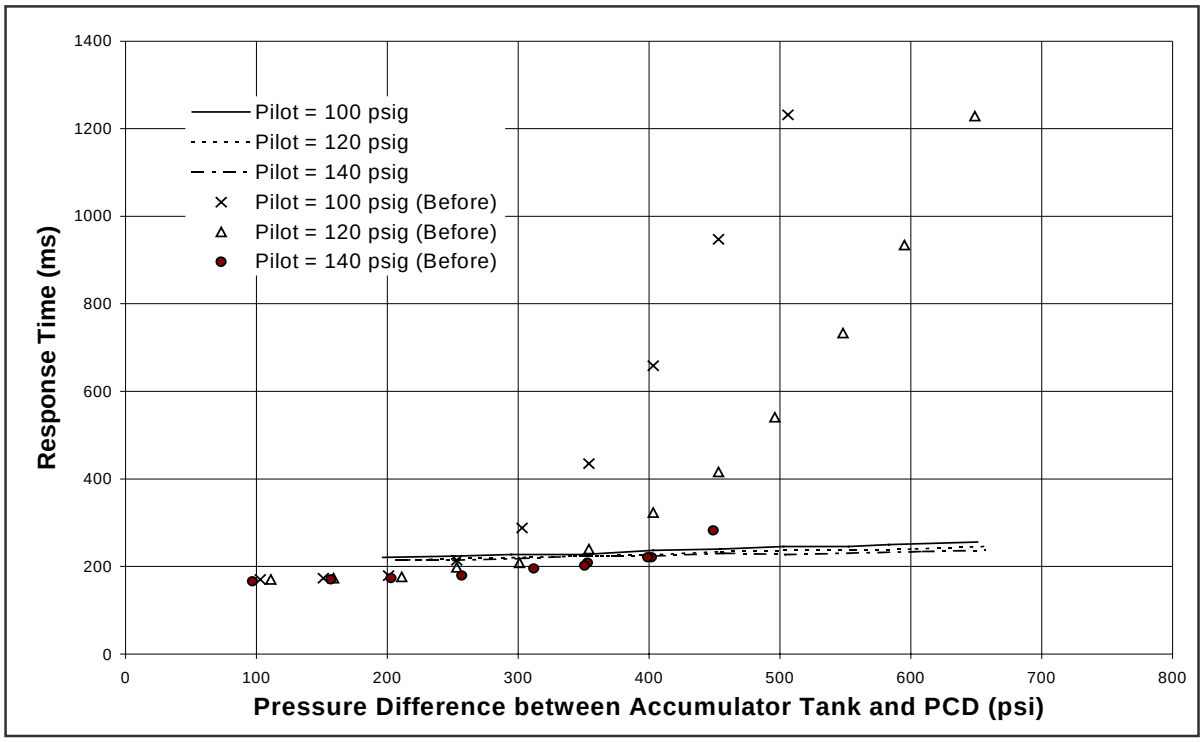

Figure 3.6-9 Response Time Vs Valve Differential Pressure for SV3112B at t = 1.2 sec

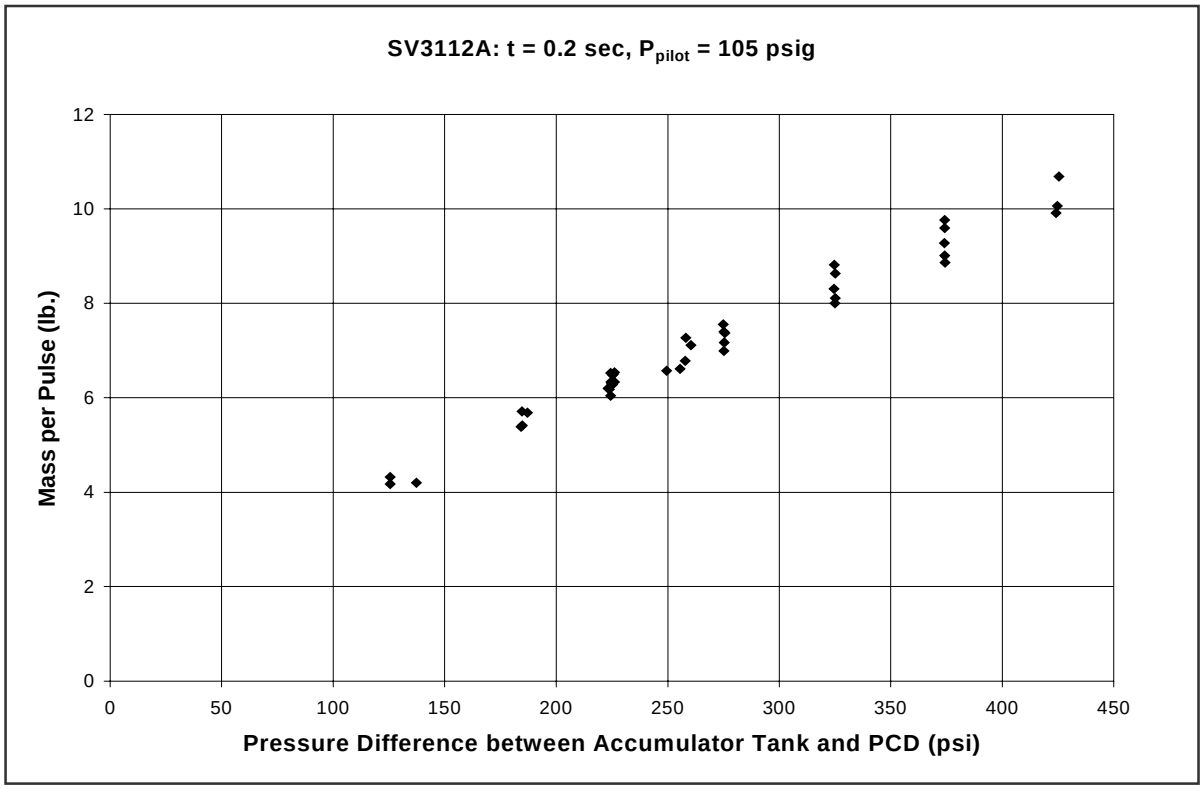

Figure 3.6-10 Mass Discharge Vs Valve Differential Pressure for SV3112A at t = 0.2 sec

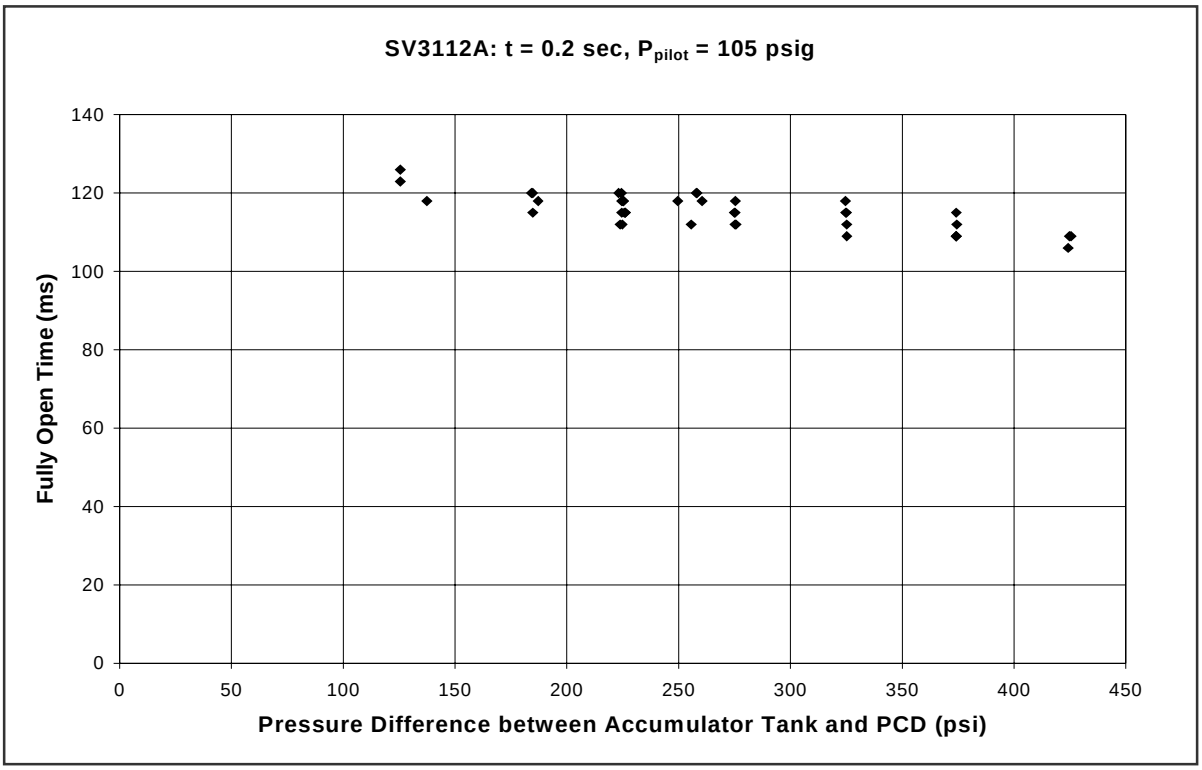

Figure 3.6-11 Fully Open Time Vs Valve Differential Pressure for SV2112A at t = 0.2 sec

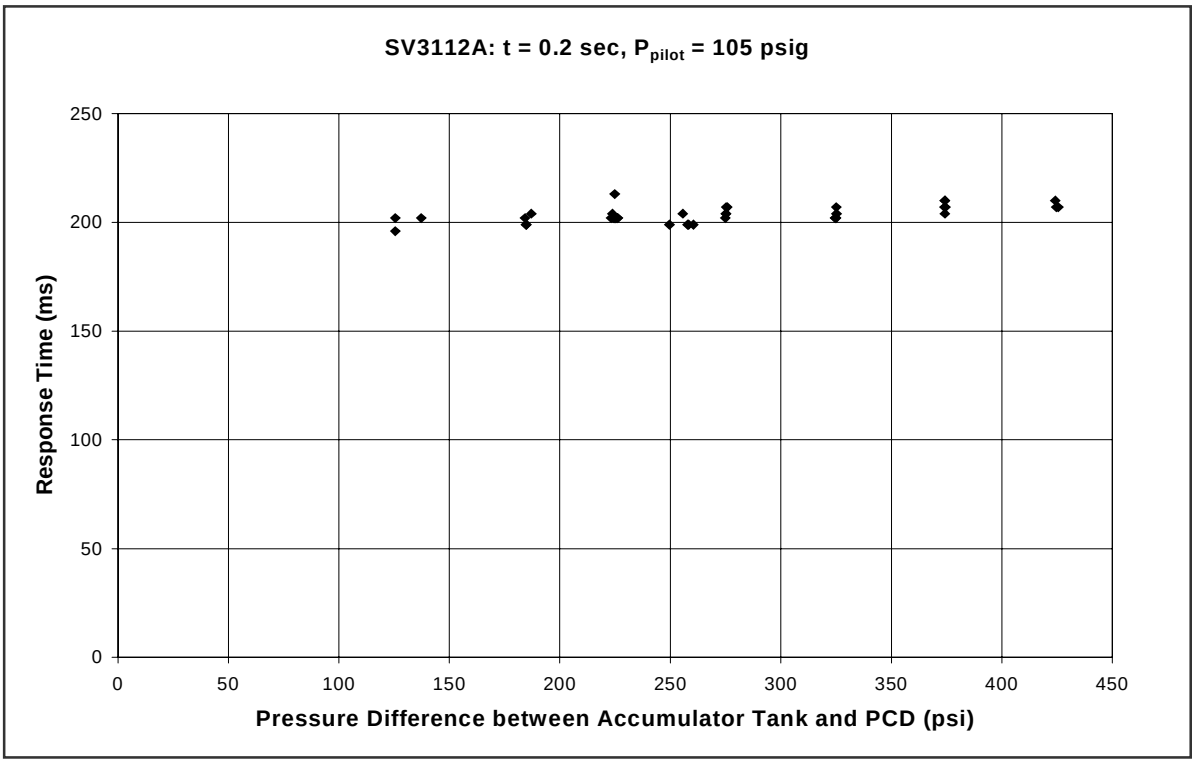

Figure 3.6-12 Response Time Vs Valve Differential Pressure for SV3112A at t = 0.2 sec

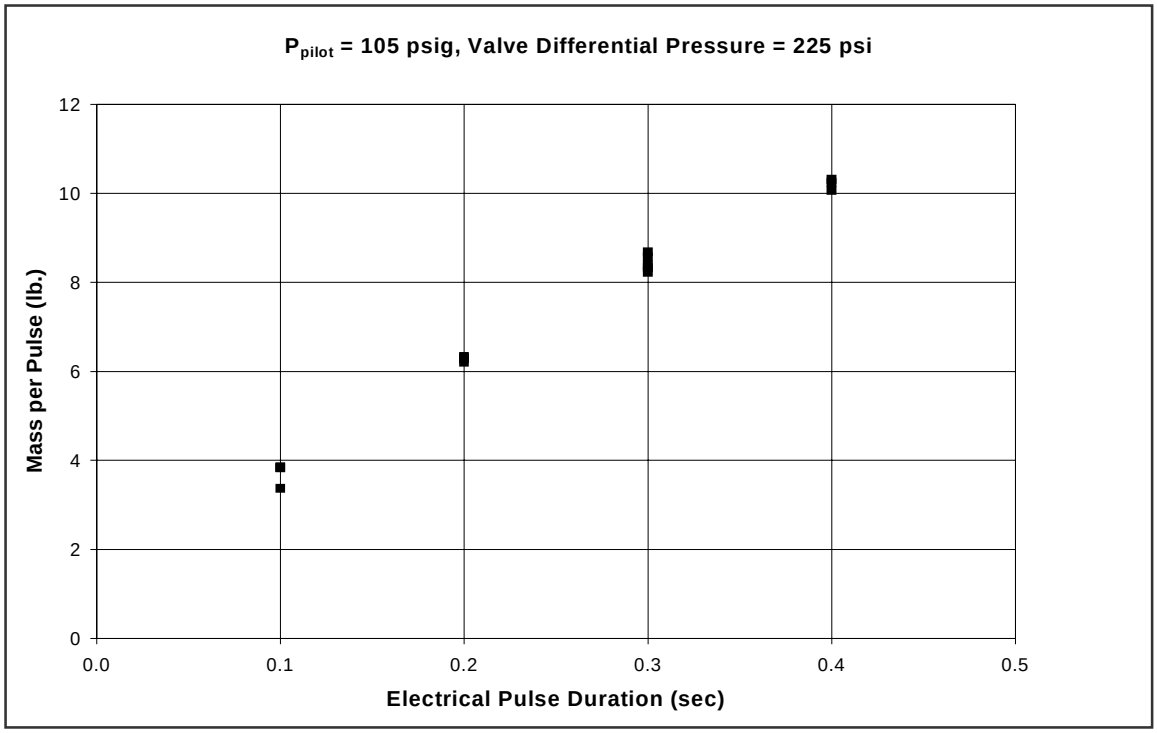

Figure 3.6-13 Mass Discharge Vs Electrical Pulse Duration for SV3112A at ΔP = 225 psi

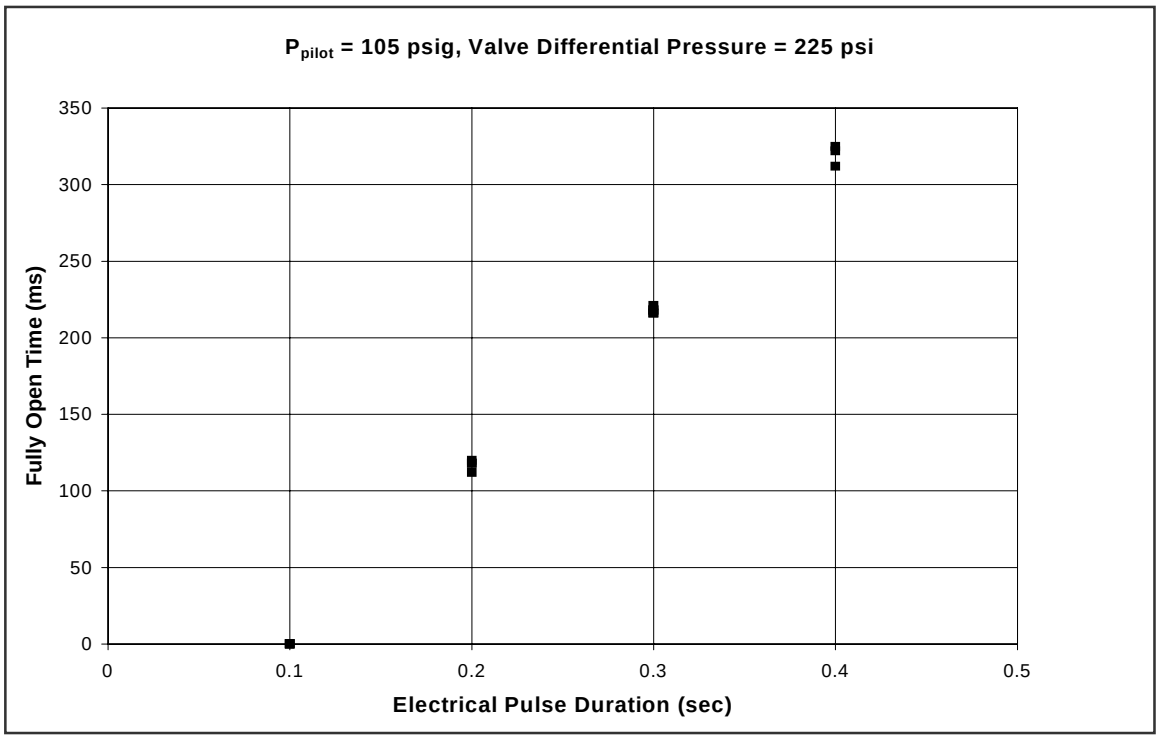

Figure 3.6-14 Fully Open Time Vs Electrical Pulse Duration for SV3112A at ΔP = 225 psi

3.7 PLENUM PRESSURE MEASUREMENTS

3.7.1 Test Objectives

Plenum pressure rises in PCD FL0301 were measured during the stable operation of TC02. The main objective of these measurements was to gather more data for better understanding the back-pulse cleaning mechanism. Another objective was to optimize the back-pulse system parameters to achieve adequate cleaning effect on the filters and minimize the negative effect of the transport reactor on the operation.

3.7.2 Introduction

Pressure rise in a plenum during back-pulse is directly related to operating parameters of the back-pulse valve, geometry of the plenum, flow resistance of the filter elements, and morphology of the ash layer. When a certain amount of mass is injected into the plenum through a Venturi device the flow resistance of the filter walls and ash layer causes a sharp pressure rise in the plenum. This pressure rise is large enough to reverse the gas flow across the filters. The ash cake is then broken by the tensile stress due to the pressurization and removed by flow drag. The whole process occurs dynamically in the open back-pulse system in a short period of time. Part of the impulse mass may bounce back to the dome during the back-pulse because the plenum is open at the top. Also, the combination of the reverse flow through the filters causes a pressure rise on the dirty-side of the PCD. These pressure changes affect the upstream and downstream subsystems, particularly the transport reactor. The stable operating condition of the whole system is upset in some situations due to the back-pulse. Therefore, the back-pulse parameters should be determined not only by the ash cleaning requirement but also by the stable operating conditions of other subsystems in the train.

A test based on operational needs for the back-pulse system information was conducted in TC02 to measure the pressure rise in plenums. The measurement provided direct data of how the back-pulse system responds to the impulse-gas injection. The findings will be used to control PCD operation, analyze filter element failures, and evaluate PCD performance.

3.7.3 Test Procedure

The test arrangement is sketched in figure 3.7-1. The pressure rise in a plenum was measured using a pressure differential transmitter (PDT3031). The measured data was actually the pressure difference across the filter elements. The absolute pressure rise in the plenum differs from the measured pressure difference since the dirty-side pressure (before filtration) varies during back-pulse. However, this pressure difference is desired since it can be correlated to the impulse-gas flow through the filters. The term "plenum pressure rise" in this report refers to the pressure difference measured by PDT3031. Also, note that the long instrument tubing contributed to a pressure loss when the pressure wave reached the transmitter. The reading from the transmitter may be smaller than the real pressure difference across the filters. This report, however, presents only the measured data, and corrections will be conducted in the future.

The top and bottom plenum pressures were measured in the test when the plenums were back-pulsed separately. The pressure change and back-pulse-valve limit switch signals were recorded by a fast data acquisition device during a back-pulse. Other system parameters were obtained from the plant information (PI) system. Various operating parameters were varied during the measurement to study their influence on the plenum pressure rise.

3.7.4 Conclusions

Results and observations are not discussed in detail in this report due to the proprietary nature of the information. However, some general conclusions drawn from the results of this work include:

- In the test range, the plenum pressure rise increased linearly with increasing valve differential pressure, mass discharge, electrical pulse duration, and time between back-pulses.

- Top and bottom plenums had different pressure rises.

- The back-pulse system worked well in TC02 with $\Delta P = 225$ psi and $t = 0.2$ sec. The transport reactor upsets were minimized and ash cleaning was satisfied.

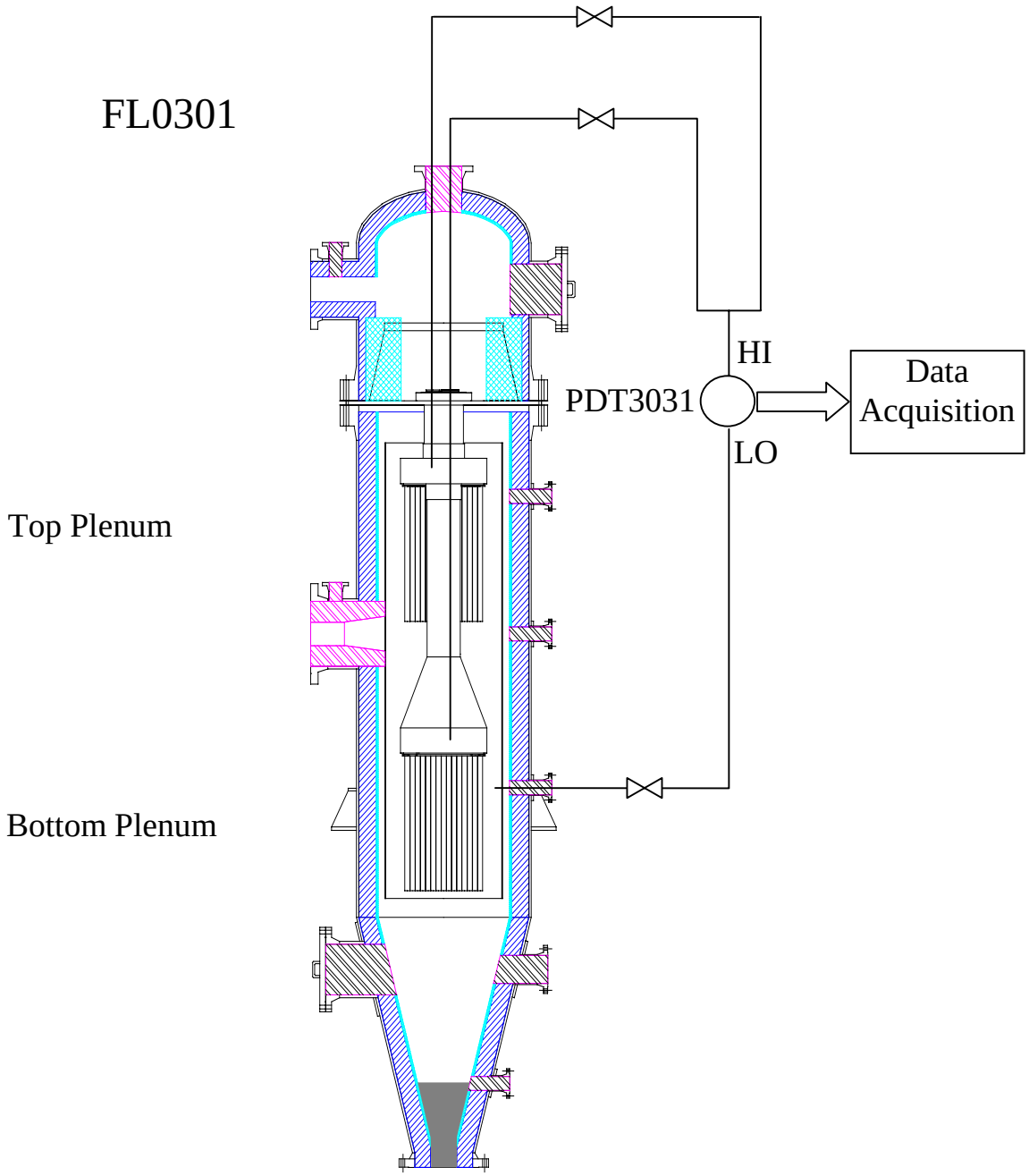

Figure 3.7-1 Schematic of Plenum Pressure Rise Measurements

3.8 COORS P-100A-1 FILTER ELEMENT OPERATIONAL EXPERIENCE AND ANALYSIS

3.8.1 Introduction

Coors P-100A-1 alumina/mullite filter elements have been used in high-temperature, high-pressure (HTHP) gas filtration test facilities essentially since the inception of research into this technology. The elements have been successfully tested at the American Electric Power Tidd Demonstration Project, the Karhula R&D Center, and at many other facilities around the world. Through the U. S. Department of Energy (DOE)-sponsored efforts of Siemens-Westinghouse, the Coors P-100A-1 material was demonstrated to be a chemically stable, reliable filter element. The alumina/mullite filter element is superior to clay bonded silicon carbide elements (Pall and Schumacher) at the 1,550°F-operating temperatures experienced by filter elements used in first generation pressurized fluidized-bed combustion (PFBC) units because the matrix does not elongate and resists gas-phase chemical attacks at that temperature.

One drawback to the filter element is its susceptibility to thermal-stress failure. This susceptibility to thermal stress has plagued the testing of the Coors P-100A-1 filters at the Power Systems Development Facility (PSDF).

The first Coor P-100A-1 filter elements were installed during the April 1997 outage. A total of 31 Coors P-100A-1 elements have been installed since that time in the Siemens-Westinghouse PCD (FL0301) on the KBR transport reactor train. Of the 31 elements, 17 failed during operation (55 percent) and one failed upon removal during an inspection. At no time was there any bridging of ash between the filters, which has caused multiple failures at other facilities. At the time of the inspections it was generally agreed that the failures were due to thermal and not mechanical stress.

It is very important to note that at all times there has been a wide variety of filter elements installed in the same filter vessel. Monolithic silicon carbide filters from Pall and Schumacher and composite filters from 3M, DuPont, and McDermott have all endured and survived the same thermal events that have caused failure of the Coors P-100A-1filters. Only two other types of filters have failed during operation: the alumina oxide filter from Blasch Precision Ceramics and the cordierite filter from Specific Surface.

However, the staff working with the filter system at the PSDF believes that it is very important, in fairness to Coors, to acknowledge that the failures were caused by *operational upsets***.** The filter elements did not fail due to poor quality, but were subjected to operational conditions that they were not designed to handle. Coors filters would probably still be in use today had the operational understanding of the transport reactor advanced to a point where these upsets had not occurred.

In this document the following topics will be discussed:

- The operational history of Coors P-100A-1 filter elements at the PSDF.
- The gathering of information which lead to a hypothesis of why the Coors P-100A-1 filters failed.
- The installation of thermocouples that provided the information needed to confirm the hypothesis.
- The thermal/mechanical model that answers why the Coors P-100A-1 filters failed and the silicon carbide and composite filters did not.
- Conclusions, on-going work, and future plans.

3.8.2 Coors P-100A-1 Test History at the PSDF

3.8.2.1 First Installation—April 1997

A thermal event caused the failure of 91 clay bonded silicon carbide elements (see section 3.8.3.3) from Pall and Schumacher on April 7, 1997, and lead to the first installation of Coors P-100-A1 elements at the PSDF. The decision was made when the filter system was opened to remove all of the existing filter elements and replace them with a mixture of Pall 326, Pall 442T, and Coors P-100A-1 filter elements. One Schumacher F40 filter element that was being evaluated by Roger Chen was installed to increase its exposure time (see section 3.8.2.2). A total of 19 Coors elements were installed, 10 on the top plenum and 9 on the bottom plenum. All of these filter elements were new and were purchased for testing at the PSDF. The location of these filters is shown in figure 3.8-1 and the individual element serial numbers are listed in table 3.8-1.

These filter elements were in service without incident for about 616 hours on coal until the next maintenance period on FL0301 in July 1997. The primary gas cooler (HX0202) was used in a bypass mode for approximately 1/3 of the 616 hours, limiting the PCD inlet temperature to below 1,000˚F. A time-vs-temperature histogram of this operating period is shown in figure 3.8-2.

3.8.2.2 Second Installation and First Failure

Siemens-Westinghouse requested in June 1997 that the PSDF perform a 1,000-hour test with the PCD limited to a maximum inlet temperature of 1,400˚F to evaluate the elongation potential of Pall clay bonded silicon carbide filter elements. Additional filter elements from Schumacher (TF20) and 3M (SiC) had been received and these were installed during the week of July 20, 1997. Selected Pall and Schumacher elements were measured and installed as part of this test plan.

DOE/FETC had been funding Dr. Roger Chen at West Virginia University to develop a vibrational response method for the nondestructive evaluation of ceramic filter elements. The PSDF had supplied as-manufactured filter elements from Coors, Pall, and Schumacher to

support this work. Dr. Chen had evaluated 12 as-manufactured Coors P-100-A1 elements at the time of this installation and 10 of these were installed in the top plenum. Eight of the 10 elements previously installed in the top plenum were removed.

Also, there was consideration of taking a nonisokinetic extractive sample from near the filter elements. Three Coors elements on the lower plenum were removed and replaced with blanks to accommodate the sampling probe. The tubesheet layout at the conclusion of the installation is shown in figure 3.8-3 and individual element numbers are shown in table 3.8-2.

The next start-up following this installation occurred in the last week of August 1997. The unit was transitioning to coal at midnight on August 31 when pieces of Coors filter elements were detected in the PCD ash removal system. The filter pieces were collected and by weight it was estimated that at least three Coors elements had failed. The decision was made to shut down the system and inspect the PCD after about 12 hours on coal.

Figure 3.8-4 shows a trace of the PCD inlet, outlet, and plenum temperatures during this transition to coal. The temperature inside the PCD increased at a rate of 325˚F/hr when coal feed began. Whereas this is high, it is well below the ramp rates evaluated by Siemens-Westinghouse in their test facility that did not produce failure. Also of interest were the three "spikes" in the lower plenum temperature (TI3014). This thermocouple is located very close to the elements which failed and initially it was believed that this was an indication of the Siemens-Westinghouse fail-safes plugging since the measured temperature approached but never exceeded the inlet temperature. However, in hindsight, this may have been an indication that there was local combustion of coal on the elements in the lower plenum.

Upon inspection, three of the filter elements (LC022 (B26), KC001 (B27), and KC004 (B28)) were broken. All three had V-shaped breaks on opposite sides of the element and were broken within 12 inches of the flange. A fourth filter element (KC008 (B9)) broke about the midpoint upon inspection and removal. The appearance of the break was not V-shaped, but circumferential. Approximately 60 to 90 degrees of the break was filled with ash indicating failure during operation with the remaining fracture surface completely clean. Figure 3.8-5 shows the location of this element relative to the three that broke during operation. The location of the "dirty" part of the break was facing elements B26 and B27. It is possible, given the orientation and nature of the crack, that the element was damaged as LC022 and/or KC001 broke. It is important to note that the Pall 326, Pall 442T, Schumacher TF20, and 3M SiC filters were not visibly affected (i.e., broken) by this event.

The decision was made during the outage to remove KC002 (B8) and KC007 (B10) for materials testing. One observation made was that the only elements that had failed were the "used" elements installed in April. There was much discussion about the cause of failure and whether the "used" elements KC017 and KC010 located in the top plenum should be removed. The possibility of coal carryover from the transport reactor was not considered at the time, so the leading theory was accumulated damage due to the many thermal transients experienced from April to July caused by coal feeder trips. A compromise decision was made that left KC017 and KC010 in the vessel but to move them to the lower plenum so that if they broke there would be minimal consequential damage to other filter elements as they fell into the ash hopper. The

tubesheet layout at the conclusion of the outage is shown in figure 3.8-6 and the list of elements installed in shown in table 3.8-3.

3.8.2.3 Second Failure—September 7, 1997

During the next transition to coal another Coors P-100-A1 filter element failed. The failure occurred at about 4:00 a.m. on the morning of September 7. The temperature plot for this failure is shown in figure 3.8-7. It was desired to control the temperature ramp rate to see what, if any, impact this would have on the PCD. This was accomplished by cycling the coal feeder on and off to gradually increase the temperature to the PCD. The "bumps" in the PCD inlet temperature from before 2:30 to 4:30 are a result of the coal feeder cycling. During this transition, the average temperature rate of rise was about 100°F/hr.

It was determined, based on the mass of pieces from the ash removal system, that only one filter had broken. There was no way to tell which filter failed but speculation was that it was one of the two elements installed in April. (This was confirmed during the November outage.) A decision to continue operation and evaluate their performance was made because the PSDF had no experience at the time on how well the Siemens-Westinghouse fail-safes would perform.

3.8.2.4 Third Failure—September 19, 1997

Testing continued from September 7 to September 19 with no failures. Particulate samples taken by Southern Research Institute (SRI) on the outlet of the PCD, shown in figure 3.8-8, revealed that the loading was quite low, below 1 ppm, indicating very good performance of the Siemens-Westinghouse fail-safe. Another Coors P-100-A1 filter failed while the unit was at steady state late in the evening on September 19. The temperature plot for this failure is shown in figure 3.8-9. The only anomaly in the graph is the temperature drop in the lower plenum thermocouple just before 6:30 p.m. This was still unexplained at the time of this report.

Operationally, the only PCD testing that occurred on September 19 was parametric testing of the pulse valves. However, the limitations of the pulse valves were recognized by this time and the range of pulse parameters used in the testing was not severe. But it is possible, since this element had survived the thermal events leading to failures of the elements on August 31 and September 7, that it was already in a weakened state and the pulse optimization was sufficient to lead to its failure.

The collection efficiency of the PCD deteriorated after September 19 for a variety of reasons (see figure 3.8-8). It was determined upon disassembly of the PCD in November that the blanks installed in July as well as the fail-safe at tubesheet location B10 were leaking (see section 3.8.2.5). The fail-safe at tubesheet location B9 was completely plugged. Therefore, it is assumed that KC010 (B9) failed on September 7, and KC017 (B10) failed on September 19. The decision was made to continue operation based on the relatively low-outlet loading (<15 ppm) and the desire to continue monitoring the fail-safe performance.

3.8.2.5 Fourth Failure—November 2, 1997

The fourth failure occurred on November 2, also during a transition from the start-up burner to the coal feeder. At about 1:00 p.m. the coal feeder plugged, so the pressure upstream of the plugging was raised in an attempt to clear the line. At the time, the coal feeder rotary valve had been turned off. When the plugging cleared, apparently the gas flow caused a "suction effect" of coal through the disabled rotary feeder. This momentary loss of control caused several fairly significant thermal cycles throughout the transport reactor and PCD as shown in figure 3.8-10. The temperature rate of rise exceeded a maximum of 350˚F/min during the upset. Almost immediately, the ash removal system plugged with pieces of Coors filter. Given the large quantity of pieces, the unit was shut down to inspect the PCD. The transport reactor was placed back on the start-up burner almost immediately after the event, so there was very little ash generated after the failure.

It was found when the plenum was removed that all 12 of the Coors P-100-A1 filters in place in early September, as well as one of the 3M filter elements (B5), had failed. Another 3M filter (B20) had a visible "nick" in one side. For the most part, all of the Coors filters had the characteristic "V" crack seen during the September outage (figure 3.8-11). A tubesheet map showing the location of the failed elements is shown in figure 3.8-12. Representatives from Coors, SRI, and Siemens-Westinghouse were all present for the inspection and filter removal.

All of the fragments as well as the fail-safes were labeled and removed. Analysis of the fail-safes showed that the 10 of the Coors element in the top plenum and the failed 3M element in the lower plenum failed simultaneously. There was very little ash in the inner bore of the 3M element, which also suggests simultaneous failure. Therefore, it is believed that the 3M element was hit as the Coors filters in the top plenum broke and fell into the ash hopper.

The Coors filters were replaced with silicon carbide filters from Pall and Schumacher to finish the 1,000-hour run.

3.8.2.6 Final Installation and Failure—January/April 1998

As part of the analysis found in sections 3.8.3 and 3.8.4 it was decided to mount thermocouples to the outside diameter (OD) and inside diameter (ID) of a Coors and a Pall 326 filter element. The purpose of these thermocouples was to determine the gradient across the filter element wall during start-up and normal operation. The thermocouples and their attachment are described more fully in section 3.8.4 and the tubesheet location of these elements is shown in figure 3.8-13. In addition to the two Coors filters installed, eight monolithic alumina oxide elements from Blasch Precision Ceramics were installed. Two of these elements were exposed elements from the Karhula R&D center and six were new elements shipped directly to the PSDF.

The first transition to coal occurred on April 9, 1998, even though these elements were installed in January. The PCD thermocouple readings shown in figure 3.8-14 indicate a relatively smooth transition to coal, but the thermocouples mounted on the filter elements recorded a very different picture (see section 3.8.4). The end result was that both Coors filters as well as six of the eight Blasch filters failed during the upset. It was very interesting to see that the

instrumented Coors filter did not fail at the thermocouple but was virtually hanging by the thermocouple wire (see figure 3.8-15).

3.8.3 Analysis of Data

Based on the lack of ash bridging, and the fact that all but one of the failures occurred during the transition from the start-up burner to coal feed, the cause of failure was generally agreed to be due to thermal instead of mechanical stress. Through literature searches, analysis of the operational data at the PSDF, testing of the filter elements exposed at the PSDF, and conversations with staff at other test facilities, the following hypotheses were developed:

- The Coors filters failed due to a thermal gradient across the filter wall.
- The Coors filters failed due to accumulated damage caused by multiple thermal transients during pulse-cleaning, coal feeder trips, etc.

3.8.3.1 What does it take to thermally break a Coors filter?

The Coors filter, which is made of monolithic ceramic material, demonstrates roughly linear elastic behavior up to the point of failure when subjected to a mechanical load. Failure is brittle and catastrophic when the maximum stress for the filter element is reached. The stress-strain curve for the Coors P-100A-1 material as measured by SRI is shown in figure 3.8-16. The average room-temperature ultimate tensile strength for the element tested was 2,478 psi and the element had a room temperature strain-to-failure of 0.00062 inches per inch.

Like most materials, ceramics expand upon heating. The unit thermal expansion curve for the Coors material is shown in figure 3.8-17. The temperature difference required to cause microcracking at the surface (~280°F in the normal operating range) is shown in the figure. This analysis assumes a uniform temperature throughout the wall of the element with the temperature difference applied at the surface that simulates the conditions during back-pulsing. The analysis is based on a flat plate but is a good approximation for a cylinder.

3.8.3.2 Analysis of PSDF Data

Once the magnitude of the gradient was determined the data from the PCD was analyzed from April 1997 to December 1997. The data was analyzed in the following ways:

- Plotting temperature difference between the inlet and outlet of the PCD.
- Plotting temperature difference between the inlet nozzle and the plenum.
- Plotting temperature difference between the plenum and outlet nozzle.
- Plotting temperature rate-of-change (dT/dt) with time intervals of 1, 15, and 60 minutes.

The final analysis revealed one significant problem. Even though the nozzle to nozzle gradients and rate-of-change during the failures was significant there were always events that could be found of a greater magnitude than the events which caused failure.

3.8.3.3 Siemens-Westinghouse Information

A significant source of information was a report by Mary Anne Alvin of Siemens-Westinghouse titled "Thermal/Chemical Degradation of Ceramic Cross Flow Filter Materials - Final Report." Siemens-Westinghouse had conducted testing on both new and used Coors filters in a series of increasing thermal transients, where the system was heated to 1,550˚F. Various air flows were introduced to the vessel to rapidly drop the temperature once the combustor flame was extinguished. The filter element temperature would drop about 200˚F in 5 seconds and about 870˚F in seven minutes depending on the test conditions. Several Coors filters failed during this testing, primarily exposed elements from PFBC units, which suggests the possibility that elements exposed to operation may be more susceptible to failure than new filters.

Thermocouples were installed on the OD of the filter and through the filter wall to measure the ID temperature during the transient testing at Siemens-Westinghouse. These thermocouples were added to determine the thermal gradient (OD temperature - ID temperature) during these thermal transients. The thermal gradient across the wall during the most severe testing was approximately 100 to 125˚F. Because the gas is flowing through a porous wall it is logical that the temperature of the element would respond quickly, minimizing the thermal gradient.

It is unlikely, based on the information in the Siemens-Westinghouse report, that the element failures in the PCD were caused by a rapid change in *gas* temperature. The analysis of the PSDF operating data indicated that the rate-of-change in bulk temperature of the gas was always well below the rate-of-change used in the testing at Siemens-Westinghouse. However, there was still consensus that the failure was due to thermal stress since there was no apparent mechanical cause of failure (e.g., ash bridging).

The first filter element supplier meeting was held at the PSDF on January 21-22, 1998, while this analysis was underway. When the preliminary results of the data analysis were presented Dr. Lippert from Siemens-Westinghouse suggested the possibility of carryover of burning coal from the transport reactor to the PCD. Initially, this was not considered the primary cause of the failure due to the experience of April 1997.

About 600 lb of coal were inadvertently fed to the transport reactor during the start-up of April 1997 while the temperature in the reactor was at about 600˚F and in the PCD at about 400˚F. The coal apparently was heated to a point where it began to smolder by the time it entered the PCD. When it entered the PCD it burned, causing a sharp rise in the PCD outlet temperature. In this event the PCD outlet temperature exceeded the PCD inlet temperature by over 200˚F, however, the actual filter element temperature was probably much higher, as almost all of the clay bonded silicon carbide filters were destroyed. The temperature traces shown in figures 3.8-4 and -7 indicated that there was a rise in the temperature of the lower plenum, but it never exceeded the PCD gas inlet temperature. However, once the Siemens-Westinghouse report was reviewed and it was apparent that the elements probably did not fail due to rapid changes in gas temperature, the carryover of burning coal to the PCD was seriously considered.

3.8.3.4 Mechanical Testing of Exposed Filter Elements

Another possible cause of failure was accumulated damage (see section 3.8.3). This could have been caused by the accumulation of microcracks in the Coors filter during temperature swings in the process caused by feeder trips, start-up, etc. It has been reported that cracking of the Coors filter can be caused by pulse-cleaning, but one of the functions of the Siemens-Westinghouse fail-safe/regenerator was to preheat the pulse gas to minimize thermal stress.

Six Coors filter elements were given to SRI for mechanical testing after the initial failure in September. Two of the filter elements, KC027 and LC026, were virgin elements. Three filters (KC005, KC011, and LC025) with about 616 hours of on-coal exposure were removed during the July 1997 outage and one filter (KC007) was removed during the outage after the first failure. KC007 had only 12 more hours of exposure than the elements removed in July and, therefore, should have been similar unless a significant event occurred during the last 12 hours of testing the strength of the four exposed elements.

Nine 1-in.-tall O-rings were cut from each of the Coors filter elements: three rings from the "top" of the filter near the flange, three from the "middle," and three from the "bottom" (see figure 3.8-18). All of these rings were tested to failure by using the SRI hydrostatic O-ring tester. The results of this testing are shown in table 3.8-4 and are shown as plotted-vs-exposure hours in figure 3.8-19.

Data in table 3.8-4 and figure 3.8-19 show that:

- The average strength of the elements made in the LC batch is slightly higher than those made in the KC batch.

- There was about a 10-percent loss-of-strength over the 616 hours of exposure. This applies to both batches of elements.

- Six of the specimens from the element removed in the September outage (KC007) had an ultimate tensile strength comparable to the strength of the elements removed in July. The three O-rings from the flanged end of KC007, however, had markedly lower strength than the rest of the filter element.

It is very unlikely that the root cause of failure was accumulated damage given that there was only 12 hours of operational experience between the filter elements removed in July and the one in September.

The three O-rings from KC007 with low strength were unique in that the fracture formed during the test was not typical. As one can imagine, a "typical" fracture for an O-ring test would be nearly vertical. The fractures on these specimens, however, were vertical on one side and diagonal on the other. As part of their normal test procedure, SRI draws a reference "centerline" down the length of the filter element before the O-ring specimens are cut. Once these specimens were placed in their original orientation it was obvious that they had failed along a crack in the element that was not evident during machining as shown in figure 3.8-20.

(The sample marked "microscopy-2" failed during machining.) This crack appears similar to the cracks observed in Coors element KC013 that failed in November 1997. Mr. Colt Pears at SRI documented the cracks in this element as shown in figure 3.8-21.

3.8.3.5 Karhula Experience With Asahi Ceramic Tube Filter

One other useful piece of information in our analysis was the experience of the Karhula staff with the operation of the Asahi Ceramic Tube Filter. Their report suggested that soot formed by their start-up burner system may have ignited once a high-enough temperature was reached in the filter system. This combustion would cause very high local temperature gradients in the filter elements, which would lead to their failure.

This information reinforced Dr. Lippert's theory that coal was being carried into the PCD from the transport reactor (see section 3.8.3.3). Very high thermal gradients would be produced that would lead to the failure of the filter element once the burning coal landed on the filter elements.

3.8.3.6 Conclusions From Analysis

Listed below are the conclusions reached based on the results of the analysis reported in section 3.8.3.5:

- The Coors P-100A-1 filter element is mechanically strong but sensitive to thermal gradients.
- A temperature gradient (OD-ID) of about 280˚F is required to initiate microcracking on a Coors P-100A-1 filter element at an operating temperature of ~1,350˚F.
- The lack of any mechanical force (i.e., bridging) and the fact that nearly all of the failures occurred while the transport reactor was either transitioning to coal or during a coal feeder upset lead to the conclusion that the Coors filters probably failed due to thermal stress.
- Coors filter elements had been tested for over 3,300 hours successfully in PFBC conditions at Tidd and Karhula but were failing at the PSDF in less than 1,000 hours.
- Review of the operational data at the PSDF was inconclusive in determining the reason for the failure.
- Testing at Siemens-Westinghouse suggests that the Coors filter elements can survive substantial rapid changes in gas temperature without failure. The filter elements in this testing survived transients much larger than transients measured at the PSDF.

- Thermal gradient measured in the Coors filter during severe gas temperature transient testing at Siemens-Westinghouse was significantly less than that required to cause the filter element to fail.

- There was about a 10-percent loss-of-strength in the Coors filter over 600 hours.

- A crack that led to a significant reduction in strength was detected in the filter element removed after the September failure.

- The characteristics of the Coors P-100-A1 filter material readily allows for crack propagation in all directions.

- Experience from the early commissioning at Karhula suggested that thermal events leading to element failure could occur from the local combustion of carbon on the filter element surface.

3.8.4 Filter Element Thermocouples

It was obvious from this analysis that the existing plant instrumentation was unable to detect the carryover of small quantities of coal into the PCD. Therefore, the decision was made to add thermocouples to two filter elements—one Coors and one Pall 326—prior to the April 1998 test campaign.

3.8.4.1 Thermocouple Installation

The thermocouples installed were Inconel sheathed 0.062-in. diameter, type K, grounded junction. Six thermocouples were installed on each element: three on the ID and three on the OD. The thermocouples were grouped into ID/OD pairs; therefore, there were three ID/OD pairs on each filter element. The locations of these three pairs are shown in figure 3.8-22. Two pairs were located near the top of the filter element (about 6 inches from the flange) and oriented 180° apart. The final pair was located about 40 inches from the flanged end of the filter element directly below the pair at zero degrees.

The installation of the thermocouples on the outer surface was relatively straightforward. A small notch was machined on the surface with a thermocouple placed in the notch and cemented in place with mullite whisker reinforced Si_3N_4 ceramic cement. Several test pieces were machined into 2-inch-tall O-rings prior to installation of the thermocouples. The O-rings were notched and the ultimate tensile strength determined using the SRI hydrostatic O-ring tester mentioned previously in this report. There was no significant decrease in the strength of the machined rings when compared to the strength of O-rings with no notches.

Installing thermocouples on the inner bore of the filter element presented a challenge. The original idea was to bore a hole into the filter element and cement the thermocouple into the hole from the OD surface, perpendicular to the longitudinal axis of the filter element. However, there were concerns that the difference in the thermal conductivity between the thermocouple

and the ceramic would cause an increased heat flux along the length of the thermocouple, which would produce misleading results. Finally, the decision was made to bore a hole through the filter wall and then insert a loop of fine wire. The thermocouple was inserted through the bore of the filter element and into the wire loop. The wire was then pulled tight, drawing the thermocouple against the ID filter wall. Notches were machined in the ID wall for the thermocouple near the flange. The wire would be secured by wrapping it around the filter element and the hole plugged with the mullite whisker reinforced Si_3N_4 ceramic cement.

The filter elements were installed adjacent to each other at tubesheet location number B15 for the Coors filter and B16 for the Pall filter (see figure 3.8-13). A picture of the two elements showing the thermocouples is shown in figure 3.8-23. The thermocouples were not recorded with the plant information (PI) system as is typical. Instead, the results from these thermocouples were recorded using a high-speed data acquisition system from Dataq.

3.8.4.2 Results From Thermocouples

The transport reactor switched from the propane-fired start-up burner to coal feed on April 9. The thermocouples on the inlet and outlet of the PCD and on the plenum showed a relatively smooth transition to coal (see figure 3.18-14). However, within a few minutes of starting coal feed, pieces of Coors and Blasch filter elements were found in the ash removal system. The unit was shut down and it was found that both the Coors and six of the eight Blasch filter elements had failed (see figure 3.8-24).

Data recorded by the Dataq system and plotted along with data from plant instrumentation show several sharp "spikes" in the filter element thermocouples (figure 3.8-25) which were not seen by the plant instrumentation. It should be noted that the data shown was recorded by the upper thermocouples on the Pall filter and not on the Coors. Additionally, the measured transients were sporadic and not uniform, neither radially nor axially, on the filter element. Only one spike was measured on the lower set of thermocouples and the spikes were less severe on one side of the filter than on the other.

The source of the transients is believed to be the carryover of burning coal from the transport reactor to the PCD. The transport reactor was at a temperature of 950˚F when coal feed began during this start-up. The coal being fed was Alabama bituminous coal that is fairly slow to react. It is believed that the transport reactor temperature was too low to sufficiently burn the coal particles before they reached the PCD and the filter elements. A very local, high-temperature gradient was produced when particles produced by the burning coal collected on the filter elements. This caused the failure of the monolithic oxide filter elements.

It would be incorrect to assume that the 360˚F-temperature rise measured was the maximum temperature rise on the filter element during this event. It is not known how close the burning coal particle was to the thermocouple. If the coal particle landed directly on the thermocouple, then 360˚F is correct. However, the coal particles could have landed several inches away and the thermocouple was only recording the rise in the wall temperature as the heat was dissipated from the burning particles. The actual local gradient may have been much more severe.

It cannot be overemphasized that the recording of this transient occurred through an enormous amount of luck. Had the filter element been in a different location, the thermocouple oriented differently, etc., the transient may have never been seen. However, there were 13 different types of filters installed in the PCD at the time of the failure in April 1998. The only filter elements that failed were from Coors, Blasch, and Specific Surface. Table 3.8-5 details the type and number of filter elements installed and the number of filter elements that failed.

A primary question remaining was why the monolithic oxide elements failed while the monolithic silicon carbide elements and the composite elements remained intact.

3.8.5 Thermal/Mechanical Analysis of Coors Vs Other Ceramic Filter Elements

As discussed in section 3.8.3.1, two important properties of ceramic filters which determine the susceptibility of a ceramic material to thermal stress is the thermal expansion and the strain-to-failure. The thermal expansion of a variety of ceramic filter materials is shown in figure 3.8-26 and the stress-strain curve for most of these materials is shown in figure 3.8-27. (The testing of the 3M oxide and SiC materials by SRI had not been completed at the time of this writing.) The coefficient of thermal expansion (CTE) and strain-to-failure is summarized in table 3.8-6. This table shows the predicted strain-to-failure for Coors, Pall, and Schumacher filters at 1,000˚F (approximate temperature when the elements failed) based on values measured at room temperatures of 1,400; 1,500; and 1,600˚F. The room temperature strain-to-failure for DuPont and McDermott is shown because elevated temperature strain-to-failure has not been measured. Dividing the strain-to-failure by the coefficient of thermal expansion provides an estimate, based on a flat plate analysis, of the temperature gradient required to initiate microcracking in a filter element.

Given the above information, the DuPont and McDermott filters are apparently less sensitive to thermal gradients than the monolithic Coors, Pall, and Schumacher filters. The microstructure of the DuPont and McDermott filters is also more "forgiving" to thermal stress. However, it is interesting that the estimate of the thermal gradient required to fail the Pall and Schumacher filters is actually lower than the Coors. Given this, why did the monolithic silicon carbide filters not fail? The answer is probably due to differences in thermal properties, such as conductivity and microstructure.

3.8.5.1 Thermal Conductivity and Diffusitivity of Coors, Pall, and Schumacher Filters

One difference between the alumina/mullite and silicon carbide filter elements is how the materials dissipate heat based on their thermal properties. A measure of a material's ability to dissipate heat is defined as the thermal diffusitivity. The thermal diffusitivity is defined as:

$$\alpha = \frac{k}{cp * \rho}$$

where:

α = thermal diffusitivity, ft^2/hr
k = thermal conductivity, (Btu-in.)/(hr*ft^2*°F)
cp = heat capacity, Btu/(lb*°F)
ρ = density, lb/ft^3

SRI measured the thermal conductivity (see figure 3.8-28) and density of the Coors, Pall, and Schumacher elements. The heat capacity value is from literature. The values determined and the calculated thermal diffusitivity are shown in table 3.8-7.

The information in table 3.8-7 shows the silicon carbide filter elements manufactured by Pall and Schumacher have a much higher thermal diffusitivity than the Coors filter. In an event where there was a local thermal transient, such as experienced on April 9, the heat would be more readily dissipated in the Pall and Schumacher elements, which would tend to minimize the thermal gradient across the filter wall. Conversely, in the Coors material, the heat of burning coal would not readily dissipate, which could provide a high-enough gradient to cause catastrophic failure. SRI and SCS used these properties in an attempt to simulate the gradient that would occur across the filter element during this transient.

3.8.5.2 Microstructure

In addition to the higher thermal conductivity of the silicon carbide materials, the microstructures of the Coors filter and the silicon carbide are fundamentally different. The silicon carbide filters made by Pall and Schumacher are composed of fairly large silicon carbide grains held together by a "glassy" binder phase. This matrix is used for support as the filtration is performed by a membrane applied to the OD surface of the filter element.

There is no membrane applied to the Coors filter element but the fine-pore size in the support structure is relied on to provide the filtration. This results in the microstructure of the Coors element being much more homogeneous than its silicon carbide counterparts.

Cracks in the Coors filter matrix tend to propagate more readily in all directions (see section 3.8.3.4). Cracks propogate less readily in silicon carbide filters because of their heterogeneous nature. Cracks in the silicon carbide matrix can either terminate at a pore or at the interface between the binder phase and the silicon carbide grains. Eventually, enough of the binder "bridges" are damaged such that the element fails. This tends to make crack propagation in the silicon carbide filters less of an issue than with the Coors elements.

3.8.5.3 SRI Flat Plate Thermal Model

SRI performed a thermal calculation as a first approximation of the thermal gradient present in the Coors material compared to the silicon carbide materials, which imposed the measured temperature rise on a flat plate of material with the thermal properties (see table 3.8-7). The boundary conditions for this model are shown in figure 3.8-29. Several assumptions made to simplify this problem are obviously not correct. However, the calculation was made to see the relative effect the thermal properties of the three ceramic materials would have on the gradient

produced. The temperature rise of 360˚F in 60 seconds was applied as a boundary condition to the uninsulated surface and then removed. This was not through a change in the bulk gas temperature, but rather as a change on the surface of the material. The results of the calculation are shown in figure 3.8-30.

The thermal diffusitivity plays an essential role in the gradient calculated. The gradient produced in the Coors material in this case was much larger than that produced for either the Pall or the Schumacher filter. Again, the model for this calculation uses many simplifying assumptions. The calculated magnitude of the gradient may be incorrect, but the influence of the thermal conductivity in the calculations is apparent.

3.8.5.4 ANSYS 3D Model

Dr. Xiofeng Guan at the PSDF generated an ANSYS model of the filter element to expand the results analyses beyond the calculations performed by SRI. Two of the assumptions used in the SRI model were removed in this case: 1) flat-plate-vs-cylindrical geometry, and 2) heat transfer on both sides of the plate. The model for this calculation is shown in figure 3.8-31. The magnitude and duration of the thermal transient used is shown in figure 3.8-32. This transient was applied to the "spot" shown in figure 3.8-31. Obviously, the size of this spot was assumed since there was no way to determine the exact size, shape, or orientation of the transient source. One assumption used by both models is that the wall is solid (i.e., there is no gas flow through the wall). Since this could have a significant impact on the calculations, SRI and PSDF personnel are working together to build a model which would accommodate this effect.

The results of this model for the Coors filter are shown in figure 3.8-33 and for the Schumacher filter in figure 3.8-34. Both images were generated at a time equal to 55 seconds, which corresponds to the peak of the thermal event, and the temperature scale is the same in both cases. From these results, it is apparent that the temperature gradient is much more localized in the Coors filter than in the Schumacher. The higher thermal diffusitivity of the Schumacher filter allows for the dissipation of heat away from the source of the thermal transient, which minimizes the thermal gradient across the wall. The thermal gradients calculated in the center of the spot for the Coors, Pall, and Schumacher filters are shown in figure 3.8-35. The curves generated are slightly different, but certainly within the magnitude of the SRI model shown in figure 3.8-30.

3.8.5.5 Does this mean that a silicon carbide filter cannot be thermally broken?

Unfortunately, no. The thermal gradient required to initiate microcracking of a Pall 326 filter is roughly 75 percent of the gradient required to initiate microcracking in a Coors filter (see table 3.8-6). For a Schumacher TF20, the gradient required to initiate microcracking is only about 60 percent of that required for a Coors filter. However, the thermal conductivity of Pall 326 is about 3 times and the Schumacher TF20 about 4 times the thermal conductivity of the Coors, so the gradient produced by any thermal transient would be less severe for the 326 or TF20 filters. In fact, the curves in figures 3.8-30 and figures 3.8-35 indicate that by these models the magnitude of the gradient produced in this event could have been sufficient to initiate microcracks, depending on the location of the thermocouple relative to the location of the hot

spot. However, the microstructure of the clay-bonded silicon carbide filters allows them to sustain greater damage without failure than Coors due to thermal gradients.

Operational experience at the PSDF has also demonstrated that silicon carbide filters can thermally fail during operation. As explained in section 3.8.3.3, a thermal event occurred on April 7, 1997, that caused the failure of nearly all of the silicon carbide filter elements installed. However, it is believed that the magnitude of the transient occurring on the filter element surface during that event was substantially greater than the transient recorded in April 1998. A second thermal event that caused the failure of five silicon carbide (four Pall 326 and one Schumacher TF20) filter elements and one monolithic oxide filter element from Ensto occurred on October 17, 1998. In this event, coal was again burned in the PCD while sand was being added to the transport reactor. At the time of this report the investigation into the cause of the event and failures had just begun; however, the staff of a hot-gas filter system must always be diligent to insure that coal is never fed to the combustor at such a time when complete combustion cannot occur before the process stream reaches the filter elements.

3.8.6 Conclusions and Future Plans

The results of this analysis provided a great deal of insight into both the operation of the transport reactor and the PCD at the PSDF as well as the strengths and weaknesses of various ceramic filter materials. The conclusions drawn from this study are described below:

- The root cause of failure for the Coors filters was most probably the carryover of burning carbon (coal) from the transport reactor to the PCD. The reason that the burning carbon was present was probably because the transport reactor was too "cool" for the type of coal being fed at the initiation of coal feeding. Therefore, the coal was not completely combusted before reaching the filter elements. The operational procedure of the transport reactor has been changed so that the reactor temperature would be much higher before coal feed starts. Since essentially all of the failures occurred during initiation of coal feed or during a coal feeder upset it is very likely that this mechanism was the root cause of all the Coors filter failures.

- When the burning coal reached the filter element a local-temperature transient occurred, creating a thermal gradient through the filter wall.

- Whether or not the thermal gradient produced a failure depended on the thermal/mechanical properties of the filter elements. The Coors filters have a relatively low-thermal conductivity that hindered the dissipation of the gradient throughout the filter body. The significantly higher thermal conductivity of the Pall and Schumacher filters allowed for rapid dissipation of the heat and minimization of the temperature gradient and thermal stress through the filter wall. However, experience at the PSDF indicates that the monolithic silicon carbide filters can fail under thermal stress.

- The composite oxide filters from DuPont, McDermott, and 3M did not fail for a variety of reasons. First, the strain-to-failure of these materials is of a greater magnitude than that of the monolithic filters. This indicates that the transient

required to fail these filters due to thermal gradients is significant and may not be possible in this application. Additionally, their structure does not readily propagate cracks through the filter wall.

- The Coors filters have performed well for extended periods (> 3,300 hours) at Tidd and at Karhula. The most likely reason for this success was the "maturity" of the two combustors at the time that the Coors filters were installed. The Siemens-Westinghouse filter systems at both facilities were installed well after the initial start-up and commissioning of the units.

- The thermal and mechanical properties of the virgin filter elements can be used to determine the susceptibility of a filter element to failure caused by thermal gradients. Mathematical models as well as finite element analysis are very useful in determining the limits that can lead to failure. Development of a "flow-through" model will be useful to better represent the thermal gradient in a ceramic filter during a transient.

3.8.6.1 Should the Coors filter be used again?

It is reasonable to ask if the Coors filter element is suitable for this application. As with most things in life the answer is, it depends. The Coors filter is mechanically one of the strongest filter elements made, and it is chemically stable in the aggressive environment of the PFBC. However, its thermal/mechanical properties make it one of the most susceptible to thermal gradients. The decision on whether to use the Coors filter will depend on the experience base and operating discipline of the operating facility. For example, the Coors filter is probably not suitable for use in the initial start-up of a new facility. However, as experience is gained and operational difficulties are overcome the Coors filter will probably last a long time in the absence of thermal events. To date, Coors filters have operated successfully for over 3,300 hours at other facilities.

The silicon carbide filter is more forgiving to thermal transients, but it will also fail if the thermal stress is severe. Additionally, literature suggests that the aggressive chemical environment of the PFBC may limit the useful life of this group of filters, especially at temperatures above 1,400˚F. However, only long-term operating experience will provide the ultimate guide for suitability.

Finally, one group of filter elements that appears to be extremely encouraging under these conditions is the composite oxide filters from DuPont, McDermott, and 3M. In general, the composite filters have a very high strain-to-failure and unique microstructure that combine to make them very unlikely to fail due to thermal stress in this environment. The operational history of these filters is rather limited, but operational experience to date at the PSDF has been encouraging. As the mechanical properties of these elements are evaluated over time, confidence in their use will improve. The relatively high cost of these elements at this time is a drawback; however, the cost is expected to decrease as the production of these filters moves out of the R&D lab.

3.8.6.2 What is left to do?

This report is a big step towards the completion of this analysis, but there is some work still outstanding. In the next several months the work listed below will be completed, at which time an addendum to this report will be issued.

- Several filter element pieces, including remaining segments of KC007, have been shipped to Coors for microstructural (SEM and EDAX) analysis.

- An exhaustive review and documentation of the PSDF data from April 1997 to date is underway to determine thermal cycles, log-pulse events, transport reactor temperatures at the time of coal feed, etc. The purpose of this is to look again, this time in hindsight, to discover what can be learned from the plant data and then use this knowledge to prevent a repeat of the same problems that occurred.

- Coors filters will probably be reintroduced into the system once PSDF staff is comfortable that the carryover issue has been resolved. The Coors filter element is mechanically strong, chemically stable, and one of the less expensive filter elements.

- Additional ANSYS simulation is being performed to calculate the stress imposed by this thermal gradient.

3.8.7 Acknowledgments for Section 3.8

This report is the culmination of about 1 year of diligent work by a large number of people. The author expresses thanks to Matt Davidson, Edwin Galloway, Xiaofeng Guan, and Patrick Scarborough at the PSDF and Jack Spain and Stuart Starrett at SRI.

Additionally, the author would like to thank the operators and mechanics who repeatedly had to take apart the PCD and ash removal system during failures. Also, very instrumental were the SRI technicians, who did a great job of machining specimens, installing thermocouples, and providing the material test data.

Thanks also for the contributions of many people who provided support and direction along the way, including Rich Dennis, Ted McMahon, Jim Longanbach, Bob Dahlin (SRI), Carl Landham (SRI), Randall Rush, Tim Pinkston, Tom Lippert, Zal Sanjana, and Mary Anne Alvin. The report by Mary Anne Alvin, "Thermal/Chemical Degradation of Ceramic Cross Flow Filter Materials - Final Report," was especially useful in helping to narrow the list of possibilities for failure.

Finally, the author would especially like to thank Eric Braaton, Rob Lucernoni, and Gary Klapper from Coors Ceramics for their help and patience as the PSDF worked to resolve the causes of failure.

3.8.8 References for Section 3.8

Asahi Ceramic Tube Filter Testing on a 10-MWth Pressurized Circulating Fluidized-Bed Combustor, Final Report, EPRI TR-102407, RP3161-01, December 1993.

Physical, Mechanical, and Thermal Properties of Coors Alumina Mullite Filter Material, Final Report to US DOE/METC, Task 7 of Contract Number: DE-AC21-89MC26233, August 1994.

Technical Progress Report for M.W. Kellogg Transport Reactor Train With Siemens-Westinghouse Particulate Control Device: January 1997-December 1997, section 3.27, prepared by
Southern Company Services. DOE Cooperative Agreement Number DE-FC21-90MC25140, December 1998.

Thermal/Chemical Degradation of Ceramic Cross Flow Filter Materials - Final Report, DOE/METC Contract No. DE-AC21-88M25034, August 31, 1995.

Table 3.8-1

Coors P-100A-1 Filters Installed in April 1997

Top Plenum				
T3 - LC025	T4 - LC024	T5 - KC011	T6 - KC012	T7 - KC009
T21 - KC020	T22 - KC019	T23 - KC018	T24 - KC017	T25 - KC010
Bottom Plenum				
B8 - KC002	B9 - KC008	B10 - KC007	B11 - KC006	B12 - KC005
B26 - LC022	B27 - KC001	B28 - KC004	B29 - KC003	

Note: The "T" designation refers to the top plenum and the "B" designation is for the bottom plenum. The number is the location on the tubesheet (refer to figure 3.8-1).

Table 3.8-2

Coors Filters Installed in July 1997

Top Plenum			
T2 - KC015 (N)	T3 - KC026 (N)	T4 - KC025 (N)	T5 - KC028 (N)
T6 - KC031 (N)	T19 - KC014 (N)	T20 - KC014 (N)	T21 - KC030 (N)
T22 - KC016 (N)	T23 - KC013 (N)	T24 - KC017 (U)	T25 - KC010 (U)
Bottom Plenum			
B8 - KC002 (U)	B9 - KC008 (U)	B10 - KC007 (U)	B11 - KC006 (U)
B12 – KC005 (U)	B26 - LC022 (U)	B27 - KC001 (U)	B28 - KC004 (U)
B29 - KC003 (U)			

Note: The (N) represents a new element from Dr. Chen and the (U) represents a used element left in the vessel from the previous run.

Table 3.8-3

Coors Filters Installed in September 1997

Top Plenum			
T2 - KC015	T3 - KC026	T4 - KC025	T5 - KC028
T6 - KC031	T19 - KC014	T20 - KC014	T21 - KC030
T22 - KC016	T23 - KC013		
Bottom Plenum			
B9 - KC010	B10 - KC017		

Table 3.8-4

Coors Filter Element Ultimate Tensile Strength

		Ultimate	Tensile	Strength	psi		
Element		KC027	LC026	KC005	KC011	LC025	KC007
Hours		0	0	616	616	616	628
	Specimen						
Bottom	1	1530	1958	1797	1346	1544	1270
	2	1700	1945	1785	1309	1618	1400
	3	1700	1913	1713	1323	1740	1610
Middle	4	1663	2062	1723	1574	1471	1380
	5	1555	1767	1625	1487	1524	1570
	6	1630	1873	1457	1472	1795	1660
Flange	7	1813	1705	1712	1562	2059	250
(Top)	8	1744	2201	1600	1534	1886	150
	9	1755	2045	1868	1542	1797	450

Table 3.8-5

Filter Elements Installed in April 1998

Manufacturer	Type	Material	No. Installed	No. Failed
3M	Oxide	Composite	6	
	Type 203	Composite - SiC	5	
Blasch		Alumina/mullite	8	6
Coors	P-100A-1	Alumina/mullite	2	2
DuPont	PRD66C	Composite	9	
IF&P	REECER	Recrystallized SiC	1	
McDermott		Composite	9	
Pall	326	SiC	14	
	442T	SiC	10	
	FeAl	Metallic - FeAl	2	
Schumacher	TF20	SiC	10	
	T10-20	SiC	10	
Specific Surface	CC-4001	Cordierite	2	1

Table 3.8-6

Coefficient of Thermal Expansion, Strain-to-Failure,
and Estimated Thermal Gradient Required to Initiate Microcracking in a Filter Element

Filter Element	Strain-to-Failure (in./in.)	CTE (in./in./°F)	Estimated Gradient (°F)
Coors P-100-A1[1]	$0.80*10^{-3}$	$2.8*10^{-6}$	280
DuPont PRD66C[2]	$1.65*10^{-3}$	$2.2*10^{-6}$	750
McDermott[2]	$2.10*10^{-3}$	$4.6*10^{-6}$	456
Pall 326[1]	$0.60*10^{-3}$	$2.8*10^{-6}$	210
Schumacher TF20[1]	$0.40*10^{-3}$	$2.4*10^{-6}$	170

Notes: 1. Probable values at 1,000°F.
2. Probable values at room temperature.

Table 3.8-7

Thermal Diffusitivity of Ceramic Filter Materials

Filter Element	Thermal Conductivity (Btu-in./hr*ft^2*°F)	Heat Capacity (Btu/lb*°F)	Density (lb/ft^3)	Thermal Diffusitivity (Ft^2/hr)
Coors	11	0.29	101	0.031
Pall 326	38	0.29	115	0.095
Schumacher TF20	52	0.29	119	0.126

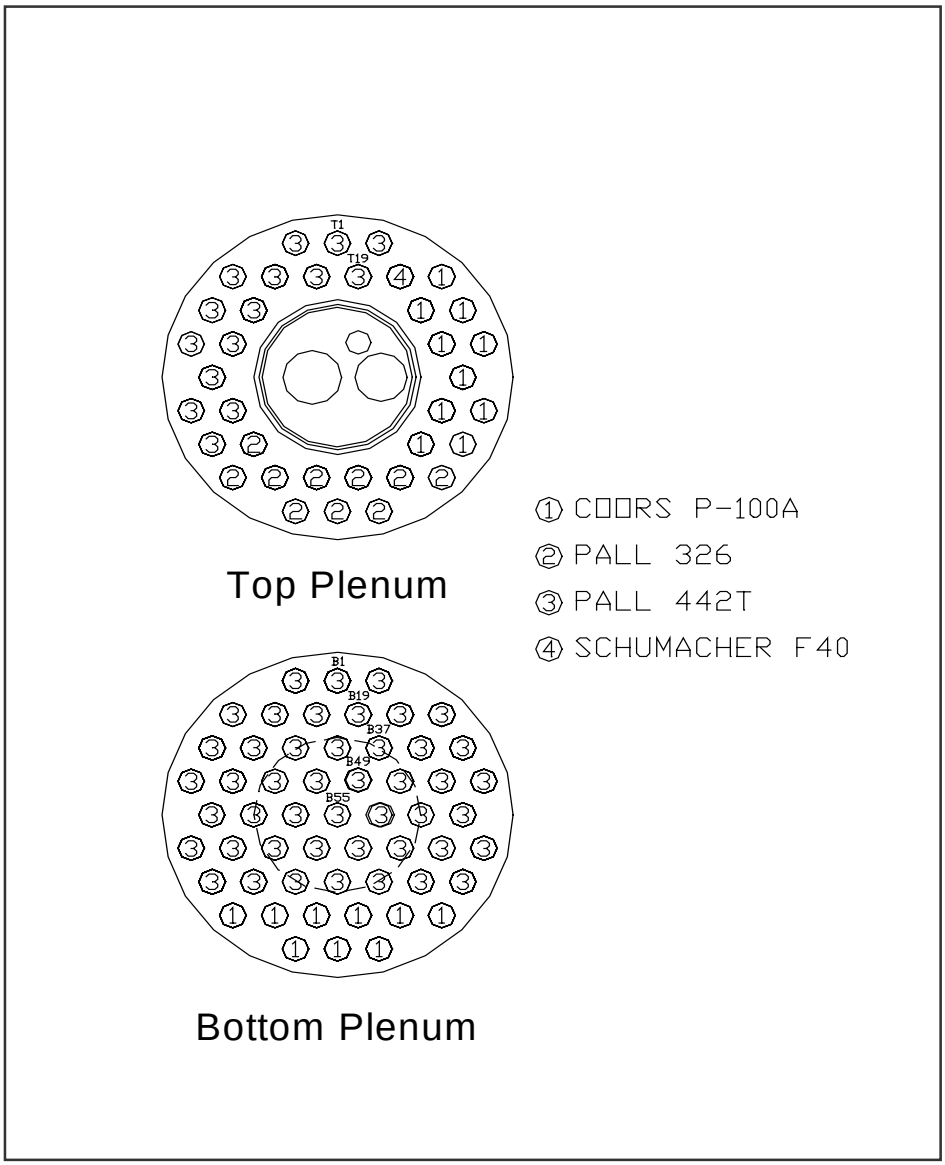

Figure 3.8-1 Tubesheet Map for April 1997

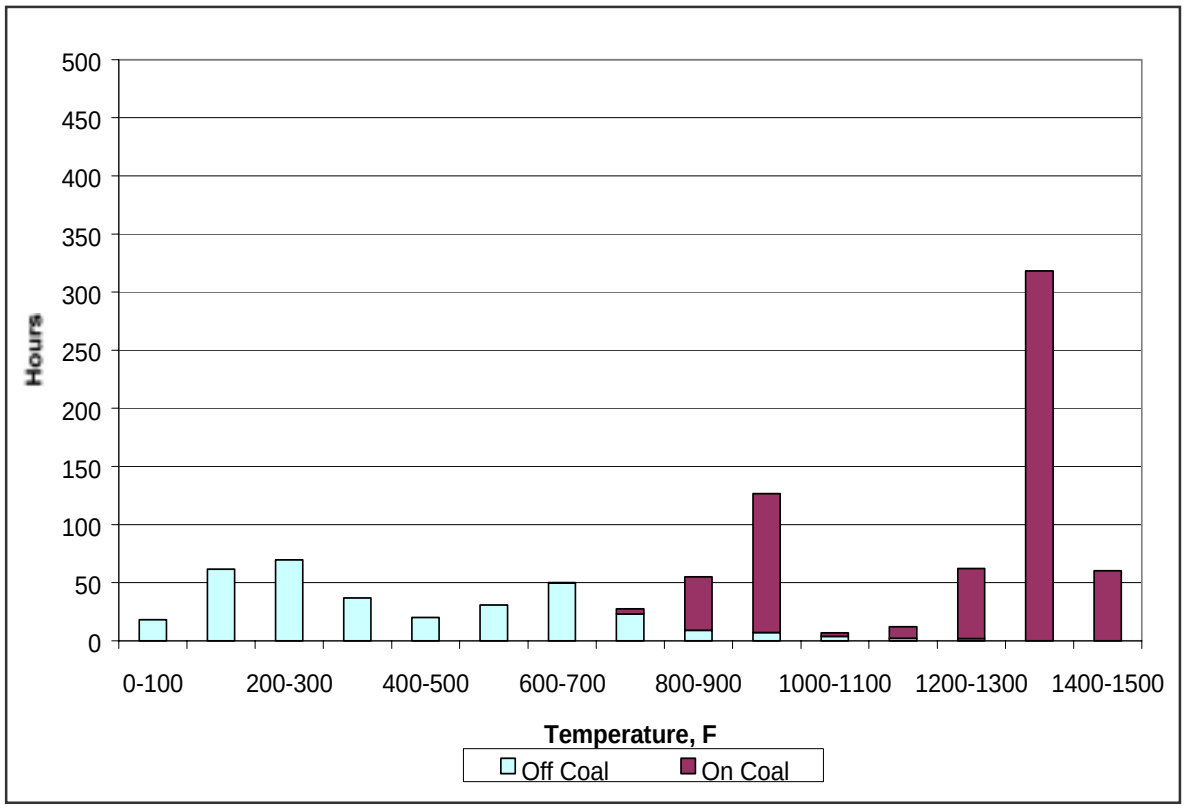

Figure 3.8-2 Time/Temperature Operating History of PCD From April 1997 to July 1997

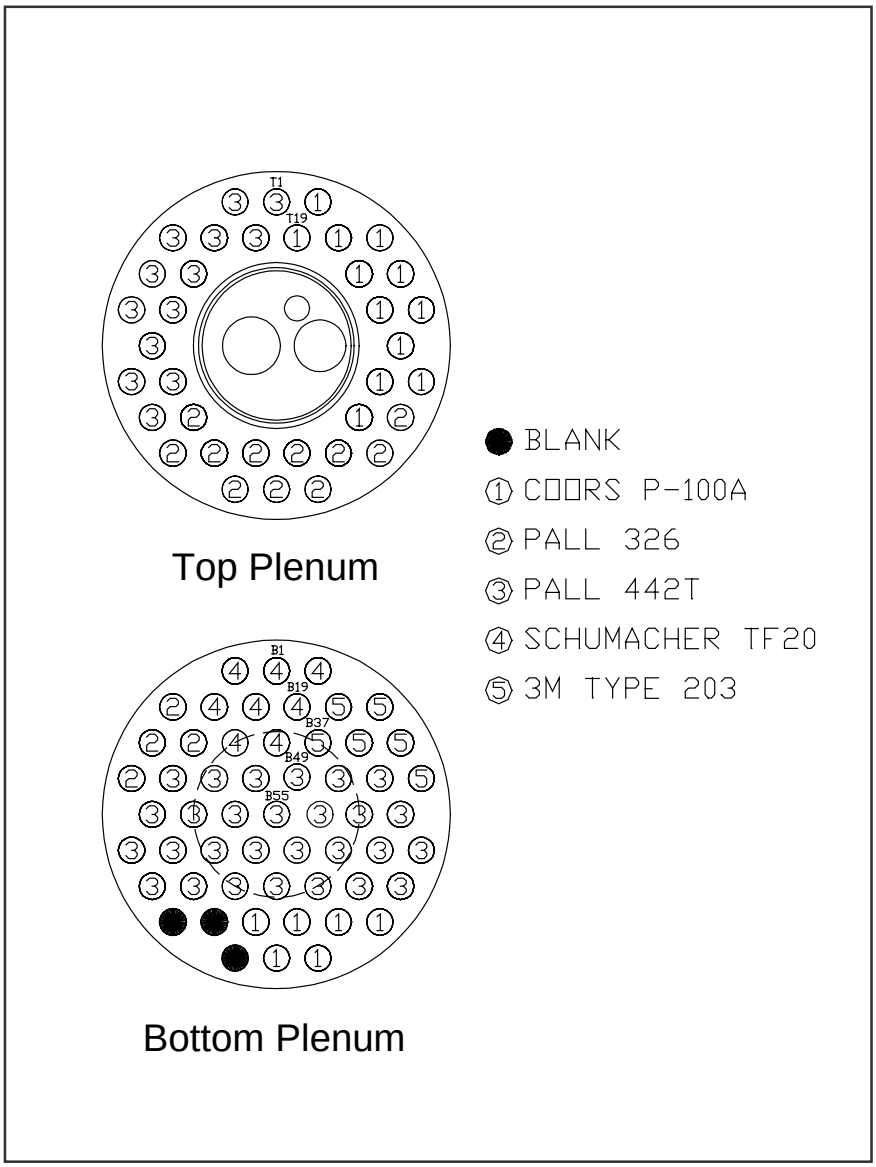

Figure 3.8-3 Tubesheet Map for July 1997

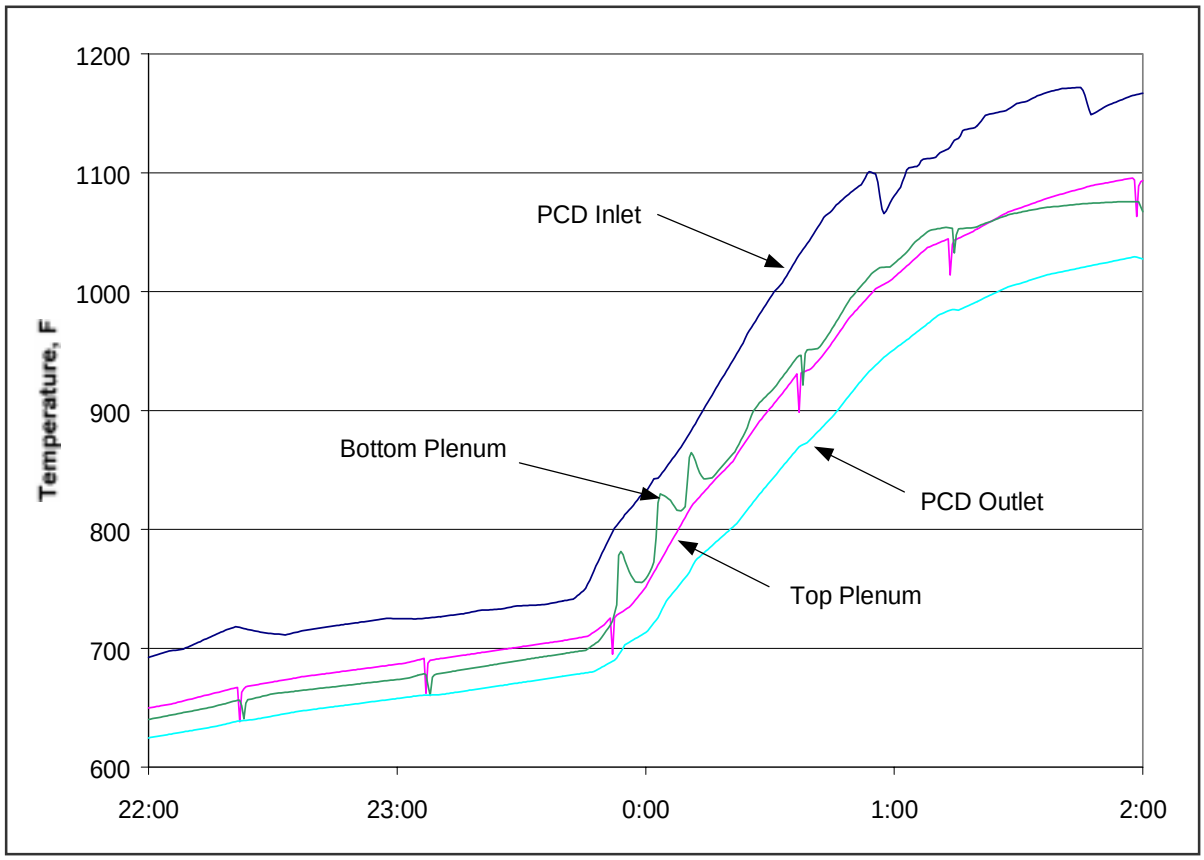

Figure 3.8-4 PCD Temperatures During Start-Up on August 31/September 1, 1997

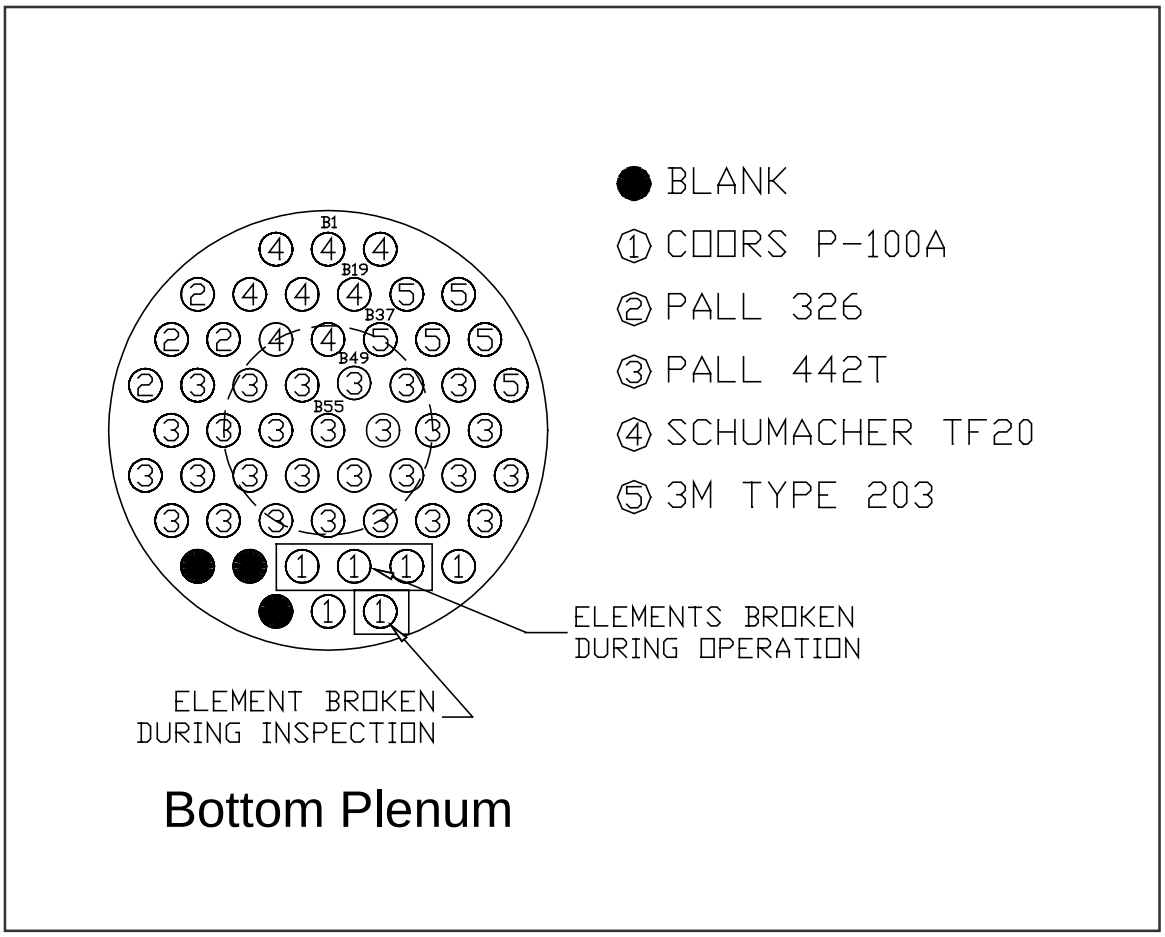

Figure 3.8-5 Tubesheet Map Showing Location of Broken Coors Filters

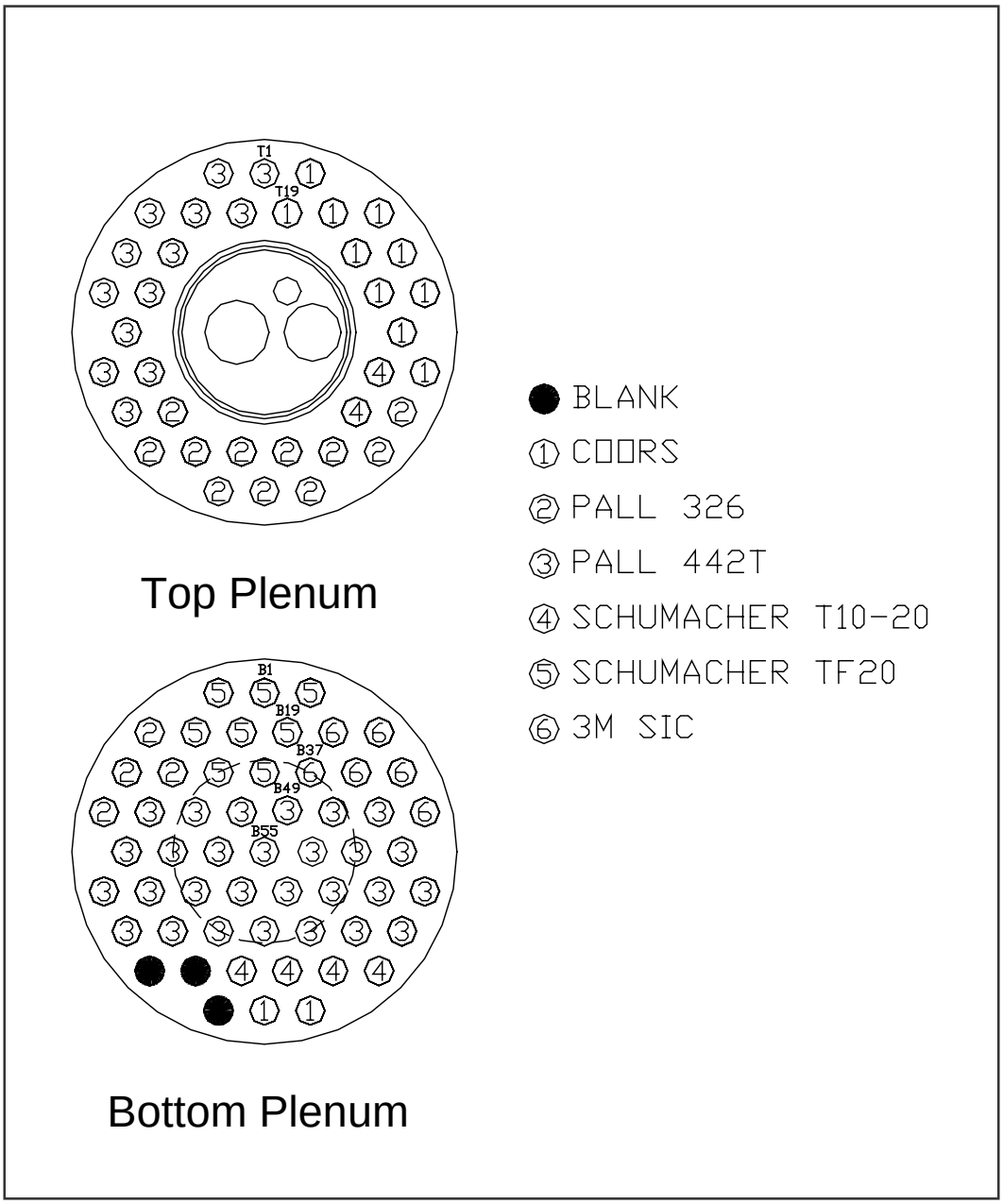

Figure 3.8-6 Tubesheet Map for September 1997

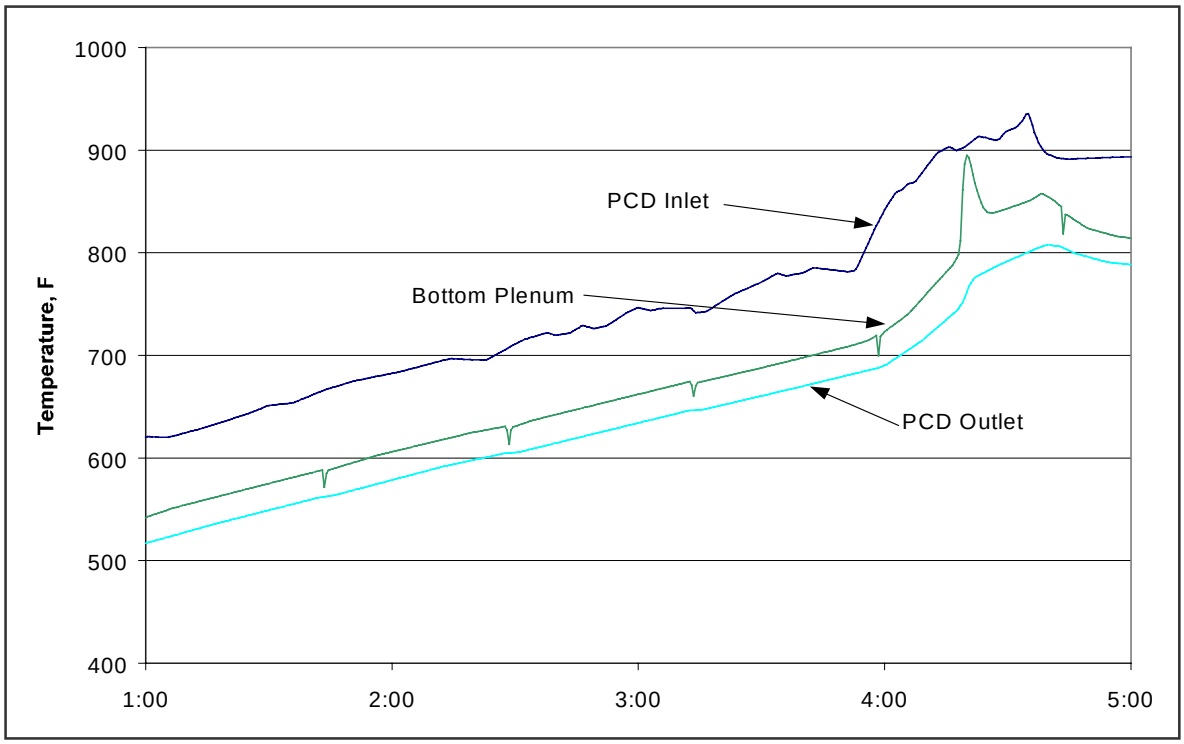

Figure 3.8-7 PCD Temperatures During Start-Up On September 7, 1997

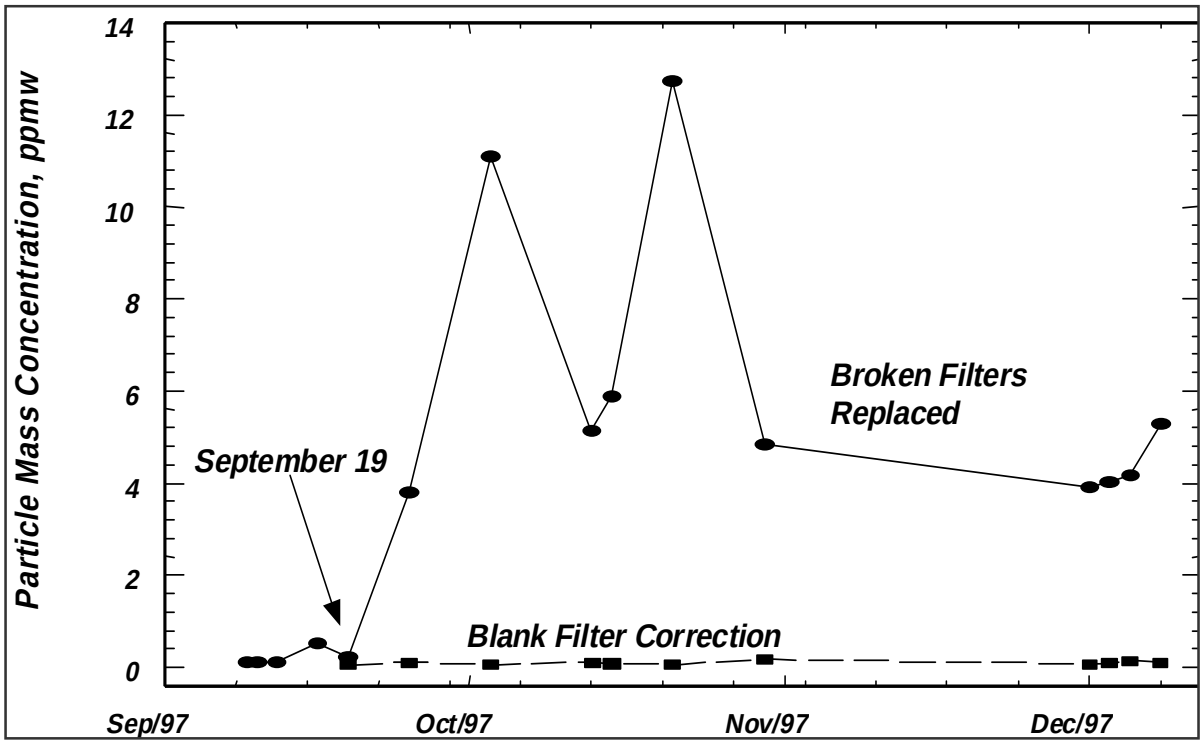

Figure 3.8-8 PCD Outlet Loadings During the September-to-December 1997 Test Campaign

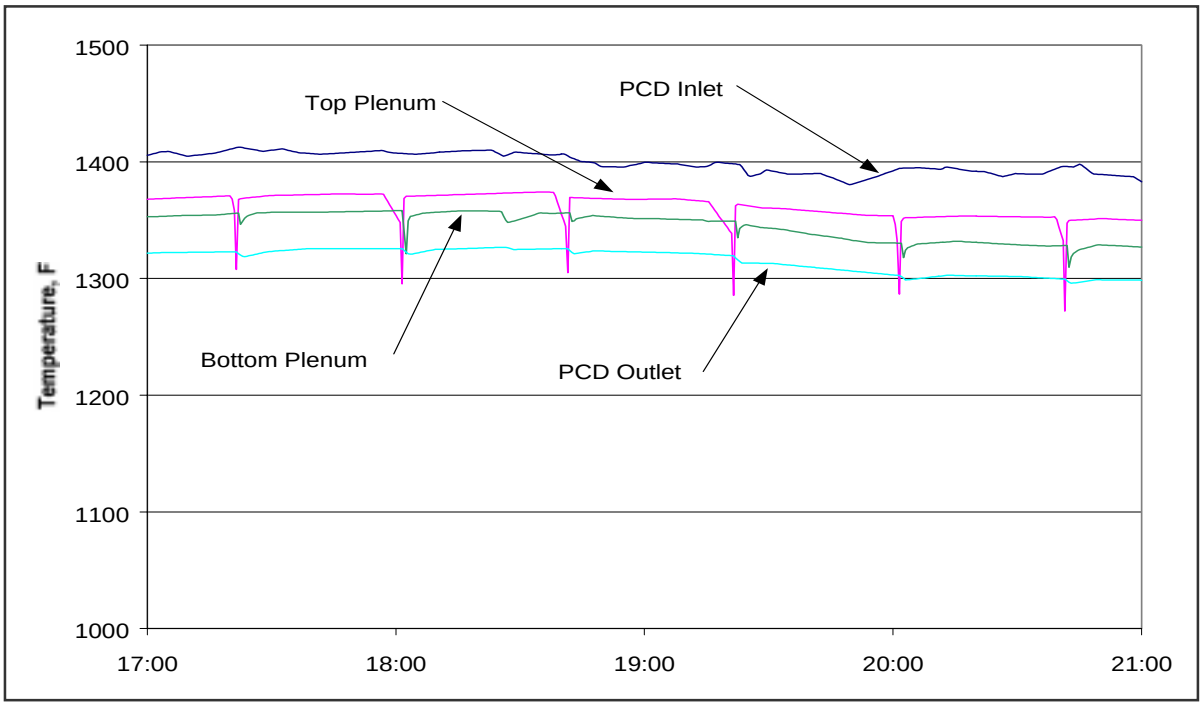

Figure 3.8-9 PCD Temperatures During Element Failure of September 19, 1997

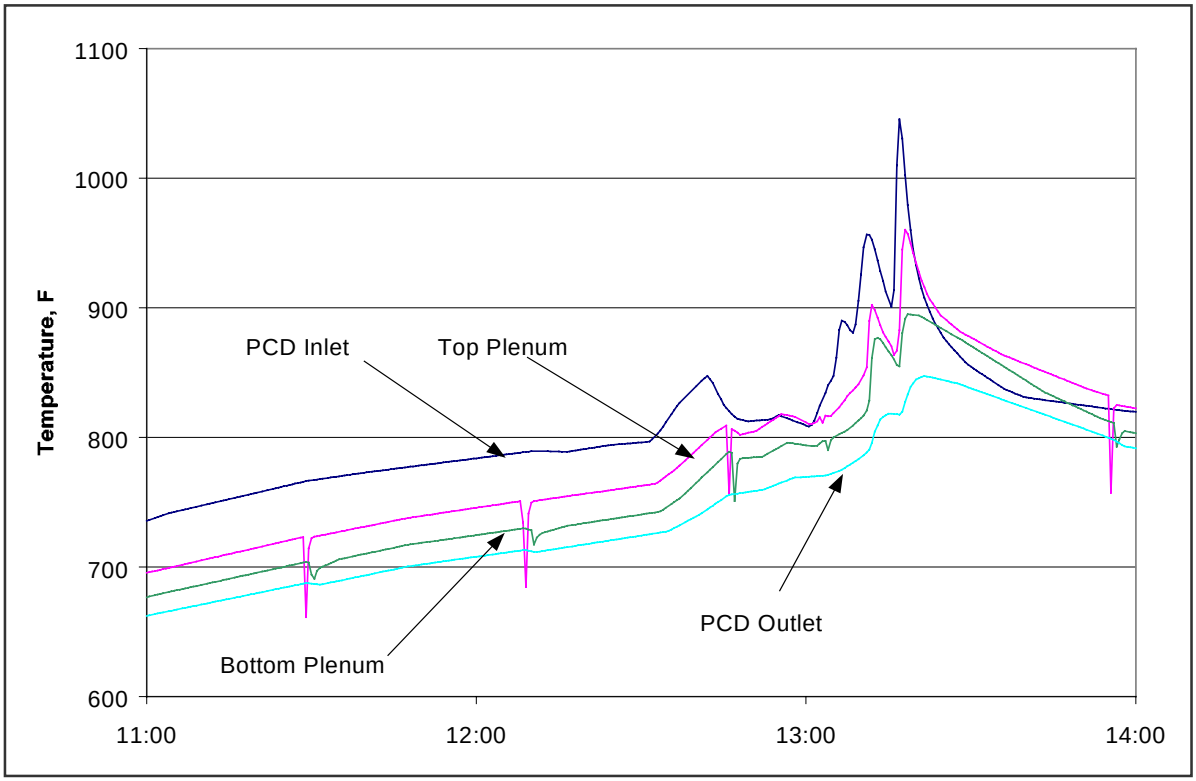

Figure 3.8-10 PCD Temperatures During Coal Feeder Upset on November 2, 1997

Figure 3.8-11 Broken Coors Filters After Transient of November 2, 1997

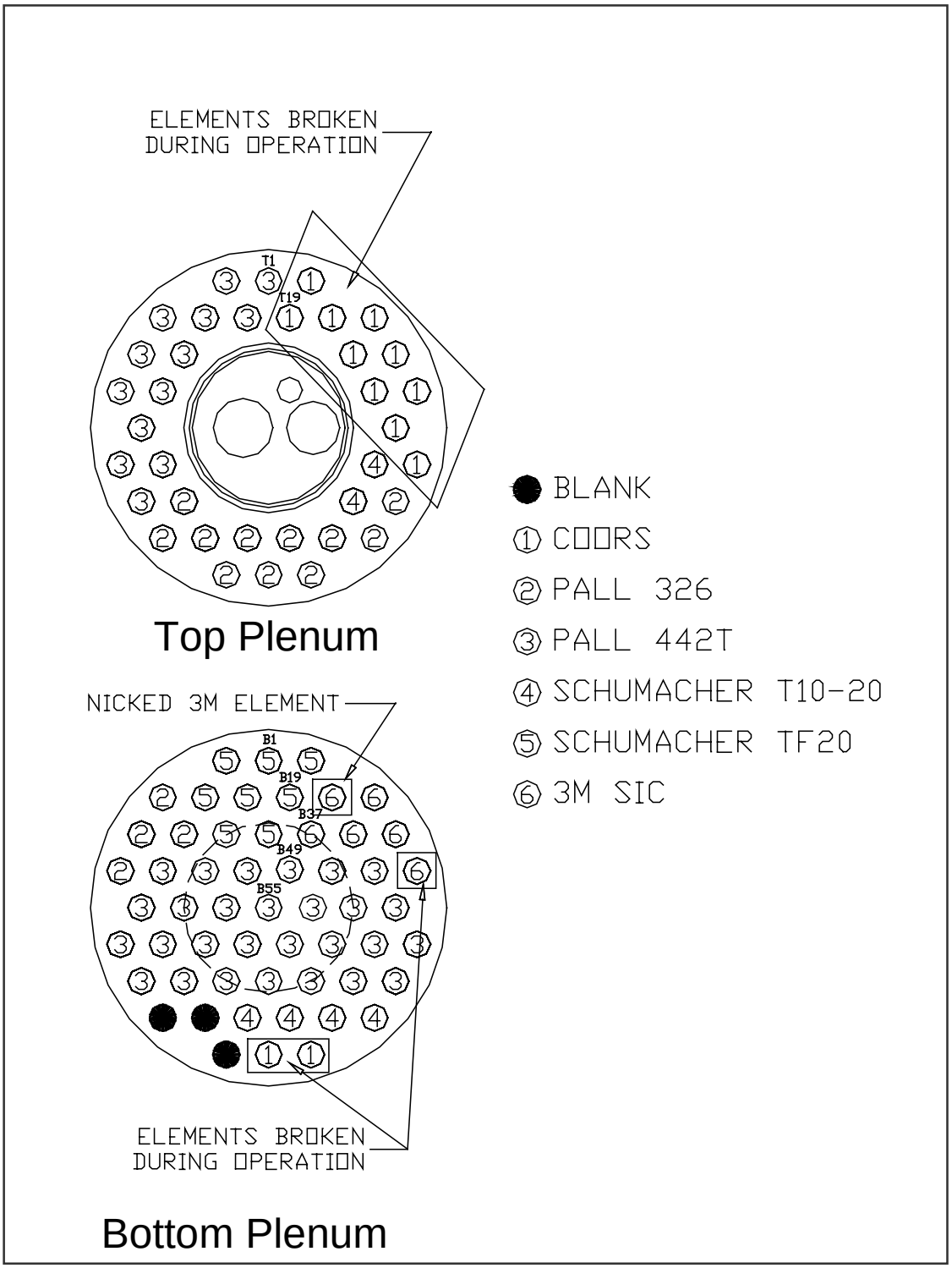

Figure 3.8-12 Location of Broken Filters After Transient of November 2, 1997

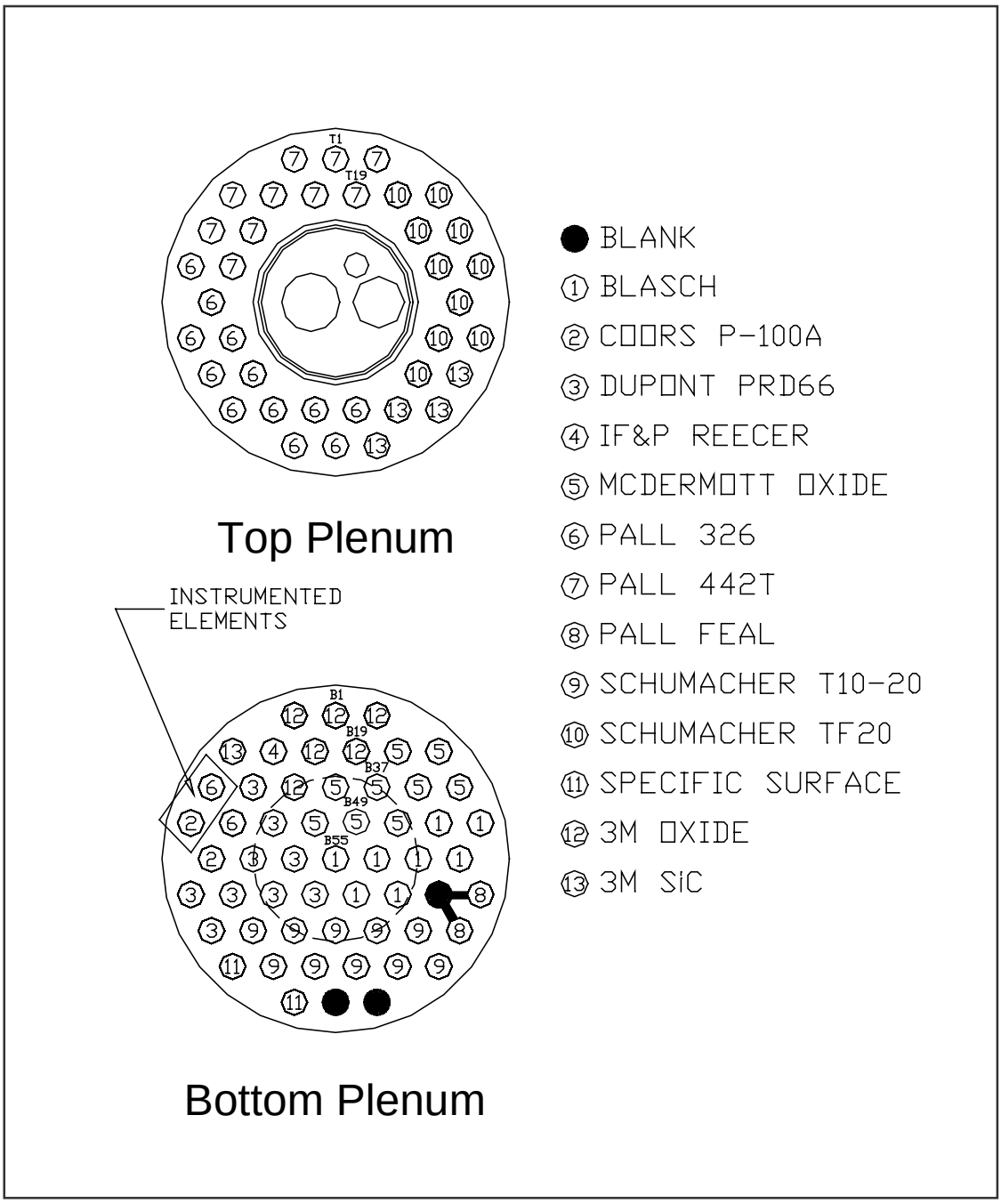

Figure 3.8-13 Location of Instrumented Filter Elements, April 1998

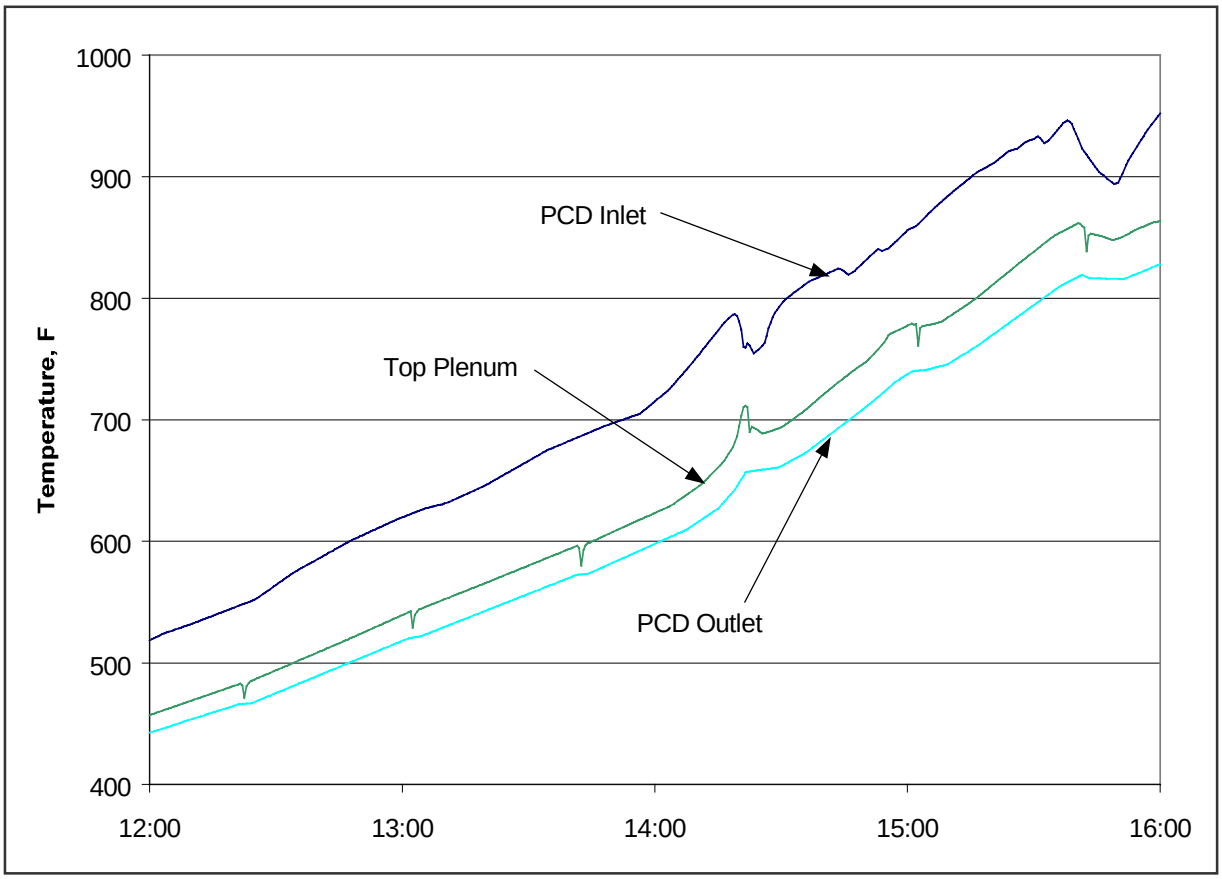

Figure 3.8-14 PCD Temperatures During Candle Failures on April 9, 1998

3.8-15 Broken Coors Filter Element Hanging From Thermocouple

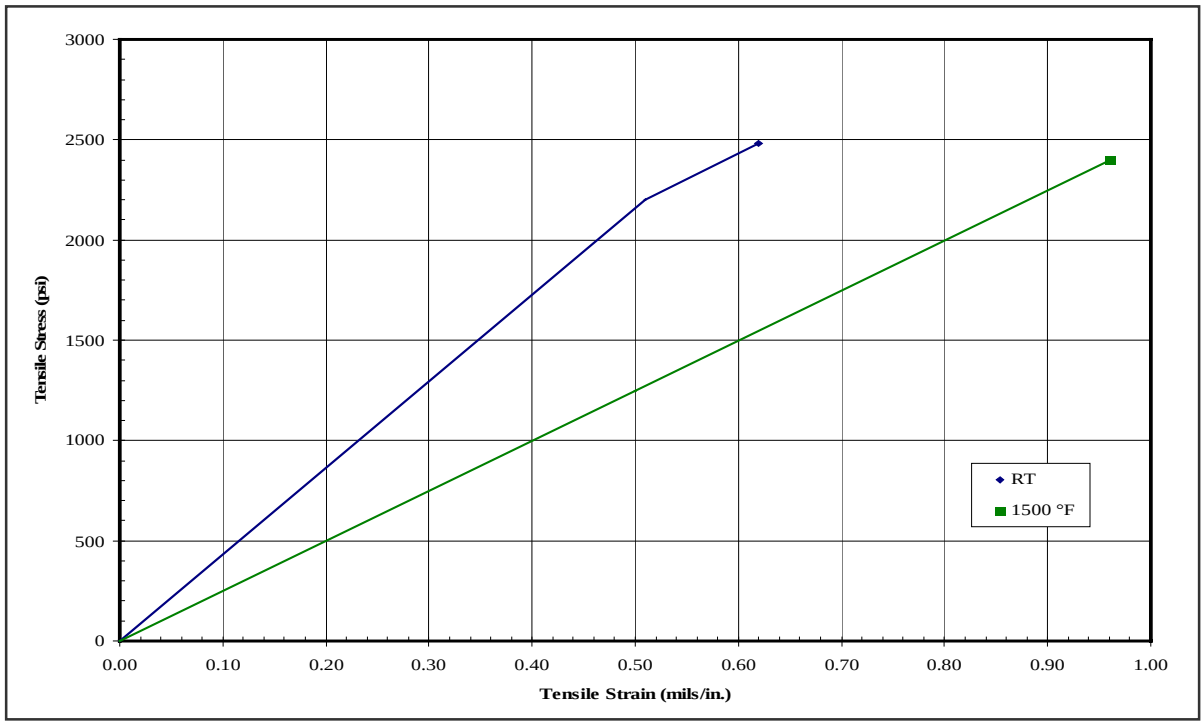

Figure 3.8-16 Probable Axial Tensile Stress-Strain Responses for Coors P-100A-1 Filter Element

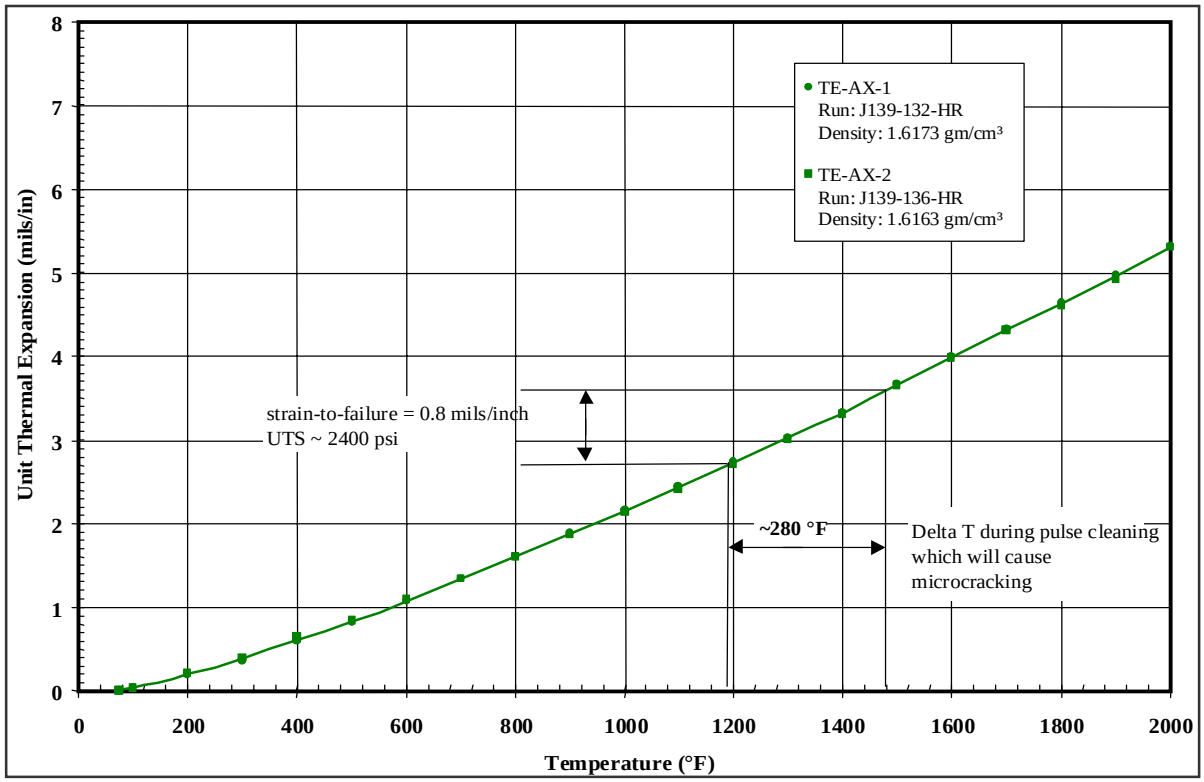

Figure 3.8-17 Thermal Expansion of Coors P-100A-1 Filter Element

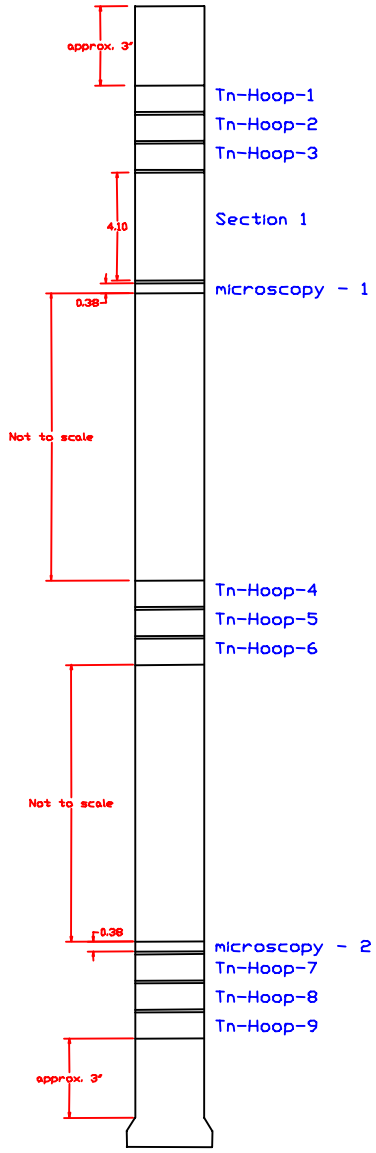

Figure 3.8-18 Cutting Plan for O-Ring Testing of Coors Filter

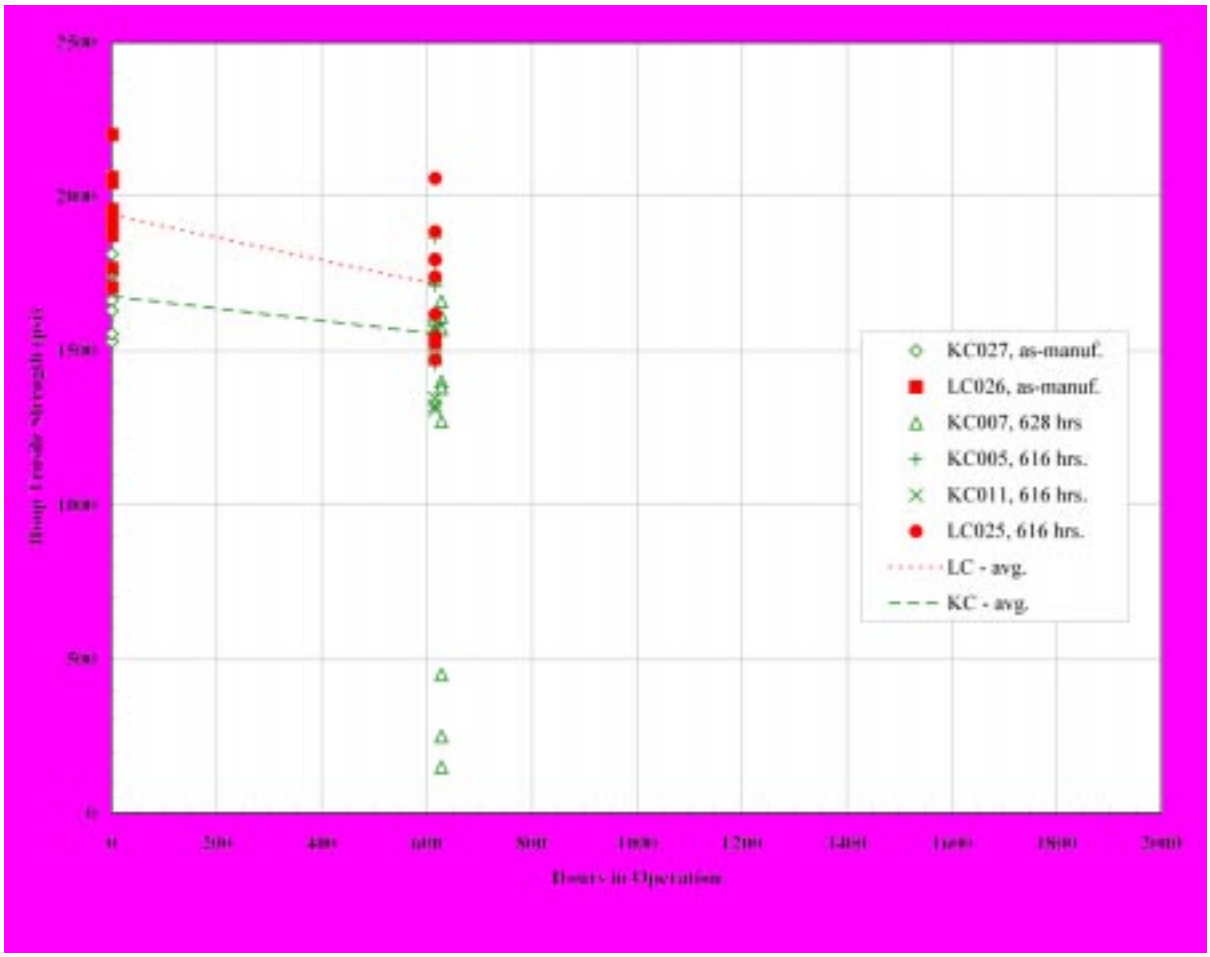

Figure 3.8-19 Hoop Tensile Strength of Coors P-100A-1

Mic-2

Tn-hoop-7

Tn-hoop-8

Tn-hoop-9

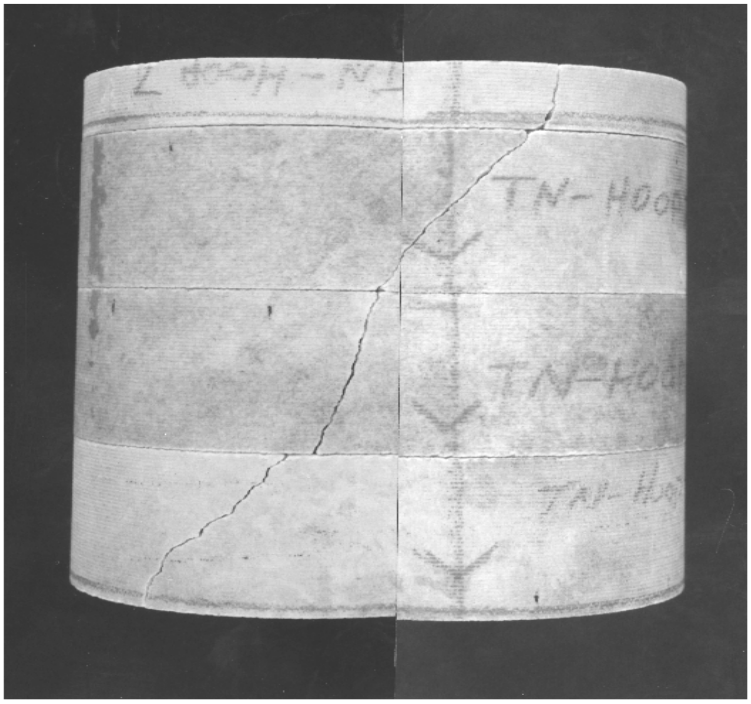

Figure 3.8-20 Crack Propogating Through Hoop Tensile Specimens of Coors Filter Element KC007

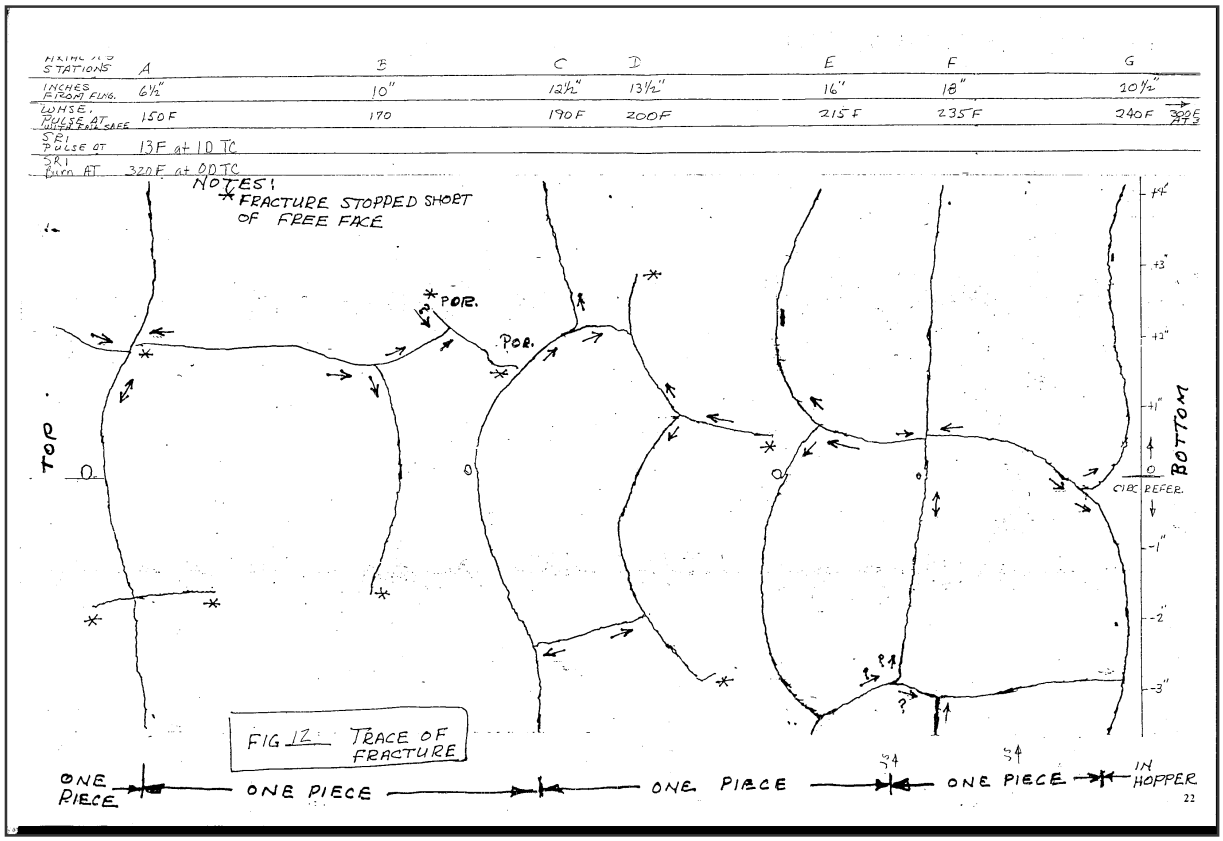

Figure 3.8-21 Diagram of Cracks in Broken Coors P-100-A1 Element KC013

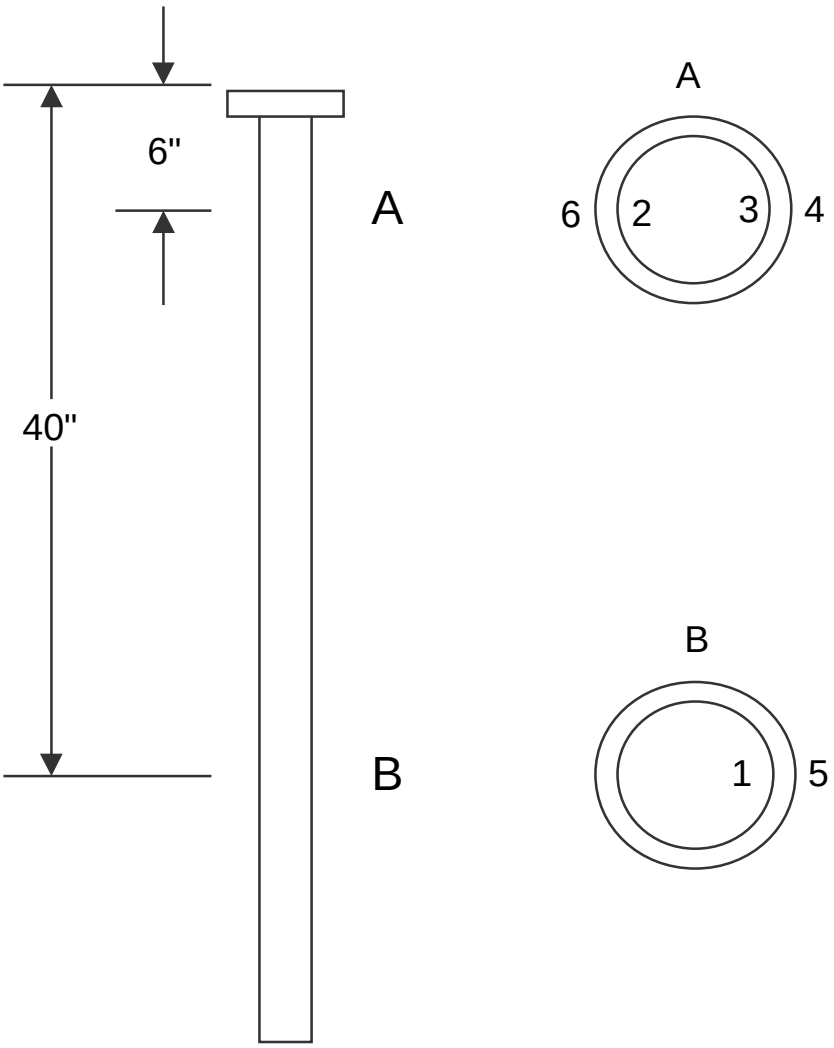

Figure 3.8-22 Approximate Locations of ID and OD Thermocouples

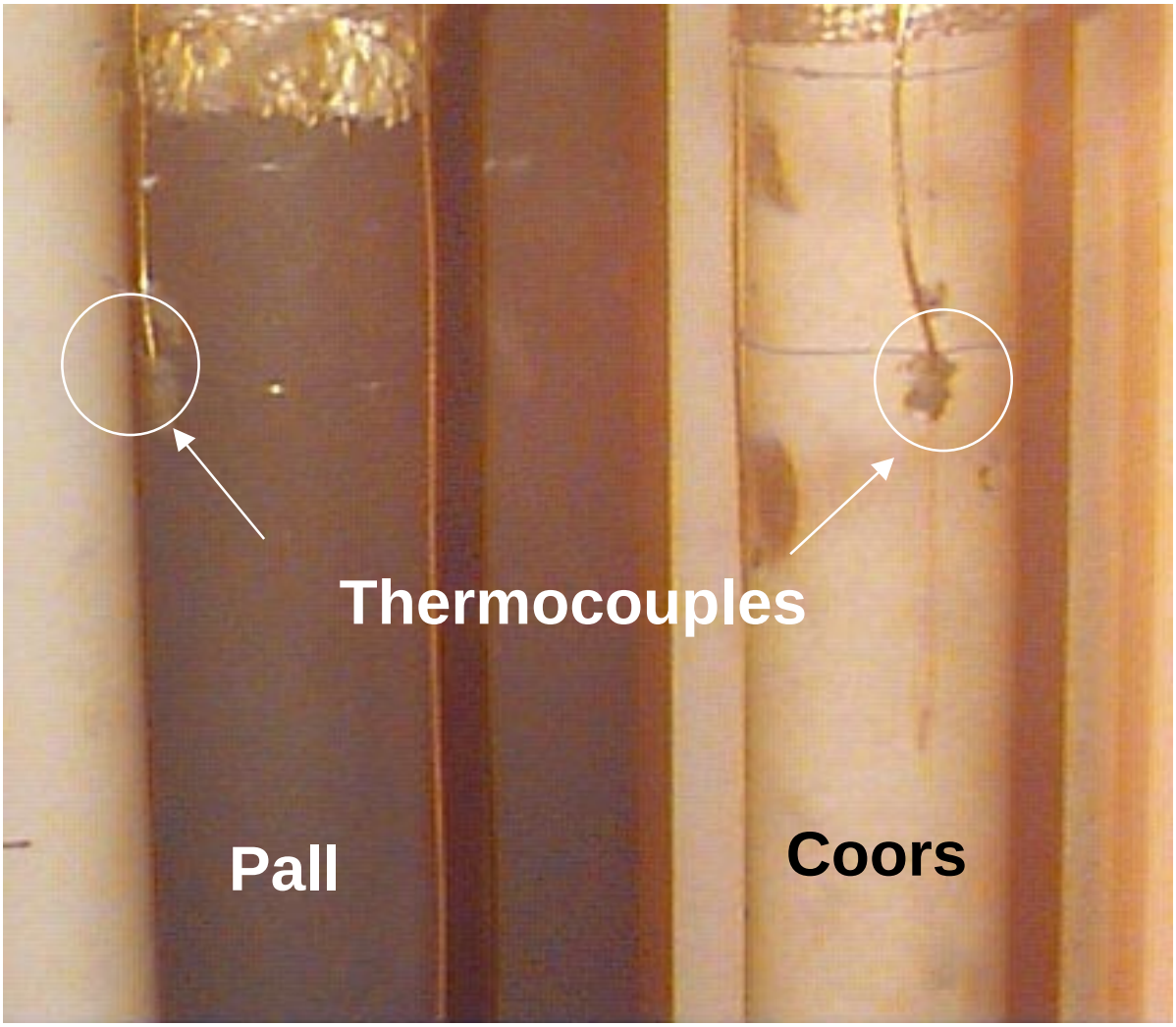

Figure 3.8-23 Thermocouples on Pall and Coors Filter Elements

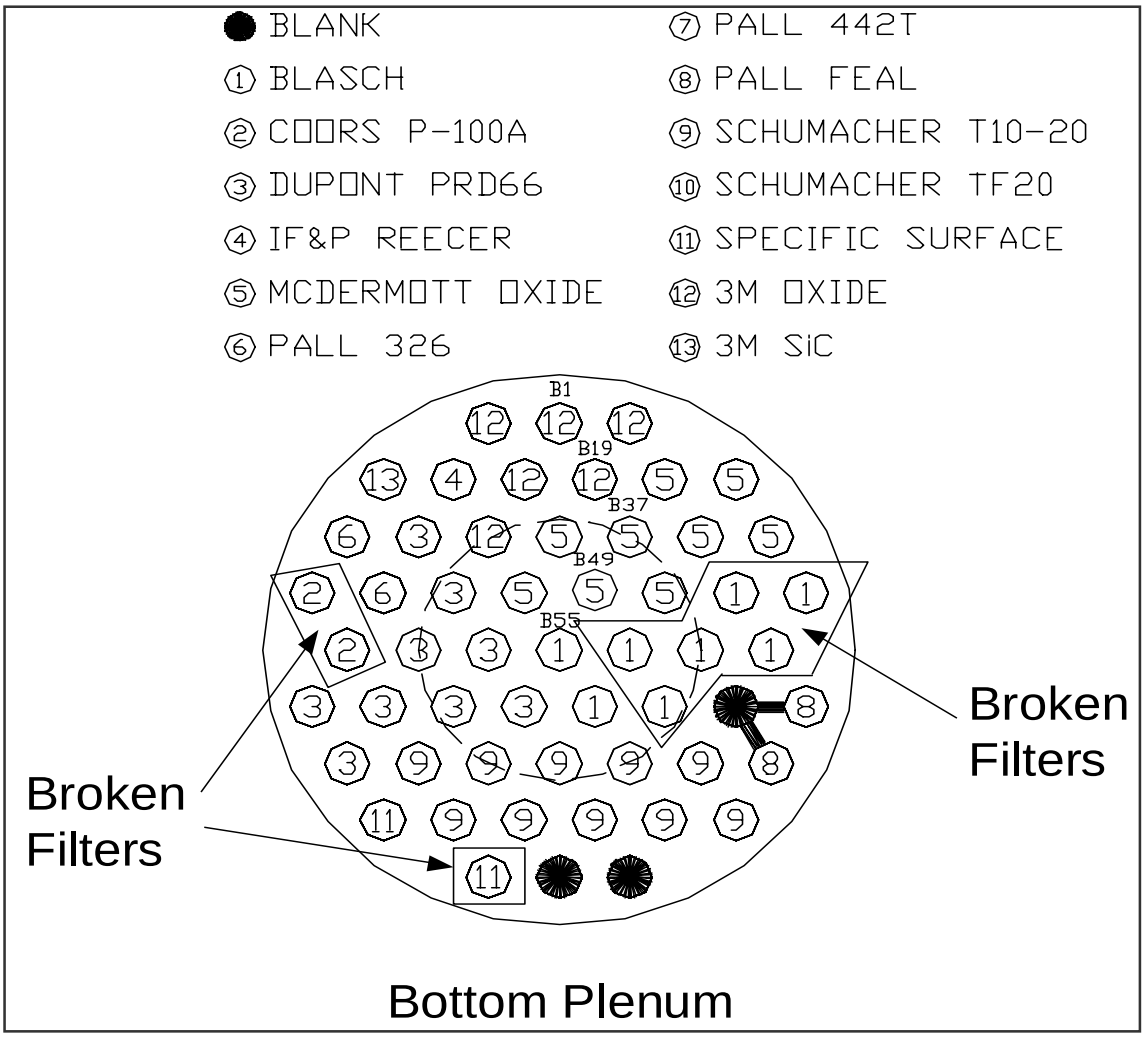

Figure 3.8-24 Broken Filters After Start-Up on April 9, 1998

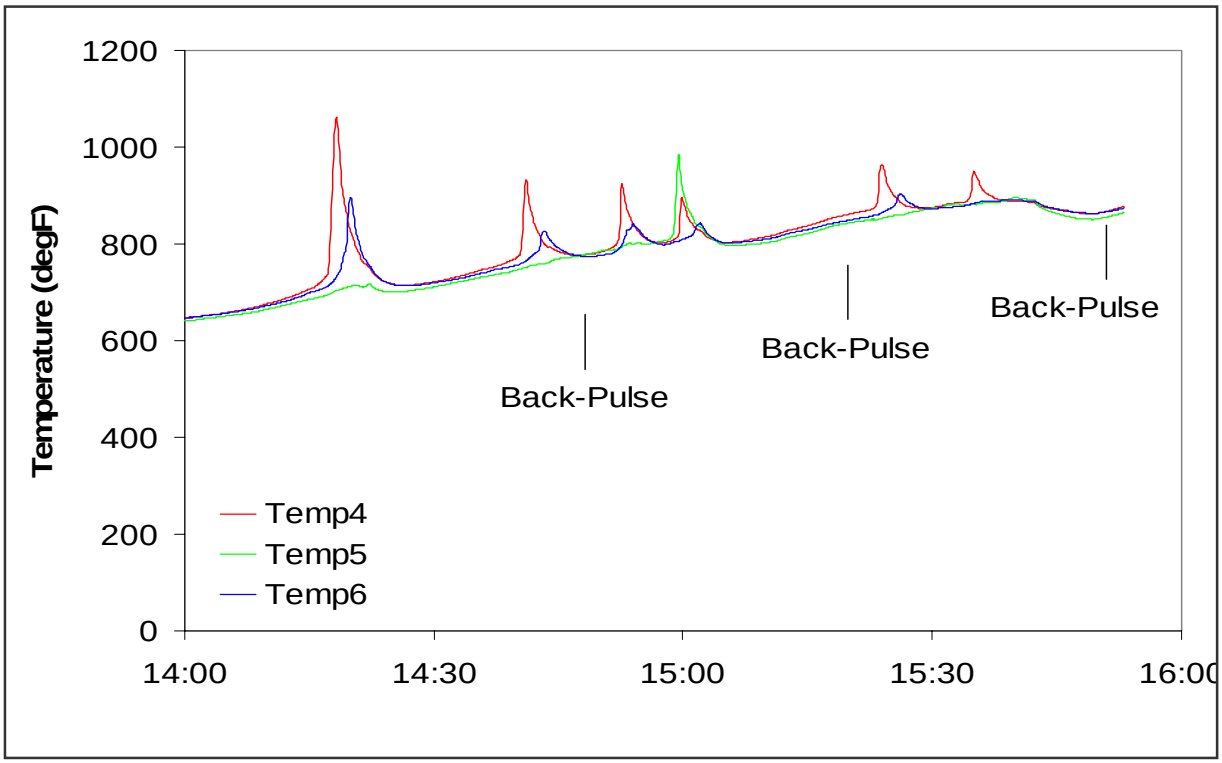

Figure 3.8-25 Pall Filter Element Thermocouple Response on April 9, 1998

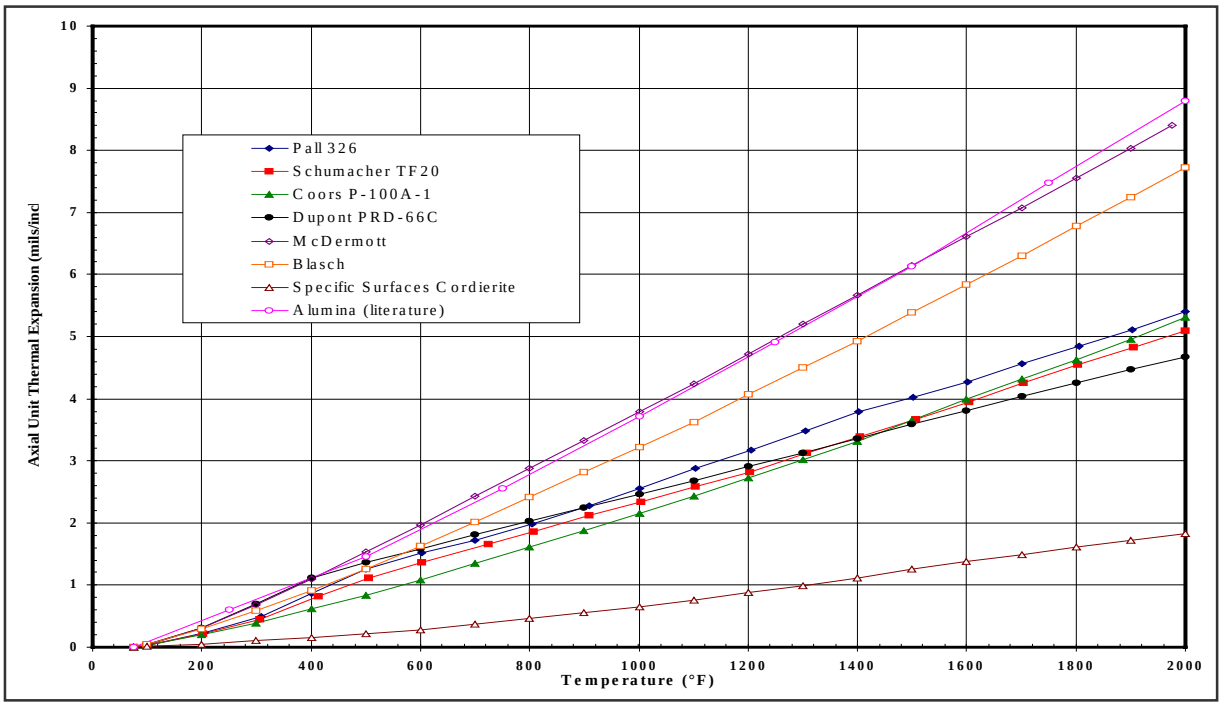

Figure 3.8-26 Thermal Expansion of Various Ceramic Filter Materials

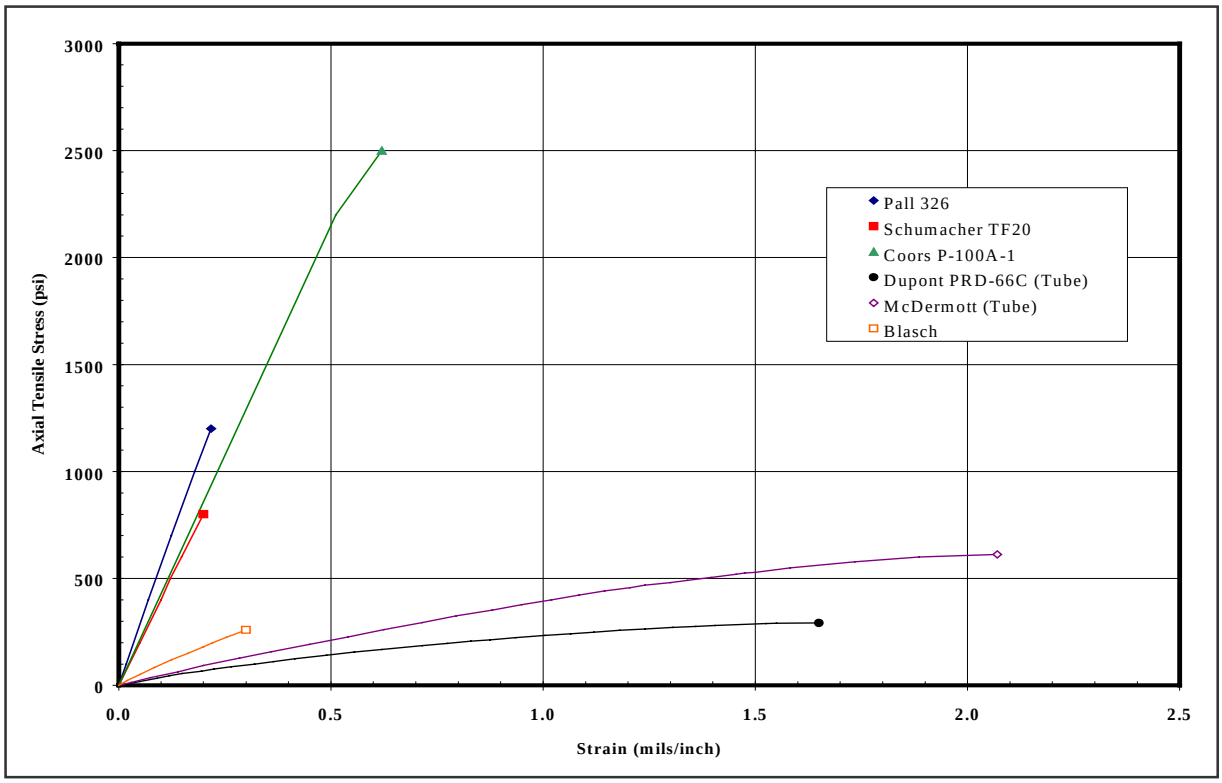

3.8-27 Axial Tensile Stress-Strain Response of Various Ceramic Filter Material

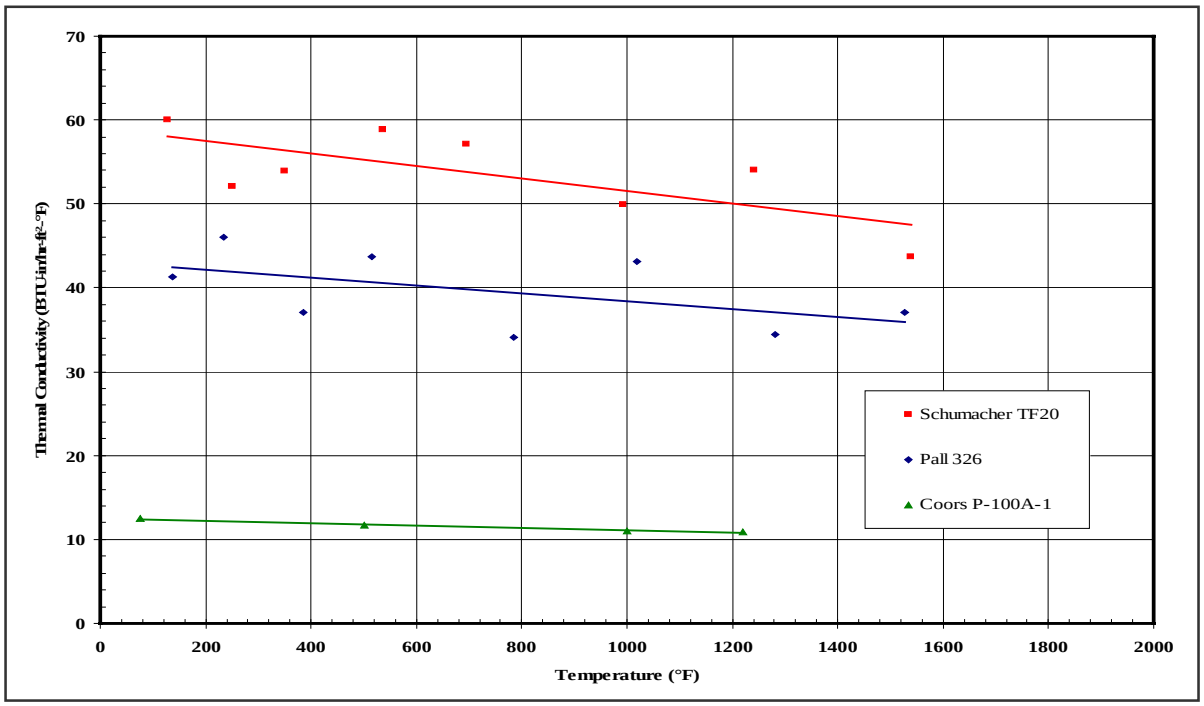

Figure 3.8-28 Thermal Conductivity of Coors, Pall, and Schumacher Filter Elements

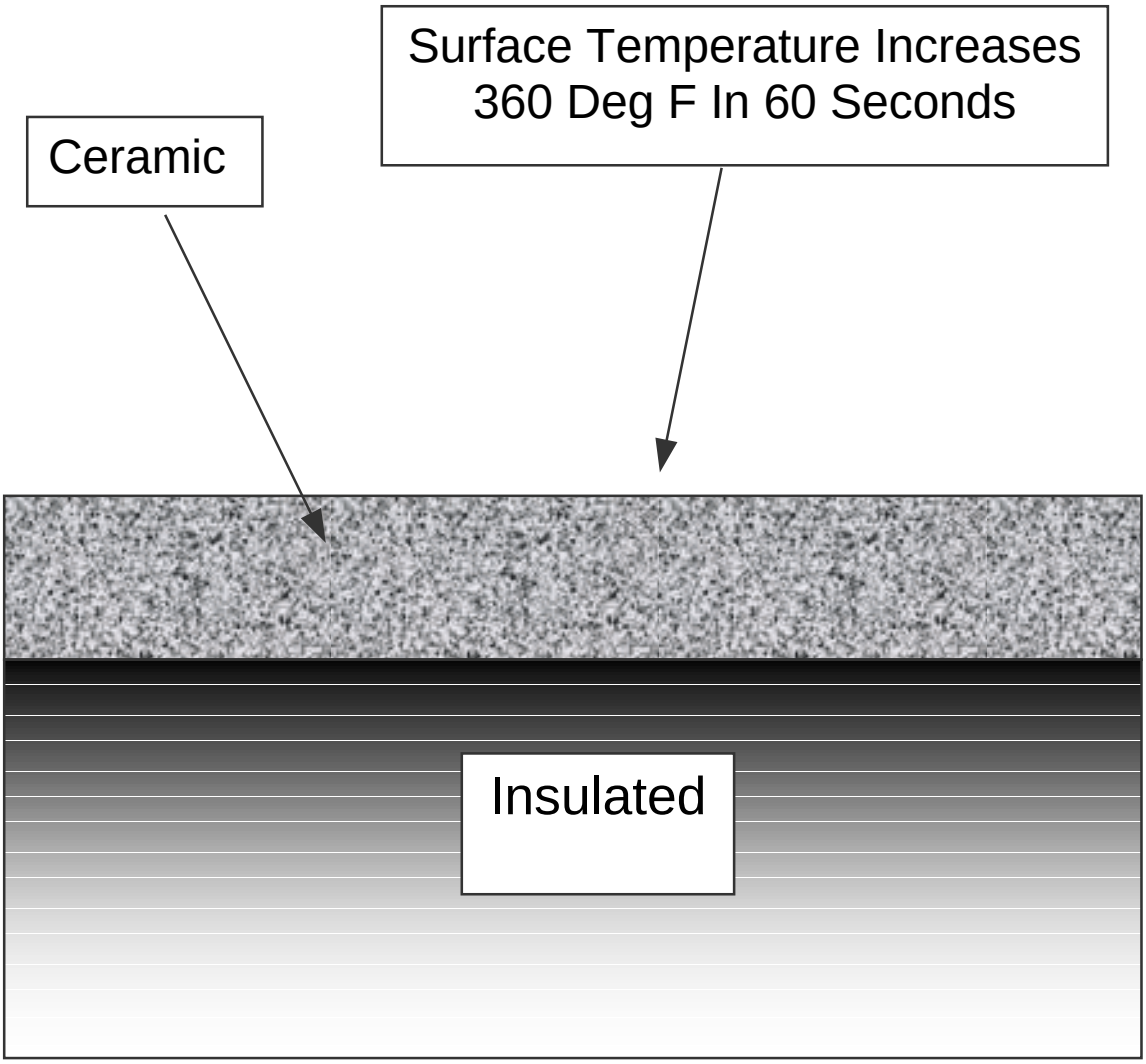

Figure 3.8-29 SRI Flat Plate Thermal Model

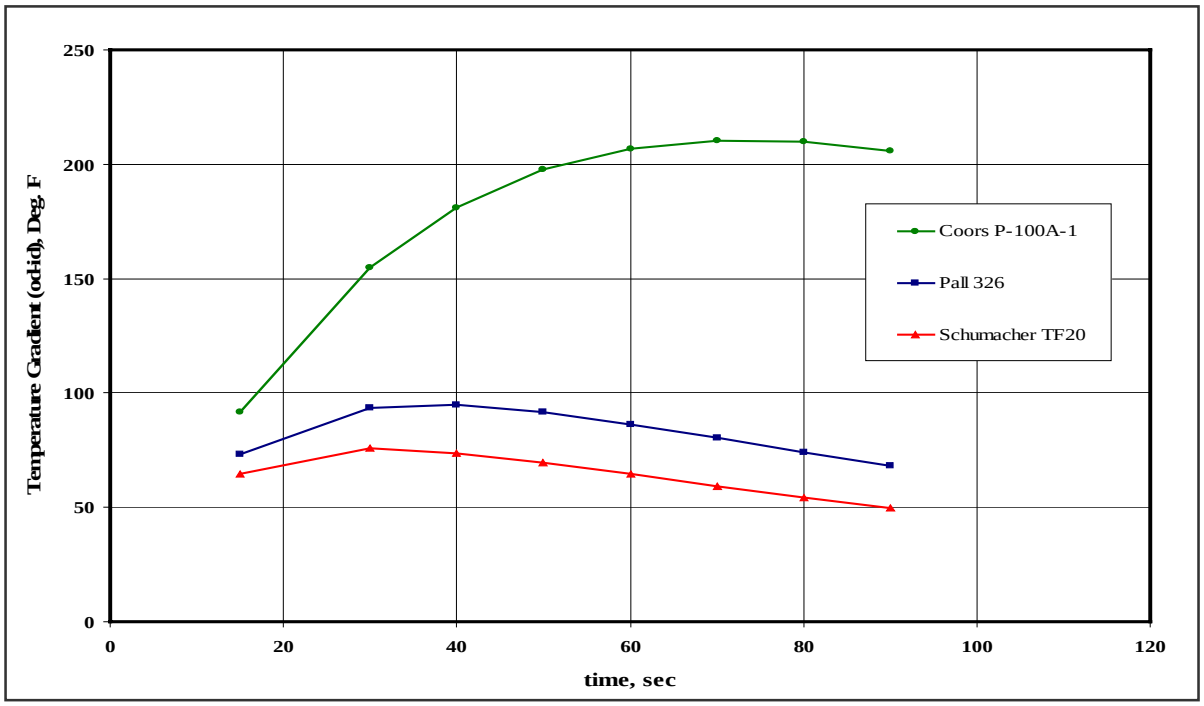

Figure 3.8-30 Calculated Thermal Gradient From SRI Flat Plate Model

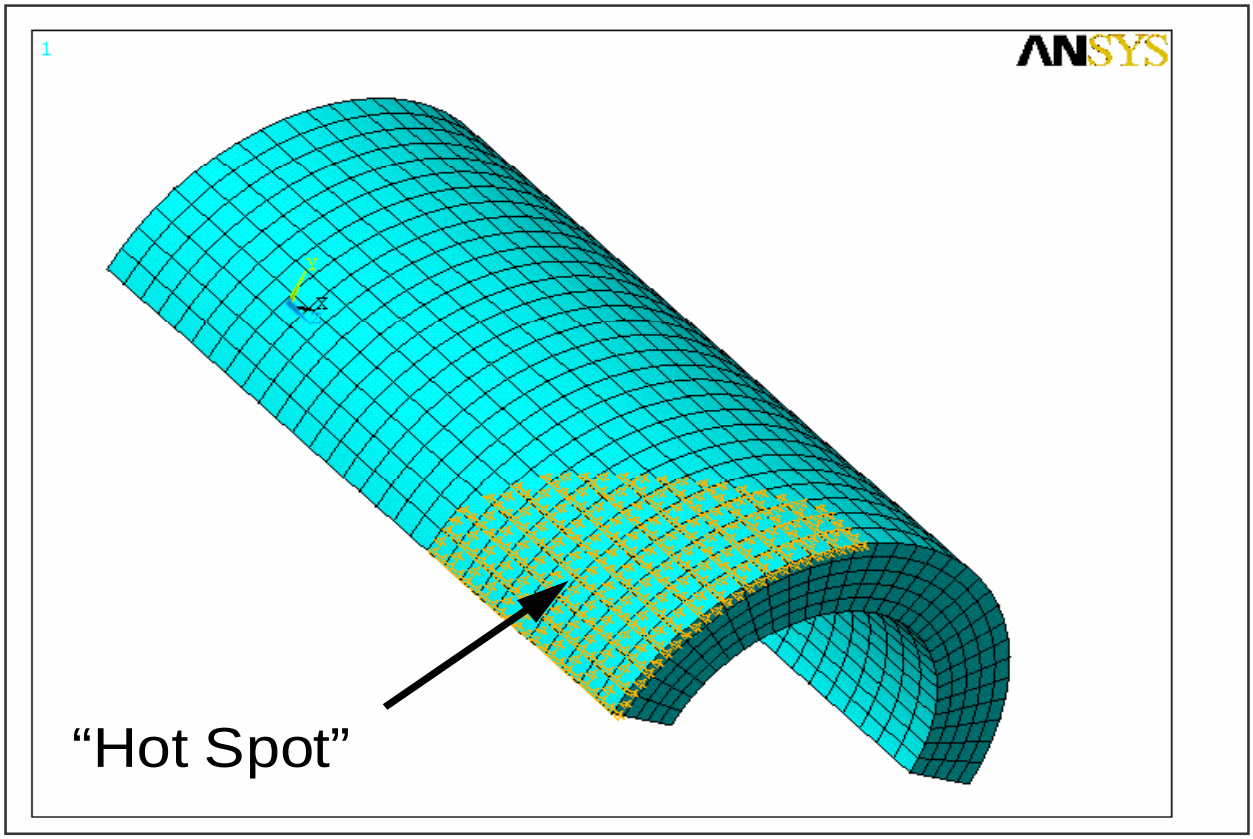

Figure 3.8-31 ANSYS Finite Element Model of Filter Element

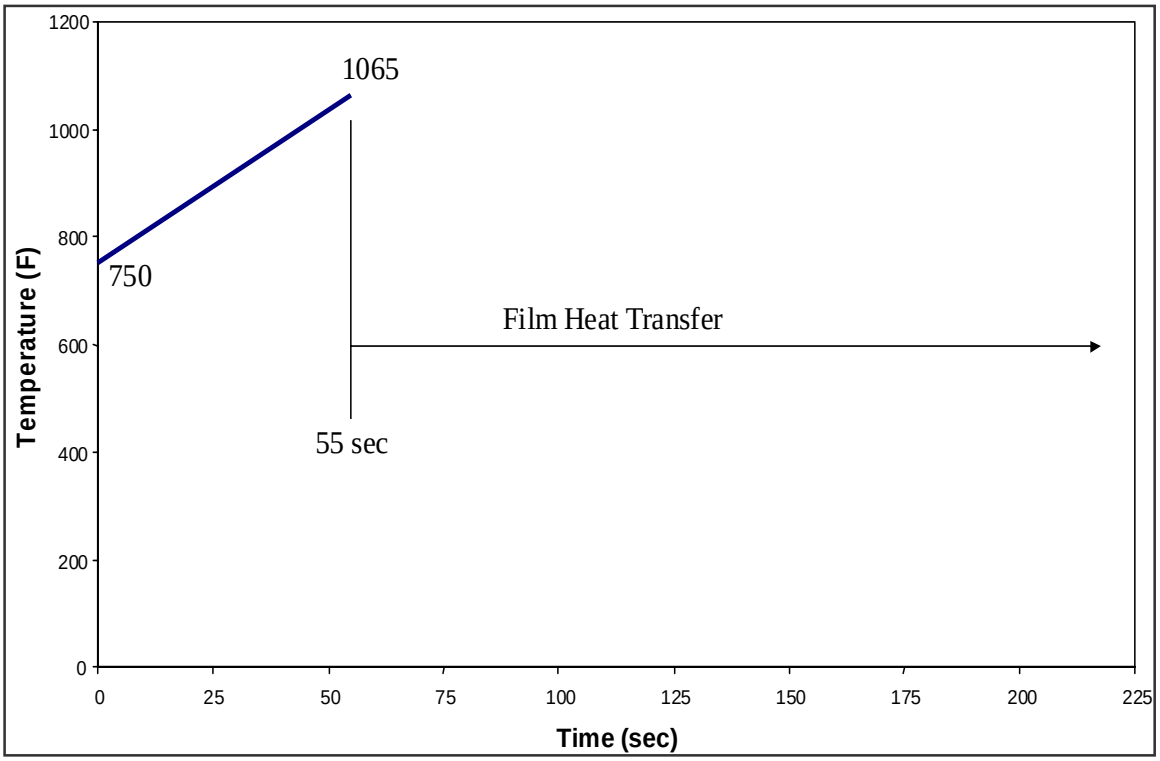

Figure 3.8-32 Thermal Gradient Applied to "Hot Spot"

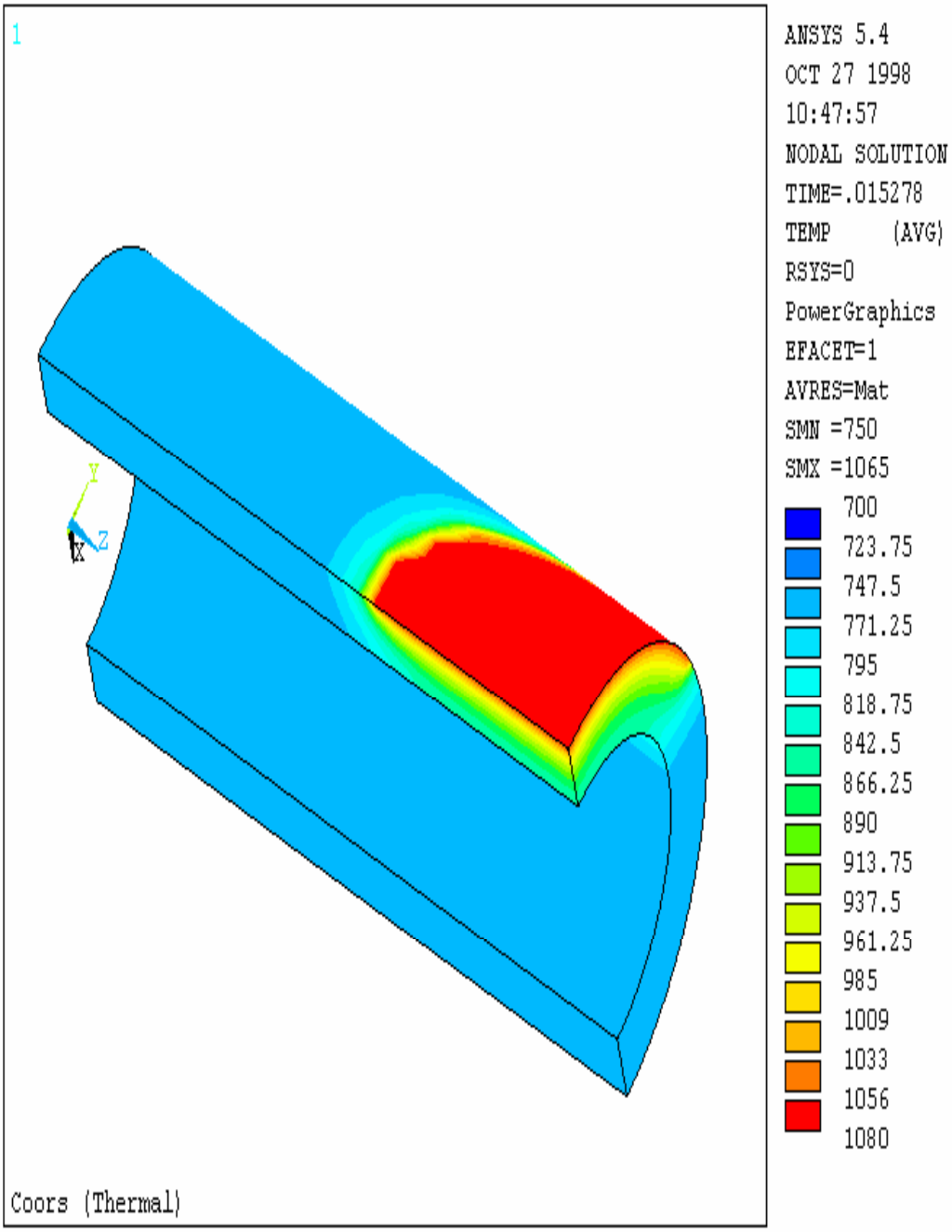

Figure 3.8-33 Results of ANSYS Model for Coors Filter

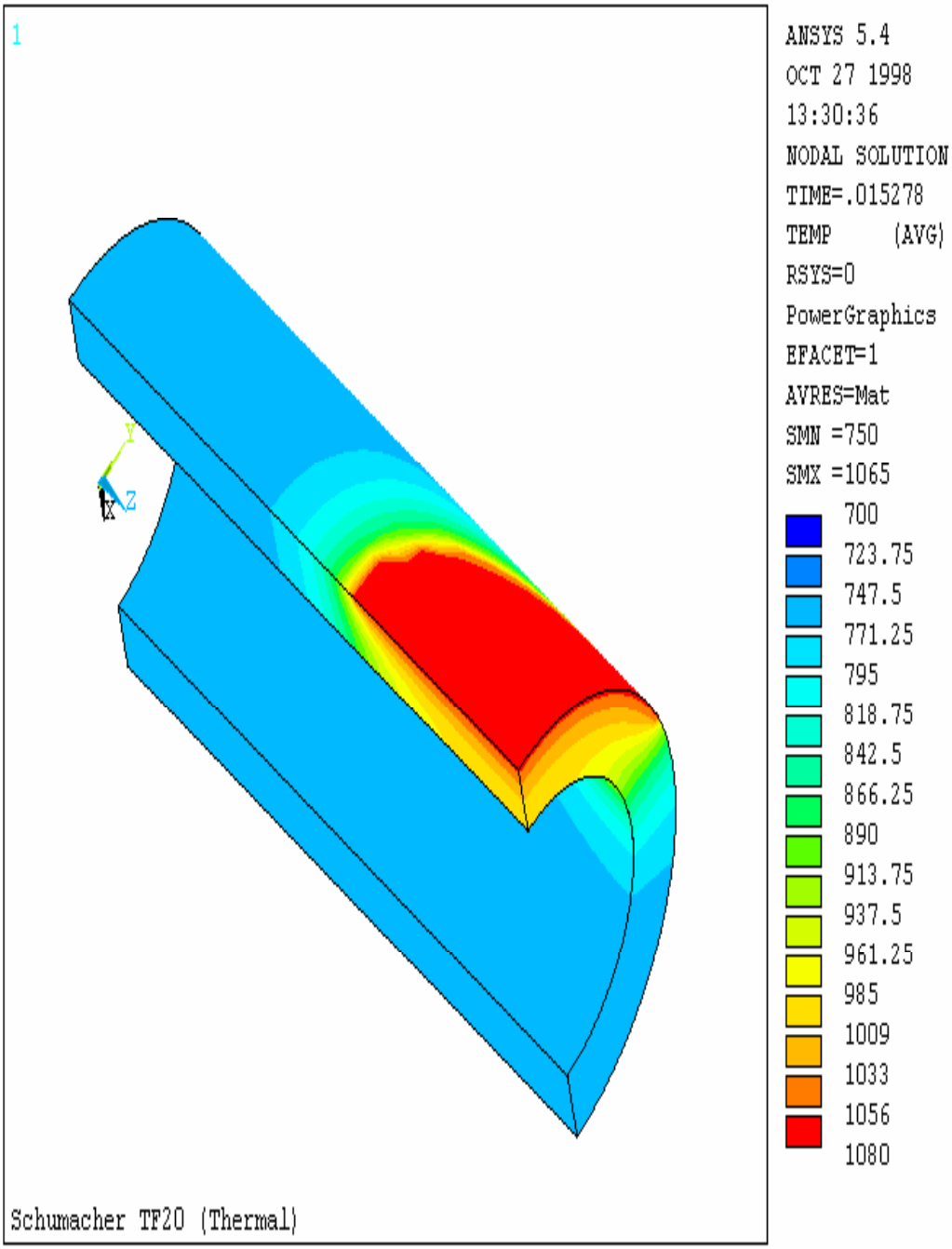

Figure 3.8-34 Results of ANSYS Model for Schumacher TF20 Filter

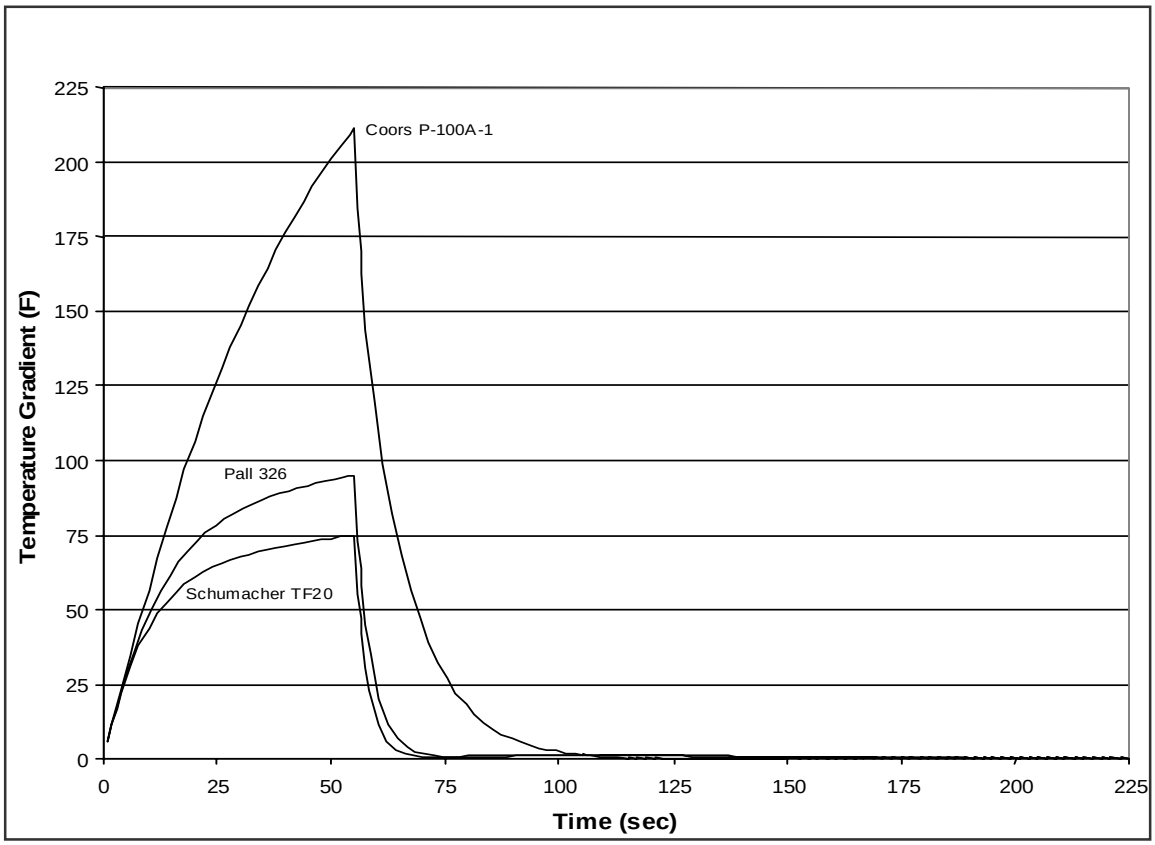

Figure 3.8-35 Gradient Calculated by ANSYS for Coors, Pall, and Schumacher Filter Elements

Section 4.0

Transport Reactor

4.0 TRANSPORT REACTOR

4.1 TRANSPORT REACTOR TC02 RUN SUMMARY

Test run TC02 was begun on April 5, 1998, in combustion mode of operation after the reactor inspections, preventive maintenance activities, and process modifications were completed. The previous test run, TC01, was focused on exposing the PCD candles to process gas for 1,000 hours at temperatures from 1,350 to 1,400°F and achieving more stable reactor operations. With this accomplished, TC02 was planned for reactor parametric testing to better quantify the effect of different variables on reactor operation. The objectives of test run TC02 for the transport reactor were:

- *Perform reactor capacity test.* Determine the maximum coal feed rate, solids circulation rate, and reactor pressure.
- *Evaluate effects of reactor conditions on NO_X emissions.* Vary excess air, primary/secondary air ratio, and operation temperature.
- *Evaluate effects of reactor conditions on SO_X emissions.* Vary Ca/S molar ratio, solids inventory, and operation temperature.
- *Investigate the effect of increasing the mixing zone density.* Decrease various aeration flows and increase solids inventory.

After the ancillary equipment was started and sand was loaded into the reactor, coal feed was started on April 9, 1998. After the start-up burner was shut down the dipleg operation was somewhat unsteady for the next 12 hours. Various reactor flows were adjusted to stabilize the dipleg operations. Once stable operations were achieved the parametric tests were started. First, the Ca/S molar ratio was varied to evaluate the effect on SO_X emissions. The final SO_X test was shortened due to ash accumulation in the PCD caused by broken candle pieces plugging the fines transporter system exit line. Due to the ash accumulation in the PCD and problems with the coal feeder system (FD0210) the reactor system was shut down on April 11, 1998. The coal feeder was inspected, the exit elbow was removed, and the dispense vessel was cleaned.

After the candle pieces and ash were removed from the PCD, coal feed was started on April 13, 1998, to evaluate the PCD outlet loading. The outlet loading was high, approximately 700 ppm, so the reactor system was again shut down to inspect the PCD. Inspection revealed that nine mullite candles had been broken. A later evaluation by the fast data acquisition device revealed that monitored PCD candle skin temperatures showed a local temperature excursion during start-up. This temperature excursion likely broke the candles. Therefore, it was decided to preheat the reactor system and the PCD to a higher temperature before feeding coal. The start-up burner firing was increased from 5.0 to 7.5 MBtu/hr, which resulted in a PCD inlet temperature of 920°F and a reactor temperature of 1,200°F prior to coal feed. Also, the burner was successfully operated up to a reactor pressure of 135 psig.

Coal feed was started on April 21, 1998, and the tests to evaluate the effect of excess air, staged air, primary air distribution, and temperature on NO_X emissions were begun. One of these tests could not be run due to dipleg instability. On April 24, 1998, the dolomite addition was halted so that an SO_2/SO_3 extractive measurement could be done. All other NO_X tests were completed by April 25, 1998.

Next, various reactor flows were adjusted to achieve a higher mixing zone density. However, these changes did not have much effect on the mixing zone density. Other parameters that affect the mixing zone density such as the solids circulation rate were not varied at this time. Other than some minor dipleg upsets and spent solids transporter system exit line plugging, operations were smooth until April 29, 1998, when the coal feeder was inadvertently tripped while working on the transport air dryer. Coal feed was restarted within 10 minutes. Operations continued to be smooth until May 3, 1998, when clumps of fine coal plugging the FD0210 exit which caused the reactor to be taken off of coal feed.

Coal feed was restarted on May 4, 1998. The potential for increasing the reactor pressure per the test plan was then evaluated. It was determined that the reactor pressure could not be increased beyond 200 psig due to problems with the recycle gas system. Attempts to run the recycle gas booster compressor during TC02 were unsuccessful due to the inability to remove condensate from the gas stream. Next, the reactor throughput was maximized within this pressure limit. Several days later, the dipleg operation became somewhat unsteady, resulting in loss of inventory from the transport reactor. Also, the solids were not circulating smoothly through the combustor heat exchanger due to plugged aeration nozzles on the heat exchanger J-leg. Due to continued problems with solids circulation through the heat exchanger the reactor was shut down on May 9, 1998.

Coal feed was again started on May 10, 1998, after the nozzles were unplugged. On May 11, 1998, the dolomite addition was stopped so that another SO_2/SO_3 extractive measurement could be taken. Operations were smooth except for intermittent unsteady dipleg operations. However, on May 13, 1998, the transport reactor was shut down due to a spheri valve seal pressure leak on the FD0520 system.

This test run was successful. The average operating conditions for the run are given in table 4.1-1 and operating plots are given in figures 4.1-1 to -12. There were 692 hours of solid circulation and 559 hours of coal feed attained. The process availability was much higher than previous test runs due to the higher reliability of all dense-phase systems. Another important factor was that the dolomite feed rate could be controlled at the desired rate and excess dolomite feed was not needed to maintain the reactor solids inventory. In addition, there were no instances where the dolomite feed rate significantly exceeded the desired rate.

Most of the tests that were planned for the test run were successfully completed. However, one staging air test could not be completed due to operations difficulties with the cyclone dipleg, and the reactor pressure was limited to 200 psig due to the capacity limitations of the main air compressor and the nitrogen system and problems with the recycle gas system. The maximum coal feed rate for this test run was achieved at 1,420 lb coal/hr.

There were several notable findings in addition to improved reactor operations during this run. Greater than 99-percent sulfur capture was achieved with dolomite at Ca/S = 1.5. A higher-than-expected sulfur oxidization was found within the reactor. Without addition of dolomite, the SO_3 level detected was approximately 2 times the SO_2 level. With addition of dolomite, the SO_3 level detected was about 1/10 of the SO_2 level detected. The NO_X emissions were low, varying from 0.08 to 0.35 lb/MBtu. The NO_X emissions increased with increased excess air and with increased air through the lower level of primary air. The NO_X emissions decreased as the amount of staging air was increased. It was also observed that the NO_X formation was significantly higher when dolomite was fed to the reactor. Analysis of both NO_X and SO_2 emissions is further covered in sections 4.3 and 4.4.

The transport reactor was inspected during the outage using a borescope. The riser and the standpipe were found to be clean with only minor cracks of these refractories. The riser crossover had some deposits on the walls and some loose material at the bottom. The north end of the riser crossover (the disengager end) had a large, dark deposit that partially obstructed the flow to the disengager. The cyclone inlet and the disengager roof each had significant refractory wear with some anchor bolts visible in the disengager.

The next test (TC03) is another 500-hour test in combustion mode of operations to evaluate different feedstocks and is scheduled to occur after a short outage. Additional issues to be addressed include the continuing challenges in operating the recycle gas system and the use of limestone for sulfur capture.

Table 4.1-1

TCO2 Operating Conditions

Start-Up Bed Material	200 μm d_{50} Silica Sand
Coal Type	Calumet Alabama Bituminous
Nominal Coal Particle Size, d_{50}	300 μm
Coal Feed Rate	400 to 1,420 lb/hr
Sorbent Type	Plum Run Dolomite
Nominal Sorbent Particle Size, d_{50}	250 μm
Ca/S molar ratio	1 to 3
Reactor Temperature	1,550 to 1,625°F
Reactor Pressure	160 to 200 psig
Riser Velocity	30 to 40 ft/s
Excess Air	15 to 35 %

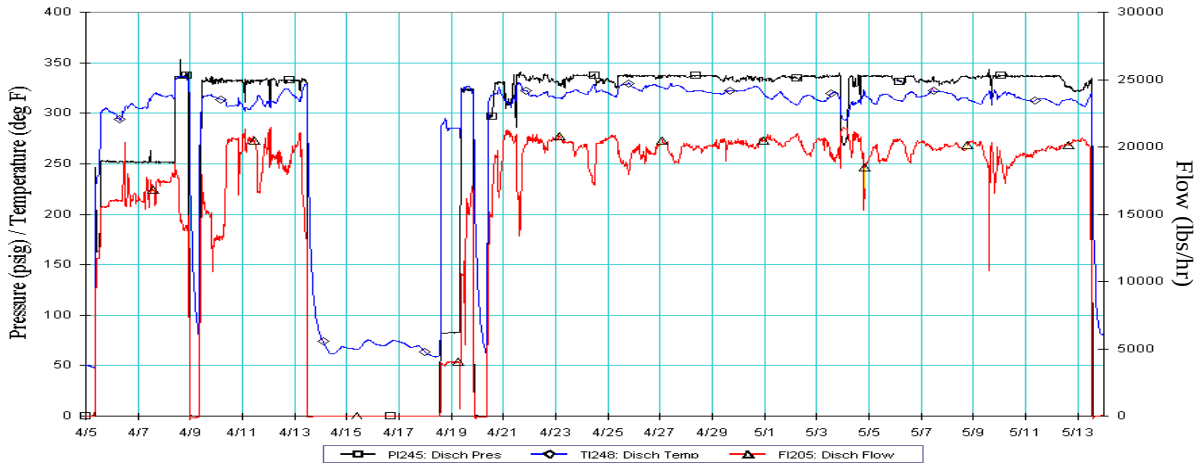

Figure 4.1-1 CO0201 System Profile

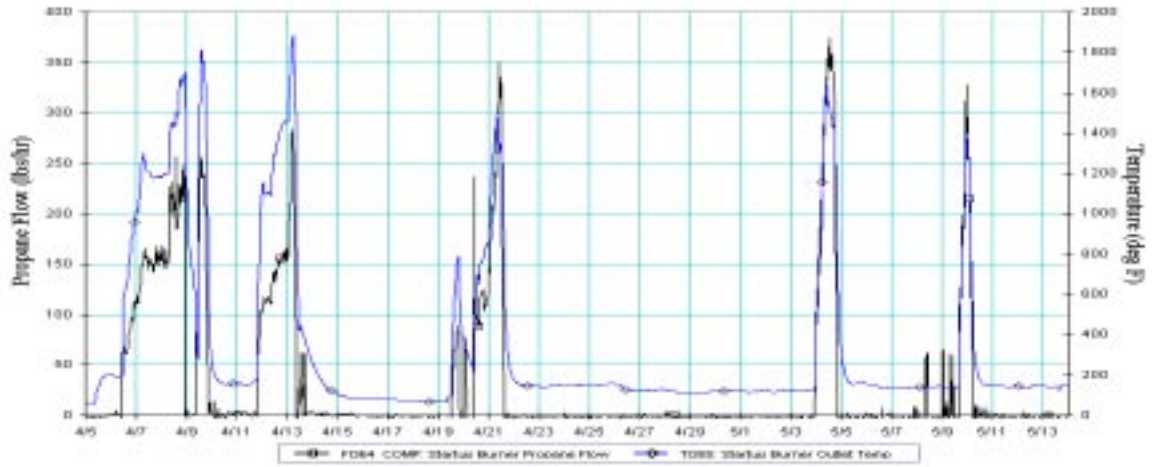

Figure 4.1-2 Start-Up Burner Flow/Temperature

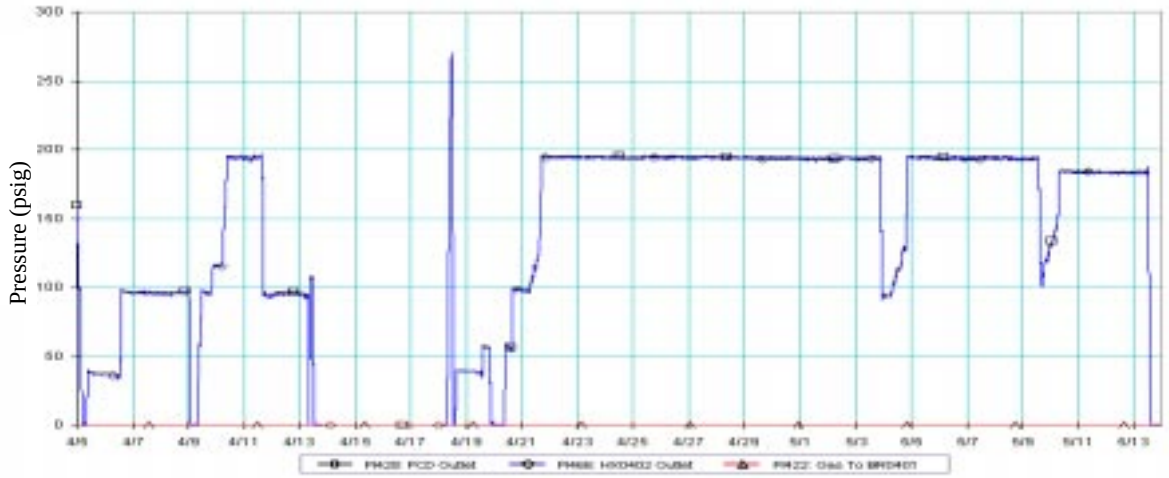

Figure 4.1-3 System Pressures Downstream of PCD

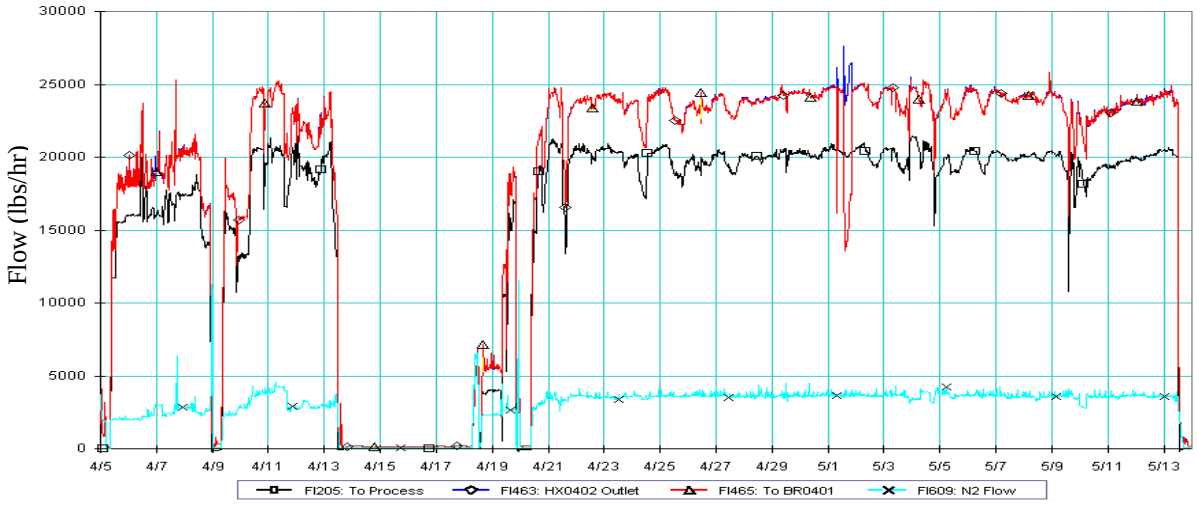

Figure 4.1-4 Total Gas In/Out Flow Rates

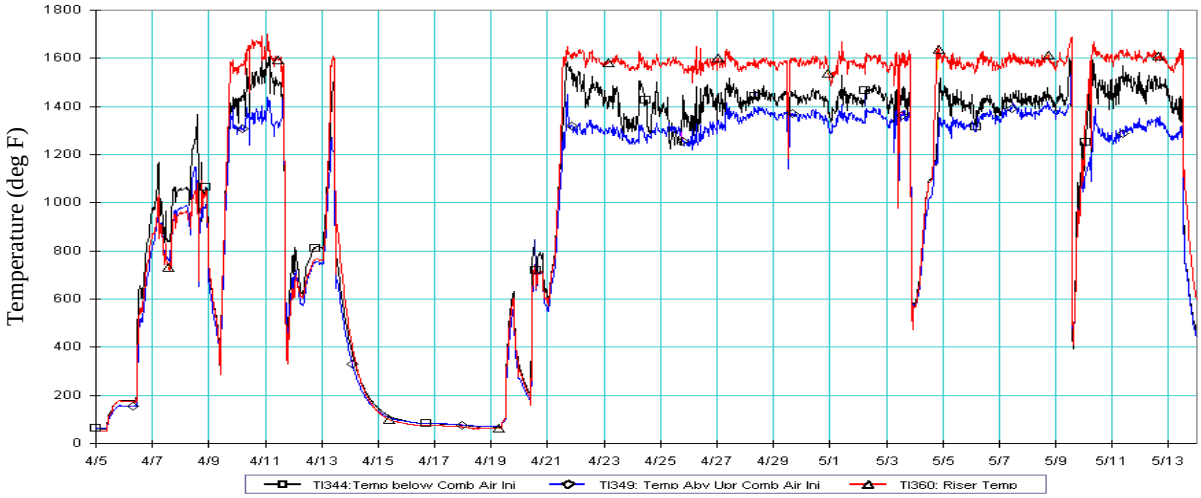

Figure 4.1-5 Reactor Mixing Zone and Riser Temperature

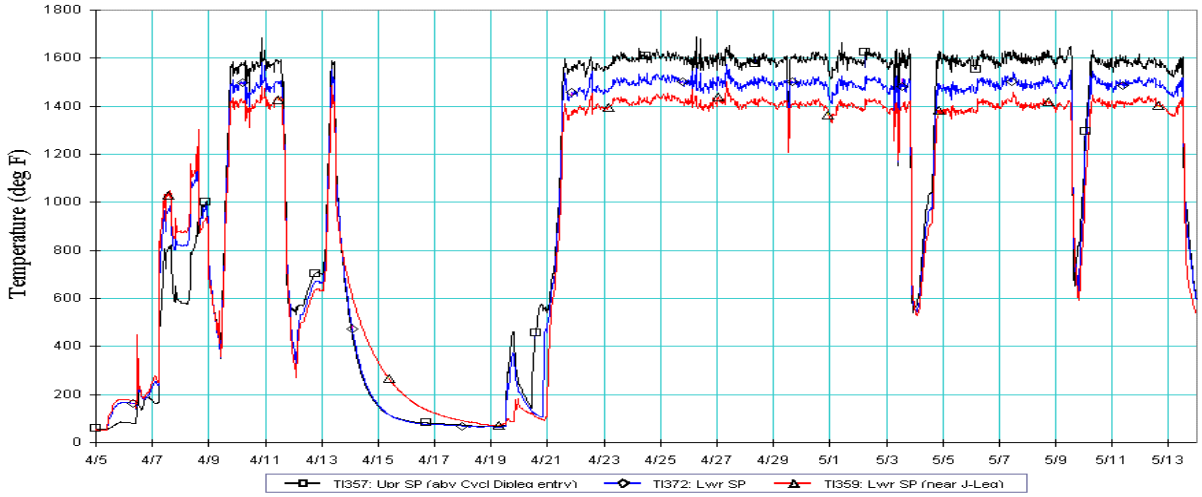

Figure 4.1-6 Standpipe Temperatures

F)

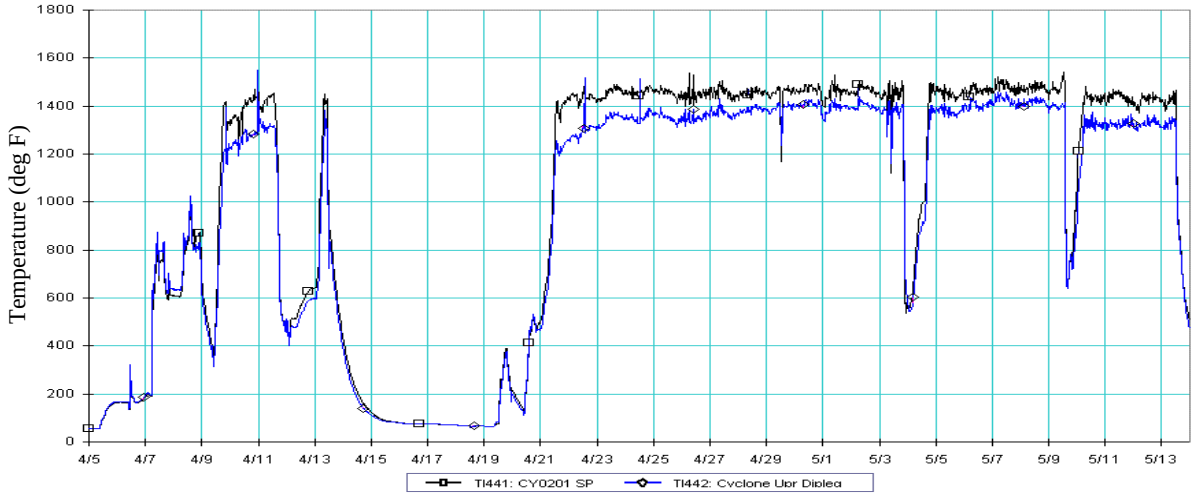

Figure 4.1-7 Cyclone Dipleg Temperatures

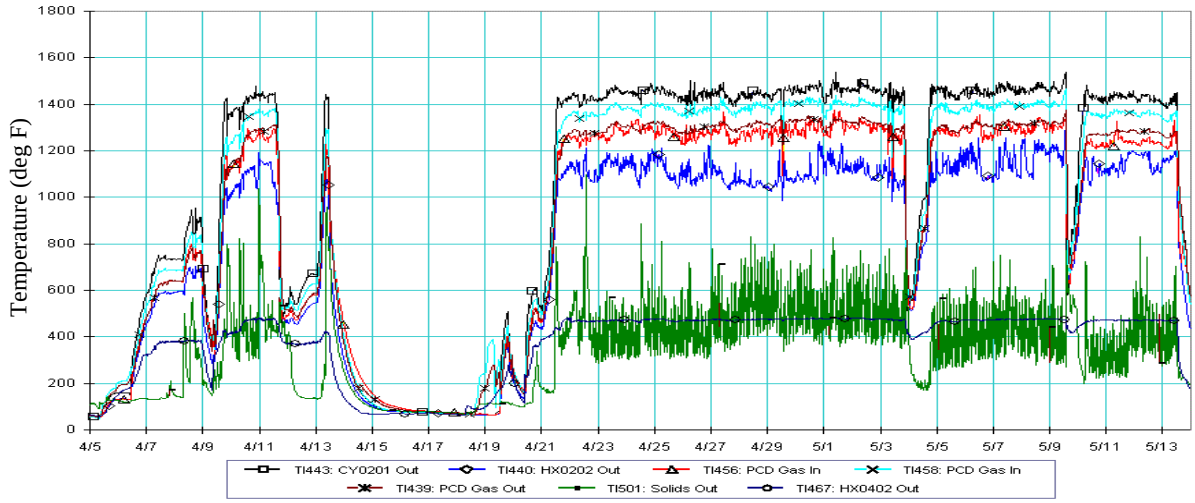

Figure 4.1-8 Temperature Profiles Downstream of Reactor

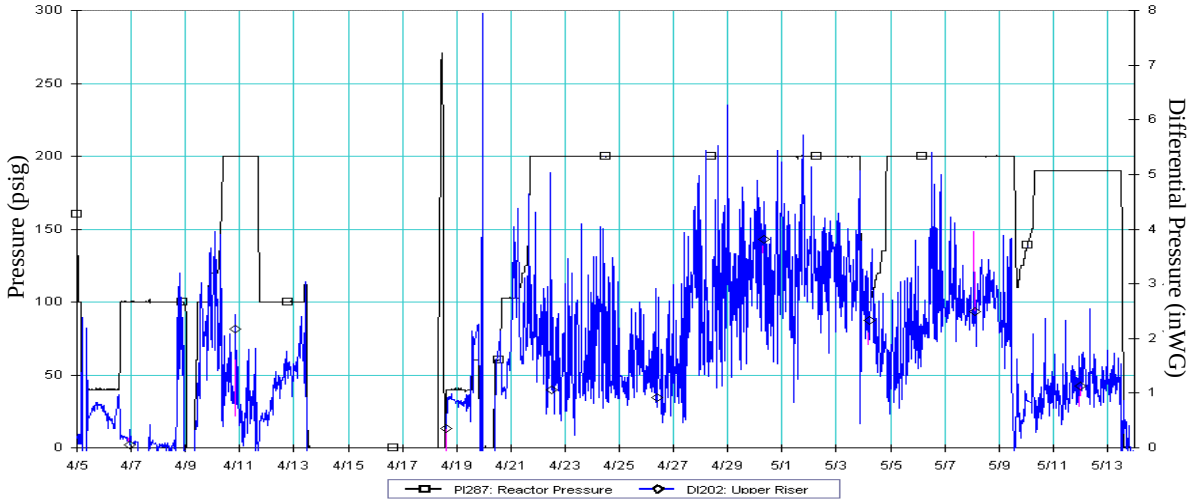

Figure 4.1-9 Reactor Pressure/Riser Differential Pressure Profiles

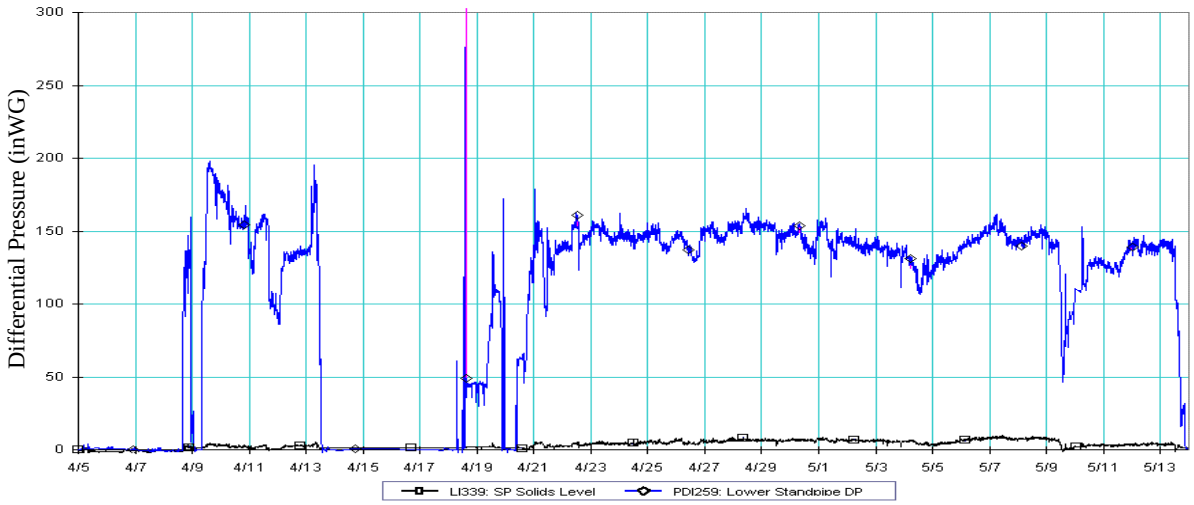

Figure 4.1-10 Standpipe Differential Pressure Profiles

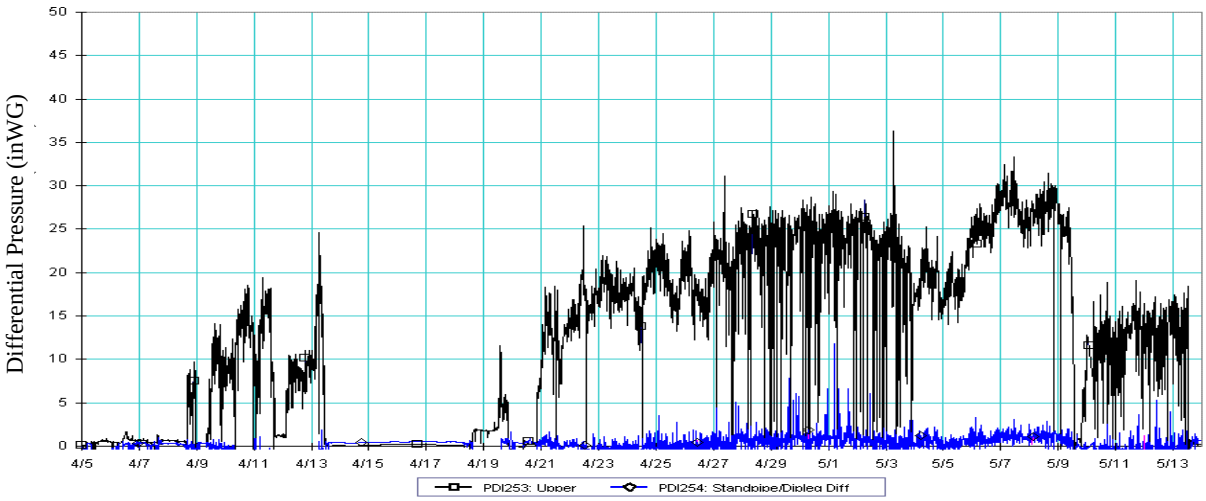

Figure 4.1-11 CY0201 Dipleg Differential Pressure Profiles

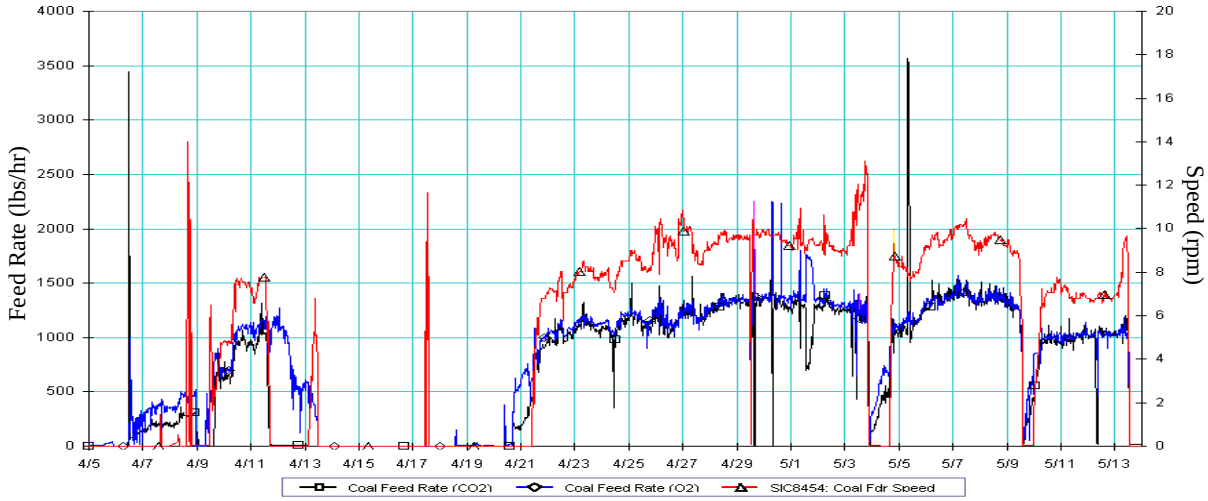

Figure 4.1-12 Coal Feed Rate Based on Gas Analysis

4.2 TCO2 HEAT AND MATERIAL BALANCE

Data from the transport reactor for the 24 hours of May 2, 1998, were used to perform a heat and material balance.

The average reactor conditions for this date are summarized in table 4.2-1. The transport reactor had been operated at very stable conditions for several days leading up to the balance period. The solids levels in the reactor, the aeration rates, and the solids feed rates were held very steady during the period.

The overall material balance on the transport reactor closed to within 3-percent difference (see table 4.2-2). This difference is typical of the percent error in material balances for the transport reactor. The solids flow rates were determined predominately with weigh cells. The coal feed rate was checked by calculating it from both the CO_2 and the O_2 content in the flue gas.

The component balances produced low-percent errors for species predominantly in the gas phase and higher errors for species predominantly in the solid phase. This is due to the difficulty in measuring solids flow rates. The elemental balances are given in table 4.2-3.

The material balances also provided some data regarding the performance of the transport reactor during this time. The sulfur capture was approximately 99 percent at a Ca/S ratio of 1.7. The NO_X emissions were only 0.14 lb NO_X /MBtu. The unburned carbon in the solids removed from the reactor and the CO in the flue gas yields a carbon conversion of 99.9 percent.

Table 4.2-1

Average Reactor Conditions on May 2

Pressure	200 psig
Riser Temperature	1,588 deg F

Table 4.2-2

Overall Material Balance

Feeds	(lb/hr)	Products	(lb/hr)
Coal	1,308		
Sorbent	100	Fine Ash	250
Air	20,166	Flue Gas	24,199
Nitrogen	3,687	Accumulation	18
TOTAL	25,261	TOTAL	24,467

Table 4.2-3

Component Material Balances

Species	Feed (lb/hr)	Products (lb/hr)	Ratio
Carbon	870	871	1.00
Nitrogen	19,176	18,832	1.02
Oxygen	4,798	4,747	1.01
Sulfur	11.4	8.5	1.34
Calcium	21.3	19.4	1.10
Magnesium	12.1	11.7	1.04

4.3 SO_2, SO_3, AND SOLIDS ANALYSES

Solid samples were collected during the test run from the coal feed system (FD0210), the sorbent feed system (FD0220), the standpipe spent solids transport system (FD0510), and the particulate control device (PCD) fine solids transport system (FD0520). These solids were analyzed for chemical composition and particle size. The SO_2 emissions were also continuously measured and recorded on the plant information (PI) system. This section will use the chemical analysis data and SO_2 emissions data to show the following:

- Process and chemical composition changes.
- Effect of sorbent on sulfur dioxide removal.
- Particle-size changes.
- Sulfur and calcium balances.
- Thermodynamic equilibrium in the sulfur dioxide/sulfur trioxide system.
- Levels of unburned carbon/combustion efficiency.
- Sulfur trioxide emissions.

Test run TC02 began on April 9, 1998, and consisted of two separate periods. The first period, April 9 to 13, 1998, lasted 4 days and resulted in a few broken candles. This testing period did not result in steady state operation and will be excluded from SO_2 and solids analysis. The second period, April 21 to May 13, 1998, was a longer-term operation and more characteristic of steady state operation. There were two coal outages during that period (on May 3 and 4, 1998, and on May 9, 1998). Figure 4.3-1 shows the daily (24-hour) averages of system pressure and upper standpipe (SP) temperature for the period April 21 to May 13, 1998.

The daily averages for the coal feed rate (by CO_2) and the SO_2 PCD exit concentrations are given in figure 4.3-2. The coal feed rate is calculated from the flue gas rate, CO_2 content of the flue gas, and the carbon content of the coal. The coal rate increased from April 21 to April 28 as the combustion heat exchanger filled up and the solids circulation rate was increased. The period from April 28 up to the outage of May 3 was characterized by good, steady operation. Steady operation is characterized as steady feed coal and sorbent rates, steady reactor temperatures and pressures, and steady reactor and heat exchanger solids inventory. This is a shorter time frame than when achieving steady chemical composition of the reactor solids, which can take weeks to level out. After the May 3 outage the heat exchanger and solids circulation rate returned to the previous steady values. After the May 9 outage the dolomite was turned off and the SO_2 exit concentration increased.

The coal used during TC02 was Alabama Calumet Mine bituminous. Figure 4.3-3 shows the sulfur and ash contents of the coal as sampled from the coal feed system during TC02. The sulfur increased slightly during TC02 from 0.8-percent sulfur to nearly 1.0-percent sulfur. The ash decreased from 18 to about 15 percent during TC02. The sauter mean diameter (SMD) (average surface area mean) of the coal sampled from the coal feeder is plotted on figure 4.3-4 along with the coal bulk density. The coal grind size was fairly consistent during TC02 with an average particle size sauter mean diameter of about 180 microns. A typical feed coal particle size distribution is given in figure 4.3-5.

Figure 4.3-6 gives the particle sizes of the feed dolomite for about half of the test period. Dolomite samples were mistakenly not taken from May 6 to May 13. The SMD started at around 140 microns, dropped to around 80 microns, and then were rising to 140 microns just before the first coal outage on May 3. The large variation in dolomite particle size was likely due to particle segregation in the silo where dolomite was stored for several months. Figure 4.3-7 gives the particle size for the feed dolomite on May 1.

Solid samples were collected on a regular basis from the PCD using the fine ash transport system (FD0520) and sent to the laboratory for analyses. The solids were analyzed for:

- Calcium (reported as CaO).
- Magnesium (reported as MgO).
- Sulfur (reported as S).
- Silicon (reported as SiO_2).
- Aluminum (reported as Al_2O_3).
- Titanium (reported as TiO_2).
- Iron (reported as Fe_2O_3).
- Potassium (reported as K_2O).
- Sodium (reported as Na_2O).
- Phosphorus (reported as P_2O_5).
- Carbon dioxide (reported as CO_2).
- Carbon (reported as carbon).

The ash minerals, silicon, aluminum, titanium, iron, potassium, phosphorus, and sodium are reported as oxides, which are the most likely form in which they exist after combustion. These compounds are from the coal ash, dolomite inerts, and sand. Calcium, magnesium, and sulfur are not present as the compounds reported in the raw data. Free energy minimization calculations (Shadle, 1997) give guidance to the calcium and magnesium compounds existing at the transport reactor operating conditions. Calculations at pressures from 150 to 200 psig and from 1,350 to 1,600°F indicate that the permissible sulfur-magnesium-calcium compounds are:

- $CaCO_3$ (limestone).
- CaO•MgO (dolomitic lime).
- $CaSO_4$.
- MgO (magnesia).

Lime (CaO) and magnesium sulfate ($MgSO_4$) are not thermodynamically stable compounds at these conditions.

The molar ratio of calcium to sulfur (Ca/S) was calculated for each sample. The Ca/S ratio is the measure of excess sorbent required for sulfur removal according to the equation:

$$SO_2 + CaCO_3 \bullet MgCO_3 + (1/2)O_2 \rightarrow CaSO_4 + 2CO_2 + MgO \qquad (1)$$

For all the dolomite to react, equal molar amounts of dolomite and SO_2 are required, which would result in the same molar amount of calcium in the solids as sulfur (Ca/S = 1.0). Solids with the minimum amount of dolomite required would then have calcium present only as $CaSO_4$ and there would be neither $CaCO_3$ nor CaO•MgO present. The higher the Ca/S ratio the more excess dolomite is used than theoretically required for 100-percent SO_2 capture.

The PCD exit SO_2 concentrations shown in figure 4.3-8 (8-hour averages) are plotted with the spent solids analysis Ca/S molar ratio and the Ca/S ratio based on the coal and dolomite feed rates. The periods when the coal feed was off are indicated in the figure. Periods when the dolomite feed was stopped are noted in the figure. The feed coal sulfur and the coal calcium are calculated from the coal feed rate and coal analysis. The dolomite feed rate is determined from a correlation between dolomite weight cell readings and dolomite feeder speed. The dolomite calcium feed rate is then determined from the dolomite feed rate and the amount of calcium in the dolomite.

The Ca/S ratio by spent solids analysis was constant at about 2.0 until April 26. Between April 23 and 26, the Ca/S by feed and spent solids analysis were in excellent agreement with each other. The dolomite feed was increased on April 26 and the feed Ca/S ratio quickly increased, resulting in an increase in spent solids Ca/S ratio. The spent solids Ca/S ratio should follow any changes in the feed Ca/S ratio. The dolomite feed rate was increased on May 1 resulting in an increase in feed solids Ca/S ratio. Both Ca/S ratios were in agreement from May 1 to May 3 just before the first coal outage.

The feeds Ca/S was higher than the spent solids Ca/S from May 5 to May 8 and then showed good agreement just before the second coal outage. The two Ca/S ratios agreed with each other at the end of the run on May 12 and 13.

The PCD exit SO_2 concentrations reacted as expected to the two dolomite shut offs (increase in SO_2 concentrations when the dolomite was shut off). The small increase in SO_2 concentration from April 25 to April 29 was probably due to calibration drift of the SO_2 analyzer. The SO_2 concentration decreased quickly once the dolomite was turned on May 11.

The sauter mean particle diameter and bulk density of the reactor bed solids taken from the standpipe using the spent solids transport system FD0510 are given in figure 4.3-9. The particle diameter slowly decreased from around 300 to 175 microns as the test progressed and the start-up sand was slowly purged from the bed. The particle size data indicated that the reactor solids were at steady state from about May 1 until the end of the run. Figure 4.3-10 gives the particle size distribution for reactor solids on May 8.

The sauter mean diameter of the solids collected by the PCD and sampled from the fine solids transport system FD0520 is given in figure 4.3-11. The sauter mean particle size for the PCD solids averaged 23 microns for TC02 and was fairly constant for the period April 22 to May 14. The PCD solids were finer than the standpipe solids and dolomite feed solids. Figure 4.3-12 gives the particle size distribution for PCD solids in the latter half of the test.

The solid compounds produced by the reactor were determined using the solids analysis and the following assumptions:

1. All carbon dioxide measured by acidification came from $CaCO_3$, hence moles CO_2 = moles $CaCO_3$.

2. All sulfur measured came from $CaSO_4$, hence moles sulfur = moles $CaSO_4$.

3. All remaining calcium not taken by $CaSO_4$ and $CaCO_3$ came from CaO•MgO.

4. All remaining magnesium not taken by CaO•MgO came from MgO.

5. All carbon dioxide was also measured from combustion as total carbon, hence unburned carbon in the solids is moles measured carbon minus moles measured CO_2.

The solids analyses by component are plotted in figures 4.3-13 and -14 where the weight percent of $CaCO_3$, $CaSO_4$, CaO•MgO, and MgO in the PCD solids are plotted against time. All are consistent with the Ca/S ratios shown in figure 4.3-8. The $CaCO_3$ weight percent is fairly constant for the entire test, around 2.0-weight percent, except when high-dolomite feed rates resulted in a high Ca/S ratio. The weight percent $CaSO_4$ slowly climbed to 16 weight percent and then remained steady despite a later decrease in dolomite feed rate and lower Ca/S ratio. The MgO weight percent increased to about 6 percent and then leveled off.

The CaO•MgO-percent solids reacted to the changing Ca/S ratio of the solids. The CaO•MgO content slowly rose with the Ca/S ratio, then leveled off when the Ca/S ratio was about 2.0, and then decreased when the dolomite feed was decreased, resulting in Ca/S ratios of about 1.0. During the final 2 weeks of testing the CaO•MgO-percent solids were nearly zero. This indicated that the measured sulfur and carbon dioxide levels were sufficient to account for all the measured calcium as $CaCO_3$ and $CaSO_4$.

The laboratory reported carbon in two forms: elemental carbon and carbon dioxide (CO_2). The measured elemental carbon is the total carbon in the sample and includes unburned carbon and the carbon dioxide. The actual elemental carbon in the solids is the difference between the measured elemental carbon and the measured carbon dioxide. The elemental carbon in the solids is a measure of combustion efficiency. Zero carbon in the solids would indicate 100-percent combustion efficiency.

The carbon content of the solids is calculated as the difference of two small numbers typically close to each other in value and, therefore, there is a large variation in the carbon content of the solids. Sometimes the CO_2 content of solids is larger than the total carbon, resulting in a "negative" unburned carbon.

The unburned carbon of the PCD solids is plotted as the difference between the elemental carbon and the carbon dioxide of the solids (see figures 4.3-15). Some of the data show less than 0.0-weight percent, an indication of the uncertainty in both the measurements and the result of taking the difference of two small numbers. All unburned carbons are at a very low level indicating about 99.9-percent combustion efficiency. The data indicates that the

combustion efficiency increased as the run progressed until May 1, then gradually decreased to May 8, and then leveled off. The circulation rate and heat exchanger level increased from the start of run until April 28. Both the circulation rate and heat exchanger were constant from April 29 to May 2. The circulation rate and heat exchanger level returned to previous high values on May 7 and 8 and then dropped to low values from May 10 to the end of the test.

Figure 4.3-15 also plots the calculated weight percent of PCD inerts against time. The inerts are defined as a mixture of sand, coal ash, and dolomite inerts and are any bed compounds not containing calcium, magnesium, or sulfur. The percent inerts started at about 95 percent and then decreased to about 75 percent as the run progressed. Sand was added to the reactor after the second coal outage, which increased the percent inerts. Operation on coal without dolomite during start-up also increases the weight percent inerts. Data presented in figure 4.3-9 for reactor solids and figures 4.3-11, -13, -14, and -15 for PCD solids show the reactor was at steady state in terms of particle size and chemical composition from about May 1 until the end of run TC02.

Southern Research Institute (SRI) obtained both SO_2 and SO_3 data from the cyclone outlet (PCD inlet) to confirm that occasional white plumes emitted from the PSDF stack were SO_3 and also to check the accuracy of readings of the online SO_2 analyzer. SRI used extractive and wet chemical techniques to obtain SO_2 and SO_3 concentrations. Two extractive SO_2/SO_3 tests were done on May 7 and May 11. The May 7 tests were done at "normal" TC02 operating conditions that produced very low analyzer SO_2 readings. The May 11 tests were done after the dolomite had been turned off (on the day before), while there were measurable SO_2 readings, and while a plume was visible coming from the PSDF stack for 5 to 6 hours.

Figure 4.3-16 plots the online SO_2 analyzer readings (hourly averages) and the spent solids calcium to sulfur ratio for the period extending from 18 hours before the May 11 extractive tests and 12 hours after the May 11 extractive tests. The SO_2 analyzer was very responsive to changes in dolomite addition. The solids Ca/S ratio decreased as expected when the dolomite was turned off and increased when it was turned on. The solids Ca/S ratio was about 1:0 at the time of the extractive testing.

Figure 4.3-17 plots the SO_2 analyzer readings (hourly averages) expressed as 6-percent O_2 and the expected SO_2 (6-percent O_2) when the dolomite was turned off for the May 11 extractive tests. The extractive SO_3 measurements (6-percent O_2) are also plotted on the figure. Sulfur oxide concentrations are expressed as 6-percent O_2 in order to better compare data taken at different amounts of excess air.

Table 4.3-1 compares the extractive SO_2 and SO_3 data taken on May 7 and 11. The average extractive SO_2 and SO_3 data are given as well as the average SO_2 gas analyzer data. Both SO_2 and SO_3 are expressed as measured and as 6-percent O_2. The average SO_X emissions in pounds of SO_X per MBtu fired and SO_X removal based on the calculated SO_X from the coal sulfur are given in the table. The Ca/S ratios for both the spent solids and feed solids are taken from figure 4.3-8.

The high-SO_3 values measured are consistent with both thermodynamics and previous results of burning coal in pressurized fluid-bed combustors with dolomite as bed material. Two papers

from literature give high measured values of SO_3 from PFBC (Wheeldon, 1985, and Burdett, 1983). Both papers reported thermodynamic calculations on the SO_2/SO_3 split for PFBC conditions. Wheeldon, et al., gives SO_2/SO_3 data for a PFBC operating at 1,220 to 1,580°F and 75 to 160 psig with both limestone and dolomite. Burdett, et al., gives SO_2/SO_3 data for a PFBC pilot operating at 1,575°F and 75 psig for both with and without limestone.

A useful way to analyze SO_2/SO_3 data is to look at the thermodynamics of the SO_2 to SO_3 reaction:

$$SO_2 + (1/2)O_2 \leftrightarrow SO_3 \tag{2}$$

Higher pressure and oxygen concentrations will lead to higher SO_3 concentrations. Equation (2) leads to the equilibrium constant, which combines the effects of pressure, sulfur oxide concentration, and oxygen concentration. The equilibrium constant K_p is defined as:

$$K_P = \frac{SO_3}{SO_2\sqrt{P(O_2)}} \tag{3}$$

The SO_3 and SO_2 concentrations are in ppm and $P(O_2)$ is the partial pressure of oxygen in atmospheres. The concentrations of SO_2 and SO_3 at equilibrium can be calculated from thermodynamic data, the oxygen concentration, the total sulfur in the gas phase, and the system pressure and temperature. Figure 4.3-18 plots the equilibrium concentrations of SO_3 and SO_2 at 10-percent O_2 and 200 psig and compares them with the concentrations measured on May 11 at 1,308°F. The formation of SO_2 is favored at high temperatures, while at low temperatures the formation of SO_3 is favored.

The measured K_p in table 4.3-2 is calculated for both TC02 data points. The temperature at which the measured concentrations are at thermodynamic equilibrium can be determined from thermodynamic data (see table 4.3-2). The equilibrium temperature can be compared to the measured temperature; the difference is called "the approach to equilibrium" and is a measure of how close the system is to thermodynamic equilibrium. The lower the approach temperature the closer the system temperature is to the equilibrium temperature and the closer the system is to thermodynamic equilibrium.

The equilibrium constant is a function of temperature. Wheeldon, et al., (1985) used the equation:

$$Kp = 2.1\text{x}10^{-5} \exp(20520/T) \tag{4}$$

The temperature, T, is in degrees Rankine. Equilibrium constants, both measured and theoretical, are plotted in figure 4.3-19. Note that the May 11 data is much closer to equilibrium than the May 7 data so less SO_3 is produced in the presence of sorbent at constant O_2 partial pressures, which agrees with the elimination of white plume once dolomite addition is resumed.

References for Section 4.3

L. Shadle, Federal Energy Technology Center, personal communication, November 17, 1997.

J. M. Wheeldon, N. A. Burdett, M. A. Freidman, and J. E. Stantan, "SO_3 measurements at the Grimethorpe PFBC," Proceeding of the Eighth International Conference on Fluidized-Bed Combustion, Vol. II, July 1985, p. 715.

B. J. Burdett, B. J. Glidden, R. C. Hotchkiss, and R. T. Squires, "SO_3 in coal-fired fluidized bed combustor," Journal of the Institute of Energy, v. 56 (September 1983), pp. 119 to 124.

Table 4.3-1

TCO2 SO_2 and SO_3 Data From May 7 and May 11

Date	5/7/98	5/11/98
Extractive Data Points	4	6
Extractive SO_3 (ppmv)	0.24	160
Extractive SO_2 (ppmv)	2.9	83
Analyzer SO_2 (ppmv)	2.0	83
Extractive SO_3 (6% O_2) (ppmv)	0.3	216
Extractive SO_2 (6% O_2) (ppmv)	3.0	113
Analyzer SO_2 (6% O_2) (ppmv)	2.1	113
SO_X From Coal (ppmv)	484	347
SO_X Emissions (lb/MBtu)	0.0055	0.9991
SO_X Removal (%)	99.6	29.90
Feed Solids Ca/S Ratio	1.7	(2)
Spent Solids Ca/S Ratio	1.25	1.0
In Situ Solids Ca/S Ratio		1.0

Notes:

1. Extractive data collected by Southern Research Institute for about 10 minutes. Extractive in situ samples taken from PCD rather than normal solids sampling location.
2. Dolomite feed turned off for this test.

Table 4.3-2

TCO2 SO_2 and SO_3 Data From May 7 and May 11

Date	5/7/98	5/11/98
Extractive SO_3 (ppmv)	0.24	160
Extractive SO_2 (ppmv)	2.9	83
PCD Outlet Temperature (F)	1,343	1,308
Pressure (psig)	200	190
O_2 (%)	6.6	10.0
K_P (atm^{-5}) (Note 1)	0.086	1.631
Equilibrium Temperature (F) (Note 2)	2,031	1,362
Approach to Eqm. (F)	689	55

Notes:

1. K_o defined in Equation (3).
2. Approach to equilibrium temperature is the difference between equilibrium temperature and actual temperature.

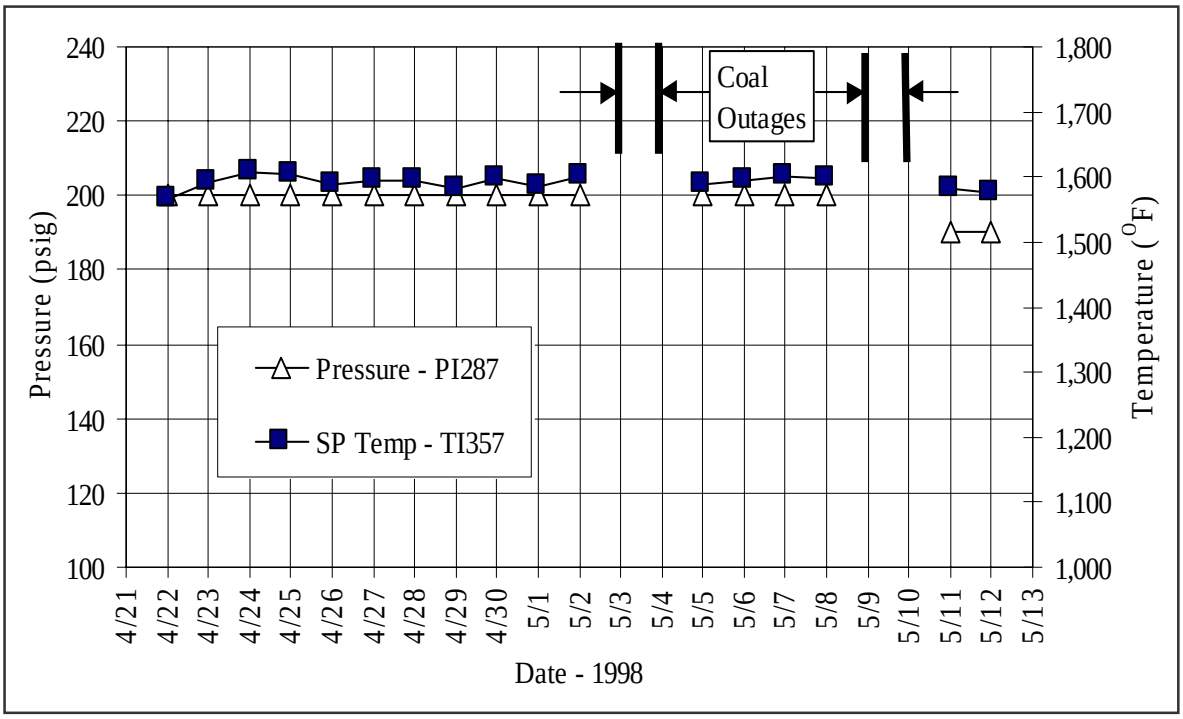

Figure 4.3-1 TCO2 Daily Average Temperatures and Pressures

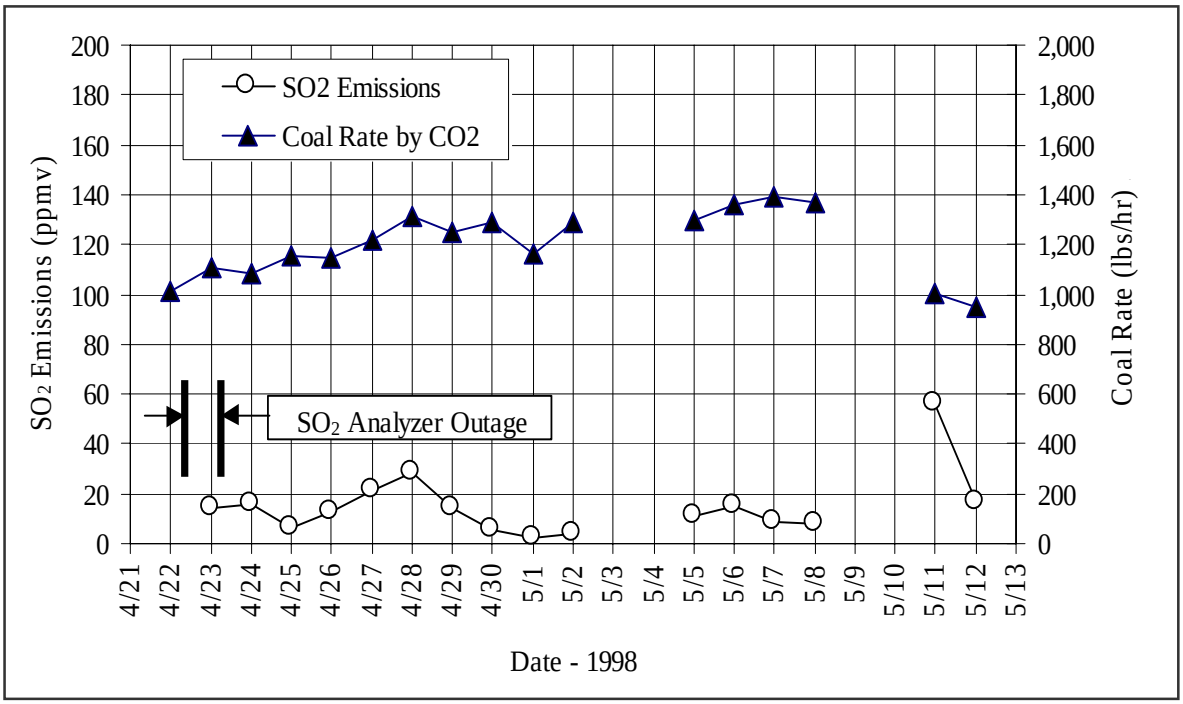

Figure 4.3-2 TCO2 Daily Average SO_2 Emissions and Coal Feed Rate

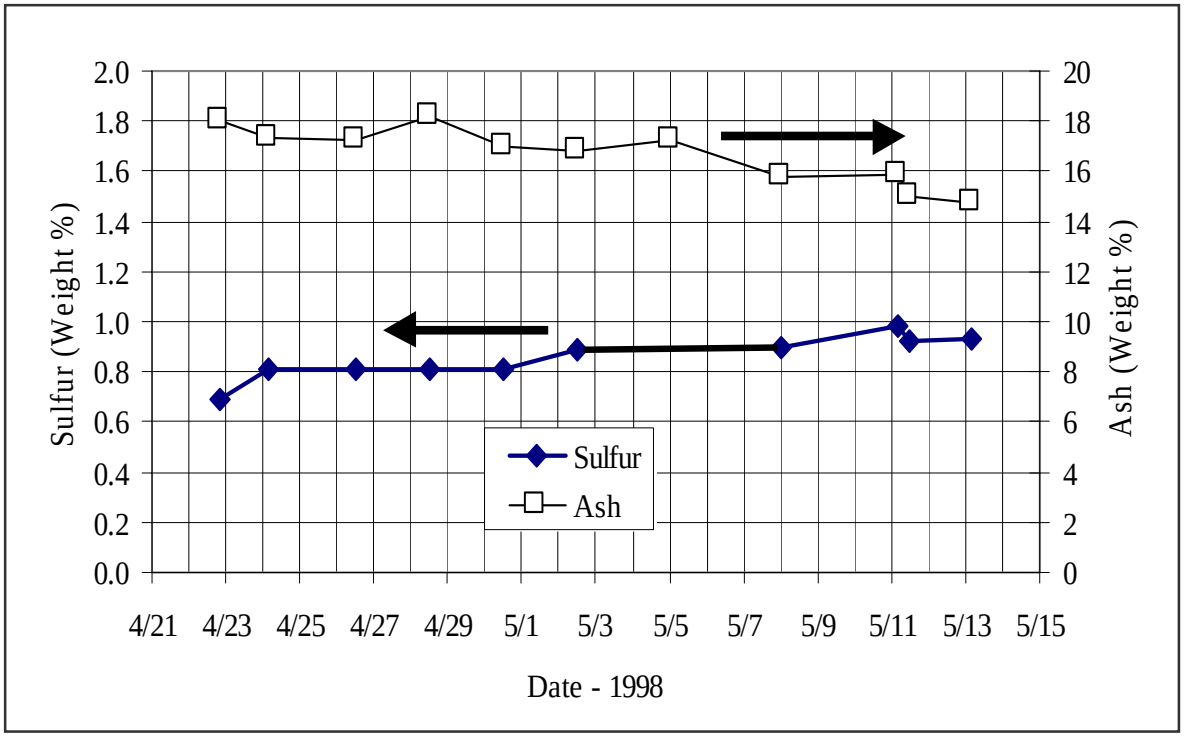

Figure 4.3-3 TCO2 Coal Sulfur and Ash Weight Percents

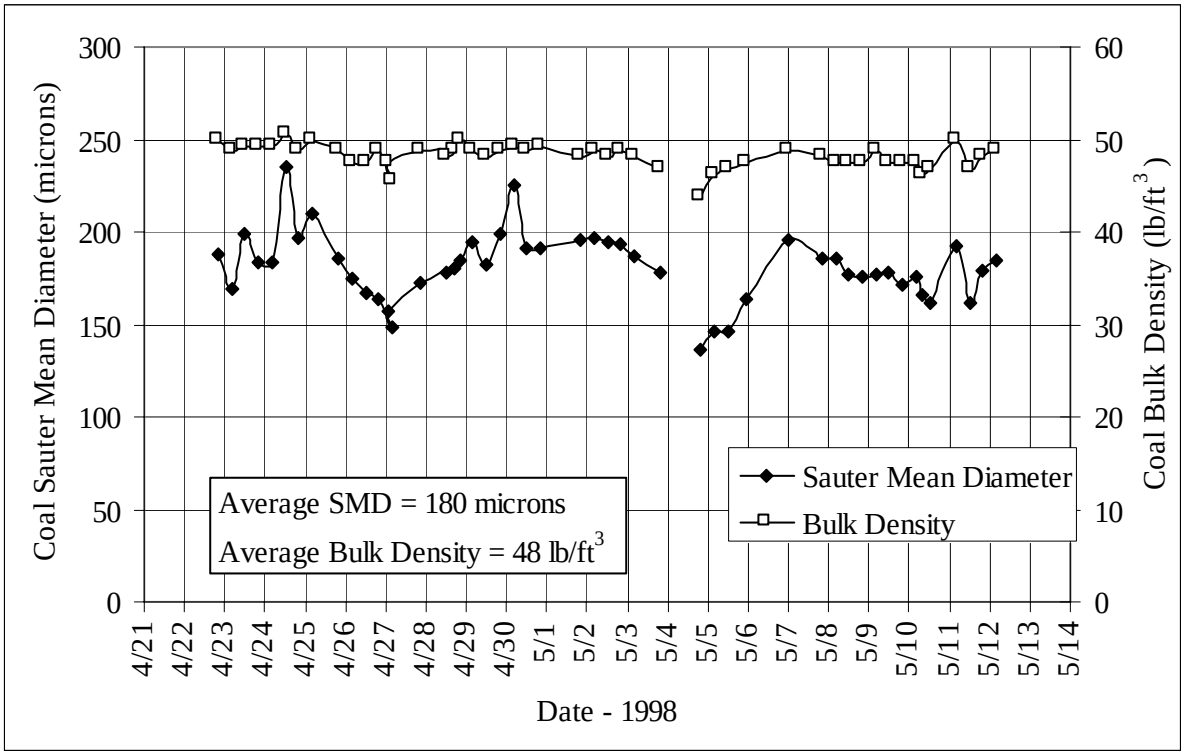

Figure 4.3-4 TCO2 Coal Particle Size and Bulk Density

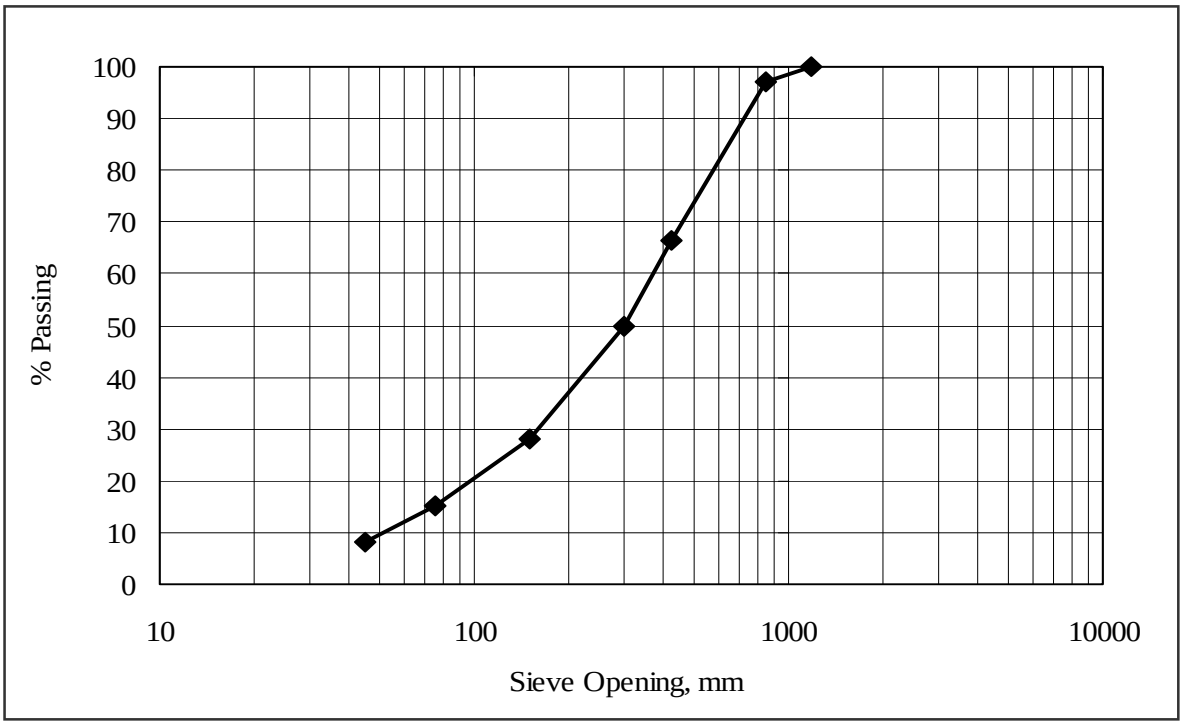

Figure 4.3-5 TCO2 Coal Particle Size Distribution May 1, 1998 (20:00)

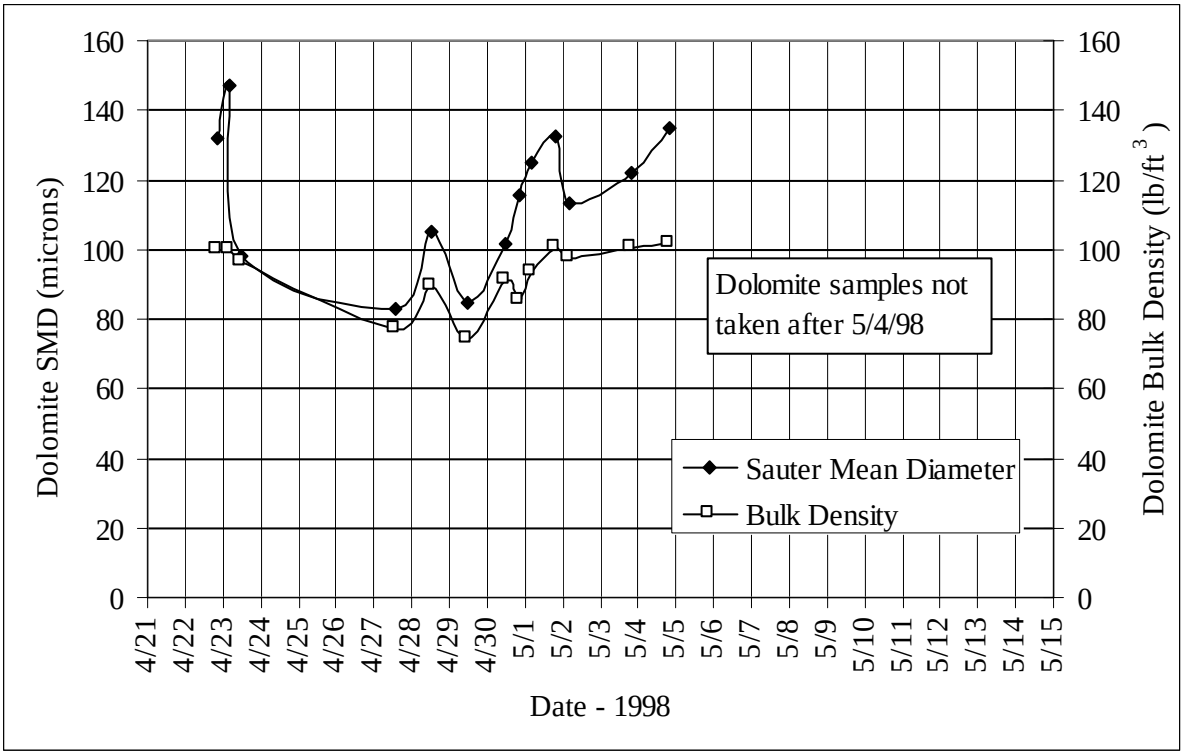

Figure 4.3-6 TCO2 Dolomite Particle Size and Bulk Density

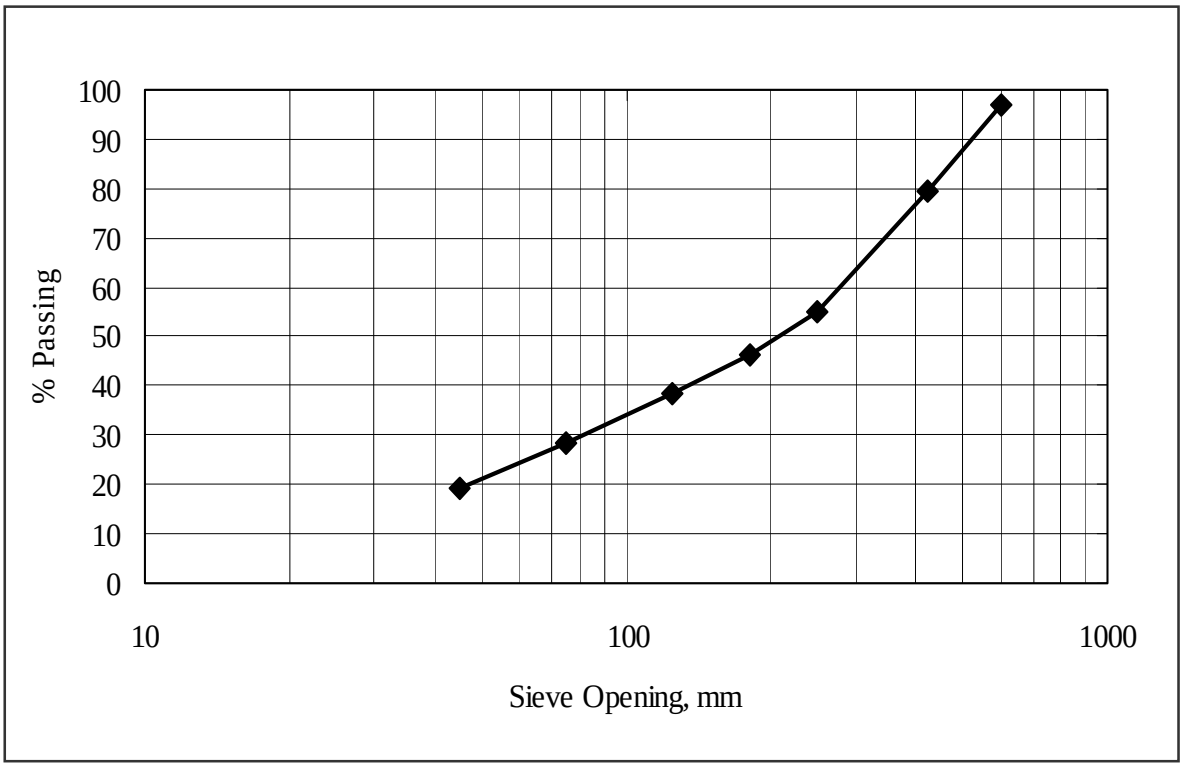

Figure 4.3-7 TCO2 Dolomite Particle Size Distribution May 1, 1998 (4:00)

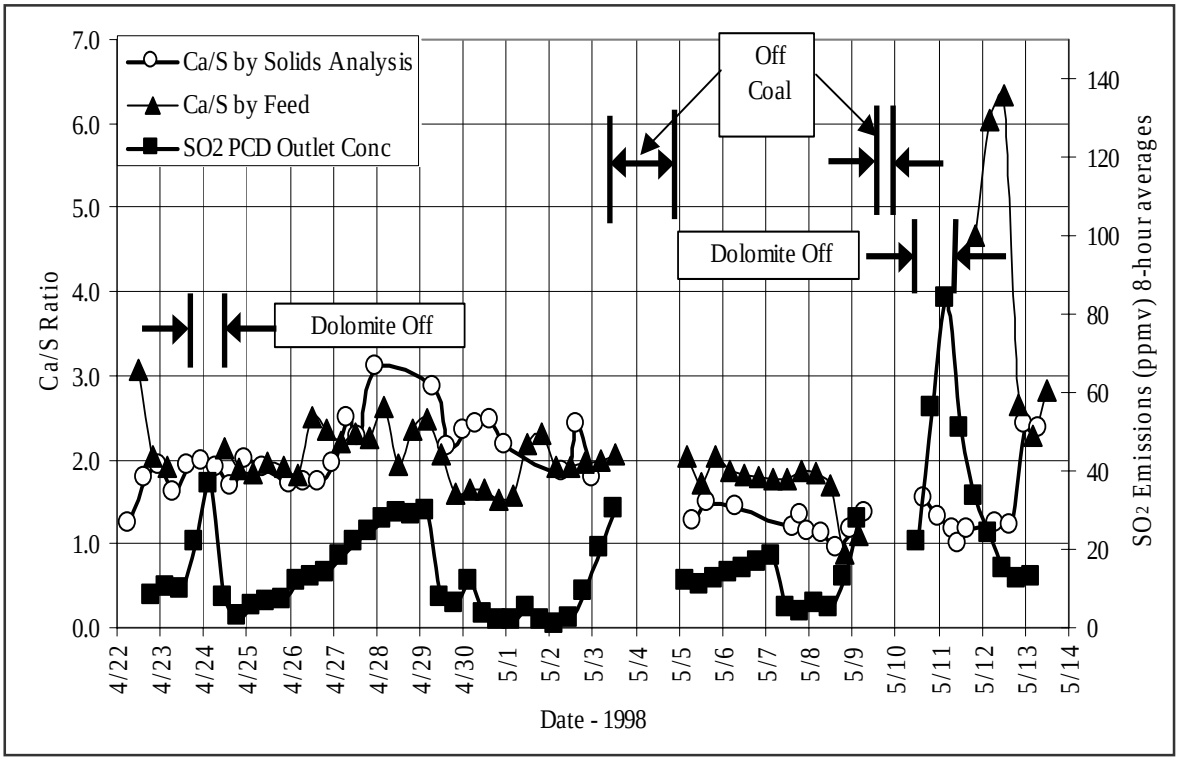

Figure 4.3-8 TCO2 Calcium/Sulfur Ratio and SO_2 Emissions

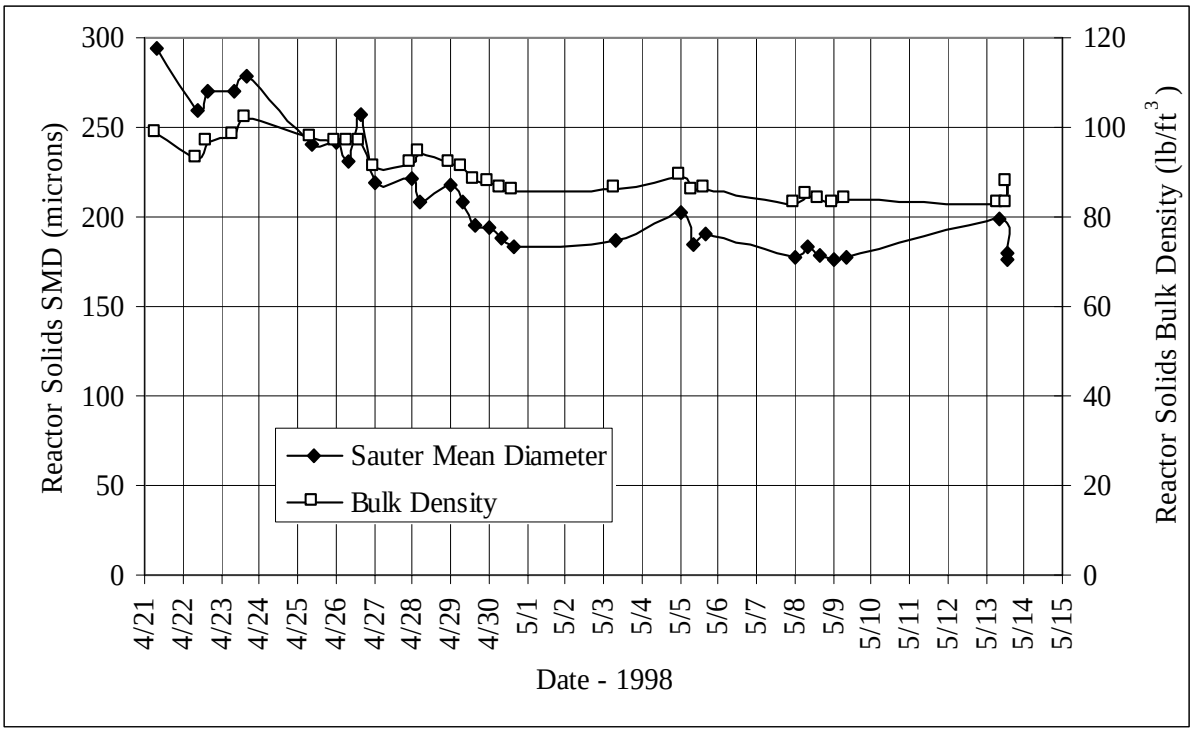

Figure 4.3-9 TCO2 Reactor Solids Particle Size and Bulk Density

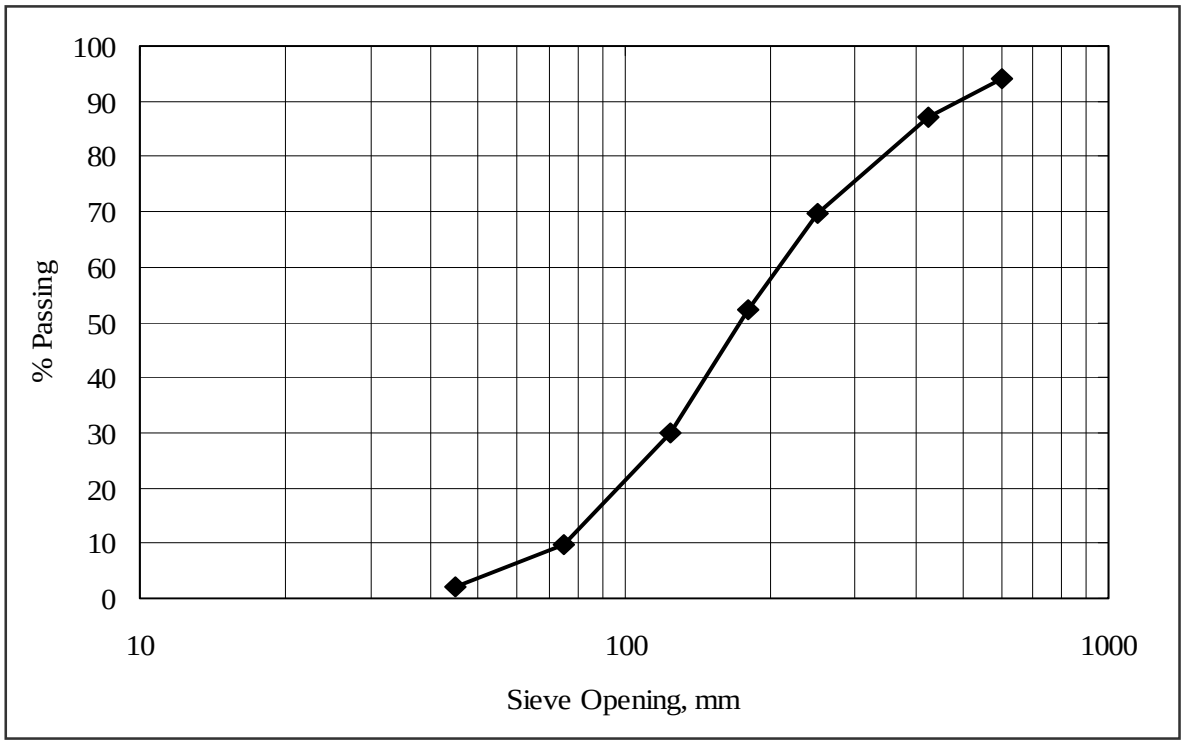

Figure 4.3-10 TCO2 Reactor Solids Particle-Size Distribution May 8, 1998 (0:00)

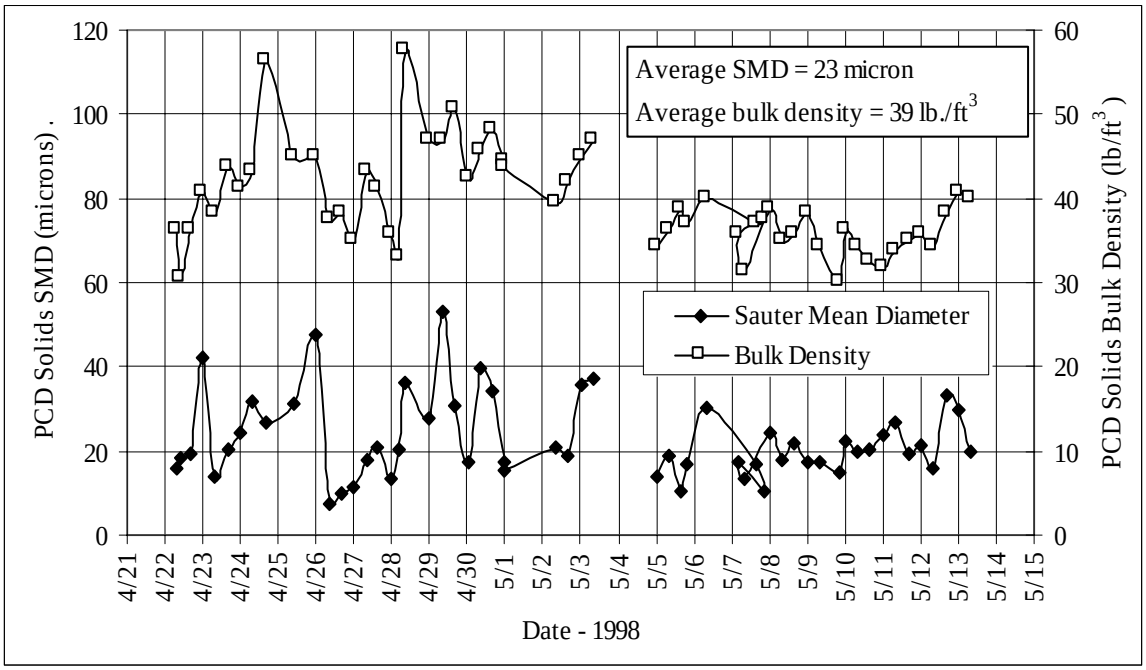

Figure 4.3-11 TCO2 PCD Solids Particle Size and Bulk Density

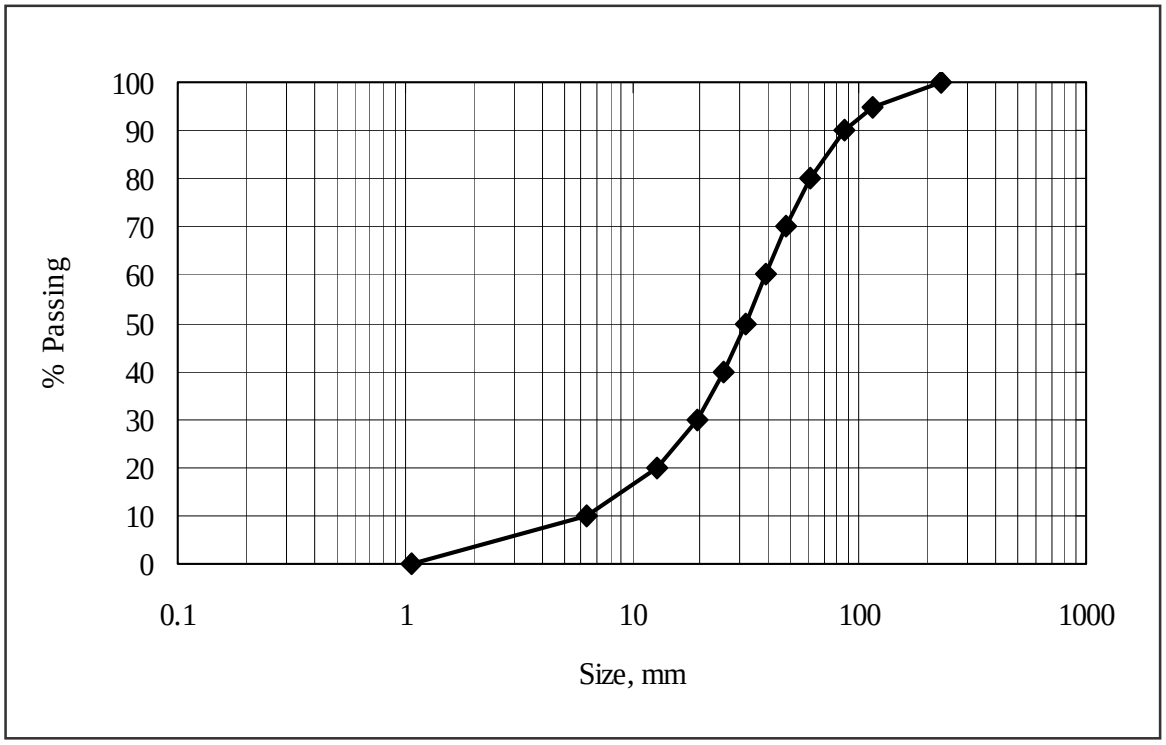

Figure 4.3-12 TCO2 PCD Solids Particle-Size Distribution May 10, 1998 (0:00)

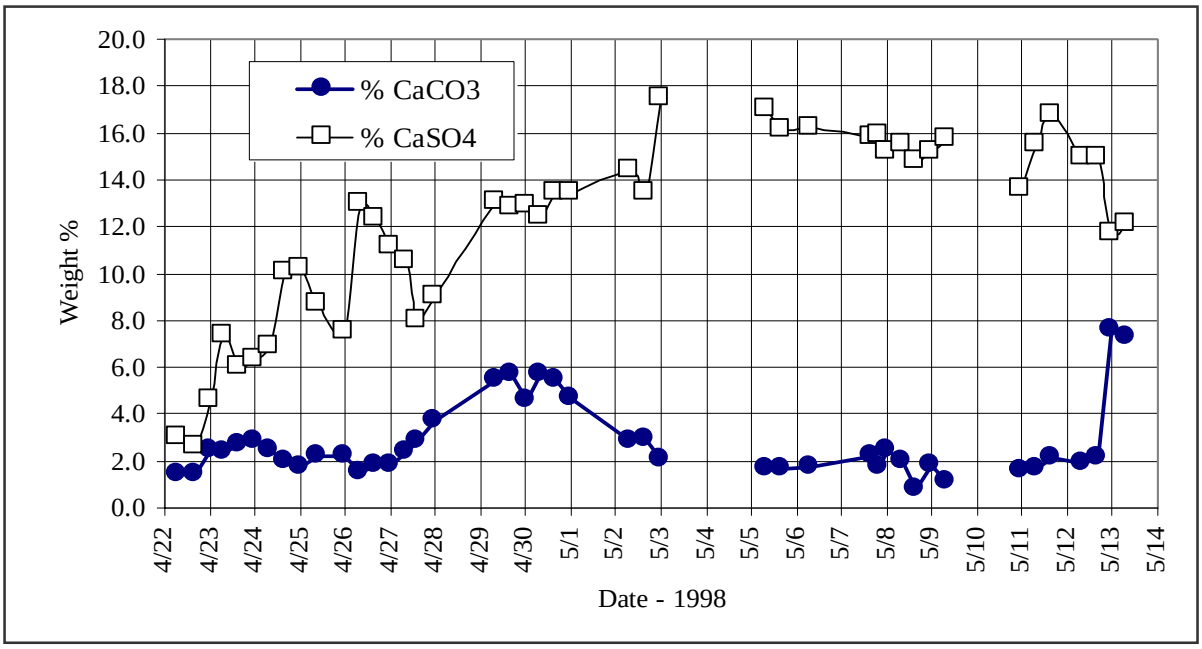

Figure 4.3-13 TCO2 PCD Solids $CaCO_3$ and $CaSO_4$ Concentrations

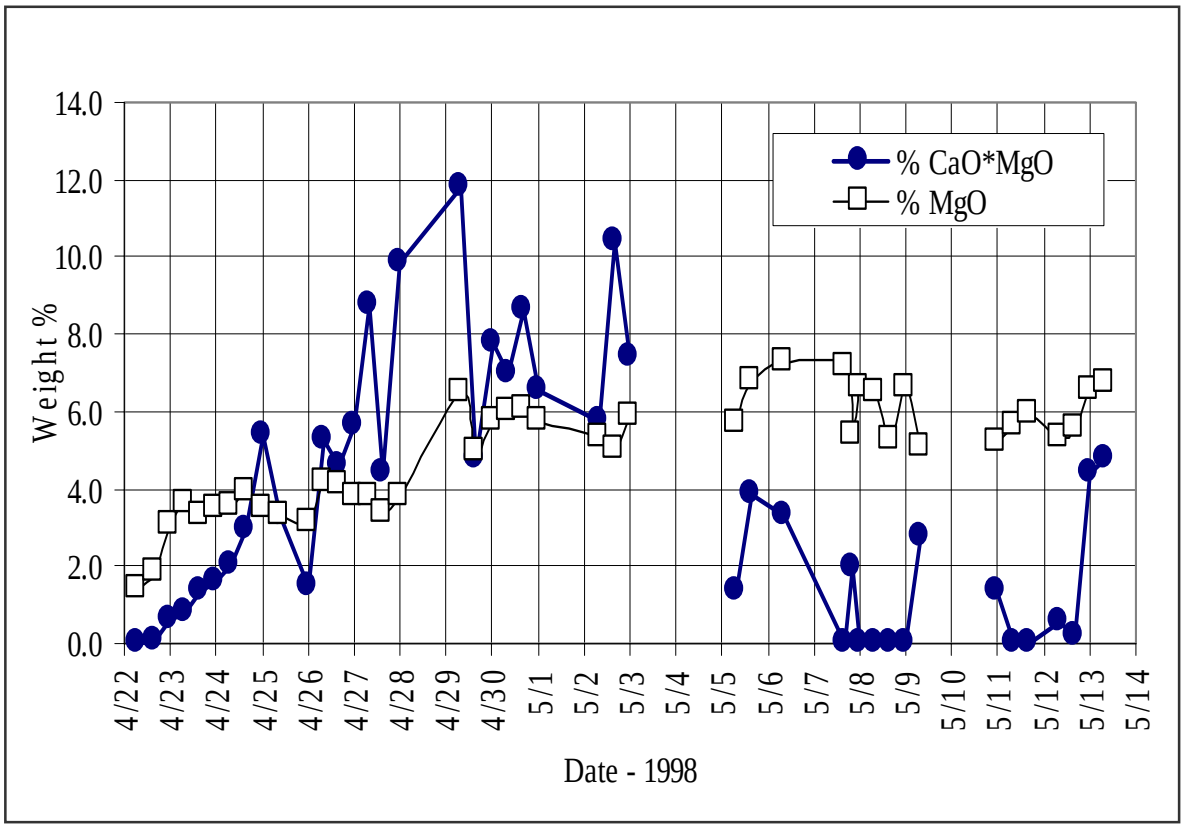

Figure 4.3-14 TCO2 PCD Solids CaO•MgO & MgO Concentrations

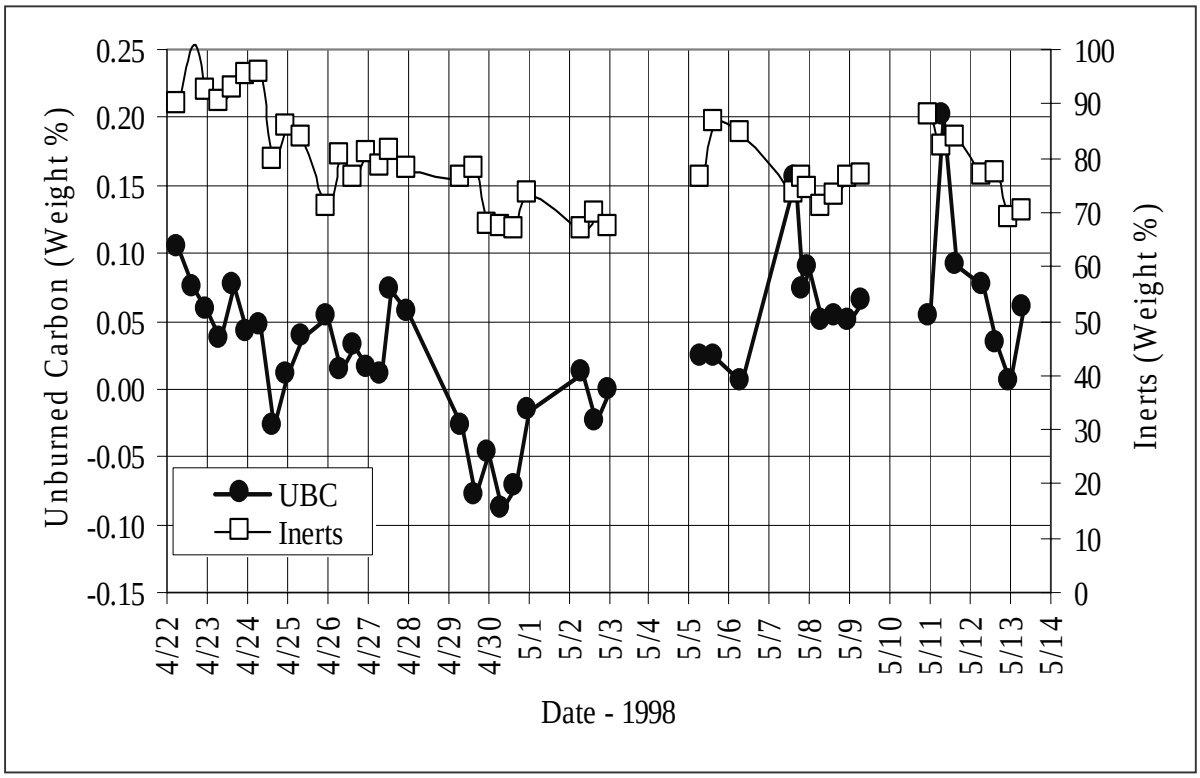

Figure 4.3-15 TCO2 PCD Solids Unburned Carbon and Inerts Concentrations

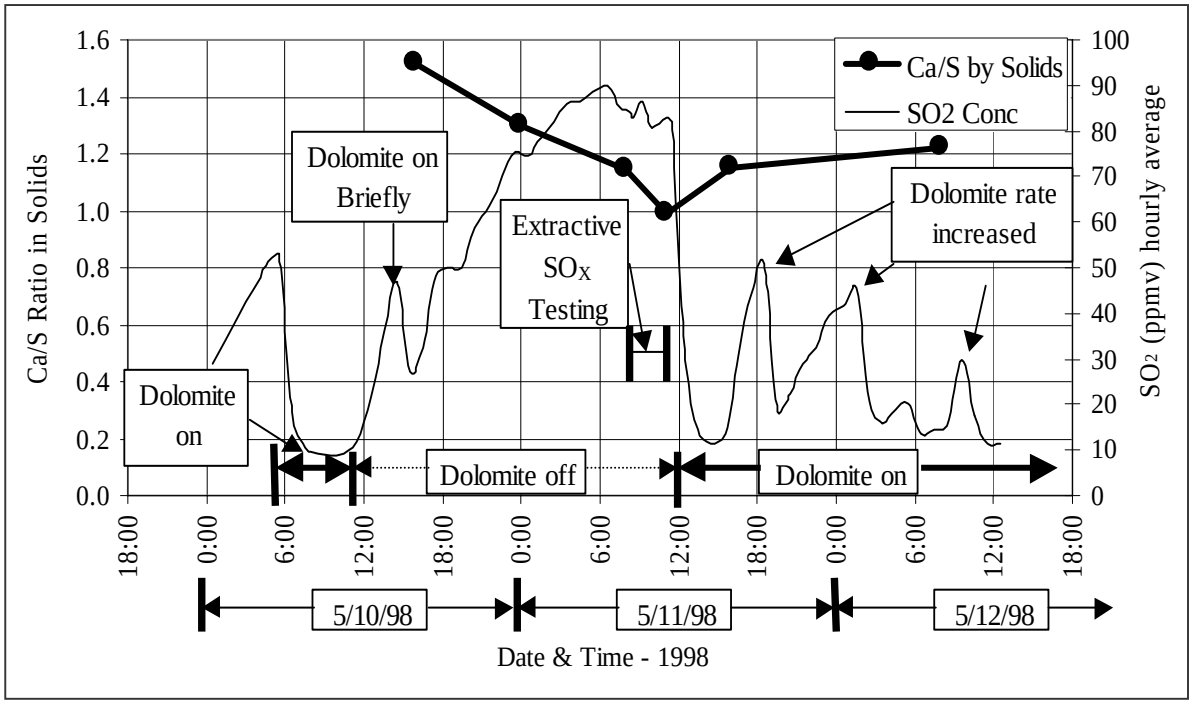

Figure 4.3-16 TCO2 May 10 to May 12 SO_2 and Ca/S Ratio Data

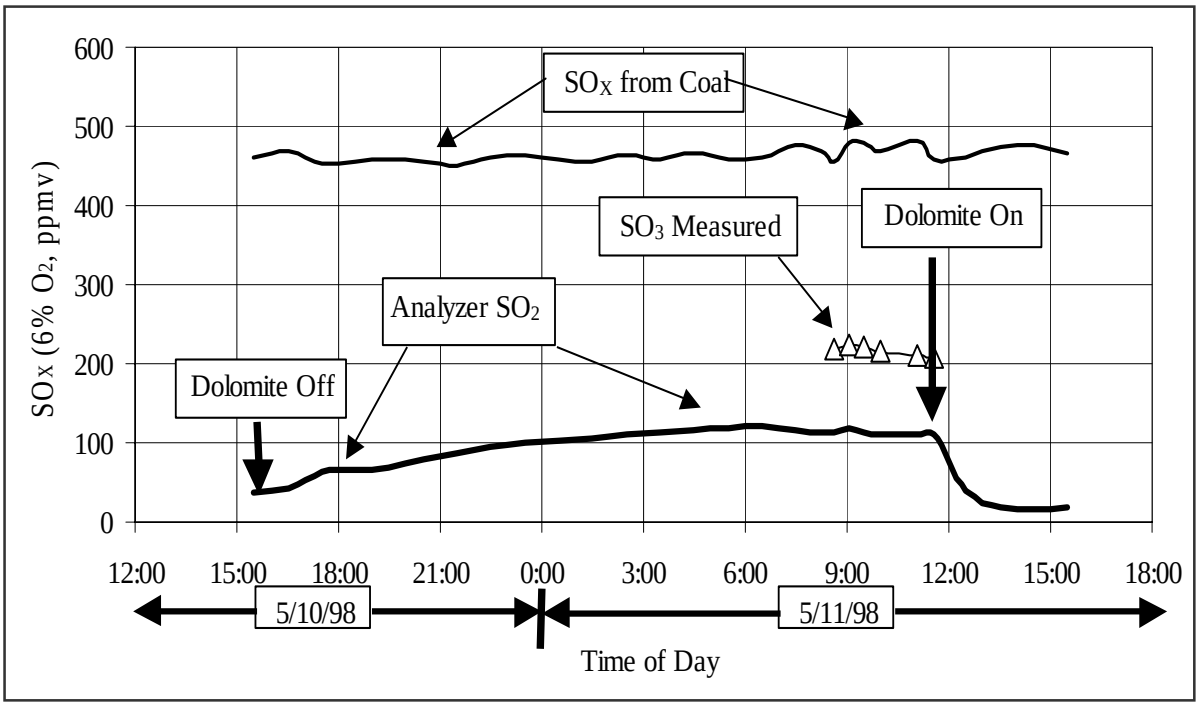

Figure 4.3-17 TCO2 May 10 to May 11 SO_2 and SO_3 Data

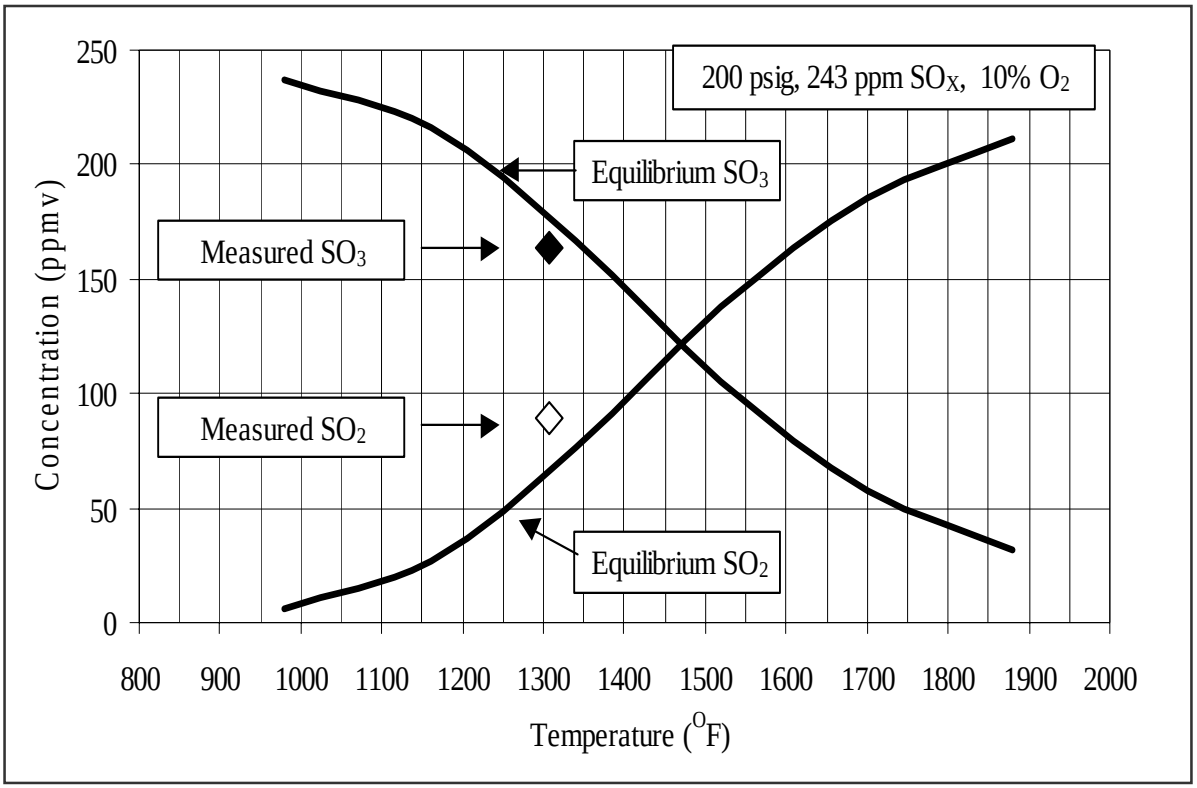

Figure 4.3-18 SO_2 - SO_3 Equilibrium and TCO2 Data for May 11, 1998

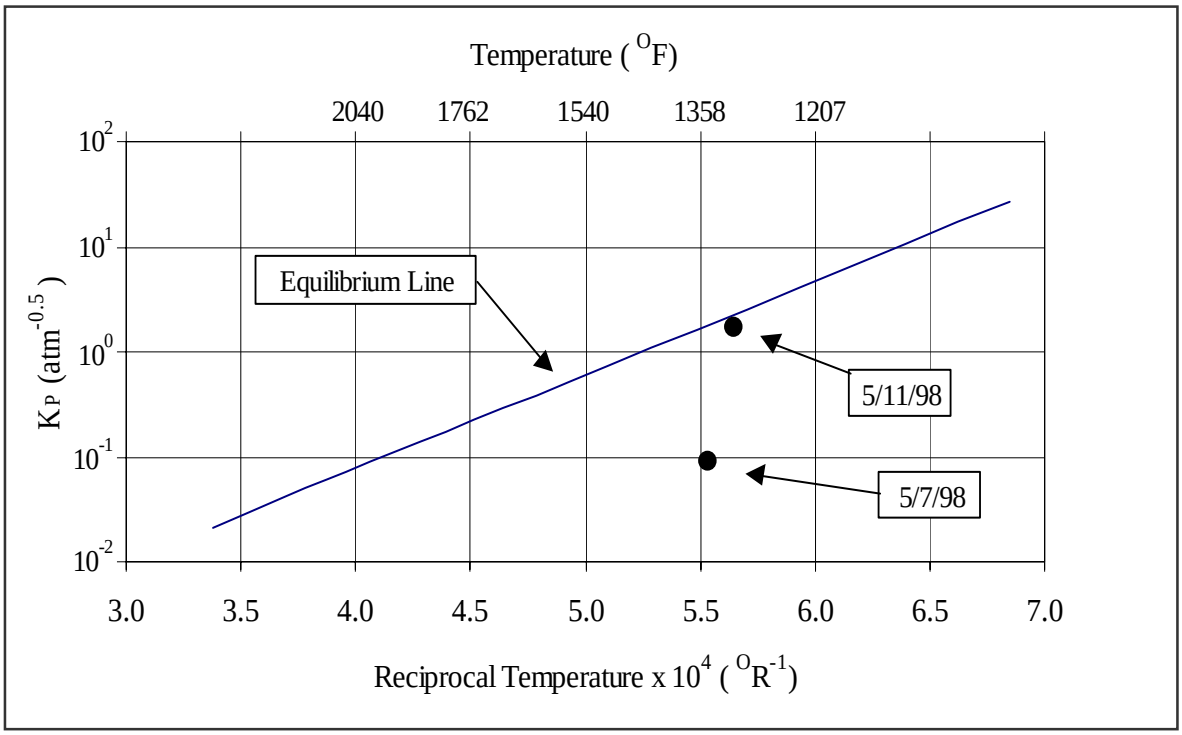

Figure 4.3-19 Equilibrium Line for SO_2 - SO_3 and TCO2 Data

4.4 NO_X EMISSIONS

Reactor operating conditions during test run TC02 were varied to study their effect on NO_X formation as measured by a NO_X analyzer downstream of the PCD. These variables included:

- Excess air.
- Staged air.
- Primary air distribution.
- Temperature.
- Coal feed rate.
- Dolomite feed rate.

This section will discuss the expected behavior and present the data collected and observations made that show the effect that these operating conditions had on NO_X emissions.

Figure 4.1-1 is a schematic of the transport reactor loop showing the air distribution locations, coal feed nozzle location, and flue-gas sample point. The combustion air can be staged with primary air being added into the mixing zone in a lower and upper level and with secondary air added into the riser in three levels. Air added into the reactor J-leg and combustor heat exchanger (HX0203) J-leg for solids circulation is also likely available for the combustion reactions. Additional air available for the combustion reactions may be added in some cases through the start-up burner (BR0201) J-leg and the bottom of the mixing zone. Air is also added into other locations downstream of the combustion zone such as the cyclone dipleg and reactor standpipe. It should be noted that this aeration air is included in the flue gas measurements since the sample point is downstream of the PCD. Aeration and fluidization air added to the cyclone dipleg, standpipe, and combustor heat exchanger is normally split with a portion of this air moving down with the solids and into the mixing zone. The split is determined by operating conditions such as circulation rate and aeration/fluidization gas velocities, and it is assumed that all aeration/fluidization gas enters the mixing zone with the solids since the split is not definitely known. This assumption introduces an error of less than 10 percent in total air available for the combustion reactions.

Figure 4.4-2 shows a plot of the NO_X emissions given in pounds of NO_X per MBtu of fuel fired (lb/MBtu) versus the oxygen concentration in the flue gas in volume percent of total flow (%) at several levels of staging. The staging percent was defined as the amount of secondary air flow divided by the total air flow to the reactor that is available for the combustion reactions. All data plotted in this section are based on 5-minute averages due to variance in coal feed rate and, therefore, oxygen concentration in the flue gas. The reactor operating conditions for this period are in table 4.4-1 listed as data set A. At 33- to 36-percent staging air, the NO_X emissions increased from about 0.15 lb/MBtu at 9-percent oxygen content in the flue gas to around 0.2 lb/MBtu at 10-percent oxygen content. At 1.4-percent staged air, the NO_X emissions increase was much less, from 0.22 lb/MBtu at about 8.6-percent oxygen concentration to 0.25 lb/MBtu at around 9.3-percent oxygen concentration.

Figure 4.4-2 also shows that at 9.0-percent oxygen concentration in the flue gas the NO_X emissions increased from 0.15 to 0.18 lb/MBtu as the staging air was reduced from 33- to 36-percent to 23-percent and further increased to 0.24 lb/MBtu at 1.4-percent staged air.

Figure 4.4-3 plots the NO_X emissions versus the oxygen concentration in the flue gas at different primary air distribution splits. The reactor operating conditions for this period are in table 4.4-1 listed as data set B. The NO_X emissions were slightly higher when all the primary air was added through the lower level.

The results from data set A operations were plotted as NO_X emissions versus reactor temperature to evaluate the effect of reactor temperature (see figure 4.4-4). The figure shows that there was a slight decrease in NO_X emissions as the temperature increased at a constant staged air.

Figure 4.4-5 plots the NO_X emissions and oxygen concentration in the flue gas versus the coal feed rate at the reactor conditions listed as data set C. The plot shows that the NO_X emissions actually decreased as the coal feed rate increased. It should be noted that it is very difficult to change the reactor temperature independently in the transport reactor. The figure shows that the oxygen in the flue gas also decreased as the coal feed rate increased because in this testing time the air flow rate was kept constant. The air flow was kept constant because the maximum capacity of the main air compressor had been reached. Also, the solids circulation rate was slightly increasing as the coal feed rate was increased. It is also possible that other reactor conditions varied and that the oxygen decrease may not have been the sole cause of the NO_X emissions decrease. The trend shows that the NO_X emissions are lowest at a lower oxygen concentration in the flue gas and a higher coal feed rate.

It was also observed that the NO_X emissions increased when dolomite was added into the reactor for sulfur capture. Figure 4.4-6 plots the NO_X emissions versus the oxygen in the flue gas with dolomite addition at a Ca/S molar ratio of 2:0 and without dolomite addition at the reactor conditions listed as data set D in table 4.4-1. The NO_X emissions were about 0.2 lb/MBtu with dolomite addition and approximately 0.16 lb/MBtu without dolomite addition at a slightly higher oxygen concentration in the flue gas.

In summary, the NO_X emissions were low, varying from 0.1 to 0.3 lb/MBtu. The NO_X emissions gradually increased as the excess air was increased, as expected. The NO_X emissions also increased as the air flow rate through the lower level of primary air was increased. The NO_X emissions decreased by 38 percent as the amount of staging air was increased from 1.4 to 36 percent. In this operating range there was a decrease in NO_X emissions as the temperature was increased. The NO_X emissions were expected to increase as the coal feed rate was increased due to increased fuel nitrogen. However, in this test period the NO_X emissions decreased because other operating conditions such as temperature and excess air could not be kept constant due to operating limitations of the reactor system. In addition, it was observed that there was a significant influence of dolomite addition on NO_X emissions. The NO_X emissions increased by 25 percent as the Ca/S molar ratio was increased from 0:0 to 2:0. This will be further analyzed in the next transport reactor test run.

Table 4.4-1

Reactor Operating Conditions

Data Set	A	B	C	D
Reactor temperature (°F)	1,540 to 1,640	1,600	1,540 to 1,580	1,600
Reactor pressure (psig)	200	200	200	200
Coal feed rate (lb/hr)	1,010 to1,230	1,030 to 1,120	1,110 to 1,230	1,030 to 1,130
Dolomite feed rate (lb/hr)	70 to 110	80 to 100	80 to 100	0 to 100
Ca/S molar ratio	1.2 to 2.0	1.5 to 2.1	1.4 to 2.0	0 to 2.0
Staged air (%)	1.4 to 36	2.6	33 to 36	2.2

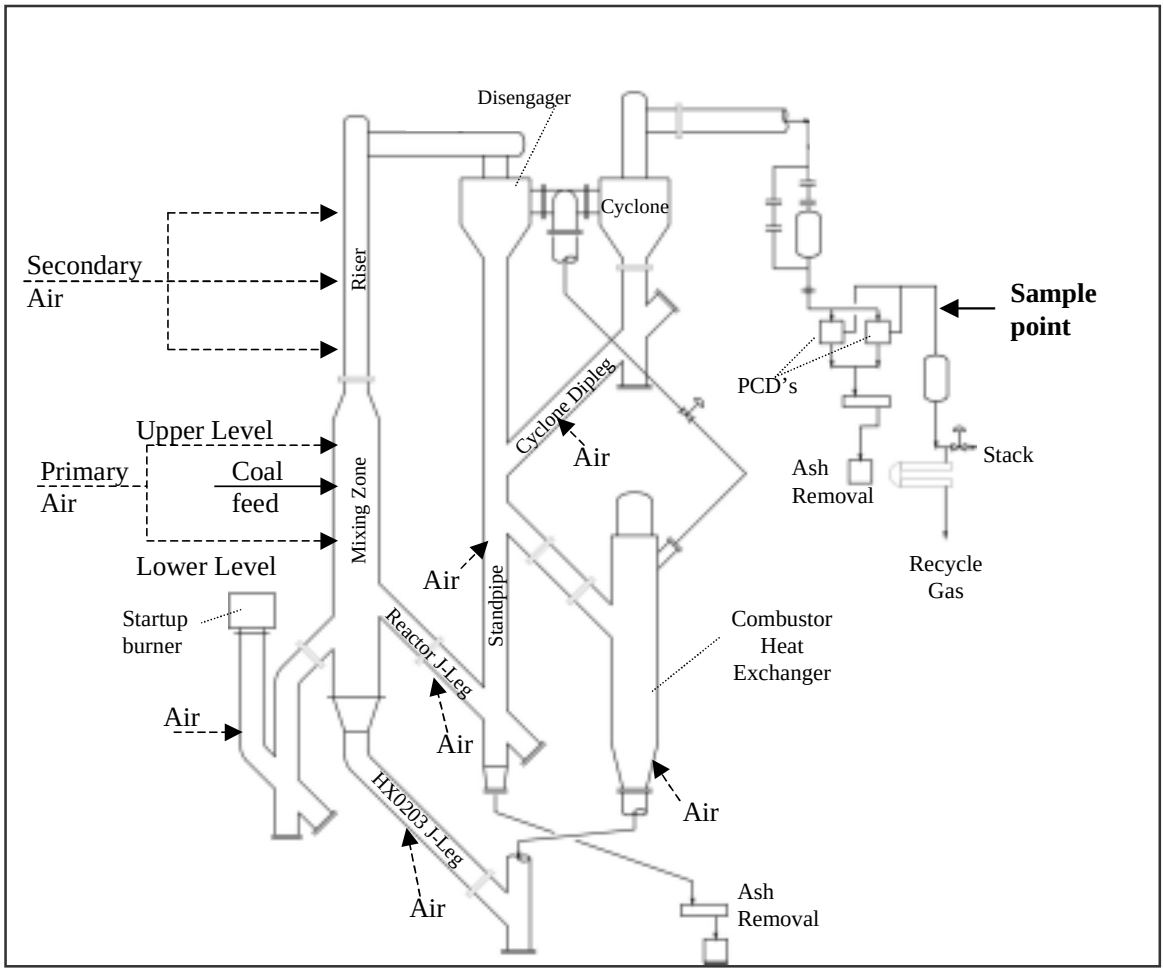

Figure 4.4-1 Transport Reactor Train Loop Schematic

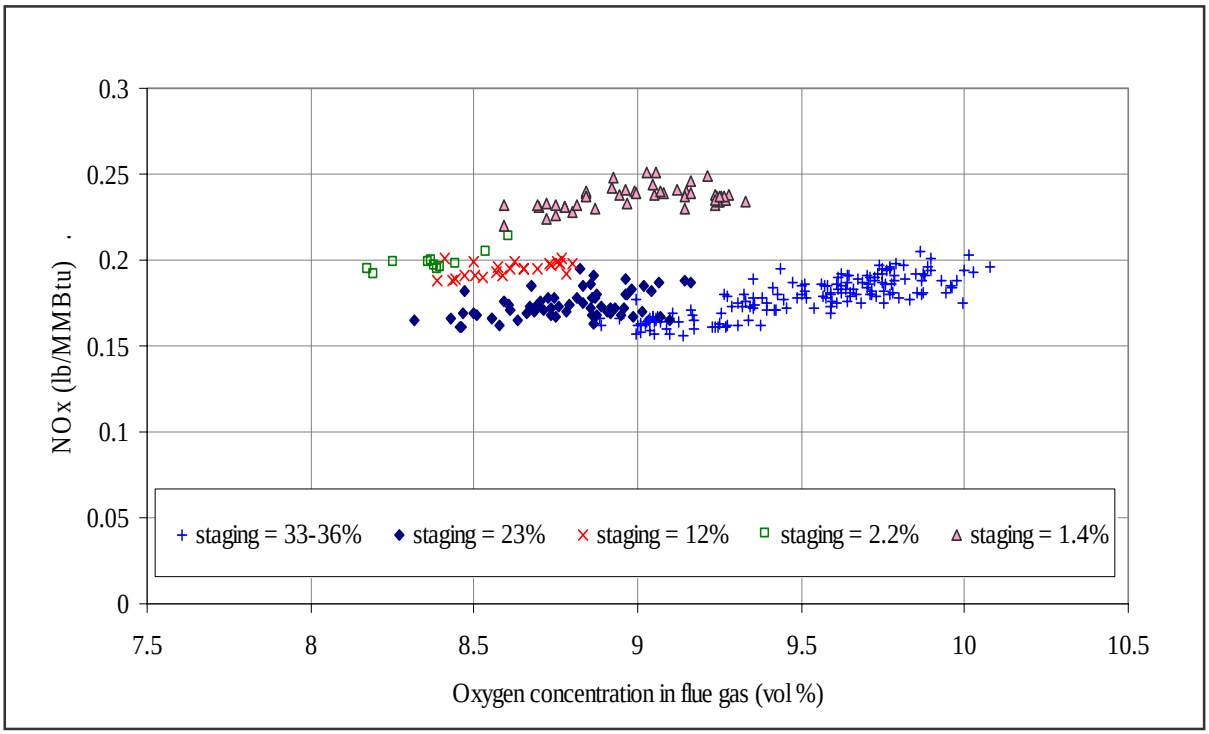

Figure 4.4-2 Effect of Staging Air and Excess Air on NO_X Emissions

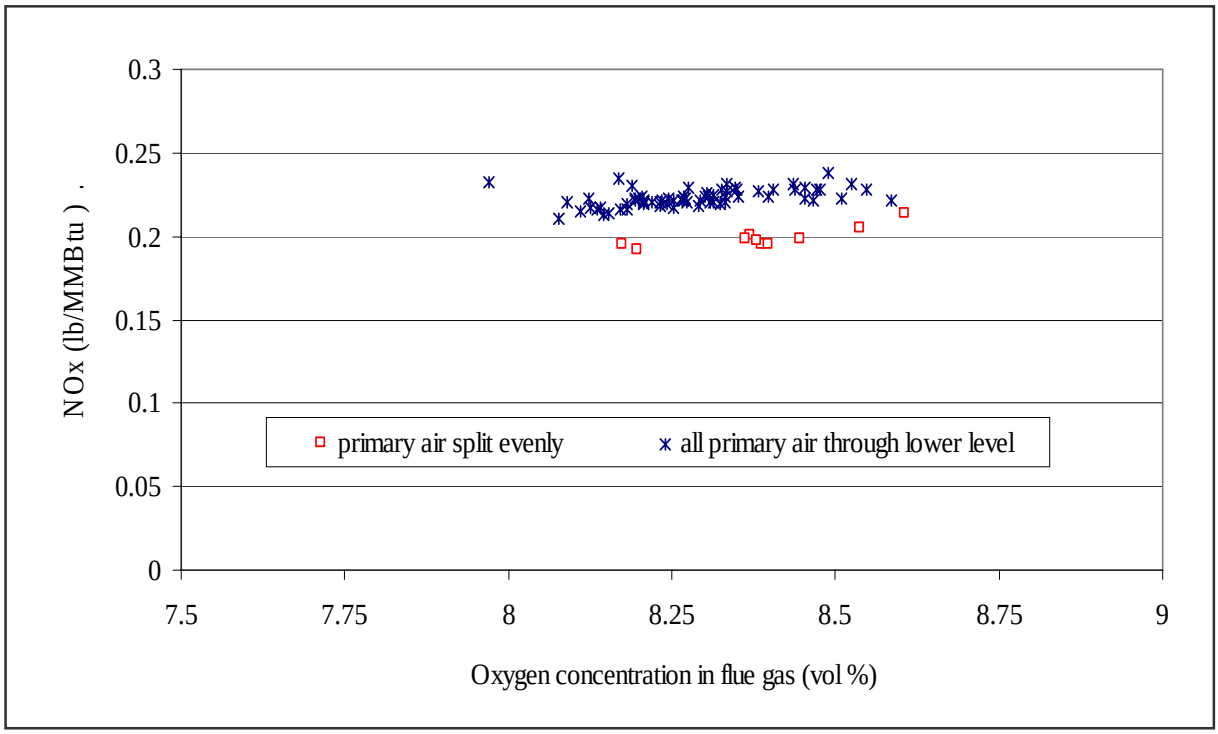

Figure 4.4-3 Effect of Primary Air Distribution on NO_X Emissions

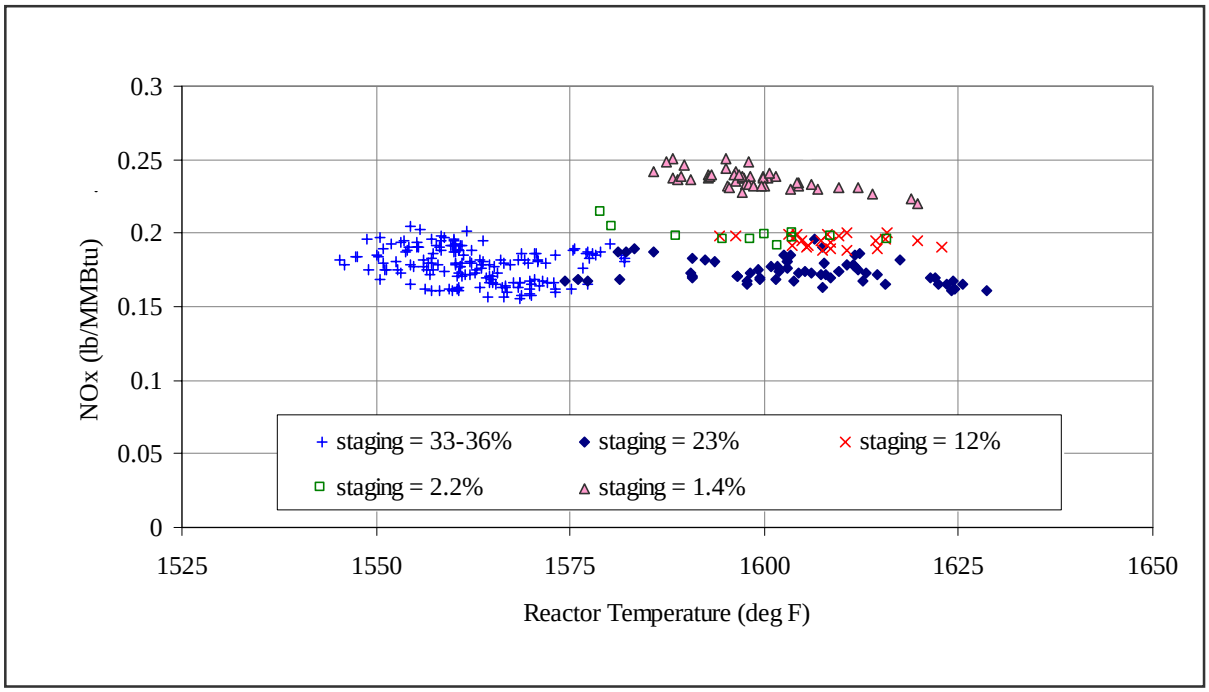

Figure 4.4-4 Effect of Temperature on NO_X Emissions

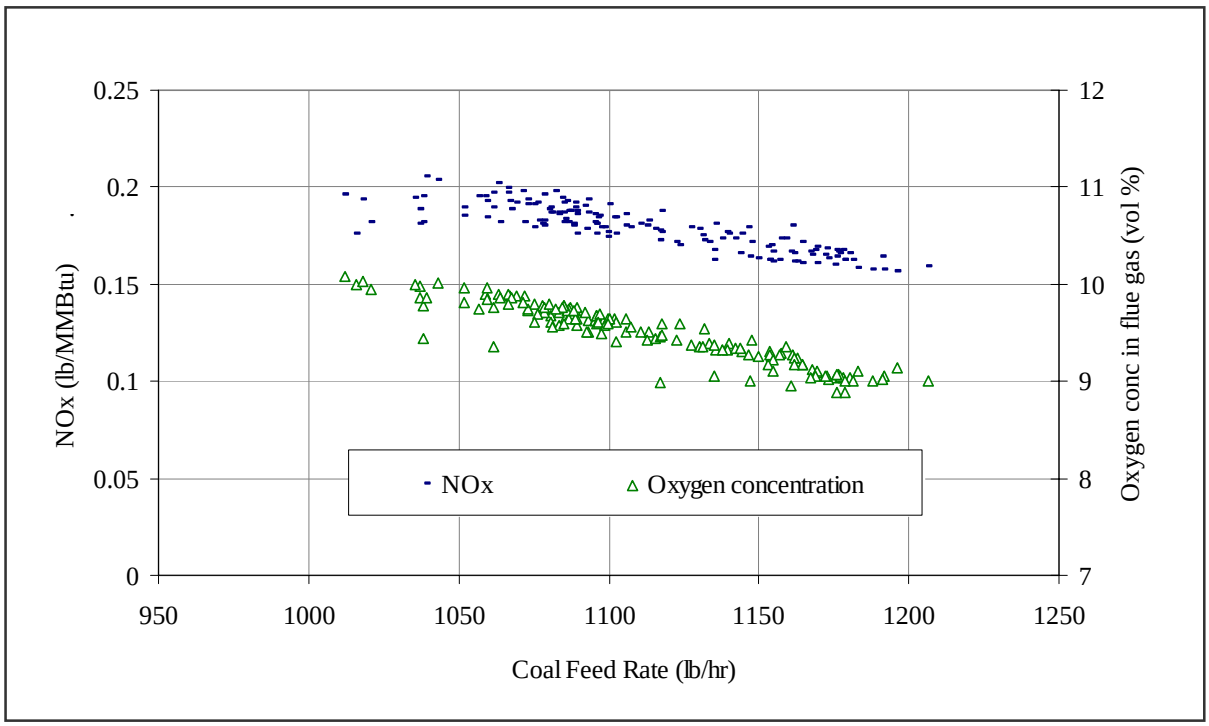

Figure 4.4-5. Effect of Coal Feed Rate on NO_X Emissions

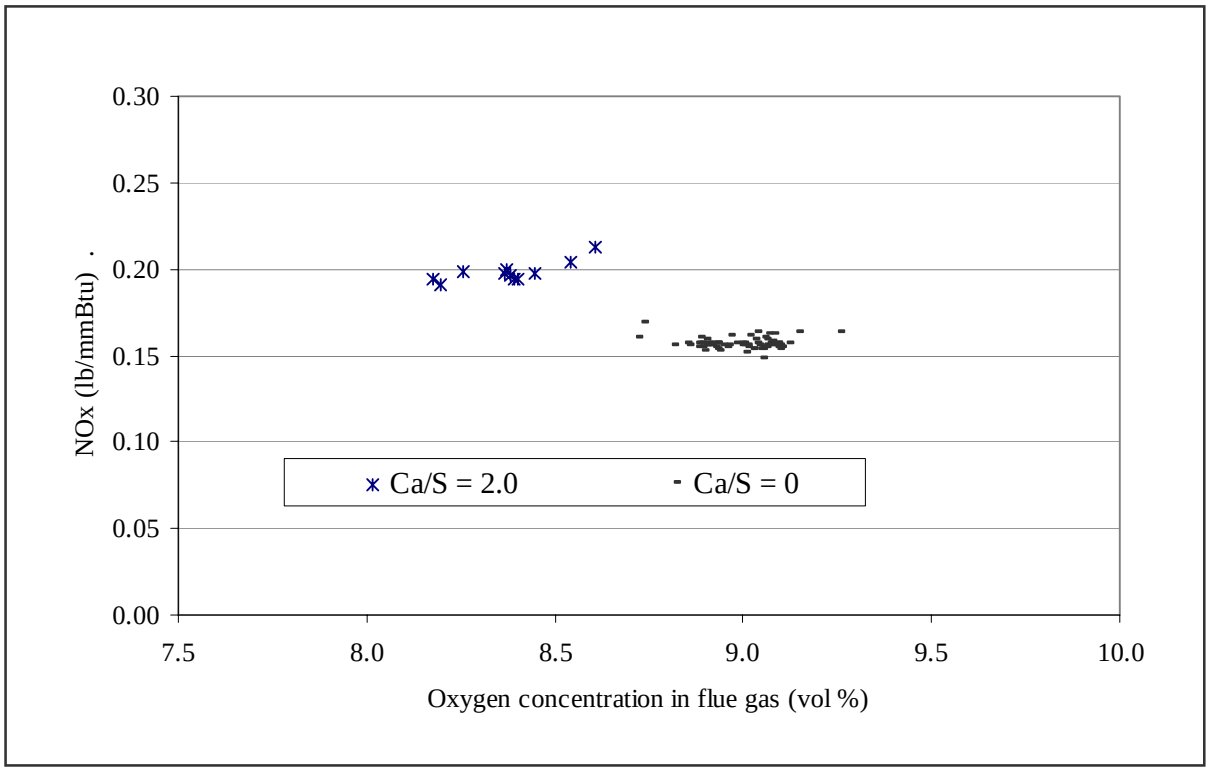

Figure 4.4-6 Effect of Dolomite Addition on NO_X Emissions

4.5 FLOW REGIMES IN THE TRANSPORT REACTOR

A critical issue in the design, operation, and scaleup of the transport reactor is the flow regimes in the different parts of the reactor loop. For example, the transport reactor was designed to have a turbulent flow regime in the mixing zone, a dilute regime in the riser, and a uniform flow regime in the standpipe. This issue will be explored in detail in this section for the purpose of both the technology development of the transport reactor and a better understanding of the flow regimes in a circulating fluidized bed.

New light may shed on this subject through the operation of the transport reactor and the observation from a cold flow model. This section of the TC02 report will focus on a review of literature data on the flow regime in the riser side of the circulating fluidized bed (CFB), and the fundamental issues that need to be addressed will then be discussed. Section 4.5-3 presents a conceptual model that can be used to describe the flow regimes in a circulating fluidized bed.

4.5.1 Literature Review on Flow Regimes in a CFB

The characterization and prediction of flow regimes can be very fruitful to technology development and the scientific advance of fluidization. The proper characterization of the flow regimes will make it possible for the process engineer to choose a proper regime for a desired result or effect. The ability to predict flow regimes will inject confidence into both the process design and operations.

Depending on different authors and on reactors, different flow regimes have been observed and various models have been proposed to predict them. The most popular, although quite misleading, flow regime definitions include fixed, bubbling, turbulent, fast, and dilute transport. Solids in a fixed bed are stationary and gas passes through a maze of complicated channels formed by packed particles. In a bubbling bed, depending on the gas velocity and the particle properties, there are apparent dense-phase and gas bubbles, which are essentially solids free. At higher gas velocity, especially with solids recycle, a churned bed with many gas and solid streaks (called turbulent flow regime) can occur. Further increases in gas velocity, but maintaining the same solids recycle (feed) rate, cause many solid clusters and extensive forward and backward mixing to occur in a bed, resulting in fast fluidization (Yerushami, et al., 1976). At a still higher gas velocity solids are more uniformly distributed into the gas phase, resulting in what is termed as dilute transport regime.

The status of the flow regime mapping can be summarized by a quote from He and Rudolph (1996): "It (a fundamental analysis) reveals that all previous models on the hydrodynamics of the riser in a circulating fluidized bed system are either incomplete or theoretically flawed." This sad situation has many causes. The fundamental reason is the complexity of the gas-solid flow itself. The second reason is that the past experiences in bubbling bed have a negative influence on the research of the hydrodynamics of CFB. Since most knowledge on fluidization is inherited from the research on bubbling bed, when a circulating loop or circulating fluidized bed is introduced, there is still heavy reliance on the previous experiences. It is not only that the experimental data are generally explained or correlated from the standpoint of bubbling bed, but also the experimental design has been influenced to a large extent by bubbling beds. There is nothing

wrong in borrowing knowledge and models from the bubbling bed. However, it becomes confusing when the circulating fluidized bed data are viewed from the bubbling bed frame of reference. The fundamental difference between the bubbling bed and the circulating fluidized bed is that the latter has net solids flow (He and Rudolph, 1996).

Although the influence of solids flow on the flow regimes has been vaguely realized from the early time of the CFB research (Yeushami and Cankurt, 1979), this factor has not been incorporated into the flow regime mapping to a degree that the flow phenomena can be better understood. The earlier efforts of the flow regime mapping, as reviewed by Kunii and Levenspiel (1991), have concentrated most on the influence of the superficial gas velocity on flow regime. Although some authors considered the influence of the solid superficial velocity (Masten, 1982) and the slip velocity (Grace and Bi, 1997) on the flow regime, none of the flow regime mapping can explain why there is a dense phase in the bottom of the circulating fluidized bed or the void fraction profile in the circulating fluidized bed. Horio (1997) presented a diagram of flow regime mapping in which the solids superficial flux (mass flow rate divided by the cross-sectional area of the total flow) is plotted against the gas phase superficial velocity. All these flow regime mappings suffer in their inability to predict the existence of a dense phase in the bed.

There is indisputable evidence that the riser side (including the mixing zone and the riser of the transport reactor) of the circulating fluidized bed has different flow patterns. Li and Kwauk (1980) presented experimental data showing an S-shaped axial void fraction profile with a dense region in the bottom and gradual transition to a dilute phase near the top of an 8-meter column. In the early development of circulating fluidized beds it was thought as a necessary condition for the coexistence of dense and dilute region in the riser of the CFB (Li and Kwauk, 1980; Takeuchi, et al. 1986). The dense phase is still in existence even if the superficial gas velocity is far above the terminal velocity of the mean particles. Svensson, et al. (1993), and Johnsson and Leckner (1995) provided experimental evidence that there are three zones in a 12-W_{th} CFB boiler in spite of superficial gas velocity far above the terminal velocity of mean size of particles: 1) a bubbling bed in the bottom, 2) a dilute bed in the top, and 3) a transition zone in the middle. This kind of void fraction profile in the riser side of the CFB has apparently eluded predictions.

Although it is quite popular (Li and Kwauk, 1980; Kunii and Levenspiel, 1991; Adanez, et al., 1994; Johnsson and Leckner, 1995) in the literature to use the exponential profile to fit the axial profile of the void fraction it is nevertheless a post hoc rationalization rather than a prediction. Recently, Kwauk and Li (1996) proposed a generalized scheme for regimizing the fluidized systems by using multiple length scales. This proposition is still heavily influenced by the bubbling bed system. The influence of the solid circulation rate on the fluidization regime is almost totally neglected. The most helpful model for the technology development purpose will be a model that can predict under what conditions the dense bed will be formed in the riser. It is the major focus of this section of the report.

In summary, the prediction of the flow regime has not been very fruitful, although progress has been made in the last 2 decades in identification of the flow regime and mapping of the transition velocity of different flow regimes. The ability to predict the flow regime in a CFB is very important in the technology development.

4.5.2 Test Results and Discussion

The purpose of this section is to explore and predict the existence of the dense bed in the bottom of a circulating fluidized bed. Experimental data is presented first from test run TC02.

The pressure drop in the riser side of the reactor is used as the measurement of the bed density. Further gravity is assumed to dominate the entire length of the riser. In this assumption the bed density becomes:

$$\rho_b = \frac{\Delta p}{gH} \qquad \text{(Equation 4.5.1)}$$

where, ρ_b, Δp, g, and H are bed density, pressure difference, gravity acceleration, and the height between the pressure difference measurement locations.

Figure 4.5-1 shows profiles of the bulk density, void fraction, and superficial gas velocity along the axial direction in the riser side of the reactor. The relative height on the x-axis is defined as any section of the reactor over the entire height of the reactor and height in the bottom of the reactor is defined as zero. The relative bulk density is then defined as:

$$\rho_R = \frac{\rho_b}{\rho_h} \qquad \text{(Equation 4.5.2)}$$

where ρ_R and ρ_b are relative and bulk densities, respectively; ρ_h is the highest bulk density in any location of the riser or the mixing zone of the reactor. The relative velocity is defined as:

$$U_R = \frac{U}{U_h} \qquad \text{(Equation 4.5.3)}$$

where U_R and U are the relative and superficial gas velocities, respectively; U_h is the highest velocity in the riser or mixing zone. The void fraction plotted on the second y-axis in figure 4.5-1 is calculated from the following equation:

$$\varepsilon = 1 - \frac{\rho_b}{\rho_p} \qquad \text{(Equation 4.5.4)}$$

where, ε and ρ_p are the void fraction and the particle density, respectively. The particle density, ρ_p, is assumed to be the same as sand (169 lb_m/ft^3).

In figure 4.5-1, the bulk density in the bottom of the mixing zone is shown as almost 20 times as high as that in the top of the riser. One apparent reason is that the gas velocity near the top of the riser is higher than that in the bottom of the mixing zone. At a given solids flux, a higher gas velocity means a higher void fraction. Also, as shown in figure 4.5-1, the gas velocity near the top of the riser is about 6 times as high as that in the bottom of the mixing zone.

An important cause of this higher density in the bottom of the mixing zone is a higher solid circulation rate. It can be imagined that at a constant superficial gas velocity, if the solid

circulation rate keeps increasing, a dense bed always forms no matter how high the gas velocity is. Since the gas carrying capacity always has a limit, increasing solid circulation rate will definitely increase the bed bulk density. The bulk density increase with the solid circulation rate has been reported in the literature many times over. A very good set of experimental data presented by Adanez, et al. (1994), clearly indicates that the bulk density in the bed increases with an increase in the solids circulation rate. Bai, et al. (1992), provided another set of data that showed that with an increase of the solids circulation rate (flux) from 39 kg/m^2 s (8.0 lb_m/ft^2 s) to 60 kg/m^2 s (12 lb_m/ft^2 s) the bulk density in the bottom of the bed changed from 3 lb_m/ft^3 to 20 lb_m/ft^3. An interesting example, which has been mentioned previously, is that Svensson, et al. (1993), who noted that for 300 μm mean particles a bubbling bed persisted in spite of the gas velocities (18 ft/s) being several times the particle terminal velocity. It is apparently due to a high-solids circulation rate. It should be noted that all of the above mentioned literature data were taken in a column that has the same diameter in the entire riser side. It is interesting to note that in spite of the different configuration of reactors, different superficial gas velocity, and different particle properties, the void fraction profile in all these reactors are qualitatively similar and also quantitatively close to one another. Ouyang and Potter (1993) reviewed various experimental data on a circulating fluidized bed and found that the void fraction in the bottom of the riser is, on the average, 0.82 in spite of the vast differences on experimental conditions among different researches. The void fraction of the bottom of the mixing zone shown in figure 4.5-1 is 0.84.

Another feature in figure 4.5-1 is that the bulk density in the bottom of the riser is higher than that in the top of the mixing zone. One reason is the gas-phase acceleration in this zone. In an accelerated gas stream at a constant mass flow rate, the wall region velocity is retarded. The lower gas velocity in the wall region causes the solids to flow downwards so that the bulk density in this region is higher. This will result in a higher solid holdup in this region so that the bulk density should be higher in a region where gas phase is accelerating. The bulk density in the top of the mixing zone is lower than that in the bottom of the riser and can be partially explained by a phenomenon called particle overshooting. Regardless of the cause of the dense bed in the bottom of the mixing zone (suggested cause being the high-solid circulation), the true gas-phase velocity (defined as the superficial gas velocity divided by the void fraction) will decrease as the gas leaves the relative dense phase and enters the relative dilute phase because of an increase in void fraction. Because the gas velocity is far above the individual particle terminal velocity, in a region immediately above the dense bed, some of the solid particles may have a velocity larger than the gas-phase velocity due to inertia. Such particle overshooting can create a relatively dilute region immediately above the dense phase region.

Still another characteristic of the transport reactor is the gas velocity profile along the axial direction, as shown in figure 4.5-1. There are three regions: 1) low gas velocity in the bottom, 2) a strong acceleration in the intersection of the mixing zone and riser, and 3) high gas velocity in the top. Three factors contribute to this gas velocity profile: 1) the reactor diameter, 2) reactor temperature, and 3) air staging.

Figure 4.5-2 gives a similar plot for a different operation period that emphasizes that the velocity, void fraction, and the bed density shown in figure 4.5-1 is representative of a normal operational period. The similarity of figure 4.5-1 and 4.5-2 is apparent. The void fraction in the bottom of the mixing zone for the operation period shown in figure 4.5-2 is 0.82 (the same

average value of literature data reviewed by Ouyang and Potter (1993)) in spite of differences in the reactor configurations, particle properties, and gas superficial velocities. The experimental data presented by Adanez, et al. (1994), also showed that the void fraction in the bottom of the riser is 0.82 under different experimental conditions.

Figure 4.5-3 gives a plot similar to the previous two figures but with a lower solid circulation rate. Comparing figure 4.5-3 with figure 4.5-1 or 4.5-2, one can clearly see that the bulk density and void fraction profiles are different. No local maximum on bulk density along the axial direction can be detected from figure 4.5-3. The void fraction in the bottom of the mixing zone is still 0.82 in spite of the difference of the bulk density profile in the riser. This is consistent with the observation by Zhang, et al. (1998), who observed that the changes in solids circulation rates and gas-phase superficial velocities will change the void fraction profile in the axial direction, but change little the void fraction in the bottom of the riser.

In summary, PSDF test data clearly show that there is a relatively dense region in the bottom of the transport reactor. This is quite consistent with the observation in the literature. The bulk density has a local maximum in the bottom of the riser when the solid circulation rate is relatively high. Although the reactor configuration, the velocity profile, and particle properties for the transport reactor are quite different from those reactors reported in the literature the void fraction profiles are all qualitatively similar. This may indicate that the solid circulation rate has the dominating influence on the bulk density profile in a circulating fluidized bed.

4.5.3 Conceptual Model and Discussion

It is easy to imagine that if we add a single small solid particle to a gas stream flowing in a vertical pipe with a velocity more than one order of magnitude larger than the particle terminal velocity the particle will be entrained with the gas stream. The trajectory of the particle will closely follow the turbulent eddies. If the particle concentration continues to increase in the gas stream, the solids concentration in the wall region will be slightly higher than the center of the pipe because the gas velocity is lower near the wall than it is in the center of the pipe. At this solid flow rate, the solids may still be flowing upward because so few particles are near the wall region and strong gas-phase shear stress can carry all the particles upwards. If the solid concentration is increased further some of the solids will be flowing downwards along the wall because the shear stress in the wall region is not strong enough to cause all solids to flow upward. This is the well-established core-annular flow region (e.g., Zenz, 1998; and Bai, et al., 1995). This core-annular flow can be viewed in the wall region as the carrying capacity of the gas phase as "supersaturated," in analogy to a solution supersaturated with solute. If the solids concentration is increased further the wall region will enlarge to the core region. A continued increase in solids flow rate means the entire pipe will be filled with a dense bed of solids. The entire flow field is supersaturated under this condition. The bubbling bed in the bottom of the reactor observed by Svensson, et al. (1993), and Johnsson and Leckner (1995) may be some evidence of supersaturation in a CFB.

It must be emphasized here that in the above described conceptual experiment, under a very high gas velocity, it remains possible to have a very dense bed of solids in the riser of a CFB. Although there are many reports on the fluidization regime mappings and many experimental findings on the void fraction profile in a CFB exist, the research and understanding on the

influence of the solids circulation rate on the fluidization regime have gained little progress due to the strong influence of bubbling bed. Emphasis is also made here that the gas-carrying capacity is the key to the different void fraction profiles along the axial direction. This issue will be addressed here theoretically so that a better understanding will be gained and a new light will be shed on this matter.

In order to grasp the essentials of the flow field and simplify mathematical manipulations, there is the assumption that there is an analogy between the core-annular gas-solids flow and gas-liquid-annular flow. This analogy is probably a portrayal of the two flow systems. In a recent paper, Zenz (1998) explicated on this analogy and calculated the annular "film" thickness by an oversimplified flooding theory. Notwithstanding his neglect of the true influence of the solid circulation rate on the flooding, the result from using such a simplified model is encouraging. The mechanism for the transition from a core-annular flow to a dense-phase flow is probably flooding. The following material briefly addresses these issues and their influence on the void fraction profile in the reactor and on the reactor design.

Once the analogy between gas-liquid flow and gas-solids flow is accepted, many of the theoretical results in the gas-liquid flow can be applied to gas-solids flow. One of the outstanding models presented by Wallis (1969) is based on the annular-turbulent flow. The result modified to the gas-solid flow can be expressed as

$$U_c^{*1/2} = C + mU_f^{*1/2} \qquad \text{(Equation 4.5.5)}$$

where:

$$U_c^* = \frac{\rho_c^{1/2} U}{\sqrt{gD(\rho_b - \rho_c)}} \qquad \text{(Equation 4.5.6)}$$

$$U_f^* = \frac{\rho_b^{1/2} U_{sf}}{\sqrt{gD(\rho_b - \rho_c)}} \qquad \text{(Equation 4.5.7)}$$

C = empirical constant
D = diameter of the reactor
m = empirical constant
U_{sf} = superficial solid velocity in the film region
U_c^*= dimensionless core velocity
U_f^*= dimensionless annular velocity
ρ_c = bulk density in the core region.

Figure 4.5-4 gives a plot of superficial gas velocity against the solid flux by application of equation 4.5.5 with m = C =1.0, bulk density of 60 lb_m/ft^3, and core density equaling the gas density of 5.0 lb_m/ft^3. It is clear under this set of conditions that to avoid flooding an increase in the solids flux must accompany an increase in gas velocity. Although equation (4.5.5) should not be deemed as an accurate expression of the flooding line in the transport reactor, it indeed gives a direction in the study of the gas-carrying capacity and the void fraction profile in the reactor.

It may be very helpful in the study of the reactor configuration and in the design of gas and solids flux in the reactor.

An outstanding feature of equation (4.5.5) is that it predicts that there will be a dense phase in the reactor no matter what is the particle size as long as the gas velocity falls below the flooding line for a given solids flux. In real operation, if the reactor is run in a dense-phase region for a given solid flux, the gas velocity should be below the flooding line. Many other models cannot predict this feature.

One advantage in using equation (4.5.5) is that this equation takes into account the influence of the reactor diameter on the gas-carrying capacity and on flooding. Figure 4.5-5 gives a comparison of the influence of the different reactor diameter on flooding by assuming that both "m" and "C" are constant in equation (4.5.5). The influence of other parameters, such as bulk density, entrance effect, and particle shape can also be studied by using equation (4.5.5).

The principle point of this subsection is that the flooding and void fraction profile in a transport reactor can be studied by using a relatively simple model by assuming an analogy between the gas-liquid flow and gas-solids flow. Other models can also be used. More study is needed to better understand the hydrodynamics of the circulating fluidized bed.

4.5.4 Summary

Findings from literature are briefly reviewed here on the void fraction or bulk-density profiles in a circulating fluidized bed reactor. Literature data clearly indicate that the bulk density in the bottom of the reactor is always higher than that in the top in a CFB. Test data from the transport reactor at PSDF showed the same trend as found in the literature, although these reactors may have different flow rate and different configurations. By speculating that flooding is the cause of the dense phase in the bottom of the reactor, it can be shown that the relationship between solids flux and gas velocity might be linear for a given reactor. This relationship should be closely examined in future tests.

4.5.5 References for Section 4.5

Adanez, J., F. Garcia-Labiano Gayan, L. F. de Diego (1994), Axial voidage profiles in fast fluidized beds, *Powder Technology*, 81, pp. 259 to 268.

Bai, D. R., J. X. Zhu, Y. Jin, Z. Yu (1995), Internal recirculation flow structure in vertical upflow gas-solids suspensions: Part I. A core-annulus model, *Powder Technology*, 85, pp. 171 to 177.

Grace, J. R. and H. Bi (1997), Introduction to circulating fluidized beds, in *Circulating Fluidized Beds* (J. R. Grace, A. A. Avidan, and T. M. Knowlton, eds.), Blackie Academic & Professional, New York.

He, Y. and V. Rudolph (1996), The volume-average voidage in the riser of a circulating fluidized bed, *Powder Technology*, 89, pp. 79 to 82.

Horio, M. (1997), Hydrodynamics, in *Circulating Fluidized Beds* (J. R. Grace, A. A. Avidan, and T. M. Knowlton, eds.), Blackie Academic & Professional, New York.

Johnsson, F. and B. Leckner (1995), Vertical distribution of solids in a CFB-furnace, *Proceedings of 13th Int. Conf. on Fluidized Bed Comb.,* (K. J. Heinschel, ed.) Orlando, Florida, pp. 671 to 679.

Konno, H. and S. J. Satio (1969), Pneumatic conveying of solids through straight pipes. *Chem. Eng. Japan*, 2, pp. 211 to 217.

Kunii , D. and O. Levenspiel (1991), *Fluidization Engineering, Second Edition*, Butterworth-Heinemann, Boston.

Kwauk, M. and J. Li (1996), Fluidization regimes, *Powder Technology*, 87, pp. 193 to 202.

Li, Y. and M. Kwauk (1980), The dynamics of fast fluidization, in *Fluidization III* (J. R. Grace and J. M. Masten, eds.), Plenum Press, New York, pp. 537 to 544.

Masten, J. M. (1982), Mechanism of choking and entrainment. *Powder Technology*, 31, pp. 21 to 34.

Ouyang, S. and O. E. Potter (1993), Consistency of circulating fluidized bed experimental data. *Ind. Eng. Chem. Res.* 32, pp. 1041 to 1045.

Svensson, A., F. Johnsson, and B. Leckner (1993), Fluid dynamics of the bottom bed of circulating fluidized bed boiler, Proceedings 12th Int. Conf. on Fluidized Bed Comb., (Rubow, L. and G. Commonwealth, eds.) San Diego, California, pp. 887 to 897.

Takeuchi, H., T. Hirama, T. Chiba, J. Baswas, and L. S. Leung (1986), A quantitative definition and flow regime diagram for fast fluidization, *Powder Technology*, 47, pp. 195 to 199.

Wallis G. B. (1969), *One-dimensional Two-phase Flow,* McGraw-Hill Book Company, New York, p. 343.

Yerushalmi, J. and N. T. Cankurt (1979), Further studies of the regimes of the fluidization. *Powder Technology*, 24, pp. 187 to 205.

Yerushalmi, J., D. H. Turner, and A. M. Squires (1976), The fast fluidized bed, *Ind. Eng. Chem. Process Des. Dev.,* 17, pp. 47 to 53.

Zenz, F. A. (1998), Predicting the degree of particle refluxing in concurrent upflow risers, *Powder Technology*, Volume 97, pp. 146 to 150.

Zhang, J., P. Jiang, and L-S. Fan (1998), Flow characteristics of coal ash in a circulating fluidized bed, *Ind. Eng. Chem. Res.*, 37, pp. 1499 to 1509.

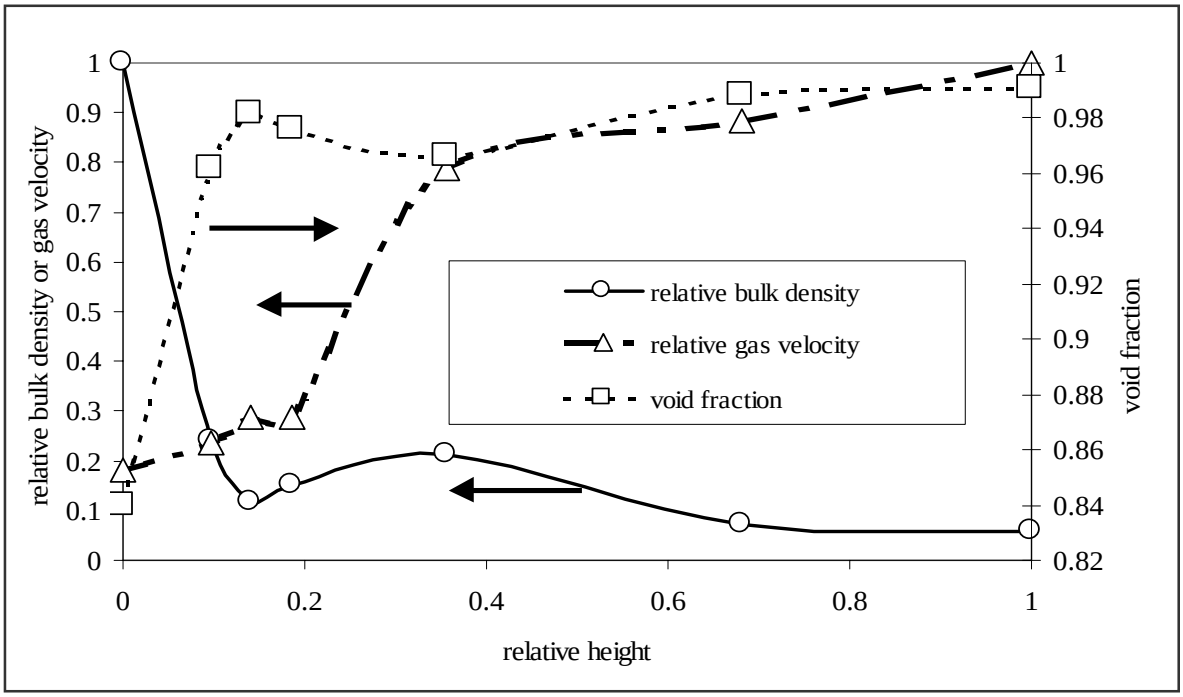

Figure 4.5-1 Bulk Density, Gas Velocity, and Void Fraction Varying With the Height of the Transport Reactor on May 7, 1998

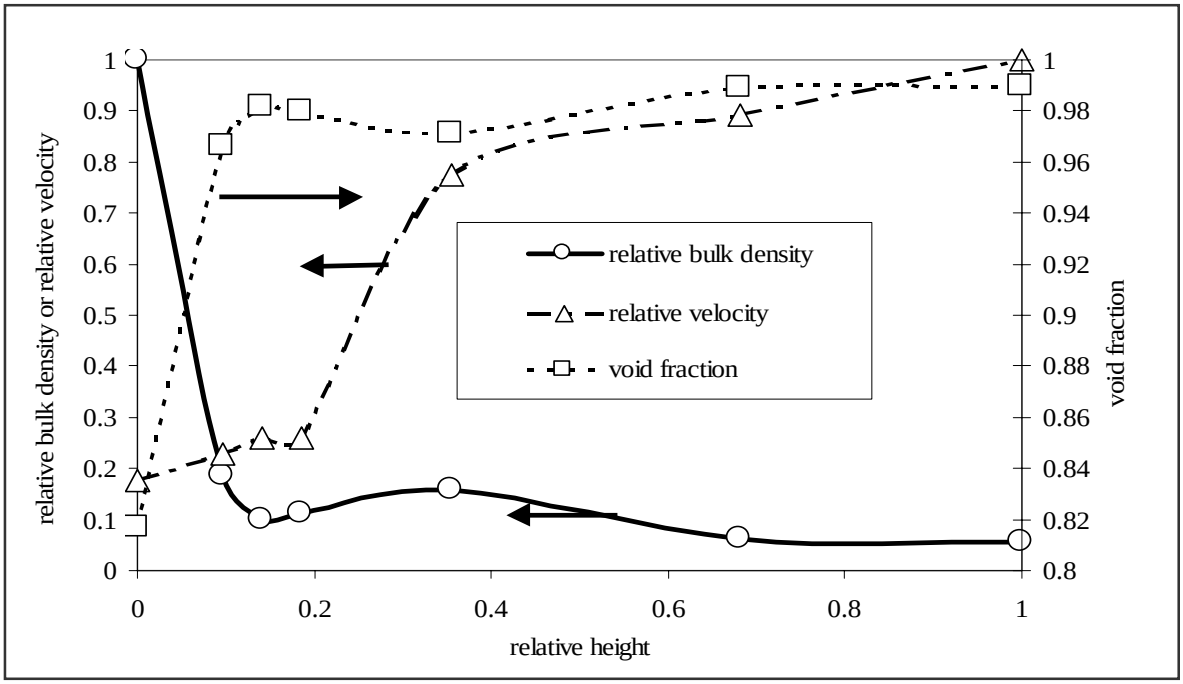

Figure 4.5-2 Bulk Density, Gas Velocity, and Void Fraction Varying With the Height of the Transport Reactor on April 29, 1998

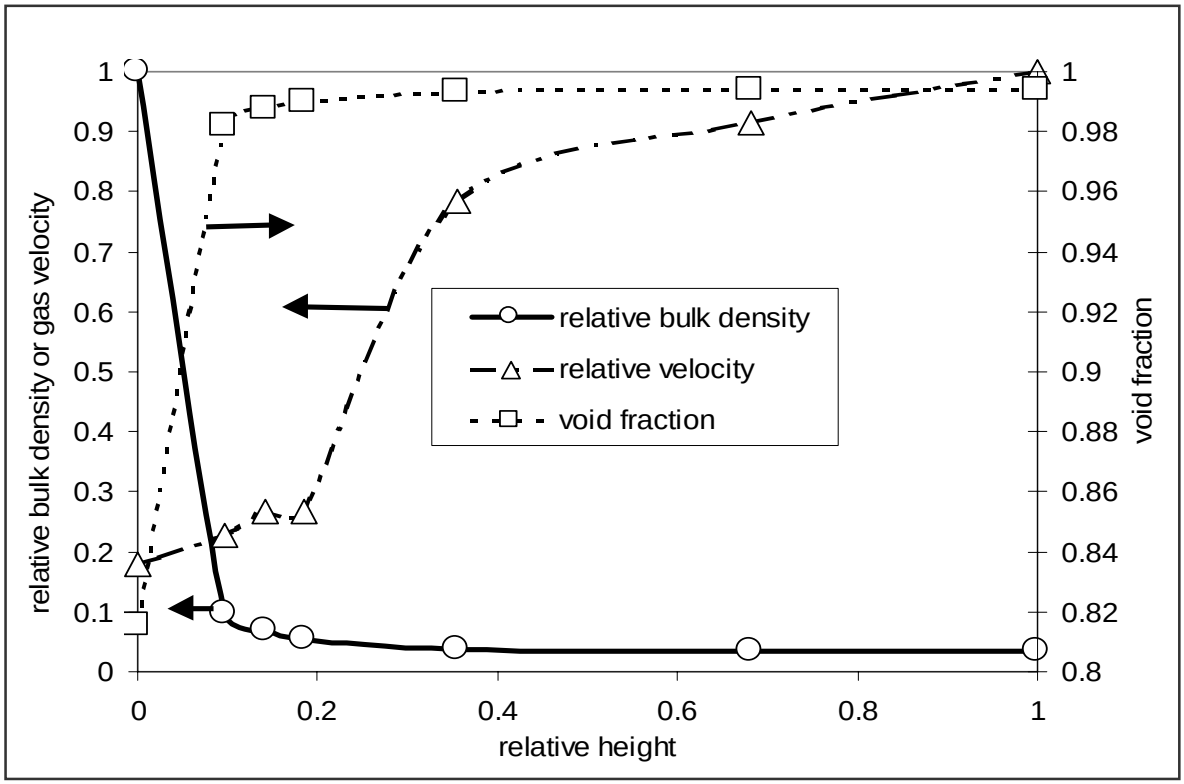

Figure 4.5-3 Bulk Density, Gas Velocity, and Void Fraction Varying With the Height of the Transport Reactor on April 22, 1998

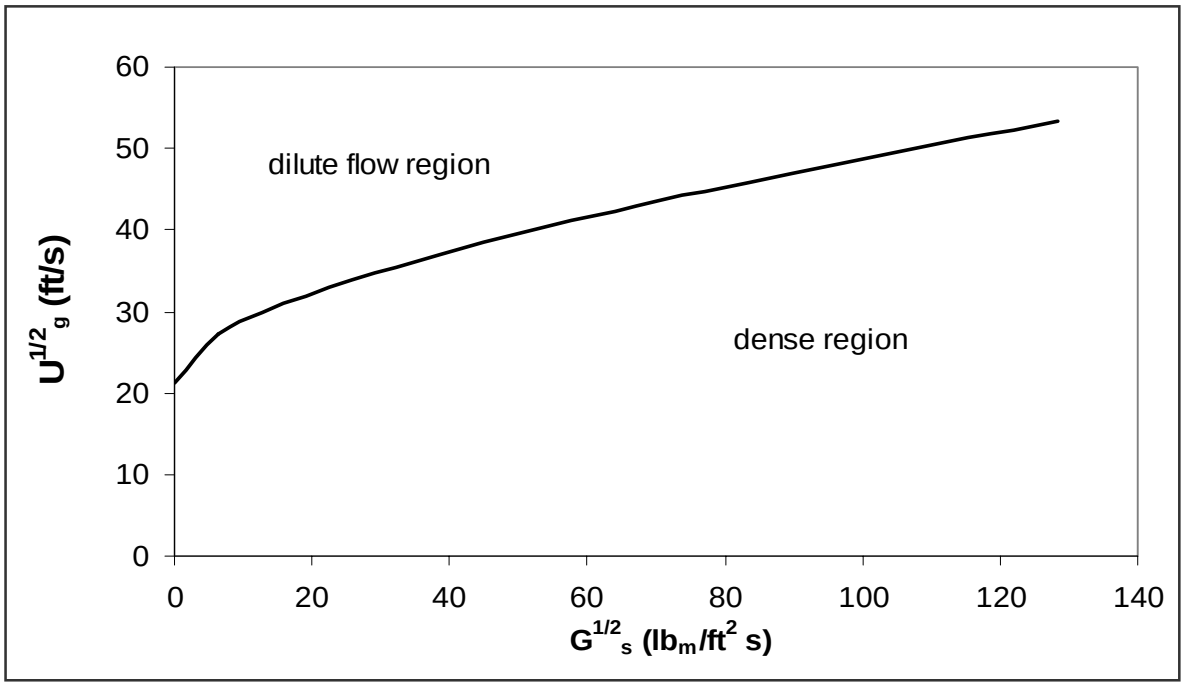

Figure 4.5-4 Illustration of an Equation of Flooding Line in the Transport Reactor

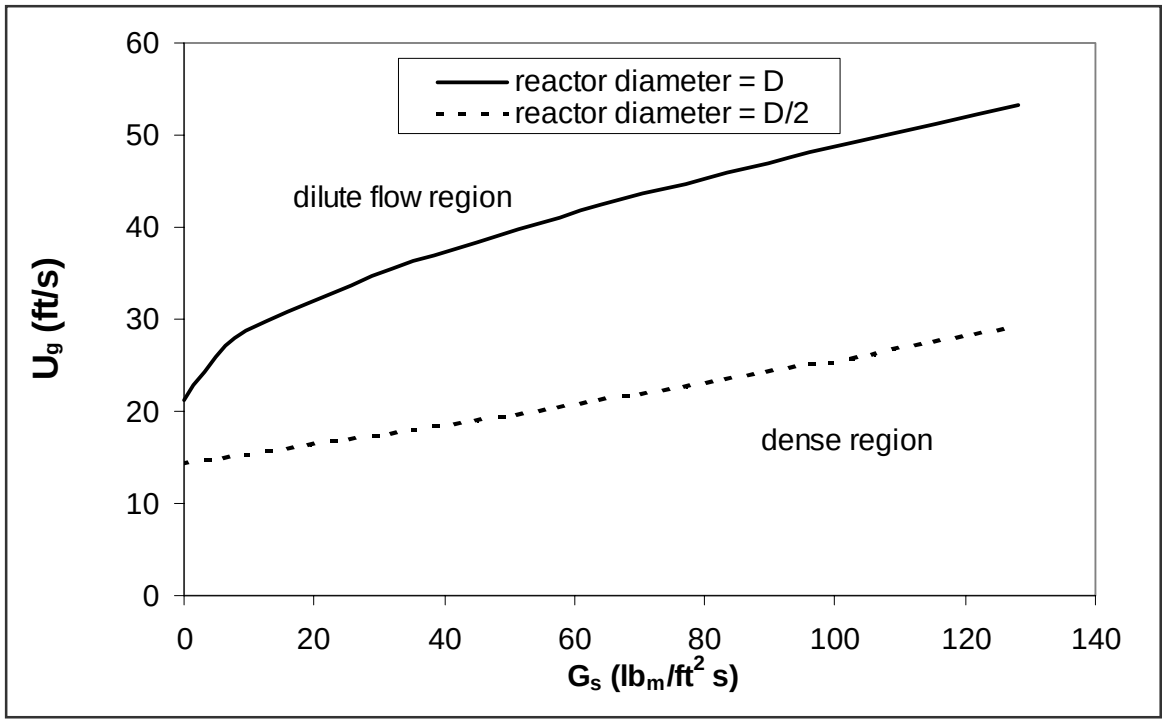

Figure 4.5-5 Illustration of an Equation of Flooding Line in the Transport Reactor

4.6 FEED SYSTEMS

4.6.1 Feedstock Preparation

There was too large a variability in coal particle size produced as feed to the transport reactor system during the first half of 1997. Tests to ascertain the sources of variation contributing to overall particle-size variation were performed and a large source of variation was found with the pulverizer inlet feedstock size.

The feedstock preparation is similar to one used by nonutility scale processes that separate and store the ground product prior to use, yet there is the additional constraint of both top- and bottom-cut sizes. The system was originally designed to have two sources of coal feeding the crushed material storage hopper (pulverizer feed hopper). The first source was the reclaim system (three-quarter-inch-by-zero coal coming from the coal pile through the hammer mill crusher), and the second was oversize particles (1,000- to 4,000-μm) coming from a scalping screen in the pulverizer system itself. This combination of coal feed sources resulted in layers within the pulverizer feed hopper. Solving the problem required consistent mixing of the smaller-size coal stream with the larger-size coal stream before feeding the mill.

The variation in mean mass grind size is less than ± 25 μm as a result of modifications and additional tuning of the coal pulverizer mill. This pulverizer modification resulted in the additional benefit of increased throughput (by 67 percent) which is almost as important as the improved control over output-particle size. The higher throughput is realized because the system no longer encounters batches of scalped coal particles, as these particles were harder or had little work performed on them in the mill and would tend to recirculate, therefore reducing the overall system throughput. The sorbent mill system performed well and no modifications have been made.

4.6.2 Reactor Feedstock Injection and Ash Removal Systems

Probably the single biggest challenge to reliable transport reactor operation has been failures of the feed injection and ash removal systems. These systems pressurize the feeds up to 20 atmospheres and depressurize the spent bed materials while moving them into and out of the process. Failures in these systems account for over 75 percent of the transport reactor train's forced outages through October 1997. The failures of the high-pressure feed and solids removal systems can be characterized into three classes: 1) material flow valve failures; 2) level probe failures and vessel bridging; and 3) starfeeder failures. However, in the past 2 years of operation, there have been only minor problems with the atmospheric dense-phase transport systems. During the same period, while working to commission (and later improve) the operation of the transport reactor, the mean time between failures of the high-pressure, dense-phase systems has been substantially increased from hours to weeks.

The reliability of the systems has improved significantly as a result of modifications made in 1997 and 1998 to all of the high-pressure dense-phase and feed systems. These modifications include the following:

- Adding high-pressure seal dump valves that provide 3 to 4 times the flow capacity of the pilot valve vent.
- Adding a low-pressure switch on the seal line.
- Adding check valves, orifices, and reservoirs in the feeder seal supply lines.
- Increasing the clearances in the starfeeder.
- Removing the epoxy lining (that was applied in error) from the coal feed system dispense vessel.
- Adding differential pressure control on the dispense vessel fluidizing nitrogen.
- Adding additional fluidization ports on the lock vessel (coal feed system) to break up cake bridges.
- Adding time delay relays to account for the elastic delay (set) in the seals returning to their original shape.
- Adjusting numerous timing and differential pressure set points in the PLC configuration.

The biggest problem involves the material flow and pressure-seal valves known as spheri valves. Rather than using typical ball valves to control the flow of solids, with the high potential for cut valve seats and seals, the spheri valves have a retractable, deflatable seal for the pressure seal and use only half of a sphere for the valve's plug. These seals are pressurized to at least 15 psig above the process pressure. Most of the failures occurred in the operation of the high-pressure (nitrogen-assisted) seals. All these systems rely on pneumatic interlocks for timing the spheri valve operation: seal deflation, valve opening, valve closing, and seal inflation. Atmospheric spheri valve systems do not have as complex an arrangement of pneumatic relays to control the seal inflation. Such simplicity has been rewarding in reliable service of these valves and seals.

The loss of a spheri valve seal also caused catastrophic header pressure loss on the nitrogen seal header. In the worst case, the seal pressure would fall so far that other seals would deflate, allowing either the hot gases or material to escape. Several such failures (with pressure loss on the seal header) seemed to be the root cause of many failures of the fine ash system spheri valves, possibly due to ash and sand getting trapped between the seal and the dome on the lower valve. Erosion on the seal was visible, indicative of the seal not pressurizing and allowing a flow path to exist long enough for channels to start eroding in the seals and/or the dome itself. Measures have been taken to minimize the rate of header pressure loss in case of a spheri valve seal failure. This provides sufficient time to isolate the failed seal and safely shut down the process.

Several shop tests were performed on the valves in an effort to better understand the hysteresis found in the seal function. The fundamental result showed that the material for high-pressure,

high-temperature use was not returning to original shape after the first few pressurization cycles. This was caused by either the material being pull-extruded by the pressure on the seal or by the seal creeping out of the clamp mechanism. Regardless, this seal growth was a major contributor to the seal failures because as the clearances are reduced the dome (which is roughcast) eventually rubs the seal causing damage. The same problem was not observed when testing the low-temperature seal materials. As a result, the low temperature seals were installed into all the spheri valves and the operating controls and procedures were modified to accommodate the lower temperature limits. Suitable high-temperature seal materials development and clamp mechanism redesign are in progress.

Level probe failures result in system operating difficulties since the level probes are the prime triggers to initiate or halt filling. These failures can cause short cycling, preventing any real movement of solids, or they can cause overfilling of the vessels as a result of plugging or bridging the vessels, which also prevents any real movement of solids. The sensitivity of the probe electronics caused by calibration in "clean" settings and then being exposed to dusty conditions has resulted in a layer of dust collecting on the probe itself, and thereby changing the probe calibration. There have also been several electronic failures of the probes. The level probes malfunctioning caused caking and bridging (especially in coal) in the vessels due to overfilling of the vessels in some cases. Secondary control signals are being developed using weight or time to assure cycle operation if the level probe fails to operate, as most of these systems are equipped with weigh cells for flow rate determination. Malfunction of the systems in some other cases was attributed to level probe failure but was actually a result of large masses of material not moving out of the vessels. The dispense vessels have been modified to provide more fluidization flow for longer periods than was originally specified, and there have also been experiments with the use of additional mechanical agitators to prevent solids bridging in vessels.

The lock vessels on the coal and dolomite/limestone feeders are directly below the surge bins. The connection is through an 8-inch pipe. The flow rate of solids from the surge bin can be very fast (as much as 600 lb in less than 5 seconds). The lock vessels would overfill and pack with such a speed that the slower reaction time of the level probes and the spheri valves would cause a loss-of-feed flow. The inlet gate valve was throttled to remain open about 1.0 inch to slow the quick overfilling. This throttling helped to reduce the packing effect in the lock vessel; however, the adjustment of the gate valve is not exact and the lock vessel will still overfill. This overfilling causes the coal to fall into the equalization line (between the lock vessel and the dispense vessel). The equalization line was rearranged to overcome this problem, with the top of the equalization line above the depressurization/vent line. The sorbent feeder sometimes will do several fill cycles without filling the dispense vessel. This indicates that the modifications made to the coal feeder should also be done on the sorbent feeder; however, loss of sorbent is less critical than loss of coal feed so changes to sorbent feed system have been delayed.

Rotary metering feeders (starfeeders) are present on both coal and sorbent feeder systems as well as on the sulfator feed system. These caused several failures that were usually the result of plugging or binding. The starfeeders were equipped with induction motors and variable frequency motor drives to adjust the injection rate of the feedstock. While such a design is very efficient and controllable in the upper half of the speed range the motors do not generate much torque (force) in the lowest quarter of the speed range. The choice of a DC motor or hydraulic motor would have been better for this application because the lower half of the speed range is

the most critical for accurate control during start-ups and low-load operation. The starfeeder is susceptible to binding by material in the clearances as well as oversized material wedged into the pockets because it relies on close clearances for sealing the star pockets. An epoxy lining was discovered in 1997 to have flaked off of the feeder vessels and was getting caught in the starfeeder, both binding the star and sometimes blinding the discharge port. The coal feed system starfeeder motor was also rewound from a 4-pole to a 10-pole design that reduced the speed by 60 percent and increased motor torque by a similar amount at the same motor speed. The functionality of the system is not compromised by such a modification because this motor is powered by a variable-frequency drive (VFD) to provide speed control. The parameters of the VFD were also adjusted to compensate for the modified speed of the rewound motor.

In summary, while these systems have been the leading cause of forced outages of the transport reactor train there has been substantial progress in the development of these systems for this application. This has been demonstrated by the significantly improved reliability of the entire transport reactor train operation in the most recent test runs.

Terms

TERMS

Listing of Abbreviations

AAS	Automated Analytical Solutions
ADEM	Alabama Department of Environmental Management
APC	Alabama Power Company
APFBC	Advance Pressurized Fluidized-Bed Combustion
ASME	American Society of Mechanical Engineers
AW	Application Workstation
BFI	Browning-Ferris Industries
BFW	Boiler Feed Water
BMS	Burner Management System
BOC	BOC Gases
BOP	Balance-of-Plant
BPIR	Ball Pass Inner Race, Frequencies
BPOR	Ball Pass Outer Race, Frequencies
BSF	Ball Spin Frequency
CAD	Computer-Aided Design
CEM	Continuous Emissions Monitor
CFB	Circulating Fluidized Bed
CFR	Code of Federal Regulations
CHE	Combustor Heat Exchanger
CPC	Combustion Power Company
CPR	Cardiopulmonary Resuscitation
DC	Direct Current
DCS	Distributed Control System
DOE	U.S. Department of Energy
E & I	Electrical and Instrumentation
EERC	Energy and Environmental Research Center
EPRI	Electric Power Research Institute
FCC	Fluidized Catalytic Cracker
FETC	Federal Energy Technology Center
FFG	Flame Front Generator
FI	Flow Indicator
FIC	Flow Indicator Controller
FOAK	First-of-a-Kind
FTF	Fundamental Train Frequency
FW	Foster Wheeler
GBF	Granular Bed Filter
GC	Gas Chromatograph
GEESI	General Electric Environmental Services, Inc.
HP	High Pressure
HRSG	Heat Recovery Steam Generator
HTF	Heat Transfer Fluid
HTHP	High-Temperature, High-Pressure

I/O	Inputs/Outputs
ID	Inside Diameter
IF&P	Industrial Filter & Pump
IGV	Inlet Guide Vanes
IR	Infrared
KBR	Kellogg Brown & Root
LAN	Local Area Network
LIMS	Laboratory Information Management System
LOC	Limiting Oxygen Concentration
LOI	Loss on Ignition
LPG	Liquefied Propane Gas
LSLL	Level Switch, Low Level
MAC	Main Air Compressor
MCC	Motor Control Center
MS	Microsoft Corporation
NDIR	Nondestructive Infrared
NFPA	National Fire Protection Association
NOx	Nitrogen Oxides
NPDES	National Pollutant Discharge Elimination System
NPS	Nominal Pipe Size
OD	Outside Diameter
OSHA	Occupational Safety Health Administration
OSI	OSI Software, Inc.
P&IDs	Piping and Instrumentation Diagrams
PC	Pulverized Coal
PCD	Particulate Control Device
PDI	Pressure Differential Indicator
PDT	Pressure Differential Transmitter
PFBC	Pressurized Fluidized-Bed Combustion
PI	Plant Information
PLC	Programmable Logic Controller
PPE	Personal Protection Equipment
PRB	Powder River Basin
PSD	Particle Size Distribution
PSDF	Power Systems Development Facility
ΔP	Pressure Drop
PT	Pressure Transmitter
RFQ	Request for Quotation
RO	Restriction Orifice
RSSE	Reactor Solid Separation Efficiency
SCS	Southern Company Services, Inc.
SMD	Sauter Mean Diameter
SRI	Southern Research Institute
SUB	Start-up Burner
TCLP	Toxicity Characteristic Leaching Procedure
TR	Transport Reactor
TRDU	Transport Reactor Demonstration Unit

TSS	Total Suspended Solids
UND	University of North Dakota
UPS	Uninterruptible Power Supply
UV	Ultraviolet
VFD	Variable Frequency Drive
VOCs	Volatile Organic Compounds
WPC	William's Patent Crusher
XXS	Extra, Extra Strong

Listing of Units

acfm	actual cubic feet per minute
Btu	British thermal units
°F	degrees fahrenheit
ft	feet
FPS	feet per second
gpm	gallons per minute
g/cm^3	grams per cubic centimeter
hp	horsepower
hr	hour
inWg	inches, water gauge
MB	megabytes
MW	megawatts
m/s	meters per second
m^2/g	square meters per gram
μ or μm	microns or micrometers
dp_{50}	particle size distribution at 50 percentile
ppm	parts per million
ppm (v)	parts per million (volume)
ppm (w)	parts per million (weight)
lb	pounds
pph	pounds per hour
psia	pounds per square inch
psig	pounds per square inch gauge
ΔP	pressure drop
rpm	revolutions per minute
s or sec	seconds
scf	standard cubic feet
scfm	standard cubic feet per minute
V	volts